Atmospheric moisture transport and dynamic precipitation controls on the Tibetan Plateau

vorgelegt von
Dipl.-Met.
Julia Curio
ORCID: 0000-0002-0361-9541

an der Fakultät VI - Planen Bauen Umwelt
der Technischen Universität Berlin
zur Erlangung des akademischen Grades

Doktor der Naturwissenschaften
- Dr. rer. nat. -

genehmigte Dissertation

Promotionsausschuss:

Vorsitzender: Prof. Dr. Martin Kaupenjohann
Gutachter: Prof. Dr. Dieter Scherer
Gutachter: Prof. Dr. Jörg Bendix
Gutachter: Prof. Dr. Christoph Schneider

Tag der wissenschaftlichen Aussprache: 17. Februar 2020

Berlin 2020

Acknowledgements

I thank my supervisor Dieter Scherer for giving me the opportunity to work on this project, for trusting and encouraging me, and for believing in me. He is a great teacher and I admire his capacity for enthusiasm. I thank everyone in the department for making it such a great place to work and for their friendship. Special thanks go to Fabien for all the scientific discussions and the hours he spent on teaching me IDL. I also would like to thank everyone in the WET project, it has been a great time and I had a lot of fun. As part of the project I had the chance to visit the Tibetan Plateau in summer 2012. This journey and experience will always have a special place in my heart.
I thank my parents, my brothers, and my grandmother for their love and for believing that I could achieve everything I set my mind to. I thank my friends and colleagues, old and new, for their friendship and support and for making it possible to feel at home in a new country. I also thank my supervisors in Reading, Reinhard, Andy, and Nick, for trusting me and giving me the time to finish my PhD.
Finally, I thank Christian, who stood by my side during this journey, never stopped trying to make me smile and showed me that we are always together even when we are apart.

Pictures taken by J. C. during the WET field campaign on the Tibetan Plateau in August 2012.

List of papers

This thesis is presented in cumulative form and is based on the following peer-reviewed papers which are reprinted in their original form in the appendix.

I: Maussion, F., Scherer, D., Mölg, T., Collier, E., Curio, J. and Finkelnburg, R., 2014: Precipitation seasonality and variability over the Tibetan plateau as resolved by the High Asia reanalysis. Journal of Climate, 27 (5), 1910-1927, https://doi.org/10.1175/JCLI-D-13-00282.1.

II: Curio, J., Maussion, F. and Scherer, D., 2015: A 12-year high-resolution climatology of atmospheric water transport over the Tibetan plateau. Earth System Dynamics, 6 (1), 109-124, https://doi.org/10.5194/esd-6-109-2015.

III: Curio, J. and Scherer, D., 2016: Seasonality and spatial variability of dynamic precipitation controls on the Tibetan Plateau. Earth System Dynamics, 7 (3), 767-782, https://doi.org/10.5194/esd-7-767-2016.

Abstract

The Tibetan Plateau (TP) is the origin of many large Asian rivers, which provide water resources for large regions in south and east Asia. Therefore, the water cycle on the TP and adjacent high mountain ranges, in particular the precipitation distribution and variability play an important role for the water availability for billions of people in the downstream regions of the TP. The respective influence of the Indian and East Asian summer monsoon on TP precipitation and regional water resources, together with the detection of moisture transport pathways and source regions are the subject of recent research.

The aim of this thesis is to gain a better understanding of the spatial and temporal precipitation variability on the TP. In order to do so we examine the moisture transport to and on the TP, analyse the underlying processes leading to enhancement or suppression of precipitation, and examine how those processes are affected by the mid-latitude westerlies and the monsoon system. A newly developed high-resolution dataset, the High Asia Refined analysis (HAR), is used to examine atmospheric water transport (AWT) and dynamical factors that influence precipitation variability in the TP region. The HAR is the result of dynamically downscaling an operational analysis. Due to the higher spatial and temporal resolution of the HAR, it better represents the complex topography of the TP and surrounding high mountain ranges than coarse-resolution data sets like reanalyses, thereby reducing precipitation biases.

Analysing the AWT, we focus on spatiotemporal patterns, vertical distribution and transport through the TP boundaries. The results show that the mid-latitude westerlies have a higher share in summertime AWT over the TP than assumed so far. High mountain valleys in the Himalayas facilitate AWT from the south, whereas the high mountain regions inhibit AWT to a large extent and limit the influence of the Indian summer monsoon. Our results show that 36.8$\pm$6.3% of the atmospheric moisture needed for precipitation comes from outside the TP, while the remaining 63.2% is provided by local moisture recycling.

We use monthly correlations of selected dynamic variables with the precipitation to analyse what controls precipitation variability on the TP and in the surrounding high mountain regions. The selected variables, called dynamic precipitation controls, are the wind speed at

300 hPa wind and the wind speed 2 km above ground, the vertical wind speed at 300 hPa, the vertically integrated atmospheric water transport, and the height of the planetary boundary layer. We focus on the seasonality and the spatial variability of the relationship between dynamic controls and precipitation.

Results show that different controls have different effects on precipitation in different regions and seasons. For example, the 300 hPa wind speed has a positive effect in the western parts of the study region in winter and spring, while it has a negative effect on precipitation on the TP in summer by cutting off deep convection. The positive correlation of AWT with precipitation is higher in winter at the high mountain ranges in the western part of the study region, than in summer on the central TP. This result shows that on the central TP the strong convection in summer is able to produce precipitation with the moisture available from local sources, emphasising the importance of moisture recycling.

Those results illustrate that the effect of dynamic controls on precipitation variability depends mainly on the dominant type of precipitation, i.e. convective or frontal/cyclonic precipitation.

This thesis shows that the impact of the midlatitude westerlies on precipitation variability on the TP is strong, not only in winter, by enhancing moisture advection for orographic and frontal precipitation in the western parts of the study region but also in summer by cutting off deep convection on the TP and in other regions and seasons where and when precipitation is mainly convective. Additionally, the westerlies deliver more moisture to the TP in summer than assumed so far.

Zusammenfassung

Das Tibetische Plateau (TP) ist der Ursprung vieler großer asiatischer Flüsse, die große Gebiete in Süd- und Ostasien mit Wasser versorgen. Daher spielen der Wasserkreislauf auf dem TP und in den angrenzenden Hochgebirgen, insbesondere die Niederschlagsverteilung und -variabilität, eine wichtige Rolle für die Wasserverfügbarkeit für Milliarden von Menschen in den dem TP nachgelagerten Regionen. Der jeweilige Einfluss des indischen und ostasiatischen Sommermonsuns auf TP-Niederschläge und regionale Wasserressourcen sowie die Identifizierung von Feuchtigkeitstransportwegen und Quellregionen sind Gegenstand aktueller Forschungsarbeiten.

Ziel dieser Arbeit ist es, die räumliche und zeitliche Niederschlagsvariabilität auf dem TP besser zu verstehen. Zu diesem Zweck untersuchen wir den Feuchtigkeitstransport zum und auf dem TP, analysieren die zugrunde liegenden Prozesse, die zu einer Verstärkung oder Abschwächung des Niederschlags führen, und untersuchen, wie diese Prozesse durch die Westwinde der mittleren Breiten und das Monsunsystem beeinflusst werden. Ein neu entwickelter hochauflösender Datensatz, die High Asia Refined Analysis (HAR), wird verwendet, um den atmosphärischen Wassertransport (AWT) und dynamische Faktoren zu untersuchen, die die Niederschlagsvariabilität in der TP-Region beeinflussen. Die HAR ist das Ergebnis des dynamischen Downscaling einer operationellen Analyse. Aufgrund der höheren räumlichen und zeitlichen Auflösung der HAR wird die komplexe Topographie des TP und der umgebenden Hochgebirgsräume besser dargestellt als bei grob aufgelösten Datensätzen wie Reanalysen, wodurch systematische Niederschlagsfehler reduziert werden.

Bei der Analyse des AWT konzentrieren wir uns auf die raumzeitlichen Muster, die vertikale Verteilung und den Transport durch die TP-Grenzen. Die Ergebnisse zeigen, dass die Westwinde der mittleren Breiten einen höheren Anteil am Sommer-AWT haben als bisher angenommen. Hochgebirgstäler im Himalaya begünstigen den AWT aus dem Süden, während die Hochgebirgsregionen den AWT weitgehend hemmen und den Einfluss des indischen Sommermonsuns begrenzen. Unsere Ergebnisse zeigen, dass $36{,}8 \pm 6{,}3\%$ der für den Niederschlag benötigten Luftfeuchtigkeit von außerhalb des TP stammen, während die restlichen 63,2% durch lokales Feuchtigkeitsrecycling bereitgestellt werden.

Wir verwenden monatliche Korrelationen ausgewählter dynamischer Variablen mit dem Niederschlag, um zu analysieren, wie die Niederschlagsvariabilität auf dem TP und in den umgebenden Hochgebirgsregionen gesteuert wird. Die ausgewählten Variablen, die als dynamische Kontrollfaktoren des Niederschlags bezeichnet werden, sind die Windgeschwindigkeit in 300 hPa und die Windgeschwindigkeit 2 km über dem Boden, die vertikale Wind-

geschwindigkeit in 300 hPa, der vertikal integrierte atmosphärische Wassertransport und die Höhe der planetaren Grenzschicht. Wir konzentrieren uns auf die Saisonalität und die räumliche Variabilität des Zusammenhangs zwischen den dynamischen Kontrollfaktoren und dem Niederschlag.

Die Ergebnisse zeigen, dass verschiedene Kontrollfaktoren in verschiedenen Regionen und Jahreszeiten unterschiedliche Auswirkungen auf den Niederschlag haben. Beispielsweise wirkt sich die Windgeschwindigkeit in 300 hPa im Winter und Frühling im Westen des Untersuchungsgebiets positiv auf den Niederschlag aus, während sie sich im Sommer negativ auf die Niederschläge auf dem TP auswirkt, indem sie die Tiefenkonvektion unterbricht. Die positive Korrelation von AWT mit dem Niederschlag ist im Winter in den Hochgebirgsräumen im westlichen Teil der Untersuchungsregion höher als im Sommer auf dem zentralen TP. Dieses Ergebnis zeigt, dass die starke Konvektion auf dem zentralen TP im Sommer in der Lage ist Niederschlag mit der aus lokalen Quellen verfügbaren Feuchtigkeit zu erzeugen, was die Bedeutung des Feuchtigkeitsrecyclings unterstreicht.

Diese Ergebnisse veranschaulichen, dass die Wirkung dynamischer Kontrollfaktoren auf die Niederschlagsvariabilität hauptsächlich von der vorherrschenden Art des Niederschlags abhängig ist, d. h. konvektiver oder frontaler/zyklonaler Niederschlag.

Die vorliegende Arbeit zeigt, dass die Westwinde der mittleren Breiten einen großen Einfluß auf die Niederschlagsvariabilität auf dem TP haben. Dieser Einfluss ist nicht nur im Winter sichtbar durch die Verstärkung der Feuchteadvektion für den orografischen und frontalen Niederschlag im Westen des Untersuchungsgebiets, sondern auch im Sommer durch die Kappung der Tiefenkonvektion auf dem TP und in anderen Regionen und Jahreszeiten in denen der Niederschlag hauptschlich konvektiv ist. Zusätzlich transportieren die Westwinde im Sommer mehr Feuchtigkeit auf das TP als bisher angenommen.

Table of contents

List of figures

List of tables

Nomenclature

Acronyms / Abbreviations

AWT Atmospheric water transport

BMBF Bundeministerium für Bildung und Forschung

CAME Central Asia - Monsoon dynamics and Geo-ecosystems (BMBF Programme)

CP Cloud particles

CS Cross section

HAR High Asia Refined analysis

PBLH Planetary boundary layer height

PKwH Pamir-Karakoram-western Himalyas region

SWJ Subtropical Westerly Jet

TP Tibetan Plateau

WET Variability and Trends in Water Balance Components of Benchmark Drainage Basins on the Tibetan Plateau (BMBF Project)

WRF Weather Research and Forecasting (model)

WS10 Wind speed at ,odel level 10 (about 2 km above ground on the TP)

WS300 Wind speed at 300 hPa

WV Water vapour

1. Introduction

1.1 Motivation

The Tibetan Plateau (TP) is the highest and largest plateau in the world. With an average height of more than 4500 m above sea level it is reaching in the mid-troposphere and alters the atmospheric circulation on a large scale, due to thermal and mechanical effects, thereby shaping the hydro-climate of its downstream regions (Hahn and Manabe, 1975).

The TP is one of the most active centres in the world water cycle and constitutes an essential source of moisture for the downstream regions in East Asia (Immerzeel et al., 2010). The TP is often referred to as the “world water tower” (Xu et al., 2008), as it is the source of many large Asian rivers such as the Indus, Ganges, Brahmaputra, Yellow River, Yangtze and Mekong, which provide water for billions of people downstream in South and East Asia (Fig. 1.1). The transport of moisture to the TP is crucial for a sustainable water supply in the downstream regions like the Yellow and Yangtze river valleys (Zhang et al., 2013). In addition, the TP and its surrounding high mountain ranges are characterised by the largest number of glaciers outside of the polar regions, giving it the name "Third Pole", large areas of permafrost and a large number of lakes. In 2009 the "Third Pole Environment" program was initiated to bring together scientists from all over the world working on the TP to use multi-national resources to gain a better understanding of the atmopshere–cryosphere–hydrosphere interactions on the TP (Yao et al., 2012a).

The TP is located in the transition zone between the midlatitude westerlies (Schiemann et al., 2009) and the Indian and East Asian summer monsoon systems (Webster et al., 1998). The TP influences the upper-level westerly flow due to thermal and mechanical forcing and the westerlies are split into two branches when encountering the planet’s largest topographic barrier and converge on its east side (Webster et al., 1998; Yanai et al., 1992). The subtropical westerly jet (SWJ) is located south of the TP in winter, with its mean position at around 28°N (Schiemann et al., 2009). The core of the jet stream is located at 200 hPa with mean wind speeds of 60 $\mathrm{m\,s^{-1}}$ (Kuang and Zhang, 2005). In spring the jet weakens and starts to move north and is located over the TP in May. The northward shift of the jet is related to

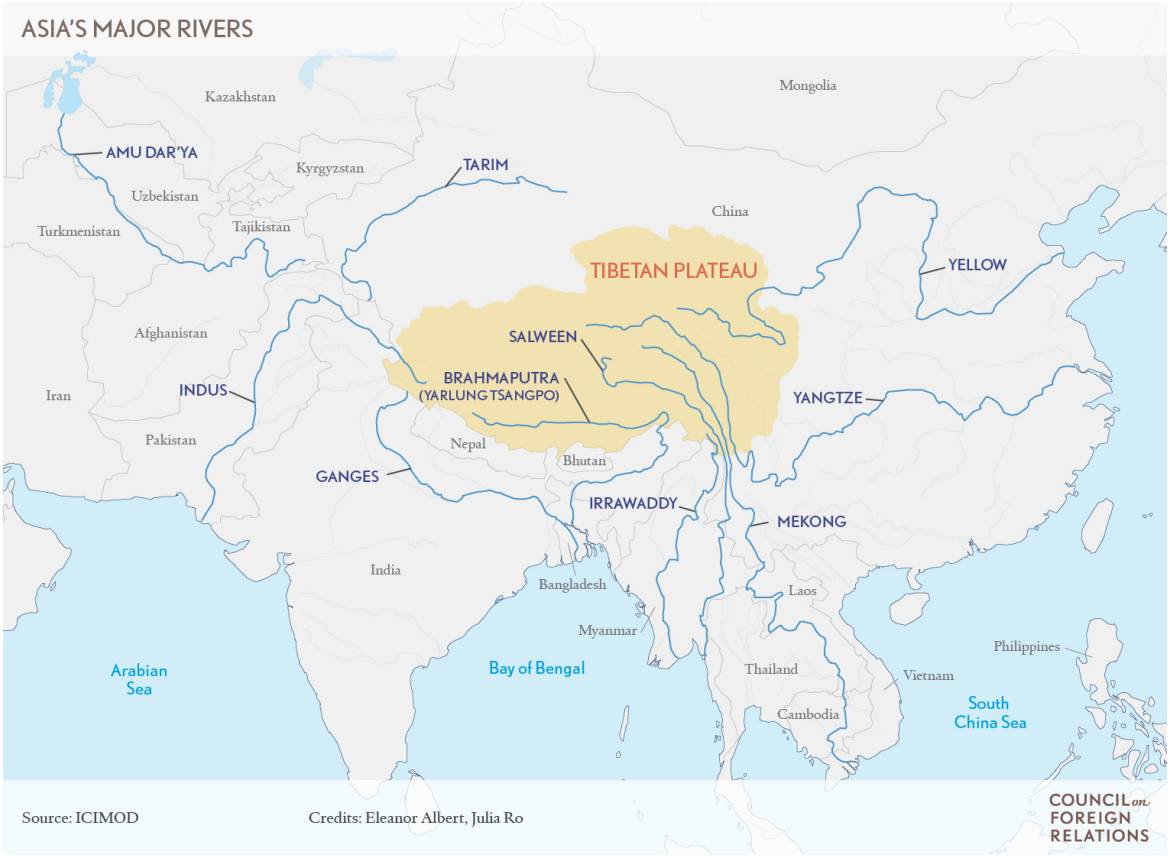

Fig. 1.1 Map of High Asia including main rivers.

the thermal contrast between land and sea due to the strong heating over the TP. Due to the height of the TP the influence of the jet stream reaches closer to the elevated surface than upstream or downstream of the TP. In summer the SWJ is located north of the TP and reaches its northernmost position at 42°N in August (Kuang and Zhang, 2005; Schiemann et al., 2009) with the mean wind speed only reaching half of its winter values. From September onwards the SWJ moves back south to its winter position south of the TP. The transition in spring is characterised by split jets and jumps while the movement is much more gradual in autumn (Schiemann et al., 2009).

The Indian summer Monsoon is thought to be the most important source of moisture for precipitation on the Tibetan Plateau. Yao et al. (2012b) and Bolch et al. (2012) list the Indian monsoon, the mid-latitude westerlies and the East Asian monsoon as drivers of climate variability in the TP. In previous studies, the influence of the westerlies and the monsoon system (Fig. 1.2) was examined on the basis of the precipitation timing and was therefore thought to be limited to winter (westerlies) or summer (Indian and East Asian summer monsoon) (Hren et al., 2009; Tian et al., 2007; Yang et al., 2014). In a recent study

(Mölg et al., 2014) showed that the westerlies influence the mass balance of the Zhadang glacier on the central TP Mölg et al. (2014) in summer and that the wind speed at 300 hPa alone explains more than 70% of the interannual mass-balance variability of the glacier.

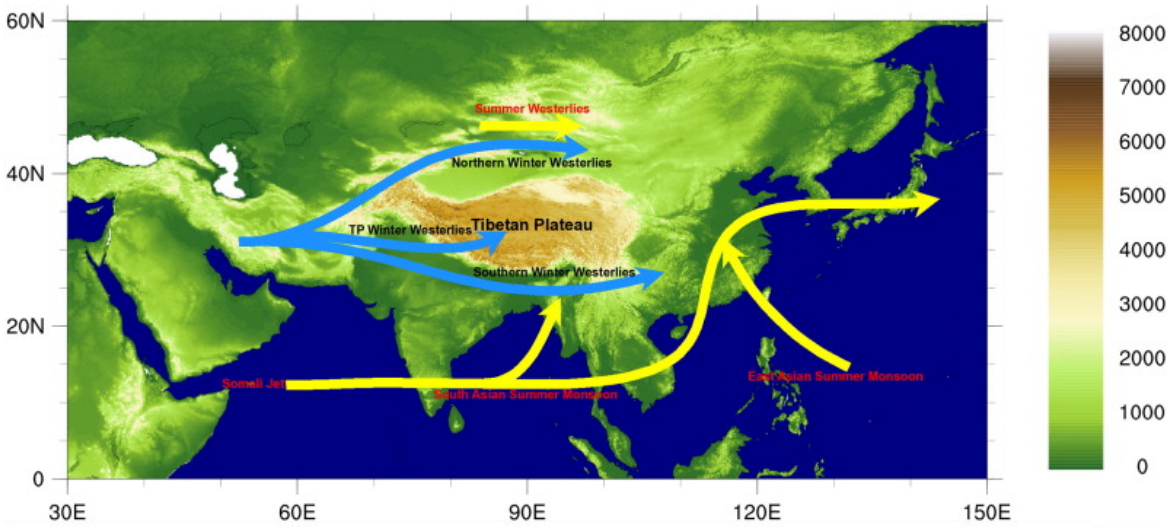

Fig. 1.2 Example for the famous Figure 1 used in many publications to schematically illustrate the influence of the westerlies and the monsoon systems on the Tibetan Plateau (Yang et al., 2014).

During the last three decades the TP experienced an overall warming and wetting (Yang et al., 2014, 2011), which has a direct impact on the hydrological cycle. The warming rate on the TP is higher than the global average (Liu and Chen, 2000). Precipitable water shows increasing trends in the eastern and western TP and decreasing trends in the central TP for the relatively short period of 2000–2010 (Lu et al., 2015). The poleward shift of the East Asian westerly jet in the period 1979–2011 and the assumed intensification of the monsoon system under climate change conditions are supposed to cause large areas of the TP to become wetter (Gao et al., 2014). Yao et al. (2012b) describe a recent weakening of the Indian summer monsoon. The glaciers and lakes on the TP have been used as proxies for past changes in the climatic conditions and for monitoring ongoing changes, e.g. ice and lake sediment cores, lake level changes, glacier retreat. Lake expansion in the central TP has intensified during the last few decades, due to global warming and its effects on the hydrological cycle of the TP (e.g. enhanced run-off from glaciers, permafrost degradation (Liu et al., 2010)). These changes in the hydrological cycle due to climate change will probably impact the water availability in large parts of South and Southeast Asia and could jeopardise the water security of billions of people.

Interestingly not all glaciers on the TP show the same mass balance changes. While most of the glaciers on the TP and in the Himalayas are shrinking, glaciers in the Kunlun Shan and

Karakoram mountain rages in the north-western part of High Asia show stable mass balances with some of them even gaining mass in recent years. This is known as the "Karakoram anomaly" (Hewitt, 2005). By analysing ice cores, Thompson et al. (2006) found evidence suggesting that the different growth rates of glaciers in different regions of the TP are not only controlled by temperature but also precipitation variability.

Many studies on atmospheric water transport (AWT) in and to the TP focus on the question of how the Indian and East Asian summer monsoon systems affect precipitation on the Tibetan Plateau, and how changes of the monsoonal circulation impact local and regional water resources (Gao et al., 2014; Immerzeel et al., 2013; Simmonds et al., 1999). The origin of the atmospheric moisture over the TP plays a key role in recent research (Chen et al., 2012; Feng and Zhou, 2012). There are three sources of moisture over the TP: the Asian monsoon systems, the mid-latitude westerlies, and local moisture recycling. The general assumption is that the main moisture source for summer precipitation in the TP is the Indian summer monsoon. The surrounding high mountain ranges, Himalayas, Karakoram, Pamir, Kunlun Shan, act as a barrier for atmospheric moisture transport. Pathways for the moisture originating in the Arabian Sea, the Bay of Bengal and the westerlies are high mountain valleys in the southern and western border of the TP, e.g. the Brahmaputra Channel in the easternmost part of the Himalayas and the meridionally orientated valleys in the central and western parts. How much moisture is transported through these channels and how much moisture the mountain ranges block highly depends on the representation of the underlying orography and therefore on the horizontal resolution of the used datasets. You et al. (2012) showed that the reliability of precipitation data from global atmospheric datasets, e.g. reanalyses, is low over the TP region, due to the unrealistic representation of the complex topography.

Shi et al. (2008) found that the representation of the meso-scale orography of the TP is important to realistically model disturbances which can impact the precipitation downstream of the TP. The weather systems originating over the TP can move off the TP and trigger extreme precipitation and severe flooding in heavily populated regions like the Sichuan basin and the Yangtze River valley (Feng et al., 2014; Tao and Ding, 1981). Moisture transport on and to the TP is influenced by mesoscale features (Sugimoto et al., 2008) and moisture transport to the TP from the south was found to be important for the development of convective clouds (Yasunari et al., 2006). The strong convection on the TP in summer facilitates transport of water vapour from the troposphere to the lower stratosphere (Tian et al., 2011).

One method to identify the sources of moisture is to analyse the isotopic composition of (i) precipitation, e.g. observed and modelled stable oxygen isotope ratios (δ^{18}O) and

hydrogen isotope values (δD) (Araguás-Araguás et al., 1998; Tian et al., 2007; Yao et al., 2013) and the isotopic composition of (ii) the water in rivers and smaller water streams (Hren et al., 2009) and of (iii) climate proxies such as ice and sediment cores (An et al., 2012; Guenther et al., 2013; Günther et al., 2011; Joswiak et al., 2013; Kang et al., 2007). During phase transitions like evaporation and condensation the isotopic composition of water, i.e. the ratio between heavy and light isotopes, changes (Dansgaard, 1964). Heavy isotopes become enriched in the liquid phase while lighter isotopes are more likely to occur in the vapour phase. This process, called fractionation of stable water isotopes, leads to unique isotopic compositions for different waters, which can indicate their source or the process that formed them.

Climate proxies can be used to analyse the moisture conditions on the plateau and its source regions in the past. An et al. (2012) analysed a sediment core from Lake Qinghai in the north-east of the TP that reaches back 32 ka. They focused on the interplay of the westerlies and the Asian monsoon and showed that there is an anti-phase relationship with periods of dominant westerlies and periods with dominant Asian monsoon. Higher monsoon activity during the current warming period is found by studying variations in the monsoon intensity in the TP during the last 1000 years using data from sediment and ice cores (Günther et al., 2011). A shift in the isotope signals implies that the contribution of westerly moisture to the ice-core accumulation was relatively greater before the 1940s (Joswiak et al., 2013).

For the present-day conditions, various studies produce different results. Both the southern Indian Ocean (Indian summer monsoon) (Yao et al., 2013) and the Pacific Ocean (East Asian Monsoon) (Araguás-Araguás et al., 1998) are identified as the dominant moisture sources for summer precipitation on the TP. The analysis of stable isotopes of precipitation samples in western China show that the southern TP receives monsoon moisture in summer and westerly moisture in winter (Tian et al., 2007). Hren et al. (2009), who sampled 191 stream waters across the TP and the Himalaya, found that the moisture entering the south-eastern TP through the Brahmaputra Channel originates in the Bay of Bengal. This monsoonal moisture is mixed with central Asian air masses the farther west and north in the TP the sampling site is located. The role of local moisture recycling as an additional moisture source is also emphasised in many studies (Chen et al., 2012; Joswiak et al., 2013; Kurita and Yamada, 2008; Tian et al., 2001; Trenberth, 1999) but its importance varies in space and time and is difficult to quantify.

Another method to investigate the moisture transport in the TP is gridded atmospheric datasets, for example global reanalysis data, regional atmospheric models and remote sensing data. Chen et al. (2012) used backward and forward trajectories to identify the sources and sinks of moisture for the TP in summer. Their results show that for periods longer than 4

days backwards, the main moisture source is the Arabian Sea, while for shorter periods, the Bay of Bengal, the Arabian Sea and the north-western part of the TP contribute moisture in the same order of magnitude. Feng and Zhou (2012) found that the main WV transport for summer precipitation takes place through the southern border of the TP and originates in the Bay of Bengal and the Indian Ocean. They also point out that the southern branch of the mid-latitude westerlies transports moisture to the TP too, but its share is distinctly lower. (Lu et al., 2015) analysed the atmospheric conditions and pathways of moisture to the TP for a wet and dry monsoon season and showed that differences in the atmospheric circulation have a direct impact on the moisture transport both to and on the TP. Meridionally orientated high mountain valleys in the Himalayas can channel water vapour and precipitation to the TP (Bookhagen and Burbank, 2010). Therefore, the representation of the underlying orography plays a key role in simulating moisture transport. Coarser resolutions tend to allow more moisture transport over the Himalayas because of a lower altitude, but on the other hand do not represent the high mountain valleys. Therefore, different studies can lead to very different result simply by choosing different regions, boundaries and datasets.

There are many studies that have explored the influence of atmospheric circulation modes, e.g. the North Atlantic Oscillation, the Arctic Oscillation, and El Niño–Southern Oscillation, on the climate and precipitation in high Asia and on the monsoon systems (Bothe et al., 2010, 2011; Liu et al., 2016; Liu and Yin, 2001; Rüthrich, 2015). Liu and Yin (2001) found that the interannual variability of precipitation on the eastern TP is closely related to the NAO and the resulting intensification or weakening of the westerly winds upstream of the TP in the Euro-Atlantic sector. The different NAO phases show opposite effects on the south- and north-eastern TP, demonstrating the combined impact of large orography and atmospheric circulation on regional climate variability. The subtropical westerly jet acts as wave guide facilitating the propagation of upstream signals to the TP region (Hoskins and Ambrizzi, 1993) and thereby connecting Asia with the Euro-Atlantic sector. Wu et al. (2012) found that the snow cover on the Tibetan Plateau modulates the teleconnection of ENSO with the East Asian Summer Monsoon (EASM). ENSO only correlates significantly with EASM in years with reduced snow cover in the TP region due to a Rossby wave response to the ENSO forcing.

Less attention has been paid to the underlying processes controlling the precipitation variability over the TP and the surrounding high mountain ranges. Since precipitation is a key feature of the water cycle of high Asia, it is important to analyse the factors controlling precipitation variability. Identifying which dynamic factors influence the precipitation may also help to estimate the impact of future climate change on precipitation variability. A number of open questions remain, for example: What is the impact of atmospherics dynamics

on the temporal and spatial distribution of atmospheric moisture, cloud development and precipitation? How large is the impact of processes in the boundary layer and in the upper troposphere on hydro-climatic conditions on the Tibetan Plateau and surrounding high mountain ranges? To which extent does the variability of atmospheric water fluxes explain the variability in precipitation over the TP? What role do dynamic enhancement and weakening of deep convection processes due to subsidence or wind shear, independent of the atmospheric moisture content, play for the precipitation dynamics?

Recently, a new high-resolution dataset, the High Asia Refined analysis (HAR; Paper I) was developed to overcome the shortcoming of scarce data availability for High Asia. The HAR is the result of the dynamical downscaling of an operational analysis and provides the opportunity for a process-based analysis of the precipitation and its variability (e.g. enhancement and suppression), due to its high spatial (30 and 10 km) and temporal (3 and 1 h) resolution. The higher spatial resolution also helps to represent the underlying orography in a more realistic way which has a big influence on the moisture transport to the TP and the precipitation variability.

1.2 Objectives

The aim of this thesis is to examine and understand factors important for spatial and temporal patterns of precipitation over the TP and its variability. Therefore, the spatial and temporal variability of atmospheric moisture transport on and to the TP and atmospheric variables affecting precipitation variability are analysed, to answer the following questions:

- Where does the moisture needed for precipitation come from?
- Which are the main moisture pathways to the TP and which role does the spatial resolution and representation of topography play?
- What controls precipitation enhancement or suppression if sufficient atmospheric moisture is available?
- Which dynamic factors control precipitation variability on the Tibetan Plateau?
- Do the different factors affecting precipitation variability act in the same way in different regions and at different times?
- How and when do the mid-latitude westerlies influence the precipitation on the TP?

The research covered in this thesis was conducted in the project 'Variability and trends in benchmark drainage basins on the Tibetan Plateau' (WET, https://www.klima.tu-berlin.de/forschung/WET/home.php) as part of the research program 'Central Asia and Tibet: Monsoon dynamics and geo-ecosystems' (CAME) funded by the Bundesministerim für Bildung und Forschung (BMBF, Federal Ministry of Education and Research).

The first objective of this thesis is to describe the characteristics of atmospheric water transport (AWT) over and to the TP as resolved by the HAR dataset. We focus on AWT spatial patterns, seasonal evolution and vertical distribution and examine the barrier effect of the topography on AWT and detect the major transport channels to the TP and quantify the importance of moisture recycling.

The second objective is to examine which dynamical factors control variability of precipitation on the TP. By analysing the spatial and temporal correlation of selected dynamical variables and precipitation we are able to to reveal the underlying mechanisms through which the variables influence precipitation variability through enhancement and/or suppression of precipitation development.

The third objective is to gain a better understanding of the roles the mid-latitude westerlies and the summer monsoon systems play in the context of the first and second objectives. We therefore assess the impact of the mid-latitude westerlies on the precipitation on the TP regarding their role in providing moisture and dynamically controlling precipitation variability.

1.3 Structure of the thesis

This thesis is based on three peer-reviewed papers.

- Paper I: Maussion, F., Scherer, D., Mölg, T., Collier, E., Curio, J. and Finkelnburg, R. (2014) Precipitation seasonality and variability over the Tibetan plateau as resolved by the High Asia reanalysis. Journal of Climate, 27 (5), 1910-1927.

- Paper II: Curio, J., Maussion, F. and Scherer, D. (2015) A 12-year high-resolution climatology of atmospheric water transport over the Tibetan plateau. Earth System Dynamics, 6 (1), 109-124.

- Paper III: Curio, J. and Scherer, D. (2016) Seasonality and spatial variability of dynamic precipitation controls on the Tibetan Plateau. Earth System Dynamics, 7 (3), 767-782.

We focus on the research conducted in Paper II (Curio et al., 2015) and Paper III (Curio and Scherer, 2016), but refer to findings from Paper I (Maussion et al., 2014) and unpublished

material to support the results. This thesis started during the development of the HAR and without the HAR (Paper I) it would not have been possible to study the moisture transport and dynamic precipitation controls over the Tibetan Plateau in such detail.

This thesis is structured as follows. Chapter 1 gives a general introduction to the study region and background for the research questions and objectives covered in this thesis. Chapter 2 provides a summary of the data and methods used to address the research questions identified in Chapter 1. The main results are provided and discussed in Chapter 3 and Chapter 4. The atmospheric water transport is analysed in Chapter 3, while Chapter 4 focuses on dynamic precipitation controls. In Chapter 5 we draw conclusions and identify future research opportunities. The thesis is followed by the three peer-reviewed research papers reprinted in their original form.

2. Data and Methodolody

Section 2.1 introduces the High Asia Refined Analysis and how it was generated. The computation of the of atmospheric water transport and the methods used to analyse its spatial and temporal variability are described in section 2.2. Section 2.3 explains how the HAR data were used to analyse the atmospheric variables acting as dynamic precipitation controls.

2.1 High Asia Refined analysis

The High Asia Refined analysis (HAR, Maussion et al. (2014)) is the result of dynamical downscaling the Operational Model Global Tropospheric Analyses (final analyses, FNL; dataset ds083.2), a gridded dataset where observations are assimilated by a global model. The FNL data are available every 6 h and have a spatial resolution of 1°. The model used to downscale these data is the advanced research version of the Weather and Research Forecasting model (WRF-ARW, Skamarock and Klemp, 2008) version 3.3.1.). For the generation of the HAR a daily re-initialization strategy was used, which makes sure that the model does not evolve too far away from the observations. A dataset created by combining the output of multiple shorter model runs in one dataset has been proven to produce more realistic atmospheric fields than continuous long-term integrations (Lo et al. 2008).

The first domain of the HAR covers most parts of south–central Asia with a spatial resolution of 30 km and temporal resolution of 3 h. High Asia and the Tibetan Plateau are the focus of a second nested domain with a spatial resolution of 10 km and temporal resolution of 1 h. In the following we will use the terms HAR30 and HAR10 when referring to the HAR datasets with 30km and 10 km horizontal resolution, respectively. A map of both domains including the location of the HAR10 domain in the parent domain HAR30 are shown in Fig 2.1.

The HAR provides meteorological fields at the surface and on 28 terrain following vertical sigma levels. The dataset covers a period of more than 14 years from October 2000 to December 2014 and is updated continuously. Different time periods were used in the different papers due to the data available at the time of the studies. The examination of the atmospheric

water transport is done for the period 2001-2012 (Paper II, Curio et al. (2015)), while the precipitation controls are analysed for the period 2001-2013 (Paper III, Curio and Scherer (2016)). HAR products are available for different time aggregation levels: hourly (original temporal model resolution), daily, monthly and yearly. One important objective of generating the HAR was to make it freely available. A website (http://www.klima.tu-berlin.de/HAR) was set up where HAR data can be downloaded after registering.

A detailed description of the HAR can be found in Paper I (Maussion et al., 2014) for the period 2001–2011. The validation of HAR monthly precipitation data against rain gauge observation and precipitation estimates from the Tropical Rainfall Measuring Mission (TRMM) can be found in Paper I and in Maussion et al. (2011) for a single event.

In this thesis, we analyse the processes on the TP and the surrounding high mountain ranges and therefore mainly use the HAR10 dataset, which provides a higher spatial and temporal resolution. we only refer to HAR30 data if a large-scale point of view is needed for the interpretation of the HAR10 results.

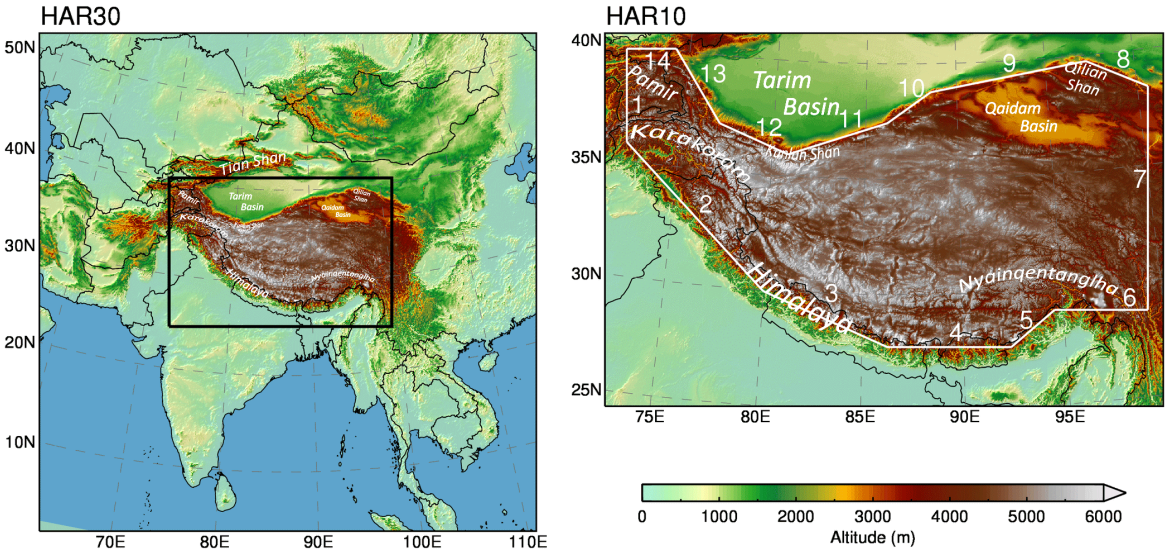

Fig. 2.1 Maps of the Weather and Research Forecasting (WRF) model domains HAR30 (south-central Asia domain, 30 km resolution) and HAR10 (high Asia domain, 10 km resolution). The transects surrounding the Tibetan Plateau (numbered 1-14) are drawn in white. The region within the defined boundaries is called "inner TP" throughout the manuscript. Geographical locations are indicated. Figure taken from Paper II (Curio et al., 2015), modified after Paper I (Maussion et al., 2014).

2.2 Atmospheric water transport

Atmospheric water transport happens through water vapour (WV) and cloud particle (CP) transport. For the CP transport we do not further distinguish between liquid (water droplets) and solid (ice) cloud particles which are both resolved by the model microphysics. WV and CP fluxes are calculated for each of the 28 original sigma levels, which are terrain following, based on the original temporal model resolution of 1 h (HAR10) and 3 h (HAR30) using the formula

$$Q = v_h \rho q \Delta z \tag{2.1}$$

where Q is the water vapour flux ($\mathrm{kg\,m^{-1}\,s^{-1}}$) or cloud particle flux, v_h denotes the horizontal wind vector ($\mathrm{m\,s^{-1}}$), ρ is the dry air density ($\mathrm{kg\,m^{-3}}$) and q is the specific humidity($\mathrm{kg\,kg^{-1}}$). Δz is the thickness of each sigma level (m), this value is not constant but increases with increasing height above ground. Since the WRF model just provides mixing ratios (r) for the three atmospheric water components (water vapour, liquid water and ice), we first calculated the specific humidity for each component using the relationship

$$q = \frac{r}{(1+r)} \tag{2.2}$$

Additionally, we integrated the fluxes over the entire atmospheric column to obtain the vertically integrated atmospheric water transport fluxes. The vertical integration is performed along the metric z coordinate along the model sigma levels from surface to top using the rectangle method.

$$Q = \int_{z=z_{sfc}}^{z=z_{top}} v_h \rho q \Delta z \tag{2.3}$$

We calculated these fluxes for the original model levels and did not interpolate them to pressure levels to avoid information loss due to the interpolation. For the analyses, 10 and 5 grid points from the HAR30 and HAR10 domain boundaries, respectively, are removed to avoid lateral boundary effects. To analyse the AWT towards the TP, we compute vertical cross sections along transects following the border of the TP. To be able to calculate a moisture budget, we defined a region which we henceforth call “the inner TP”, with 14 transects attempting to follow the highest elevations in the mountain ranges and to cut across the high mountain valleys which we assume to be pathways for atmospheric moisture. The location of transects is included in Fig. 2.1. The u and v components of AWT are then rotated to the transect coordinate system to compute the normal fluxes towards the cross section.

2.3 Precipitation controls

The selection of precipitation controls relies on well-studied relationships of these factors with precipitation variability (e.g. Back and Bretherton, 2005; Garreaud, 2007; Shinker et al., 2006). So far, these controls were not investigated at high spatial and temporal resolution in high-mountain Asia. The analysis of dynamic precipitation controls in paper III is based on the HAR10 dataset for the study period 2001–2013 (all entire years available at that time). Starting point is an analysis of the precipitation seasonality on the TP using the k-means clustering method (e.g. Wilks, 1995). This analysis follows the approach used in Paper I to detect glacier accumulation regimes based on precipitation seasonality on the TP. For the analysis of dynamic precipitation controls the clustering was extended to the entire TP and surrounding areas, using all grid points of the HAR10 domain.

The percentages of monthly contribution to annual precipitation and not the precipitation amounts were used to define seven classes with different precipitation seasonality. This has the advantage that, in an area like high Asia where the differences in precipitation amounts vary strongly between regions and seasons, the regions were made comparable by this method. We conducted the cluster analysis with other numbers of classes (5–9; see supplementary to Paper III), but the chosen number of seven classes led to the best ratio between coherent patterns and sufficient distinction between classes.

For all further analysis daily averaged HAR data are used. Because we are only interested in precipitation days, the dataset is stratified using a daily precipitation threshold. This is done month-wise. For example, all analyses for July depend on the data for each July day during the period 2001–2013; these are 31 x 13 days, i.e. 403 days in total. Precipitation days for a grid point are defined as days with a mean daily precipitation rate of at least 0.1 mm, which is a commonly used minimum value to define precipitation days (e.g. Polade et al., 2014; Liu et al., 2011; Bartholy and Pongracz, 2010; Frei et al., 1998). The threshold was used to filter out numerical artefacts and not to exclude events from the database.

The daily precipitation rate at each grid point is calculated as the mean precipitation rate for all grid points within an area of 15 x 15 grid points around the grid point. The time mask for precipitation days is then applied to the four variables used as precipitation controls. The number of precipitation days can vary distinctly between regions and seasons.

In order to analyse the relationship between dynamic controls and precipitation each of the dynamical variables is correlated with the precipitation using the Spearman rank correlation. This is done month-wise for all precipitation days in a specific month during the study period and for each grid point in the HAR10 dataset. Using correlations avoids problems associated with the exact precipitation rates and amounts falling on the TP, which

are hard to measure and to model exactly. The Spearman rank correlation uses the ranks of the values and not the values itself, which makes the correlations independent of the real data and more robust against outliers. This makes it easier to compare regions with very different precipitation amounts with each other and helps to reduce the effects of extreme events on the correlation results. We are aware of the fact that ranking the data leads to a slight information loss compared to the real values. We are sure that for our purpose the advantages are bigger than the disadvantages. Only correlations, which are significant at the 95% level, are plotted.

3. Atmospheric water transport

This chapter describes the spatial and temporal patterns of atmospheric water transport (AWT) to and on the Tibetan Plateau and surrounding high mountain ranges using a 12-year climatology of AWT derived from/based on the HAR. Section 3.1 focuses on the annual cycle of water vapour transport to detect the mean patterns and transport channels, while Section 3.2 examines the vertical structure of the atmospheric water transport for selected levels. The transport through the boundaries of the TP is analysed in Section 3.3 to quantify atmospheric water input and verify the importance of the detected transport channels. In Section 3.4 we calculate a moisture budget for the TP in order to analyse/determine the importance of moisture recycling.

3.1 Annual cycle

To get started answering the question where the moisture for precipitation on the TP is coming from we first examined the climatology of the annual cycle and spatial patterns of the water vapour transport over and to the TP. Fig 3.1 shows the temporal and spatial distribution of the water vapor transport over and to the Tibetan Plateau. In winter the westerlies are dominant over the entire domain and result in transport from west to east. The highest WV transport over the TP occurs where the westerlies encounter the mountain barrier at the western border of the TP. Most of the WV is then transported along the northern and southern borders to the TP. The highest values in the domain occur south of the Himalayas where the WV is transported eastward along the southern slopes of the Himalayas and into the TP in the southeastern corner of the TP, where the Brahmaputra channel is located. Where the flow starts to converge again in the eastern part of the domain where the orographic barrier is lower in the northern (Qaidam Basin) and south-east TP (Brahmaputra channel) the WV transport is higher then on the central TP. Some WV is still transported to the TP directly through the western boundary. The prevailing wind direction leads to transport from west to east on the TP, but the transport amount is low directly over the TP. Most of the WV transported to the western border is redirected or rained out over the Karakoram / Pamir

region. This region exhibits a winter spring precipitation regime (Fig. 3.2, Fig. 8 and 9 in Paper I).

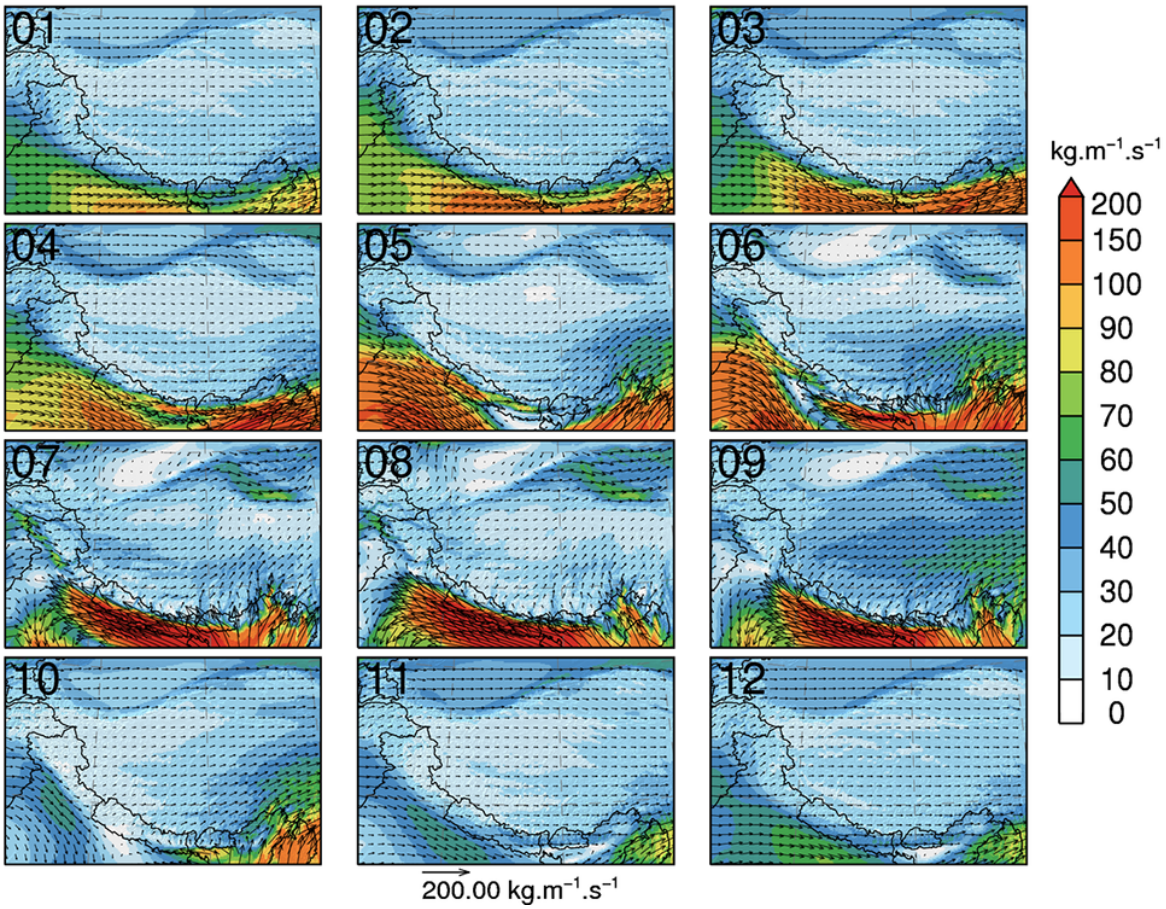

Fig. 3.1 Decadal average of the vertically integrated water vapour flux ($\mathrm{kg\,m^{-1}\,s^{-1}}$) in every month for HAR10. Colour shading denotes strength of water vapour flux, arrows (plotted every eighth grid point) indicate transport direction (length of arrows is proportional to flux strength up to 200 $\mathrm{kg\,m^{-1}\,s^{-1}}$ and is constant afterwards for more readability).Figure taken from Paper II.

An intensification of the WV transport occurs from May to July, with the beginning of the change in circulation prior to the monsoon onset. In summer the Subtropical westerly jet shifts to a position north of the TP (Schiemann et al., 2009) and the monsoon circulation establishes. In the southeast corner of the domain the WV flow starts to encounter the barrier from the south, resulting in higher WV transport north of the Himalayas. This transport is then redirected eastwards on the TP. This WV transport intensifies with the evolution of the Indian summer monsoon, when large amounts of WV are transported towards the Himalayan foothills from the Bay of Bengal (Fig. 3 in Paper II). The largest share of this WV transport is blocked by the Himalayas which act as an orographic barrier and is the

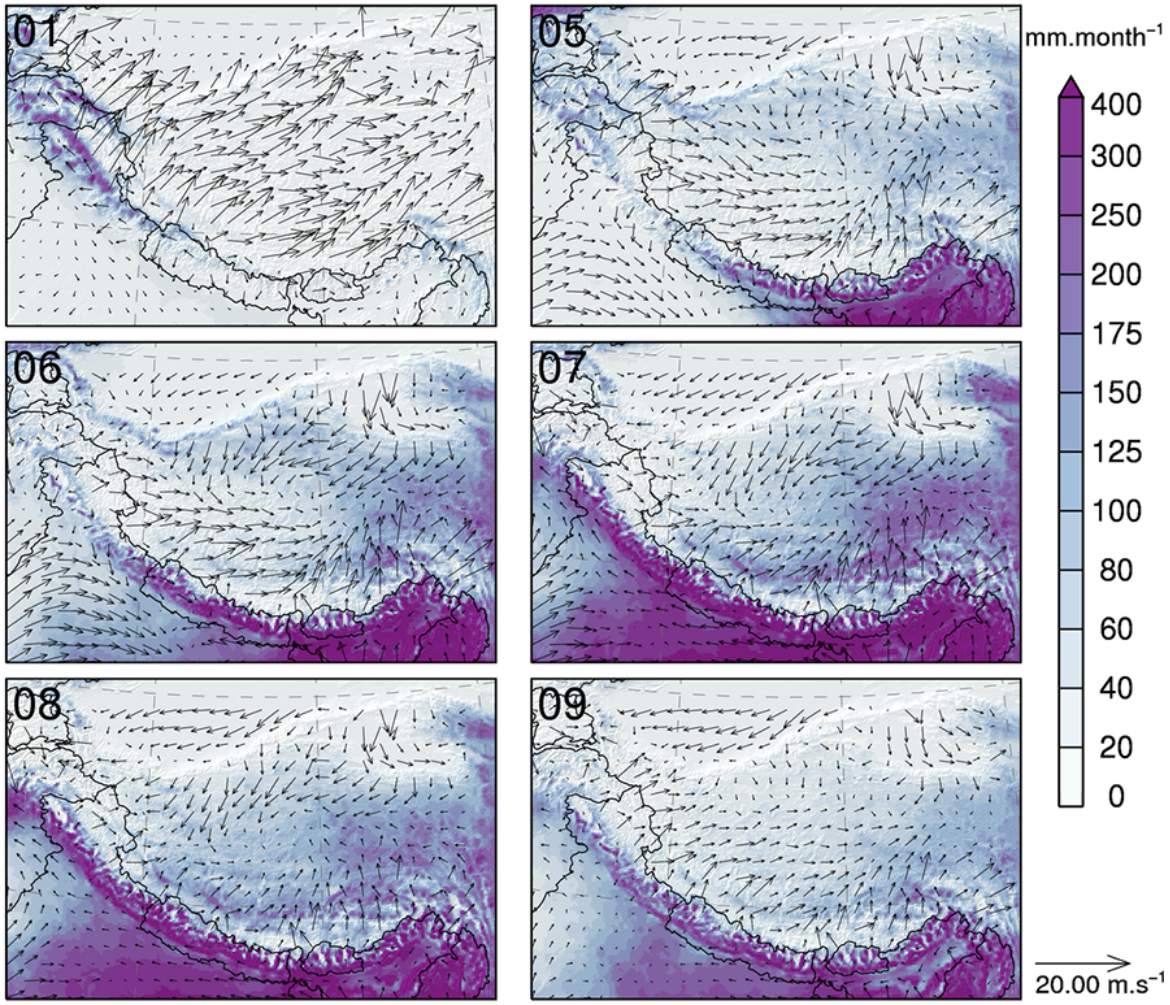

Fig. 3.2 Decadal average of precipitation (mm month^{-1}) in January (01), May (05), June (06), July (07), August (08), and September (09) for HAR10. The arrows show the 10 m wind field (every ninth grid point plotted). Figure taken from Paper II.

redirected westwards along the Himalayan foothills. Transport from south towards the TP is only possible through meridionally orientated high mountain valleys in the Himalayas. The transport towards the TP from the southwest also increases over summer and does not originate from the monsoonal flow but is provided by the southern branch of the mid-latitude westerlies (Fig. 3 in Paper II). Since the transport of moisture on the TP starts furthermore in the west the monsoonal flow reaches westward along the southern foothills of the Himalayas, it appears that this moisture is not provided by the monsoon but by the westerlies and/or the TP itself. The westerlies also contribute moisture to the TP through valleys in the western parts of the southern boundary by the southern branch of the westerlies. This implies that moisture entering the TP from the south-west can be transported there either by the westerlies

or the monsoon, depending on the how far these systems extend eastward or westward along the southern slopes of the Himalayas, respectively.

Interestingly the water vapour transport over the TP shows the highest transport amounts in September. Reason for this is the fact that the precipitation amount is lower in September than in summer (Fig. 3.2). So the moisture evaporating from the wet TP surface, caused by the high precipitation rates in summer, can be transported away from its source region without being rained out. Another reason for higher transport amounts is the wind speed recovery after the withdraw of the monsoon, which is visible in the wind field (Fig. 3.2 and Fig. 9 in Paper I), and facilitates higher evaporation rates and therefore higher transport amounts. In October there is only transport to the TP in the eastern and central parts of the Himalayas, because the monsoon circulation weakens and the fluxes do not reach as far westward into the Ganges valley as before. The flux from the westerlies reaches far more to the east along the southern slopes of the Himalayas. In November, this pattern becomes more intense, there is no westward flux south of the Himalayas visible, the monsoon circulation collapses and wintertime conditions are established.

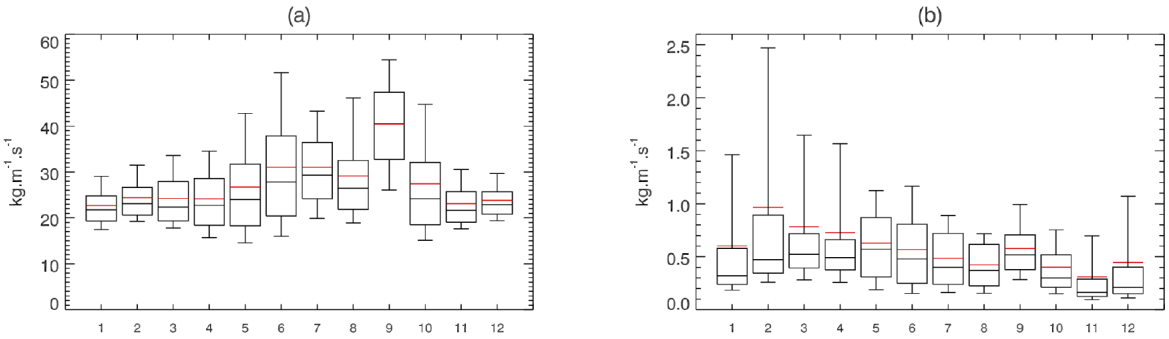

Fig. 3.3 Boxplots of the decadal average of vertically integrated water vapour flux (a) and cloud particle flux (b) on the inner TP for HAR10. The boxes represent the range from the 25th to the 75th percentile. The boxes are divided by the median value (black) and the mean value (red). The whiskers represent the 10th and 90th percentile, respectively. Note the different scales of the y-axes. Figure taken from Paper II.

Previous studies focused on WV transport and did not consider cloud particle (CP) flux. The assumption so far has been that the CP transport is so small compared to WV flux, that it does not have a significant influence on the total AWT. The median value of HAR10 WV transport for the inner TP is between 20 and 40 $\mathrm{kg\,m^{-1}\,s^{-1}}$ throughout the year, while it only reaches between 0.2 and 0.6 $\mathrm{kg\,m^{-1}\,s^{-1}}$ for the CP transport (Fig. 3.3).These values could lead to the assumption that the CP transport is not relevant. Differences in the annual cycle of the two components are clearly visible: the WV transport has its peak in summer and the CP transport in winter. The boxplot also shows that the range between the 10th and

90th percentile for the WV transport is largest in June. The large range might reflect the interannual variability in the timing of the Indian summer monsoon onset.

To examine the relevance of CP transport for AWT, we looked at the transport patterns and amounts and calculated the contribution of the CP flux to AWT as a monthly decadal average in January and in July (Fig. 3.4). Our results show that the contribution of the CP flux to the entire AWT is not negligible in winter in the Pamir and Karakoram (the western and south-western border of the TP) contributing up to 25% of the total AWT. This pattern matches the wintertime precipitation pattern in this region (Fig. 3.2). CP transport also plays a role in the eastern TP, a region where cyclones are frequent in summer.) The fact that the CP transport plays a role in the Karakoram and western Himalayas, the regions which are controlled mainly by the westerlies, suggests a strong role of moisture advection. The horizontal motion is dominant in advective processes while vertical motion is dominant in convection. This means that clouds developed in advective processes, for example frontal processes, can be transported further away from their origin than convective clouds.

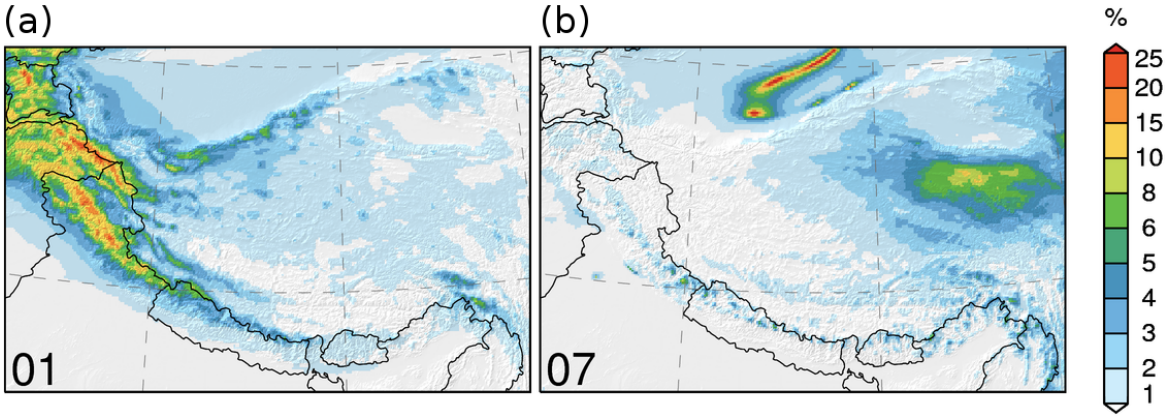

Fig. 3.4 Decadal average of the contribution (%) of cloud particle flux to atmospheric water transport in (a) January and (b) July for HAR10. Figure taken from Paper II.

3.2 Vertical structure and circulation features

Looking at the vertically integrated fluxes only does not reveal the complexity of the AWT over and towards the TP but shows the dominant patterns. To understand the vertical structure of AWT we analysed the transport occurring on different model levels in Paper II. We looked at the transport at all of the 27 model levels and then selected levels from near surface to around 5 km above ground with the most interesting features and the levels where changes compared to the patterns in other levels occur. We selected six levels from near surface to around 5 km above ground: levels 1 (∼25 m), level 5 (∼450 m), level 8 (∼1200 m), level

10 (∼2200 m), level 12 (∼3200 m) and level 15 (∼5500 m). The height of each terrain-following model level is the average height of this model level above ground over the Tibetan Plateau.

The vertical structure of AWT in Fig. 3.5 shows that the transport near the surface is generally low over the TP due to the relatively low wind speed over the TP in summer. Low wind speed leads to a low transport amount even if there is atmospheric moisture evaporated from the surface, since AWT is a product of both moisture availability and wind speed and direction. Another influencing factor could be the higher turbulent mixing in the boundary layer due to thermal eddies and turbulent eddies generated by the air flow being disturbed by the friction from the surface. (explain how more mixing and eddies influence the AWT)

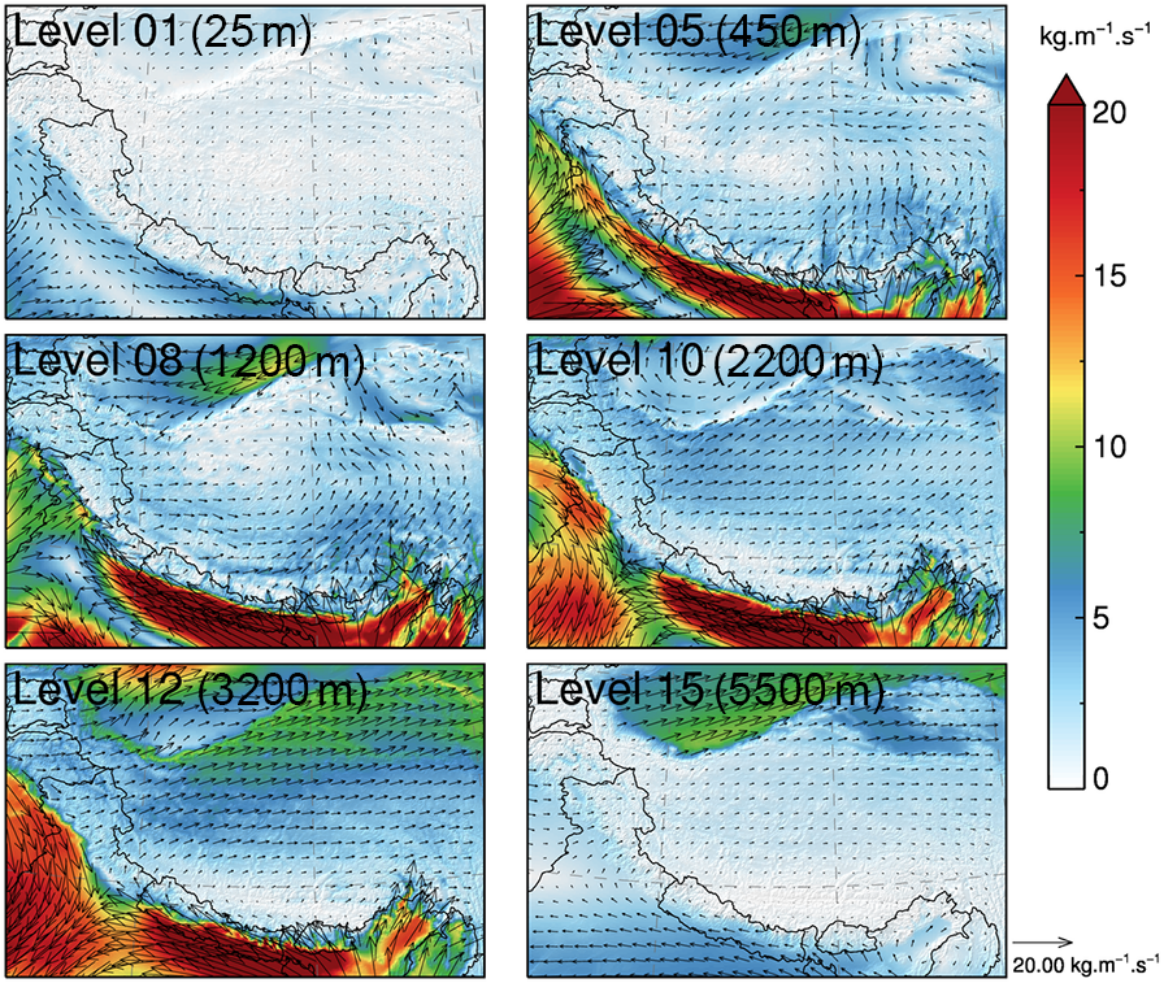

Fig. 3.5 Decadal average of the water vapour flux ($\mathrm{kg\,m^{-1}\,s^{-1}}$) for single selected model levels (1 (25 m above ground in Tibet), 5 (450 m above ground in Tibet), 8 (1200 m above ground in Tibet), 10 (2200 m above ground in Tibet), 12 (3200 m above ground in Tibet) and 15 (5500 m above ground in Tibet)) in July for HAR10. Figure taken from Paper II.

Therefore, the moisture transport first increases with height up to level 12 where the highest transport amount occurs. The higher wind speed at higher levels presumably together with larger moisture availability in the atmosphere leads to higher transport rates. It appears that the higher moisture availability occurs because more moisture can reach the higher levels of the atmosphere than the surface. The moisture laden air from the south has to cross the orographic barrier and this is only possible over the top of the mountain ranges or through high mountain valleys. The atmospheric moisture available near the surface appears to originate from local sources (e.g. evaporation form lakes, permafrost, glacier runoff). Not only the amount of transported atmospheric water is important but also where it is coming from. The AWT pattern at the different levels show the general atmospheric circulation, but one has to keep in mind that the AWT is influenced by wind and moisture availability. The Tibetan heat low with its centre at the central TP is visible at the lower levels (1 and 5) and at level 8 but shifted to the northern TP. A completely different picture is revealed by the upper levels (12 and 15) where the high-tropospheric Tibetan anticyclone with its centre in the southern TP directly north of the Himalayas is visible. This is one of the atmospheric features known since the early years of research about the TP and was first reported in the western literature by Flohn in 1968, who stated that it starts to form in May or early June. Higher up in the atmosphere the anticyclonic circulation weakens and the westerlies become dominant over the TP. The level between the cyclonic circulation at the lower levels and the anticyclonic circulation at the upper levels could be called equilibrium level (level 10).

At level 5, monsoonal air and moisture is transported relatively far to the western (north-western) part of the TP. This air mass originating in the tropical oceans and transported to the TP by the Indian summer monsoon circulation is then included in the cyclonic circulation over the TP. In the higher levels (10–15), this cyclonic circulation is replaced by the westerlies and extra-tropical air masses are transported to this region. Therefore, we find air masses and consequently moisture from different sources at one place. This finding should be considered in the analysis of stable oxygen isotopes in precipitation samples, lake water, sediment and ice cores. In those regions precipitation originating in the boundary layer will result in a monsoonal signal in the isotopes while precipitation originating from deep convection could have an isotope signature pointing to the westerlies as the main moisture source.

In the dry Tarim Basin north of the TP, we can see an anticyclonic circulation above the boundary layer at level 10 and transport of WV from north-east to south-west following the northern boundary of the TP. Therefore, the air at this level tends to descend. This means that only below this level clouds in the boundary layer are possible. These clouds can only provide small amounts of precipitation due to their low vertical extent. Above this level, the transport of WV is admittedly higher and in the opposite direction, but does not result in

precipitation. Deep convection is inhibited by the subsidence tendency at the lower level. The higher transport rate is also an indication for higher wind speeds in the upper levels, related to the southern edge of the subtropical westerly jet.

In the south-western part of the domain, the border region between India and Pakistan, we see a similar pattern. There it leads to higher differences in the precipitation patterns between the affected region and the direct surroundings (Fig. 3.2) and affects a region with a high population density. We see an anticyclonic circulation of the WV transport in the levels 10 and 12 (and in between). The transported amount is nearly as high as the WV transport associated with the ISM along the southern slopes of the Himalayas. However, if we look at the precipitation patterns, we see that there is a precipitation minimum in this region (Fig. 3.2). The development of deep convection is suppressed by subsidence. In the lower levels, the heat low over Pakistan (Bollasina and Nigam, 2010) is visible in the transport patterns (Fig. 3.5) and in the 10 m wind field (Fig. 3.2). Saeed et al. (2010) point out that the heat low over Pakistan connects the mid-latitude wave train with the Indian summer monsoon. In the surrounding region where we do not see this anticyclonic circulation in the levels above the boundary layer, the large amounts of transported WV result in high amounts of precipitation.

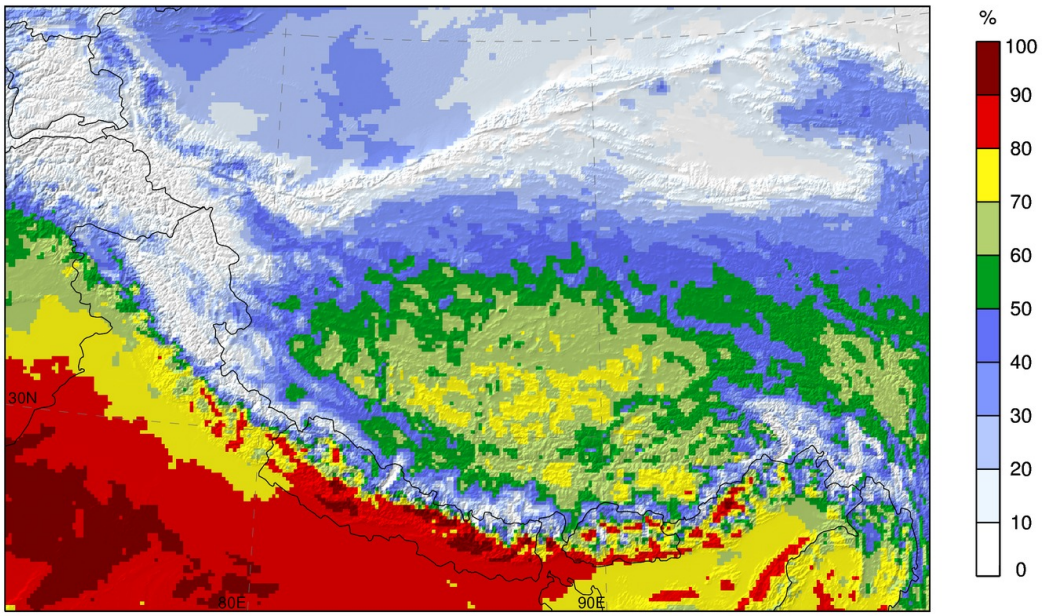

Fig. 3.6 Contribution (%) of convective precipitation to the total annual precipitation for HAR10. Figure taken from Paper I.

In Paper I the border region between India and Pakistan was identified as one of the regions with higher precipitation variability by analysing the occurrence of strong precipitation events

(less than 15% of the precipitation days suffice to reach 50% of the annual precipitation amount) and regional anomalies of the annual coefficient of variation, which is defined as the ratio between the standard deviation and the mean precipitation (Fig. 12, Paper I). Due to its location in the confluence zone between the westerlies and the Indian monsoon flow the region appears to be more sensitive to shifts in the atmospheric circulation than the neighbouring regions. The potential for strong precipitation events is given (e.g. strong solar forcing and high atmospheric moisture content) but the mean atmospheric circulation might inhibit the development of deep convection. In this region, where 90-100% of the precipitation are of convective nature (Fig. 3.6), a slight shift in the atmospheric circulation could make the difference between a dry and a wet summer. These results can provide an indication of the processes, which lead to the risk of droughts and floods in Pakistan, e.g. the severe floods in July 2010 (Galarneau et al., 2012; Houze, 2012; Webster et al., 2011).

3.3 Transport through the TP borders

From the analysis of atmospheric moisture transport so far we got a qualitative picture of how much of the moisture is transported to the TP by the Indian monsoon system and the mid-latitude westerlies. In a next step we calculated the atmospheric water transport through vertical cross sections along the border of the TP in order to quantitatively analyse the in- and output of moisture to and from the TP. The area surrounded by the transects is called "the inner TP" in the following (Fig. 2.1). We decided to do this and not only to look at the most interesting regions, where the majority of the transport takes place (Fig. 3.1) to be able to calculate the moisture budget for the inner TP (Sec. 3.4). The cross sections allow us to examine the moisture pathways and their connection to the underlying topography in more detail than looking at the horizontal patterns alone. This analysis also completes the picture at which heights the moisture is transported to the TP.

Figure 3.7 shows the transport through all cross sections for winter and summer. The separate cross sections were divided into two groups, southern and northern boundary, and then combined to single plots, respectively. This makes it easier to analyse the transport through the borders, especially the Himalayas as one system. As expected the southern boundary exhibits the highest transport amounts in summer in the lower levels of the atmosphere (Fig. 3.7 a). The transport rate decreases with height and the largest amounts are transported towards the TP where the elevation is lower compared to the direct surroundings. These regions are the meridionally orientated high mountain valleys which become only visible when looking at high resolution datasets as HAR10 (Fig. 3.8).

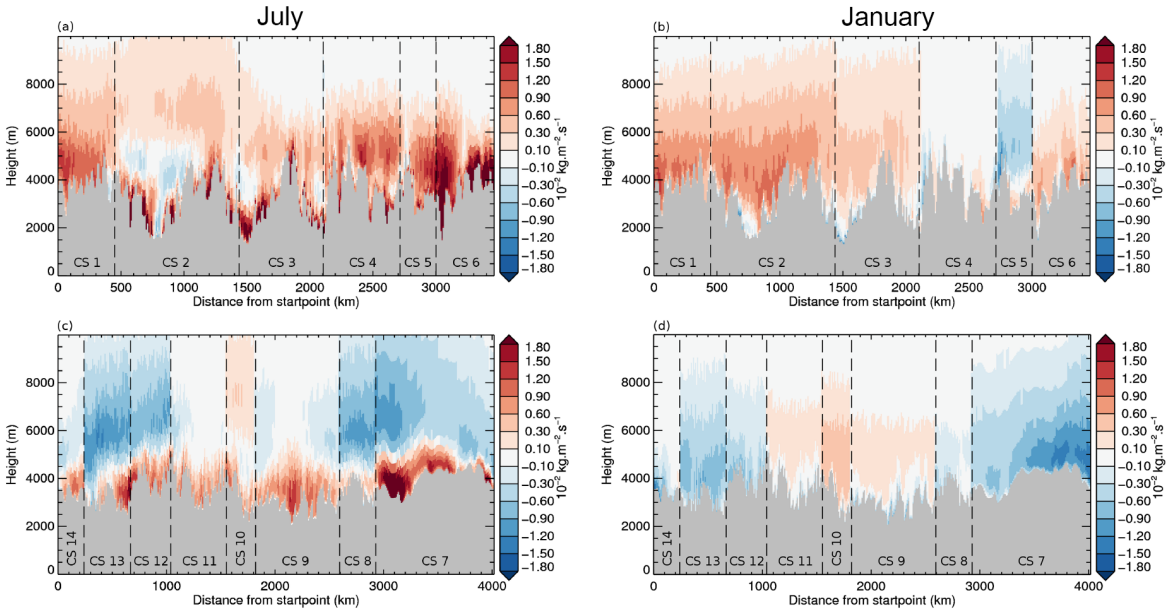

Fig. 3.7 Decadal average of the atmospheric water transport through cross sections 1–6 (a and b) (from left to right, dashed lines indicate border between the cross sections) in July (a) and January (b), and for cross sections 14–7 (c & d) in July (c) and January (d) for HAR10. Red colours denote transport towards the TP, while blue colours indicate transport away from the TP. The underlying topography is represented in grey. Figure taken from Paper II.

One of these valleys is the Brahmaputra channel in the eastern Himalayas (CS 6) which is one of the major moisture pathways to the TP. The Brahmaputra channel is wider than the other valleys and the AWT as part of the monsoonal flow encounters this part of the Himalayas directly from the south. The moisture transported to the TP through this channel arrives further north in the TP than moisture entering the TP in the central Himalayas, in the lower levels the moisture is then transported to the northern central TP with the cyclonic circulation around the thermal low and to the east with the prevailing westerlies in the upper levels. This in combination with the cross section for the eastern boundary (CS 7) shows that the TP gets moisture supply from the outside in the lower levels but provides moisture to the downstream areas in the upper levels. This is also true for the north eastern and northwestern boundaries in summer, but there, averaged over the atmospheric column, the transport away from the TP is dominant.

The AWT through the western boundary (CS 1) (Fig. 9a and b, and Table 1) is higher in winter than in summer, as it is for CS 2 in the westernmost region of the Himalayas. These regions are dominated by atmospheric water input by extra-tropical air masses, transported to this region by the westerlies. In sum, the AWT in CS 2 is still almost as high as the AWT

in CS 6. CS 6 contains the Brahmaputra Channel, which is often referred to as one of the main input channels for atmospheric moisture (Tian et al., 2001).

AWT from the TP to the south is negligible in summer and occurs only in CS2 and CS3 (Fig. 3.7a) as a recirculation in a level above the moisture input to the TP from the south. Since the air masses have to rise to overcome the orographic barrier a smaller share of this moisture might be then transported further up and then back to the south instead of further into the TP. The AWT patterns do not show any transport from north to south for the selected levels (Fig. 3.5), so it appears to be a local recirculation of moist air.

Table 3.1 shows the monthly decadal average of AWT input to the TP through the individual cross sections converted to a theoretical equivalent precipitation amount on the inner TP. We picked CS 1, the western boundary, and CS 6, including the Brahmaputra Channel, for a closer comparison (they are of the same length). From November to April the transport through the western boundary (CS 1) is distinctly higher than that through CS 6. From May to October CS 6 shows higher transport amounts, but the differences are smaller than in winter. In July the input through the western boundary (CS 1) is around 90% of the transport through the Brahmaputra Channel region that (CS 6). This is the month where the differences are smallest.

We can see that for almost every month, CS 2–3 exhibits the largest input amounts. AWT through this cross section is controlled not only by the ISM but also by the southern branch of the mid-latitude westerlies.

The main WV input to the TP takes place through the southern and western boundaries, confirming the results of Feng and Zhou (2012), even if their western boundary is further east. The WV entering the TP through the eastern part of the southern boundary originates in monsoonal air masses, while the WV entering the TP through the western boundary originates in the mid-latitude westerlies. The moisture input through the western boundary (CS1) is only slightly higher in winter than in summer and reaches its maximum in spring. The spring maximum is probably caused by (i) higher moisture availability in the mid latitudes due to higher water temperatures in the Mediterranean region and (ii) higher wind speeds due to the position of the SWJ directly over the TP. The latter would increase the moisture advection towards the western boundary. The transport through the south-western (CS2) boundary is much lower in winter compared to summer because of the absence of the warm moist air flow hitting the Himalayas from the south. But even in winter the input of AWT is dominant. The relatively high input through the western boundary shows that the westerlies are not fully blocked by the TP orography and not all moisture transported with them is redirected north or south. The magnitude of this WV input is similar to that of the input through the Brahmaputra channel. This agrees with the findings of Mölg et al. (2014), who found that

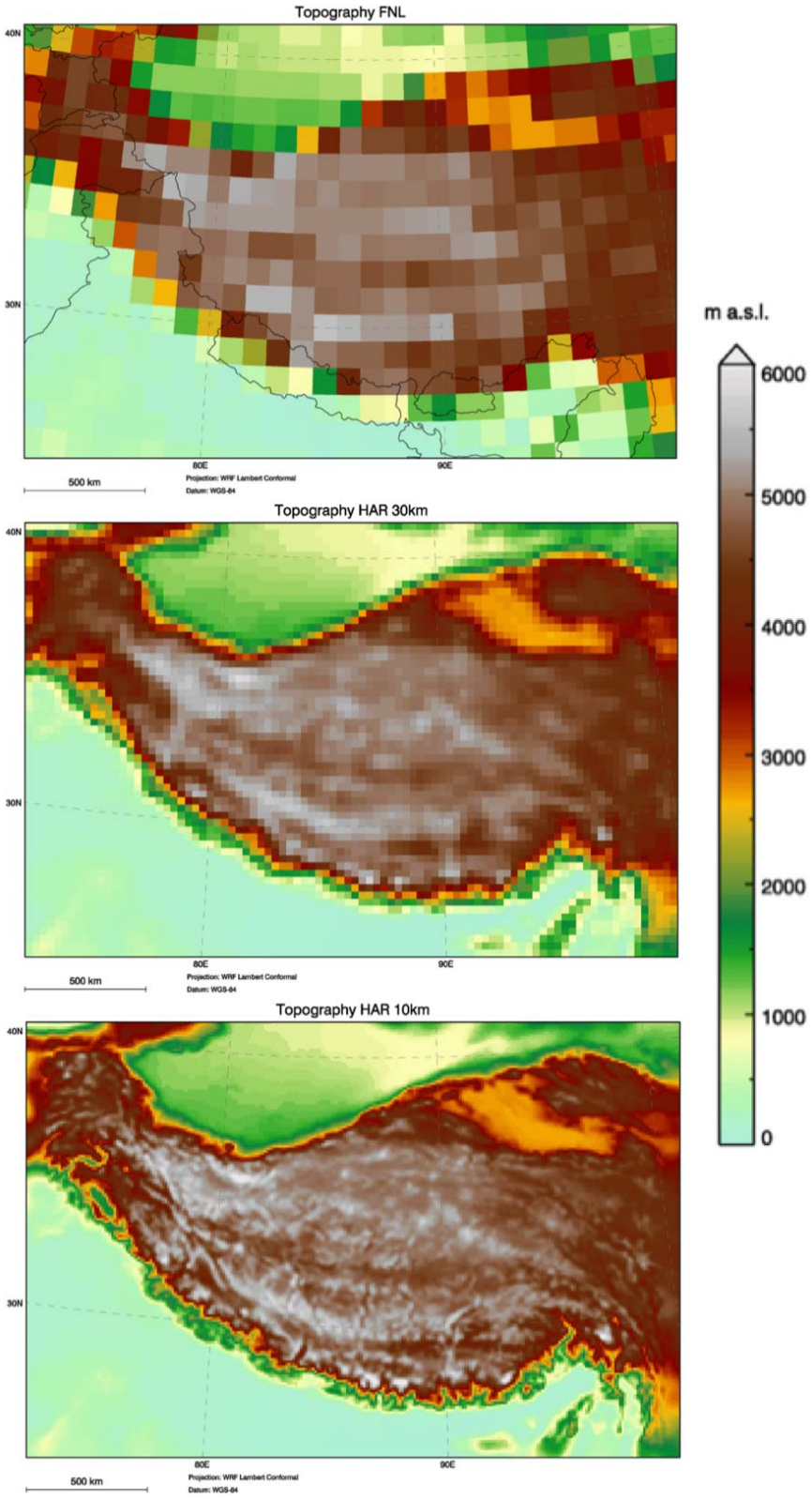

Fig. 3.8 Topography (m) for the FNL dataset (top), HAR30 (middle), HAR10 (bottom).

the westerlies play a role for precipitation and glacier mass balance in summer also, and they challenged the assumption that the westerlies contribute moisture only in winter or just in the northernmost parts of the TP in summer (Hren et al., 2009; Tian et al., 2007).

The main WV output from the TP takes place through the eastern boundary (CS 7), as also found by Feng and Zhou (2012), and the TP is a source of atmospheric water for the downstream regions east of the TP for all months (Table 3.1 and Fig. 3.7 c and d). Chen et al. (2012) and Luo and Yanai (1983) have shown that the TP contributes precipitation to its downstream areas, e.g. the Yangtze River valley, in summer. Our results confirm the importance of the TP as a source of moisture and precipitation to the downstream areas, e.g. the Yangtze River valley, as pointed out by Bin et al. (2013), Xu et al. (2011) and Chen et al. (2012), who called the TP a transfer or re-channel platform of moisture for the downstream regions in East Asia.

In January, there is only eastward moisture transport (output) through the eastern boundary (Fig. 9d). For all other months we find additionally transport towards the TP in the lower layers near the surface. The transport towards the TP through eastern cross section (CS 7) has its peak in July (Fig. 3.7 c) in the northern part of the boundary where the elevation is distinctly lower than in the southern part. There is still eastward AWT away from the TP in the higher levels. However, if we look at the total of the AWT amount through the eastern boundary (CS7 in Table 3.1), we see that the transport from the plateau towards the east is still dominant in summer.

The input to the TP through the northern boundary (CS 14–8) is lower than that from the west and south in January and July (Fig. 3.7 d and c, Table 1). There is less moisture available north of the TP that could enter the TP. Additionally, we find a strong gradient in altitude and fewer passages through which the atmospheric water could enter the TP than in the Himalayas. For the westernmost northern cross sections (14–12) the transport from the TP to the north is dominant. The reason for this is the north-eastward transport in the western TP, which also explains the lower transport amounts towards the TP. The AWT within the northern branch of the westerlies north of the TP is blocked by the high-altitude TP. AWT then follows the northern border of the TP to the east, where the elevation is lower in some regions (CS 9–11), e.g. at the border to the Qaidam Basin (CS 9). There, the input of atmospheric water to the TP is dominant for all months and the maximum input takes place in spring. AWT from the north to the Qaidam Basin is also visible in Fig. 3.1 for all months. This transport takes place in the lower layers of the atmosphere. The transport from the plateau northwards has its peak at the easternmost northern CS (CS 8) in July, August and September, when the TP can provide large amounts of atmospheric water, as shown in Sect. 3.1 in Fig. 3.1.

Table 3.1 Decadal average of the atmospheric water flux converted to a theoretical precipitation amount (mm month^{-1}) through vertical cross sections (1, 2–3, 4–5, 6, 7, 8, 9, 10–11, 12–14) and standard deviations (SD) for HAR10 (positive values denote transport towards the TP and negative values denote transport away from the TP). Decadal average of the precipitation (mm month^{-1}) and its standard deviation (SD) on the inner TP and of the contribution (%) of the atmospheric water flux to the precipitation for HAR10. Table adapted from Paper II.

Month/CS	1	2-3	4-5	6	7	8	9	10-11	12-14	Sum	TP prcp	Ratio (%)
01	12.8	41.2	−5.0	5.9	−34.0	−2.1	3.7	7.2	−17.7	12.1	22.9	52.6
02	15.8	47.4	−4.7	5.4	−31.5	−2.6	3.8	7.5	−21.1	20.0	33.5	59.7
03	19.8	35.4	−6.0	7.6	−37.8	−2.9	8.1	11.1	−31.5	11.5	33.9	33.9
04	17.8	33.4	−4.7	9.1	−36.2	−3.3	9.5	10.6	−22.8	13.4	42.7	31.4
05	17.1	21.5	9.1	21.3	−44.3	−5.6	8.5	10.4	−19.1	18.9	55.3	34.2
06	12.3	26.4	18.6	22.2	−42.4	−6.4	9.1	7.7	−14.5	32.9	72.3	45.5
07	14.9	34.4	24.3	16.5	−19.4	−12.2	4.2	5.3	−22.5	45.4	98.0	46.4
08	11.7	33.7	22.5	16.1	−22.9	−12.7	6.2	6.8	−22.6	38.8	91.8	42.2
09	12.3	44.0	20.3	19.0	−55.1	−11.3	2.4	5.1	−21.9	14.8	57.6	25.7
10	15.4	21.3	9.6	18.4	−56.3	−5.0	3.6	6.2	−17.3	−4.1	23.6	−17.5
11	16.9	24.4	−5.7	4.9	−35.5	−2.5	5.8	9.4	−20.5	−3.0	11.9	−25.2
12	15.0	36.5	−6.6	3.3	−34.2	−2.1	4.9	8.9	−20.5	5.3	15.8	33.7
Sum	181.6	399.6	71.7	149.8	−449.8	−68.8	70.1	96.2	−244.2	206.0	559.2	36.8±6.3
SD	59.4	47.6	15.5	22.1	44.1	8.4	12.7	12.8	24.5	42.6	77.1	
SD (%)	32.7	11.9	21.6	14.8	9.8	12.3	18.1	13.3	10.0	20.7	13.8	

Table 3.2 The same as Table 3.1 but for HAR30. Table adapted from Paper II.

Month/CS	1	2-3	4-5	6	7	8	9	10-11	12-14	Sum	TP prcp	Ratio (%)
01	13.6	43.1	−7.9	6.4	−35.9	−2.6	3.9	7.6	−19.9	8.3	24.3	34.0
02	16.7	49.8	−7.4	6.1	−33.7	−3.2	4.1	8.1	−23.8	16.8	35.7	47.0
03	21.5	36.9	−9.1	9.3	−41.1	−3.4	8.6	12.1	−27.5	7.3	36.7	19.9
04	19.6	35.2	−8.3	11.1	−39.5	−3.7	10.1	11.3	−26.6	9.2	46.0	20.0
05	19.0	21.4	7.5	23.3	−47.3	−5.9	9.2	10.9	−22.3	15.9	60.0	26.5
06	13.4	25.1	20.1	23.2	−47.1	−6.5	10.1	7.5	−16.1	29.8	76.2	39.1
07	16.2	32.2	27.6	14.1	−24.0	−12.6	4.9	3.9	−24.0	48.3	98.8	38.8
08	12.2	32.1	25.5	14.0	−27.3	−13.4	7.0	5.2	−23.7	31.6	91.8	34.5
09	13.4	43.2	22.8	19.3	−60.7	−12.1	2.9	4.5	−24.2	9.1	58.4	15.5
10	17.1	20.2	8.6	19.7	−59.2	−5.8	4.0	6.8	−20.3	−8.9	25.1	−35.6
11	18.4	24.5	−9.6	5.0	−37.1	−3.1	6.1	10.2	−23.6	−9.1	12.9	−71.1
12	16.0	38.2	−10.1	3.3	−35.9	−2.7	5.2	9.5	−23.0	0.4	16.7	32.7
Sum	197.2	401.9	59.7	154.9	−488.6	−75.0	76.1	97.4	−274.9	148.7	582.5	25.5±7.4
SD	25.4	53.2	18.3	23.5	212.7	9.4	13.8	13.5	27.8	47.4	81.0	
SD (%)	12.9	13.2	30.6	15.2	43.5	12.5	18.1	13.9	10.1	31.9	13.9	

3.4 Moisture budget

So far we have analysed the AWT transport over the TP at different levels and to the TP through its boundaries. In the next step we quantify how much of the moisture necessary for the precipitation falling on the inner TP is supplied by external sources and how much is provided by the TP itself from local sources and moisture recycling.

Table 3.1 displays the monthly decadal average of AWT through the individual cross sections and the sum for all cross sections, the precipitation falling on the inner TP and the ratios between them. To make the comparison with the precipitation easier, we converted the net atmospheric water input to a theoretical precipitation equivalent ($\mathrm{mm\,month^{-1}}$), which results in an annual mean AWT input of 206.0 $\mathrm{mm\,year^{-1}}$ for HAR10. The mean annual amount of precipitation falling on the inner TP (the area enclosed by the cross sections) is 559.2 $\mathrm{mm\,year^{-1}}$. The ratio of net input of atmospheric water to the precipitation falling on the inner TP reveals that, on average, AWT through the borders accounts for 36.8% of the precipitation during the year. According to this, the remaining 63.2% of atmospheric water needed for precipitation must be provided by the TP itself. This moisture supply probably takes place via moisture recycling from local sources, e.g. evaporation from numerous large lakes, soil moisture, the active layer of permafrost, snow melt and glacier run-off. The share of moisture from external sources is highest in winter when the TP cannot provide moisture for precipitation by itself, followed by summer, where the largest net input occurs. In October and November the ratio is negative, which means that the TP provides more moisture than it receives from external sources. These are the two months where the output of moisture from the TP is larger than the input; this is possible because the moisture imported to the TP in summer is available for export in autumn. On a monthly basis, there certainly is a time lag between the moisture input and the precipitation, making the analysis of monthly ratios difficult. The standard deviations for HAR10 in Table 3.1 show that the atmospheric water input varies more between the years than the precipitation falling on the TP. This implies that the evaporation from local sources (moisture recycling) stabilises the precipitation falling on the inner TP. These results highlight the importance of local moisture recycling as already emphasised by Kurita and Yamada (2008), Joswiak et al. (2013) and Chen et al. (2012). For the northern Tibetan Plateau, Yang et al. (2006) detected that 32.06% of the precipitation is formed by water vapour from ocean air mass and 46.86% is formed by water vapour evaporated from local sources. They found that at least 21.8% of the precipitation is formed by water vapour evaporated on the way and then transported by the monsoon circulation. Yang et al. (2007) also showed that for two flat observation sites in the central eastern part of the TP, the evaporation is 73% and 58% of the precipitation amount. This is in a good

agreement with our results that 63.3% is provided by local moisture recycling. The question is what will happen with the atmospheric water which is transported to the TP. Does it remain on the TP or is it lost as run-off? Could this moisture input be an explanation for the observed lake level rises (Yang et al., 2014)?

The comparison of the net atmospheric water input to the TP through the cross sections, the precipitation falling on the inner TP and the ratio between them for HAR10 (Table 3.1) and HAR30 (Table 3.2) shows that the different horizontal resolutions lead to different results. On an annual basis, the different horizontal resolutions result in an AWT input difference of 57.3 mm year^{-1} and a precipitation difference on the inner TP of 23.3 mm year^{-1}, with HAR30 showing the lower AWT input but the higher precipitation amount. This leads to a difference of 11.3% in the ratio of AWT to precipitation between the HAR10 (36.8%) and HAR30 (25.5%) datasets. Nevertheless, HAR30 exhibits higher transport amounts for both input and output for almost every cross section and every month. Due to the fact that the output values are also higher, the annual net input for HAR30 is lower than for HAR10. On an annual basis HAR30 shows just three-quarters of the HAR10 AWT input. Lin et al. (2018) show that a horizontal resolution of 10 km appears to be the best compromise between computational costs and high enough resolution to minimise precipitation biases by realistically representing the underlying topography in High Mountain Asia and therefore moisture pathways and the blocking of moisture input. Our study shows that for a quantification of AWT and the spatiotemporal detection of its major pathways and sources it is important to realistically represent the complex topography of High Asia using a dataset with a high spatial resolution (Fig. 3.8).

Shi et al. (2008) showed that a higher horizontal resolution and more realistic representation of the topography is also important for the development of disturbances on the TP leading to precipitation events in the downstream regions of the TP like the Yangtze River valley. The AWT in Figure 3.9 and the 10 m wind field in Figure 3.10 show a meso-scale cyclonic circulation/disturbance developing on the central TP on 9 July 2004 and moving eastward on the TP during the following days while intensifying. The system appears to facilitate moisture transport from south of the Himalayas to the TP through the valleys in the Himalayas (3.9). Fig. 3.10 shows that the system is associated with precipitation amounts of up to 50 mm day^{-1} . Disturbances like this are called Tibetan Plateau vortices and are the major precipitation-triggering systems on the TP (Wang, 1987).

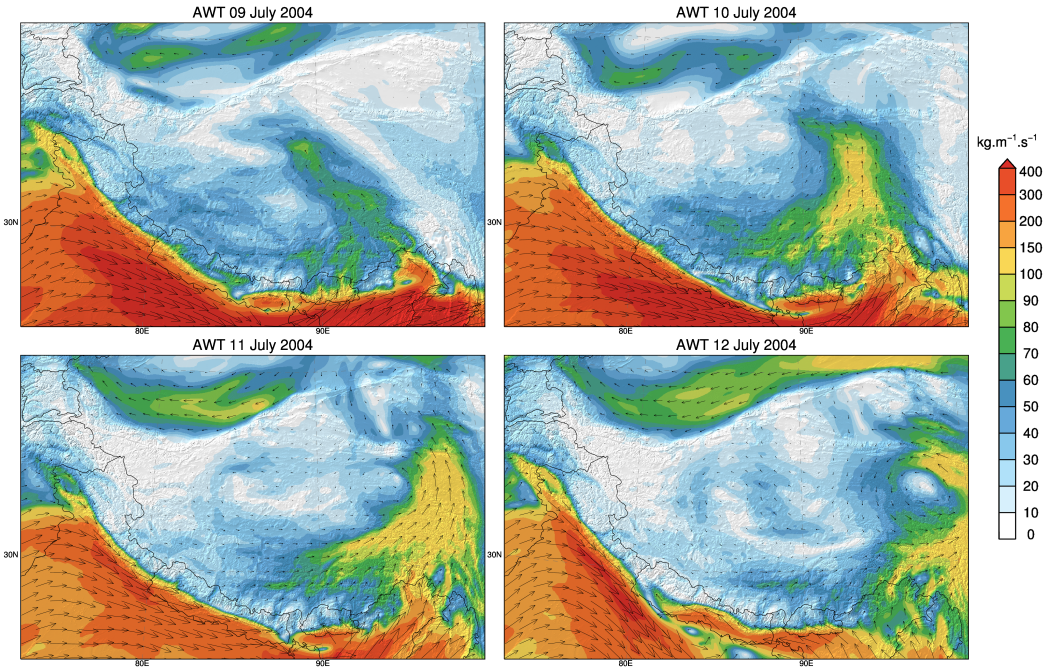

Fig. 3.9 Vertically integrated water vapour flux ($\mathrm{kg\,m^{-1}\,s^{-1}}$) for 9–12 July 2004 for HAR10. Colour shading denotes strength of water vapour flux, arrows (plotted every eighth grid point) indicate transport direction.

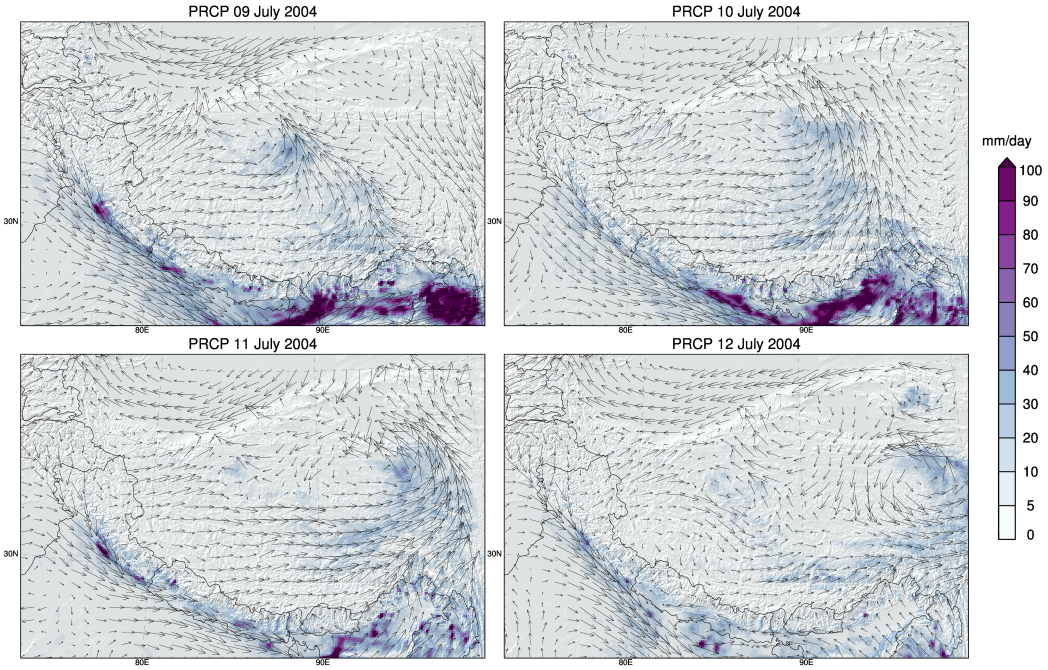

Fig. 3.10 Precipitation ($\mathrm{mm\,day^{-1}}$) for 9–12 July 2004 for HAR10. The arrows show the 10 m wind field (every ninth grid point plotted).

4. Dynamic precipitation controls

This Chapter describes how different dynamic controls influence precipitation variability by enhancing or suppressing precipitation development. We provide the motivation for this study in Section 4.1 and introduce the selected controls in Section 4.2. To be able to better understand precipitation variability we first establish the precipitation seasonality for the TP and surrounding regions using a clustering approach (Section 4.3). In Section 4.4 we then examine the correlation patterns of each of the variables with precipitation to determine which controls are when and where most efficient.

4.1 Motivation

We have shown in Paper II (Curio et al., 2015) that high atmospheric water transport over a region does not always lead to the development of precipitation. Figure 4.1 shows the correlation between atmospheric water content and precipitation. As expected the correlations are positive throughout the year, which means that higher atmospheric moisture content is associated with more precipitation at all times and in all regions. But interestingly the correlations are not of the same strength everywhere and in every month. This shows that where the variance of the vertically integrated atmospheric water contents explains only part of the variance of precipitation, dynamic precipitation controls must be at play. Therefore, there must be other factors controlling precipitation variability by dynamically enhancing or suppressing precipitation development in addition to atmospheric moisture essential for precipitation.

We selected five variables as dynamic precipitation controls: horizontal wind speed at 300 hPa (WS300) and at model level 10 (WS10, about 2 km above ground), vertical wind speed at 300 hPa (W300), vertically integrated atmospheric water transport (AWT, and the height of the planetary boundary layer (PBLH).

It is known that these factors have an influence on precipitation variability, but on the basis of coarse-resolution datasets it was not possible to analyse the relations spatially and temporally differentiated for the TP and the surrounding high mountain ranges as it is now

using the HAR. The different precipitation controls have effects on different spatial scales. While the horizontal and vertical wind speeds at 300 hPa (WS300 and W300) are large-scale controls, the horizontal wind speed in the boundary layer (WS10) and the planetary boundary layer height are effective at the mesoscale. The atmospheric water transport (AWT) is effective on both scales and across large distances connecting the large-scale with the mesoscale. We do not claim completeness for the list of precipitation controls but assume that these four factors belong to the most important dynamic precipitation controls. It is important to keep in mind that the precipitation controls are not independent of each other and can have combined effects on precipitation variability or cancel out each other; but this is not the focus of Paper III.

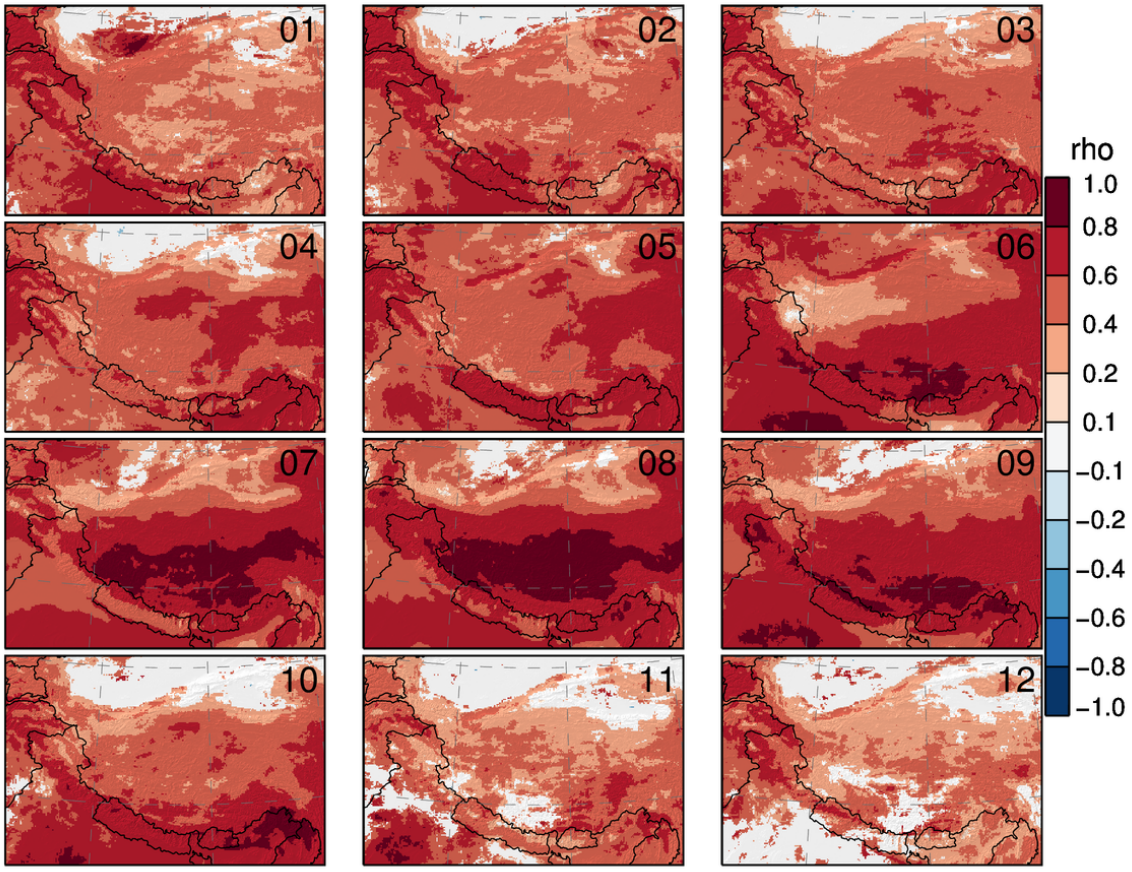

Fig. 4.1 Coefficient of correlation (rho) between daily column integrated atmospheric water content (AWC) and precipitation for all months (01–12). Positive correlations are denoted in red, while negative correlations are denoted in blue. Figure taken from supplementary of Paper III.

4.2 Selected controls

In this section we briefly introduce the selected controls and their possible impacts on precipitation variability.

The horizontal wind speed at the 300 hPa level has two main effects on precipitation variability. High WS300 can inhibit or cut off deep convection and thus suppress precipitation development (e.g. Findell and Eltahir (2003); Zhang and Atkinson (1995). In this case only shallow convection can form, which does not lead to considerable precipitation amounts. Mölg et al. (2009) showed that convective precipitation events on tropical mountain summits correspond to low horizontal wind speeds. On the other hand, higher wind speeds can have positive effects on moisture advection and orographic lifting and can, at lower levels, enhance evaporation from the surface and therefore convection (e.g. Johansson and Chen (2003); Roe (2005)). This process is most interesting during the warm half of the year, when surface moisture from local sources like lakes, soil moisture, the active layer of permafrost, snow- and glacier melt is available. Moisture recycling plays an important role in precipitation on the TP (e.g. Araguás-Araguás et al. (1998); Trenberth (1999)); on average, more than 60% of moisture needed for precipitation falling on the inner TP is provided by the TP itself (Paper II).

The core of the subtropical westerly jet (SWJ) occurs at the 200 hPa level. Over the Tibetan Plateau the jet reaches down to 300hPa and still has an effect there and also at lower levels. This was shown for the HAR in Paper I (Fig. 2). The strength and location of the jet influences the hydro-climate of the Tibetan Plateau and central Asia (e.g. Schiemann et al. (2009)). The precipitation seasonality in the north-western parts of the study region is especially related to the position of the jet (Schiemann et al., 2008). Garreaud (2007) pointed out that stronger than normal low-level westerlies lead to more precipitation on the windward side of meridionally orientated mountain ranges (orographic precipitation), while high wind speeds at mountain tops lead to rather dry conditions because of intensified downdrafts. This process is called the rain shadow effect. But he also shows this could lead to more precipitation on the lee side because more cloud particles are advected and disturbances can overcome the topographic barrier with the help of higher wind speeds, which would lead to more frontal or cyclonic precipitation. This case already shows that the influence each of the dynamic controls has on precipitation depends on many factors and that this influence may vary highly in time and space.

The influence of the vertical wind speed on precipitation depends on the direction of the vertical wind, i.e. on whether it is an updraft or a downdraft (Rose and Lin, 2003). Updrafts have a positive impact on precipitation because they can boost or enhance convection and are

a key element for orographic precipitation on the windward side of mountain ranges, while downdrafts (e.g. on the lee side of mountain ranges) and subsidence lead to the inhibition of convection and cloud dispersal. The expectation is that we have mainly positive correlations of vertical wind with precipitation: high upward winds cause higher precipitation and higher down- ward winds cause less precipitation.

Atmospheric water transport (AWT) is not only a dynamic precipitation control since it is a product of atmospheric moisture content and wind speed (and direction). The positive effect of AWT on precipitation variability due to moisture supply is described in e.g. Barros et al. (2006) and Giovannettone and Barros (2009). We assume that there is always a positive correlation between AWT and precipitation. But high AWT does not automatically lead to precipitation development, which we have shown in this thesis in Paper II for the Qaidam Basin where the prevailing atmospheric subsidence inhibits convection.

The height of the planetary boundary layer (PBLH) shows the turbulent mixing of the lower atmosphere. It is influenced by solar forcing, turbulent processes, convective activity (Yang et al., 2004), moisture content and temperature of surface and air, and wind speed. Gentine et al. (2013) point out that dry soil surface accelerates the growth of the PBL. The TP has one of the highest PBLs in the world, due to its high altitude and strong solar forcing, but the TP PBL is not fully understood yet because there are only few observations. During daytime in spring and summer the PBL is higher than in the other seasons in this region (Patil et al., 2013) and can exceed heights of 3000 m or more (Ma et al., 2009; Yang et al., 2004) in some regions on the TP due to strong solar forcing and convective activity. The horizontal wind speed influences the PBLH by facilitating the mixing of the atmosphere and the entrainment of air from above the PBL. The PBLH is not a purely dynamic precipitation control, but entrainment as a dynamic factor has great impact on PBLH (Gentine et al., 2013; Medeiros et al., 2005). In the HAR the PBLH is determined dynamically by using the Mellor–Yamada–Janjic turbulent kinetic energy scheme (Janjic, 2002) for PBL parameterisation.

4.3 Precipitation seasonality

To examine when and where these factors impact precipitation variability we first establish a spatial and temporal analysis of precipitation using a clustering approach (see Section 2.3). This will help to identify regions with similar precipitation seasonality which might enable us to connect different regions using the results from the analysis of dynamic controls. Only the integrated analysis of precipitation seasonality, water transport pathways, the impact of the westerlies and the dynamic controls can enable us to understand the complex picture. Figure

4.2 shows the seven defined clusters of precipitation regime and the mean annual cycle of the monthly contribution of precipitation to the annual precipitation (called precipitation fraction in the following) in each cluster.

The TP and the surrounding high mountain ranges show a high spatial variability in precipitation seasonality. The central TP and the region south of the Himalayas in India, Nepal, and Pakistan (blue, cluster 6) exhibit the precipitation maximum in summer and the minimum in winter. In this cluster the precipitation fraction increases rapidly from June onward coinciding with the onset of the Indian summer monsoon. Therefore, we refer to this cluster as the monsoonal precipitation cluster. During July and August more than 50% of the annual precipitation falls in these regions, while from October to May the monthly precipitation amount is below 5% of the annual precipitation. The yellow cluster (3) has a much broader and less pronounced summer precipitation maximum and the increase and decrease proceed with similar rates. The annual cycle of precipitation in this cluster is determined by the seasonal cycle of solar forcing and therefore convective activity. The green cluster (1) represents a transition zone between the monsoonal and convective clusters where the monsoon can have an influence but is not dominant. This means that both monsoonal precipitation and/or only solar forced convective precipitation can occur. The naming convention does not mean that the monsoonal cluster precipitation is not of convective nature, but it emphasises that the precipitation (development/variability) is influenced by the monsoon, which is associated with the advection of tropical air masses. The timing and strength of the precipitation maximum indicate a different forcing. In the monsoonal cluster the precipitation maximum is higher, starts during the Indian summer monsoon onset, and persists for a shorter time period. The monsoonal cluster is divided into a northern and southern part by the Himalayas.

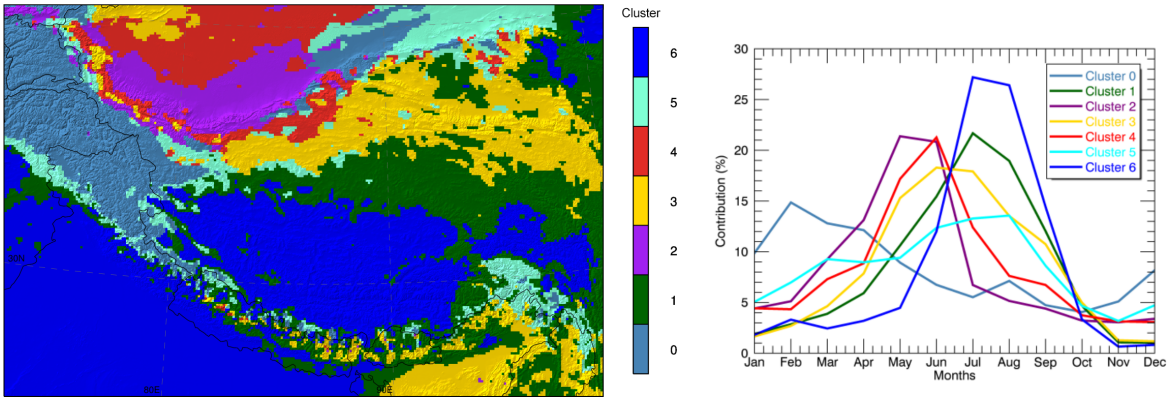

Fig. 4.2 Precipitation clusters (left) and the mean annual cycle of percentage contribution of monthly precipitation to annual precipitation for each cluster (right). Figure taken from Paper III.

The grey-blue cluster (0) shows a winter precipitation maximum and is dominated by the influence of the midlatitude westerlies. This cluster occurs mainly in the Pamir–Karakoram–western Himalayas (PKwH) region, as one coherent pattern, and additionally in the eastern part of the Tarim Basin. Fractional precipitation values are between 5 and 15% throughout the year so that the annual cycle is less pronounced than for the summer precipitation clusters. This may imply that the influence of the midlatitude westerlies is more constant year-round, while the monsoon has a stronger but temporally more limited influence on precipitation on the TP and its surrounding regions.

The light blue cluster (5) surrounds the grey-blue cluster at the southern flank of the western Himalayas (western notch),and occurs in the eastern Tarim Basin and in the south-eastern TP. In the light blue cluster the annual cycle of precipitation is less pronounced than in the grey-blue cluster with a more evenly distributed seasonality of precipitation during spring and summer with a minimum in November. It is interesting that the region in the south-east of the TP, where the Brahmaputra Channel enters the TP, belongs to a different cluster than the surroundings, which are divided between the three clusters dominated by convection: blue, yellow, and green. There might be a stronger influence from AWT (due to being located around the Brahmaputra channel, one of the major moisture pathways for monsoonal air masses to the TP) which would make this region more similar to the surroundings of the PKwH region regarding the factors controlling precipitation variability. Another possible reason could be the occurrence of extratropical disturbances which propagate eastward along the southern side of the Himalayas and can get terrain-locked in the eastern notch of the Himalayas (Norris et al., 2015). This would lead to a higher moisture supply to the region and therefore higher amounts of orographic precipitation. This kind of terrain locking of the westerly flow in winter is described in detail for the western notch of the Himalayas by Norris et al. (2015). This mechanism would explain the higher shares of winter precipitation in the region around the Brahmaputra Channel and the affiliation to the same cluster occurring at the southern flank of the western Himalayas in the western notch.

The remaining two clusters – red (4) and purple (2) – almost only appear in the Tarim Basin. They are both characterised by a spring and early summer precipitation regime but also show some differences. The fraction of precipitation in the purple cluster increases sharply from March to May and June, when the maximum with a value of slightly above 20% occurs. The decrease is even sharper so that in July already only 6% of the annual precipitation occurs. The annual cycle of the red cluster seems to be delayed relative to the purple cluster, and the period of maximum precipitation is only one month long. In spring the values are lower but higher in late summer and autumn, while these two clusters exhibit almost the precipitation fraction during winter.

The high mountain ranges of the Himalayas and Kunlun and Qilian Shan exhibit a complex structure of different clusters over relatively short distances and therefore exhibit no coherent patterns. This holds true also for the border area between the Karakoram and the Tarim Basin. The mountainous region of the Pamir and Karakoram is represented by only one cluster, which implies that this region is mainly influenced by one atmospheric forcing (midlatitude westerlies) or that different controls have the same impact in this region. The other mountain ranges lie in regions where an interplay of different controls occur, and the temporal and spatial variability of precipitation is larger on smaller scales. As we have shown in Paper II the water vapour transport to the TP from the southern border is controlled by the westerlies or the monsoon in summer depending on how far each of the flows reaches east or west along the southern foothills of the Himalayas.

Rain-gauge observations from the National Climatic Data Center (NCDC) were used to compare the results of the precipitation clustering approach with observations. Overall, 27 of the 65 stations (41.5%) fall in the same cluster as the nearest HAR grid point (Fig. 12 in Paper III). For 38 stations (58.5%) this is not true, but most of them fall in clusters with a very similar annual cycle or in clusters which are spatially very close to the cluster to which the HAR grid point belongs (Table 1 in Paper III). This is especially the case in the mountain regions in the western, the south-eastern, and north-eastern parts of the domain, where at least four different clusters occur on very small spatial scales. One has to take into account that there is always a distance up to a few kilometres between the NCDC stations and the respectively associated HAR grid point. This also can cause huge differences between the elevation and altitude of stations and grid points due to the complex topography of the study region, which in turn has an effect on the precipitation distribution. Additionally, the quality of the station data is not always satisfactory and the time series often show gaps, leading to a smaller database.

4.4 Variability of precipitation controls

In this Section we describe the spatial and temporal correlation of selected dynamical variables and precipitation to reveal the underlying mechanisms through which the variables influence precipitation and therefore act as controls of precipitation variability.

4.4.1 Horizontal wind speed at 300 hPa

The correlations between the horizontal wind speed at 300 hPa (WS300) and precipitation are shown in Figure 4.3. There are high positive correlations in winter in the PMwH region;

this is the time of the year when the majority of precipitation falls in this region (Fig. 8 and 9 in Paper I and Fig. 3.2 (Fig. 6 in Paper II)). The precipitation in the PMwH region is mainly cyclonic/frontal precipitation and is associated with western disturbances (Dimri et al., 2015). There are only negative correlations in the southern and eastern parts of the TP in winter, which enlarges over spring and covers most of the central and north-eastern TP and large parts of the central Himalayas, with the highest negative correlations in the central TP. The reason for the negative correlations in these regions is that they are dominated by convective precipitation (Paper I), and higher wind speeds in winter inhibit the deep convection. This also explains why there are negative correlations almost everywhere in summer. The region of negative summer correlations covers almost the same area as the convective and monsoonal precipitation clusters (Fig. 4.2) combined, so the impact of WS300 explains some of the precipitation clusters.

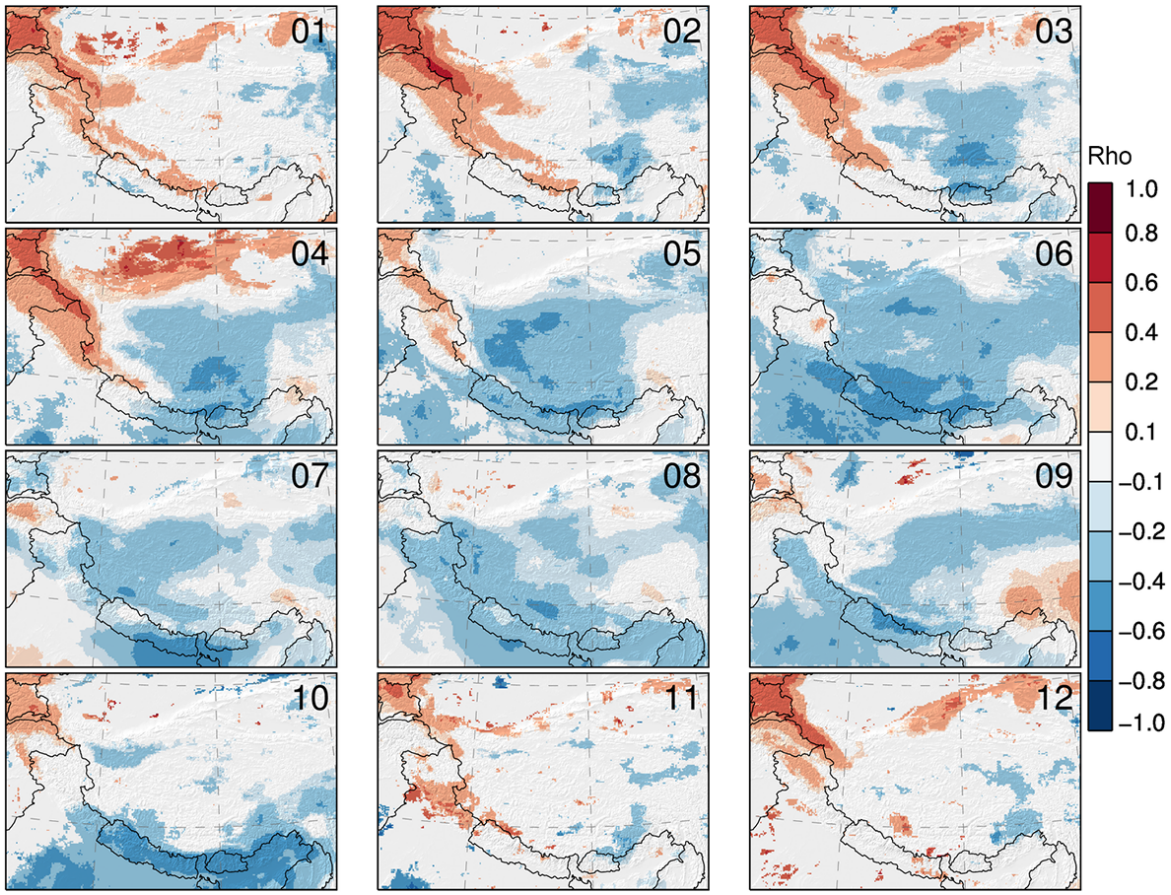

Fig. 4.3 Coefficient of correlation (rho) between horizontal wind speed at 300 hPa (WS300) and precipitation for all months (01–12). Positive correlations are denoted in red, while negative correlations are denoted in blue. Figure taken from Paper III.

This confirms the findings of Mölg et al. (2014), who showed that the flow strength at the 300 hPa level above the TP, during the onset period of the Indian summer monsoon, exhibits strong negative correlations with precipitation and explains 73% of the interannual mass balance variability of the Zhadang glacier, located at the Nyainqênthangla range in the central TP. They argue that weak flow conditions favour convective cell growth. This, together with the high positive correlations in regions and seasons where frontal or cyclonic precipitation is dominant, shows the strong influence of the subtropical westerly jet (midlatitude westerlies) not only on the western parts of the study region but also on the TP itself, which previously has mostly been described as mainly influenced by the monsoon system (Hren et al., 2009; Tian et al., 2007; Yang et al., 2014). Previous studies have stated that the precipitation on the TP is controlled by the midlatitude westerlies in winter and the Indian and east Asian summer monsoon in summer (Hren et al., 2009; Tian et al., 2007; Yang et al., 2014). This assumption is based only on precipitation timing, but we have shown in Paper II and so have Mölg et al. (2014) that the midlatitude westerlies also have an impact on summer precipitation. The current study confirms their findings by the detection of the negative influence of the high horizontal wind speeds on precipitation (development, variability, amount) on the TP in summer. Spiess et al. (2015) showed that in summer, increased horizontal wind speeds at 400 hPa have a positive effect on the height of the equilibrium line altitude at glaciers in different regions on the TP; they assumed that this could be caused by a reduction in convective precipitation due to high wind speeds. Exactly this process is shown by the strong negative correlations between horizontal wind speed at 300 hPa and precipitation in summer on the TP (Fig. 4.3).

In spring there is a second region with positive correlations north of the TP in the Tarim Basin and the bordering Kunlun and Qilian Shan. This area is reached by the northern branch of the midlatitude westerlies, which delivers moisture for precipitation. The area around the Brahmaputra Channel exhibits slightly positive correlations, due to enhanced moisture transport by higher wind speeds. The region of high positive winter correlations exhibits no or slightly positive correlations in only a small area in summer, and in some parts of the region the positive correlations are replaced by negative ones. Since there is a non-negligible amount of precipitation falling in this region in summer (20–40 percent points, see clusters 0 and 5 in Fig. 4.2), the lack/absence of positive correlations and the occurrence of negative correlations means that a different factor controls precipitation variability and/or the same control works in a different way due to higher shares of convective precipitation, especially in the eastern part of the Pamir–Karakoram region.

4.4.2 Horizontal wind speed in the boundary layer

Figure 4.4 shows that the correlations between the horizontal wind speed at model level 10 in the boundary layer (WS10) and precipitation are positive in the PMwH region in winter as they are for WS300, but the region is larger, especially the region with correlations > 0.6. The reason for the positive correlations is again the enhanced moisture supply due to higher wind speeds and therefore also more orographic precipitation. The positive correlations in the Brahmaputra Channel region (and south of it) are more pronounced, and the structure of the Brahmaputra Channel itself is clearly visible. The moisture supply is enhanced due to strengthened winds from the south, bringing moisture from the Indian Ocean to the Himalayas. There are high positive correlations between the WS10 and precipitation over the Tibetan Plateau in summer, while the correlations with WS300 are negative in summer. This is because of the fact that the wind speed in the boundary layer can enhance evapotranspiration from the surface (e.g. lakes; snow, glacier, and permafrost melt), which leads to more moisture in the lower atmosphere available for precipitation. This correlation again emphasises the importance of moisture recycling on the TP. In winter the correlations on the TP are mainly negative because the effect of enhanced evapotranspiration is not active due to the fact that all potential moisture sources are frozen during this time of the year. Strong negative correlations occur south of the Himalayas and in northern parts of India in summer. When the air flow from the south hits the mountain barrier, parts of the flow are redirected to the south-east and north-west. The flow becomes divergent, which forces the air above to descend,which in turn leads to unfavourable conditions for growing convection and therefore precipitation.

The identified positive correlations of the wind speed in the boundary layer with precipitation in summer on the TP agree with the findings of Back and Bretherton (2005), who detected positive correlations between near-surface wind speed and precipitation only when convection can be triggered easily. Their study region was the Pacific ITCZ, but we assume that their findings are also valid for the TP in summer, where the convective activity is high and enough moisture is available at the surface.

4.4.3 Vertical wind speed at 300 hPa

The correlations between vertical wind speed at 300 hPa (Fig. 4.5) and precipitation are mainly positive due to the positive effect of ascending air motion on precipitation development, as expected, especially in summer when most of the precipitation is convective. Therefore, the positive correlations are higher in summer than in winter when almost no precipitation falls on the TP, although the mean vertical wind speeds (up- and downdrafts)

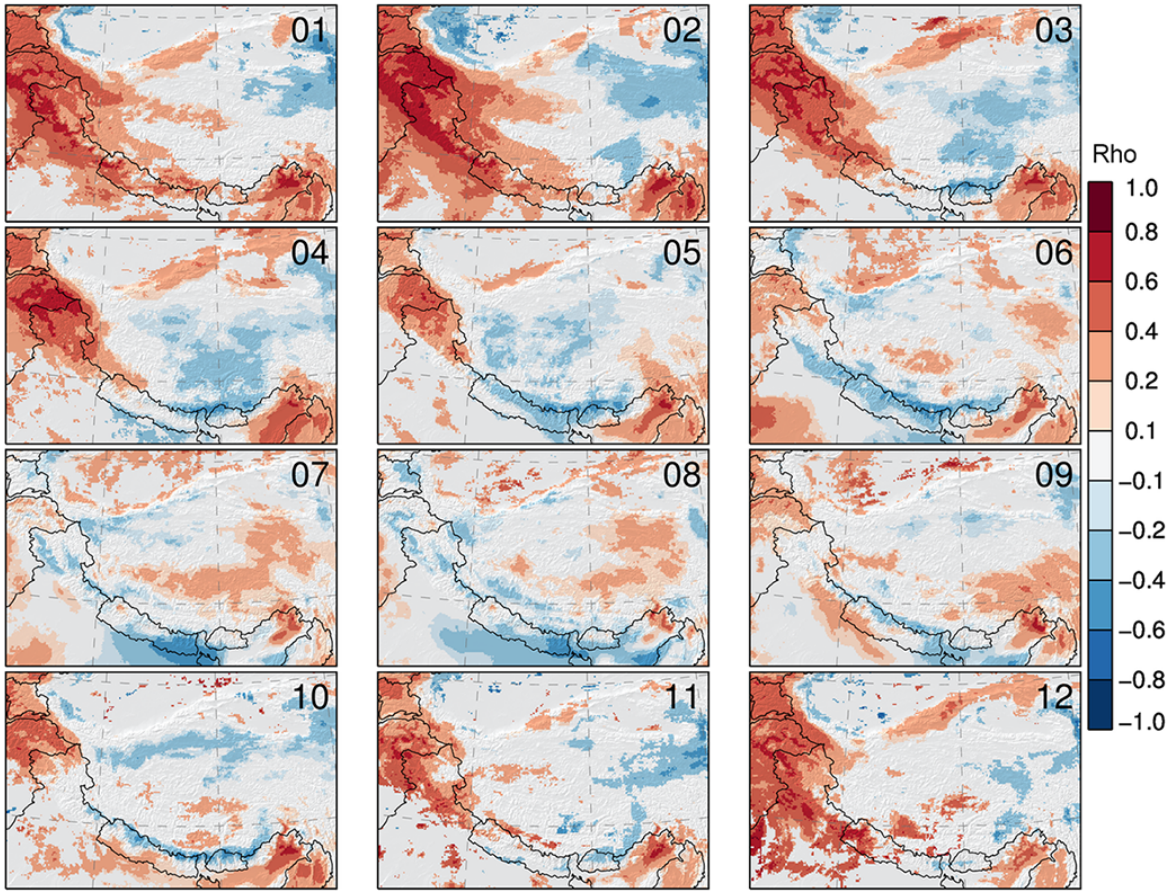

Fig. 4.4 Coefficient of correlation (rho) between horizontal wind speed at model level 10 (WS10) and precipitation for all months (01–12). Positive correlations are denoted in red, while negative correlations are denoted in blue. Figure taken from Paper III.

are higher in winter than in summer (Fig. 6 in Paper III). This shows that higher values of one precipitation control alone do not necessarily lead to higher correlations and therefore more precipitation but that usually other conditions favourable for precipitation development have to occur. This supports the interpretation that precipitation variability is mostly caused by combined effects of different precipitation controls.

The high mountain ranges of the Pamir and Karakoram show a pattern of alternating positive and negative correlations between vertical wind speed and precipitation. It was expected that the correlations between the vertical wind speed would be positive on both sides of the mountain ranges. But the negative correlations can be explained physically. If an air flow hits a mountain range, the barrier causes orographically induced flow patterns, with updrafts on the windward side and downdraft on the lee side of the mountain range. This causes the precipitation to be smaller on average on the lee side because the downdrafts suppress precipitation development. In the case of a stronger horizontal flow to the mountains, there

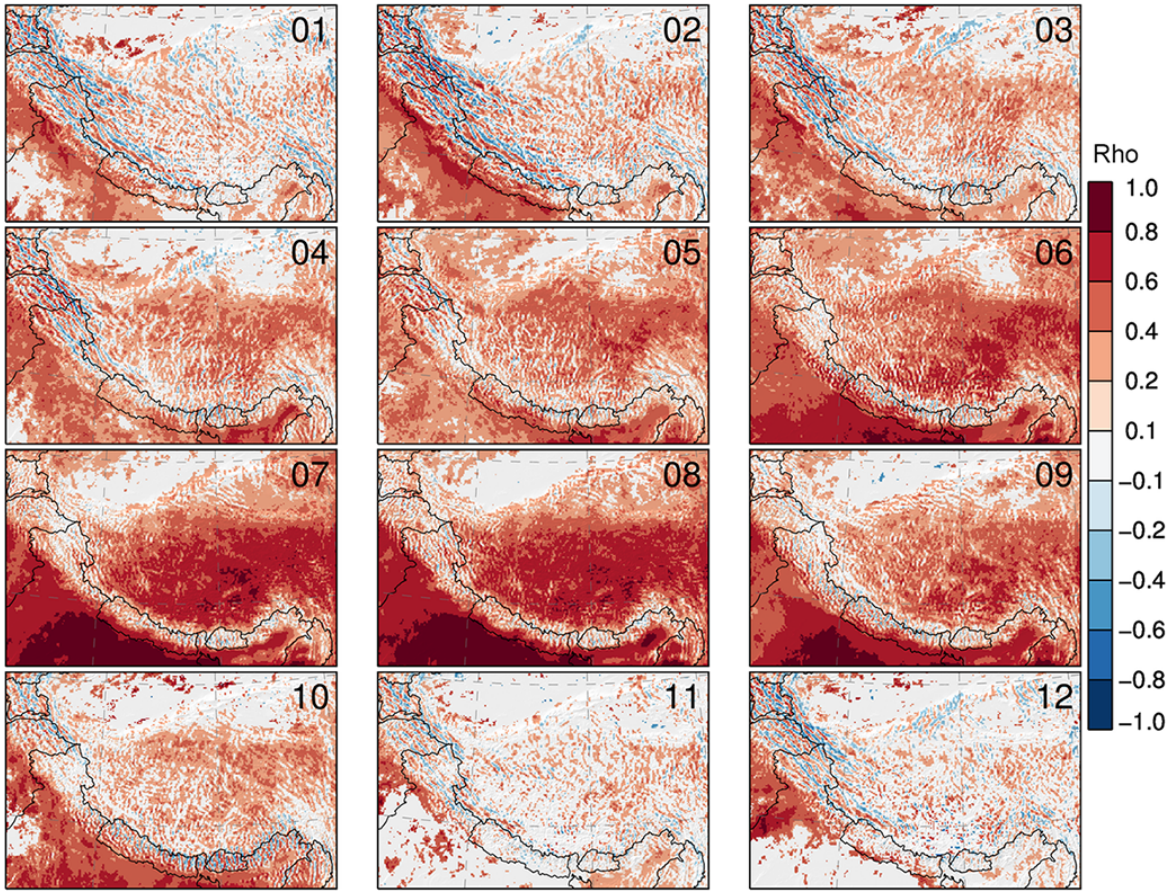

Fig. 4.5 Coefficient of correlation (rho) between vertical wind speed at 300 hPa (W300) and precipitation for all months (01–12). Positive correlations are denoted in red, while negative correlations are denoted in blue. Figure taken from Paper III.

is stronger moisture advection and orographic precipitation, and therefore the downdrafts on the lee side are no longer able to suppress precipitation. This leads to the simultaneous occurrence of precipitation and downdrafts, which is the reason for the negative correlation patterns on the lee side of mountain ranges found in the western parts of the study region.

4.4.4 Atmospheric water transport

Figure 4.6 shows the correlations between AWT and precipitation. The entire study region is dominated by positive correlations in all months. The highest positive correlations occur in winter and early spring in the PKwH region, where the correlation coefficient exceeds 0.8 in most regions. This is the time of the year when the maximum precipitation occurs in this region (Fig. 4.2 and Fig. 8 and 9 in Paper I). The annual contribution of convective precipitation in this region is below 10 percent points (Fig. 3.6), but the region exhibits

orographic precipitation triggered by the advection of moist air masses with the westerly flow and westerly disturbances (Cannon et al., 2014). Therefore, a higher moisture supply naturally leads to more precipitation. The positive correlations in the western part of the study region persist during the course of the year, even if their extent and strength varies. The positive correlations extend to the TP, the whole Himalayan arc, and along the northern border of the TP (Kunlun and Qilian Shan). These seem to be the moisture supply routes along the branches of the midlatitude westerlies. A second centre of persistent positive correlation occurs in the south-east of the TP, the region where the Brahmaputra Channel enters the TP. This region exhibits less convective precipitation on annual timescales (Fig. 3.6), but it is surrounded by regions with high convective precipitation rates. This explains the fact that this region belongs to a different precipitation seasonality cluster than its surroundings (Fig. 4.2).

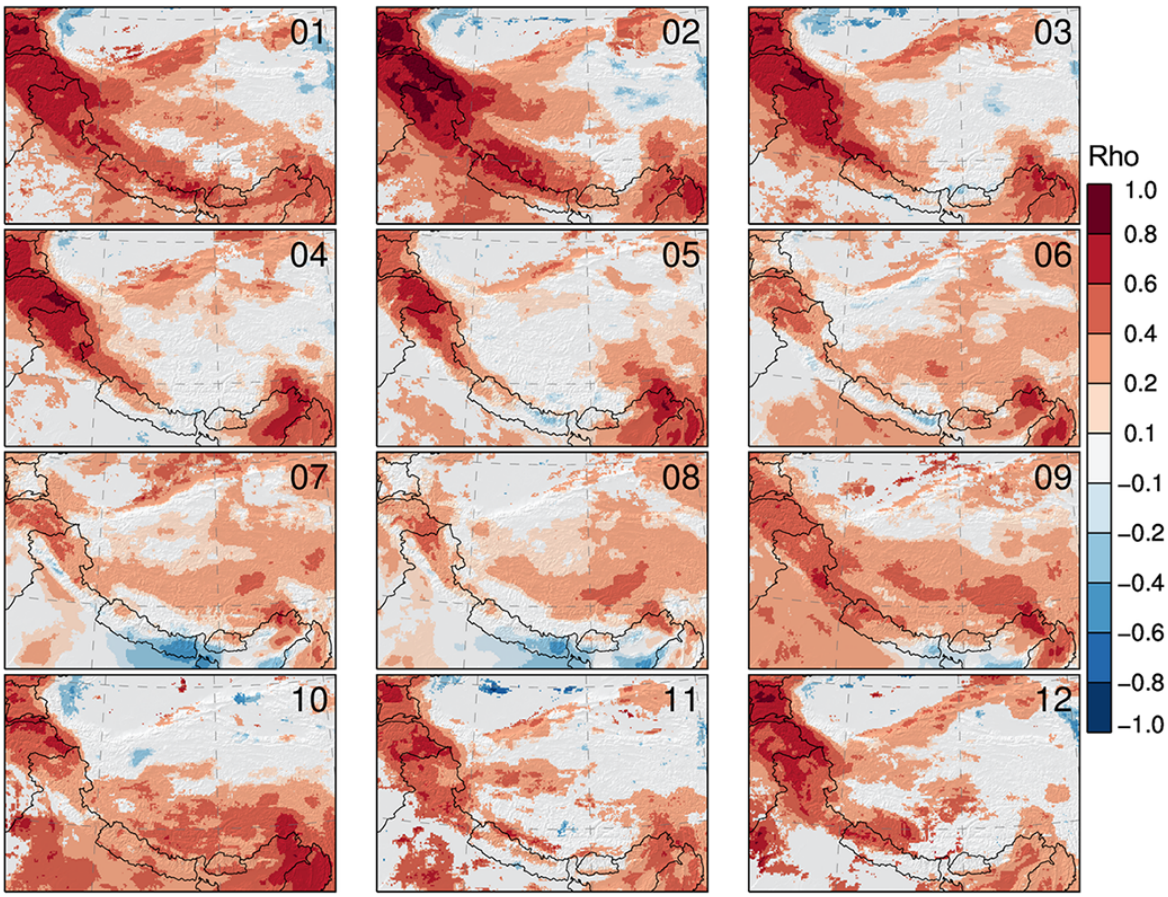

Fig. 4.6 Coefficient of correlation (rho) between column integrated atmospheric water transport (AWT) and precipitation for all months (01–12). Positive correlations are denoted in red, while negative correlations are denoted in blue. Figure taken from Paper III.

In January and February, the Himalayan arc exhibits mostly positive correlations and connects the area in the western parts of the domain with the other positive centre in the south-eastern TP around the Brahmaputra Channel. The spatial minimum of the positive correlations occurs in May, whereas the correlations are very high ($r > 0.6$) in the western and south-eastern centres. In May the central TP exhibits no significant correlations which may be caused by the fact that the AWT is very low on the TP in May (Fig. 3.1). From then on the area with positive correlations enlarges but the strength of correlation decreases. The minimum values of the positive correlations occur in July and August. But then there are positive correlations in the central TP, but they are not as high as in the western and south-eastern parts of the domain during winter and spring. This shows that the precipitation during this time of the year is mostly convective and that the moisture comes from local sources, so that the advection of moist air masses is less important. In large areas of the domain, the precipitation maximum occurs in July and August; 30% of the annual precipitation falls on the central and southern TP during this time (Fig. 8 in Paper I). The regions where the highest positive correlations occur are the regions where the precipitation maximum occurs during winter, matching the grey-blue precipitation seasonality cluster (Fig. 4.2). There are only a few regions and months where negative correlations occur, in the Tarim Basin during winter and in the central Himalayas and northern India during summer.

The fact that the positive correlation of AWT with precipitation in summer on the central TP is not as high as in the western parts of the study region in winter means that here the convection is able to produce precipitation using the moisture from local sources, which emphasises the importance of moisture recycling, as shown in Paper II using HAR data and by Chen et al. (2012), Joswiak et al. (2013), and Kurita and Yamada (2008), among others. Nevertheless, AWT still has a positive effect on precipitation, but it is not an essential control during this time of the year on the central TP.

4.4.5 Boundary layer height

In Winter the correlation between the planetary boundary layer height (PBLH) and precipitation (Fig. 4.7) are mainly positive, especially in the PKwH Himalaya region, forming a coherent pattern, and along the northern and southern border of the TP, with some interruptions, and in the eastern TP around the Brahmaputra Channel. PBLH is a precipitation control which is itself controlled by horizontal wind speed, among others. The positive correlations in winter in the Pamir/Karakoram region can be explained by higher horizontal wind speeds and thereby more moisture advection leading to more precipitation, as described earlier. Higher horizontal wind speeds lead to higher entrainment rates at the top of the PBL whereby the depth of the PBL increases. During the year this picture changes and negative correlations

become dominant. The negative correlations occur in regions and seasons dominated by convection and consequently convective precipitation. Higher PBLH are caused by higher horizontal wind speeds which have a negative effect on precipitation by cutting off deep convection, as previously pointed out in this thesis. In May we see positive correlations left only in the centre of the Pamir/Karakoram region and in the eastern TP, while in summer just small and scattered areas with positive correlations occur. Most of these areas on the central TP match the large lakes, e.g. Nam Co, Serling Co, and Tangra Yumco.

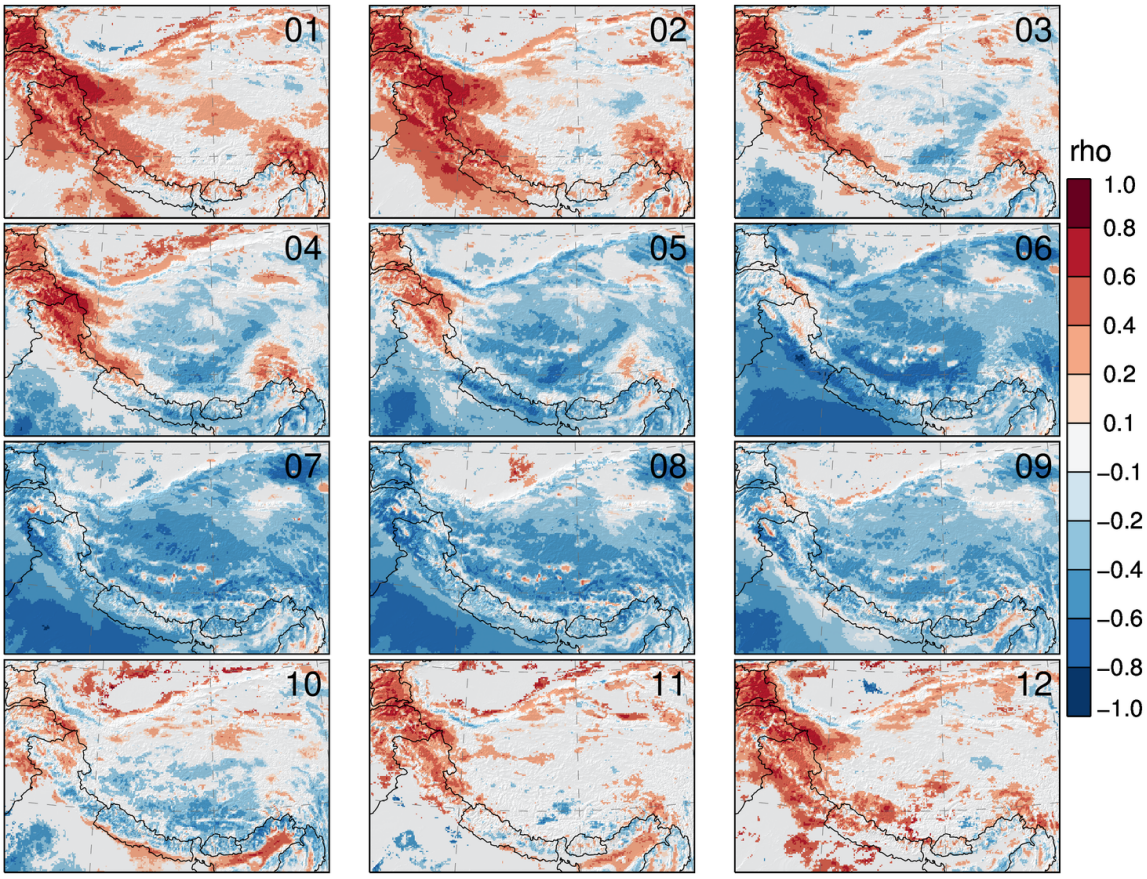

Fig. 4.7 Coefficient of correlation (rho) between planetary boundary layer height (PBLH) and precipitation for all months (01–12). Positive correlations are denoted in red, while negative correlations are denoted in blue.

To understand these contrary correlations, compared with the direct surroundings of the lakes, we have to look at the PBLH itself. Figure 4.8 shows the averaged daily mean and daily maximum PBLH for May as an example. The lowest PBLHs (mean and maximum) in the domain are found at the high mountain ranges bordering the TP, because of the high altitudes and low temperatures, and above the large lakes on the central TP. Reason for this seems to be the fact that during daytime when the air temperature above land is higher than above the

lakes, the air above the land starts to ascend and there is strong convective activity which is amplified at the slopes of the surrounding mountain ranges (due to higher solar insulation). Recirculation of the ascending air leads to subsidence of air above the lakes which lowers the PBLH and suppresses precipitation. Suppression of precipitation by subsidence was already described in Paper II for larger regions like the Qaidam Basin and the north-western parts of India and Pakistan.

The positive correlations above the lakes, mean that higher PBLHs lead to more precipitation in this area. These higher PBLHs occur when the wind speeds are higher, which leads to more entrainment, which causes a deepening of the PBL above the lakes. This effect slightly equalises the PBLHs above the lakes and the surrounding land and the differences become smaller. Due to the increase of the PBLH, the prevailing subsidence above the lakes weakens and precipitation development becomes possible.

In this chapter we presented simulated relationships, which have limitations. As always the uncertainty of the results mainly depends on the accuracy of the data themselves, the aggregation of hourly data to daily means, and the statistical methods used to analyse the data. The HAR precipitation and other variables, e.g. wind speed and direction and temperature, have been validated against other gridded data sets – global reanalyses and remote sensing data – and observations from weather stations by (Maussion et al., 2011, 2014). The analysis of PBLH was not included in Paper III (Curio and Scherer, 2016) since the PBL itself is strongly influenced by the horizontal wind speed and is determined in the HAR by using the Mellor–Yamada–Janjic turbulent kinetic energy scheme (Janjic, 2002) for PBL parameterisation. Therefore, one has to be cautious with these results and it would be preferable to repeat this analysis using observations. Studies using observations confirm a very high boundary layer over the TP, e.g. Yang et al. (2004).

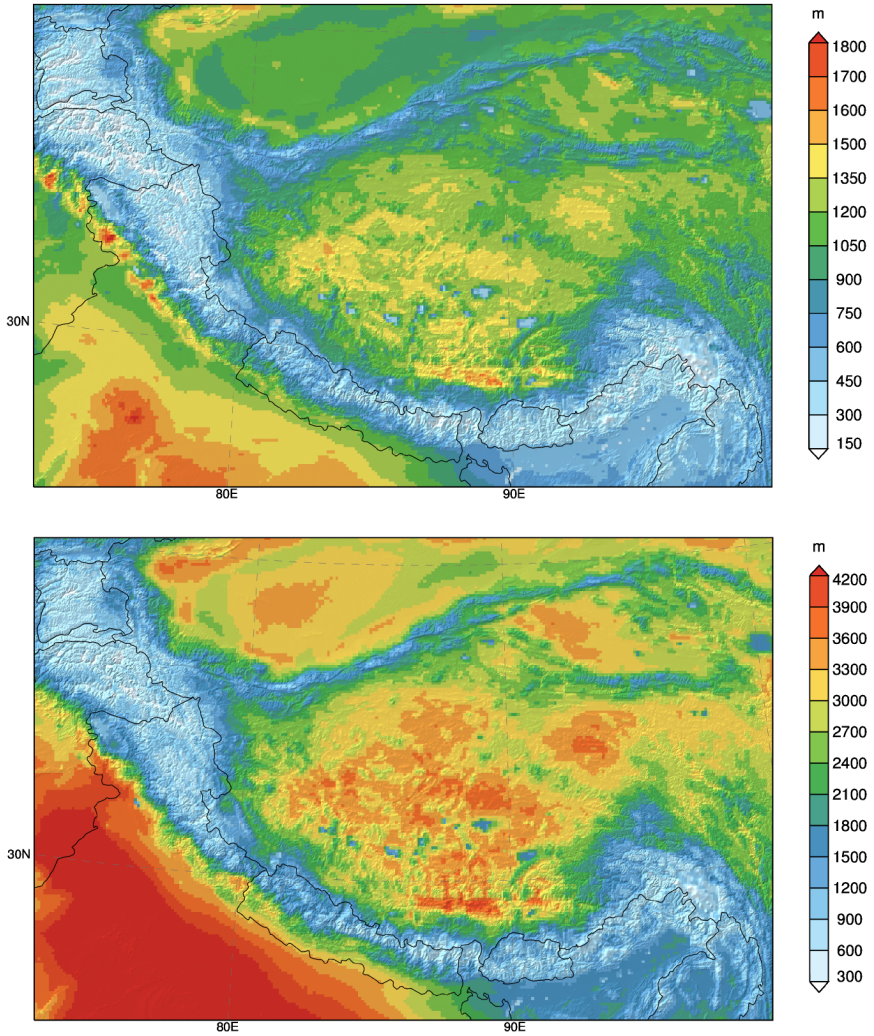

Fig. 4.8 Planetary boundary layer height (m) daily mean (top) and mean daily maximum (bottom) in May (2001-2013).

5. Conclusion and outlook

The TP plays a key role in Asian water cycle, as it is the origin of many large Asian rivers providing water for billions of people downstream in South and East Asia. The TP experiences high precipitation variability leading to dry spells and droughts, as well as to severe snow- and rainfall events and subsequent floods. However, there are strong differences between regions and seasons which are not yet well understood under present-day climate conditions, making statements for past and future climates highly speculative.

The aim of this thesis was to gain a better understanding of the spatial and temporal precipitation variability on the TP. In order to do so we used a newly developed high-resolution dataset, the High Asia Refined analysis (HAR; Paper I, Maussion et al. (2014)) which allowed us to examine atmospheric water transport to and on the TP, and variables dynamically controlling precipitation variability.

The first objective of this thesis was to examine the characteristics of the atmospheric water transport over and to the TP as resolved by the HAR dataset. Concerning the first objective, we focused on the seasonal evolution and vertical distribution of atmospheric water transport to detect the main moisture pathways and to quantify how much moisture necessary for the precipitation on the TP is provided from outside the TP and how much moisture comes from local sources on the TP, i.e. through moisture recycling.

It was found that the main atmospheric moisture input to the TP takes place through the southern and western boundaries while the main output takes place through the eastern boundary making the TP a source of moisture for its downstream regions.

Our results show that there is direct atmospheric water transport through the western boundary of the TP by the mid-latitude westerlies in summer. This result highlights that the westerlies are not fully blocked by the TP. They deliver more moisture to the Tibetan Plateau than assumed so far and their influence is not limited to winter. Additionally, the westerlies contribute moisture to the TP through valleys in the western part of the Himalayas (Himalayan arc) by the southern branch of the westerlies in summer. This implies that moisture entering the TP from the south-west in summer can be transported there either by the westerlies or the monsoon flow, depending on how far these systems extend eastward or

westward along the southern slopes of the Himalayas, respectively. The examination of the interplay of the two flows and what controls how far their respective influence reaches along the Himalayan foothills would be an interesting topic for future work.

Our results using the high-resolution HAR show that high mountain valleys in the Himalayas facilitate AWT from the south, whereas the high mountain regions inhibit AWT to a large extent and limit the influence of the Indian summer monsoon. The realistic representation of the topography of the high mountain ranges surrounding the TP is essential for modelling AWT to and from the TP. Lin et al. (2018) conclude that a resolution of 10 km, as provided by the HAR, presents the best compromise between computational costs and high enough resolution to minimise precipitation biases.

Shi et al. (2008) showed that it is also important to realistically represent the mesoscale topography of the TP itself to be able to simulate mesoscale disturbances influencing the precipitation variability on the TP and in the regions downstream. Therefore, the HAR could be used to further examine meso-scale disturbances, as shown in this thesis for one case in July 2004, and to analyse their role in facilitating moisture transport to the TP.

The water budget for the inner TP calculated in Paper II (Curio et al., 2015) reveals that local moisture recycling is an important factor and provides more moisture than the input from external sources (on average 60% versus 40%).

In future work, it would be interesting to analyse if and how the atmospheric water stored in snow in winter contributes to the atmospheric water transport and precipitation of the following warm season. Due to this storage term, the westerlies could play an even greater role in the hydrological cycle of some regions of the TP in summer. Studying moisture recycling in detail, e.g. how monsoonal moisture could reach the north-eastern parts of the TP via multiple moisture recycling as mentioned by Yang et al. (2006), could help to gain a better understanding of the water cycle on the TP. Additionally, the mixing of water vapour sources as seen in the examination of the vertical structure of the transport shows that the general question of where the moisture at a specific location is coming from often cannot be answered by naming a single source. This can make the identification of moisture sources using isotope signals difficult. Therefore, examining the part of the atmospheric column where precipitation forms and an in-depth analysis of the atmospheric water transport fluxes on individual levels could help to identify the moisture sources for precipitation in specific regions. Additionally the remaining components of the water balance, e.g. evaporation and run-off, should be considered in further studies.

Another research opportunity is to analyse if there are significant differences in the AWT patterns in wet and dry years to find out whether the extremes are influenced by changes in the atmospheric circulation or only by a change of the transported amount of atmospheric

water. Previous studies have identified large-scale teleconnections, such as the influence of the North Atlantic Oscillation (NAO) mode during wet and dry periods, have been analysed for longer periods by, e.g. Liu and Yin (2001) and Bothe et al. (2010, 2011). The novel HAR dataset offers the opportunity to re-examine their findings with the advantage of its higher spatial and temporal resolution, more realistic representation of the complex topography of the study region and better representation of mesoscale atmospheric processes.

In addition to atmospheric moisture availability dynamical effects influence precipitation enhancement and suppression. For example, large amounts of atmospheric water over the dry Qaidam Basin do not result in precipitation due to upper level subsidence. Therefore, the second objective of this thesis was to gain a better understanding of the relationship between dynamical variables and precipitation variability and the underlying processes since precipitation is the key element of the hydrological cycle of the TP and the surrounding high mountain ranges. Precipitation variability has a large impact on the water availability and therefore security in the densely populated downstream regions of India, Pakistan, and south-east Asia by governing river runoff directly through precipitation or with a time lag through snow and glacier melt.

Concerning the second objective of this thesis, we analysed the relationship between 5 selected atmospheric variables and precipitation variability on the TP in Paper III (Curio and Scherer, 2016). The results show that different factors influence precipitation in different regions of the TP and adjacent high mountain ranges during different times of the year and in different ways. For example, the 300 hPa wind speed has a positive effect in the western parts of the study region in winter and spring, while it has a negative effect on precipitation on the TP in summer.

The positive correlation of AWT with precipitation is higher in winter at the high mountain ranges in the western part of the study region than in summer on the central TP. This result shows that on the central TP the strong convection in summer is able to produce precipitation with the moisture available from local sources, emphasising the importance of moisture recycling as shown in Paper II (Curio and Scherer, 2016).

Different dynamical factors controlling precipitation variability are not independent from each other. For example, the AWT is influenced by processes in the boundary layer and higher horizontal wind speeds enhance evaporation and lead to higher transport rates. On the other hand high AWT does not lead to precipitation development in regions dominated by convective precipitation if high wind speeds cut off deep convection. Therefore, a future research opportunity could be to analyse the combined effects of precipitation controls. A combination of a principal component analysis of the dominant patterns and cluster analysis to detect control regimes, as in Forsythe et al. (2015), could be employed to obtain a climate

classification for the Himalayan arc and its surroundings. These regimes could help to explain regional features of glacier mass balance, like the Karakoram anomaly (Hewitt, 2005) or observed lake level changes (Liu et al., 2010; Zhang et al., 2011), which show a different behaviour compared to the surrounding regions. Other factors affecting precipitation variability , e.g. dust particles originating in the arid regions could play a role in precipitation suppression (Han et al., 2009)

The third objective of this thesis was to gain a better understanding of the roles the mid-latitude westerlies and the summer monsoon system play for atmospheric moisture transport to the TP and precipitation variability on the TP.

Concerning the third objective, we have shown in Paper II (Curio et al., 2015) and Paper III (Curio and Scherer, 2016) that the impact of the midlatitude westerlies on precipitation variability on the TP is strong, not only in winter, by enhancing moisture advection for orographic and frontal precipitation in the western parts of the study region but also in summer by cutting off deep convection on the TP and in other regions and seasons where and when precipitation is mainly convective.

Therefore, the TP and the entire study region can be partitioned by considering the dominant form of precipitation that occurs: cyclonic/frontal or convective precipitation. This enables us to more clearly determine the relevance of the monsoon system and the midlatitude westerlies for the precipitation distribution. Perhaps it is possible to say that the precipitation on the central TP in summer is influenced by the monsoon system regarding moisture supply; however, moisture recycling is also important, and the mid-latitude westerlies act as a control regarding the suppression or enhancement of precipitation due to the strong negative effect of high horizontal wind speeds on the development of deep convection.

The classification of precipitation has been determined by a cluster analysis using the percentage of monthly contribution to annual precipitation amounts and shows a mostly monsoonal influenced cluster, a convective cluster, and a hybrid cluster in between. The hybrid cluster shows that, climatologically, there is no delineation of the extent of the monsoon and how far its influence reaches on the TP. There is a relatively broad area between precipitation influenced by the monsoon and solely convection-dominated precipitation caused by the inter-annual variability of monsoon strength and other factors like the position and strength of the subtropical westerly jet.

References

An, Z., Colman, S. M., Zhou, W., Li, X. X., Brown, E. T., Jull, a. J. T., Cai, Y., Huang, Y., Lu, X., Chang, H., Song, Y., Sun, Y., Xu, H., Liu, W., Jin, Z., Liu, X. X., Cheng, P., Liu, Y., Ai, L., Li, X. X., Liu, X. X., Yan, L., Shi, Z., Wang, X., Wu, F., Qiang, X., Dong, J., Lu, F., and Xu, X. (2012). Interplay between the Westerlies and Asian monsoon recorded in Lake Qinghai sediments since 32 ka. *Scientific reports*, 2(619).

Araguás-Araguás, L., Froehlich, K., and Rozanski, K. (1998). Stable isotope composition of precipitation over southeast Asia. *Journal of Geophysical Research: Atmospheres*, 103(D22):28721–28742.

Back, L. E. and Bretherton, C. S. (2005). The relationship between wind speed and precipitation in the Pacific ITCZ. *Journal of Climate*, 18(20):4317–4328.

Barros, A. P., Chiao, S., Lang, T. J., Burbank, D., and Putkonen, J. (2006). From weather to climate—Seasonal and interannual variability of storms and implications for erosion processes in the Himalaya. *Geological Society of America Special Papers*, 398(02):17 –38.

Bin, C., Xiang-De, X., and Tianliang, Z. (2013). Main moisture sources affecting lower Yangtze River Basin in boreal summers during 2004-2009. *International Journal of Climatology*, 33(4):1035–1046.

Bolch, T., Kulkarni, A., Kaab, A., Huggel, C., Paul, F., Cogley, J. G., Frey, H., Kargel, J. S., Fujita, K., Scheel, M., Bajracharya, S., and Stoffel, M. (2012). The State and Fate of Himalayan Glaciers. *Science*, 336(6079):310–314.

Bollasina, M. and Nigam, S. (2010). The summertime "heat" low over Pakistan/northwestern India: evolution and origin. *Climate Dynamics*, 37(5-6):957–970.

Bookhagen, B. and Burbank, D. W. (2010). Toward a complete Himalayan hydrological budget: Spatiotemporal distribution of snowmelt and rainfall and their impact on river discharge. *Journal of Geophysical Research*, 115(F3):F03019.

Bothe, O., Fraedrich, K., and Zhu, X. (2010). The large-scale circulations and summer drought and wetness on the Tibetan plateau. *International Journal of Climatology*, 30:844–855.

Bothe, O., Fraedrich, K., and Zhu, X. (2011). Large-scale circulations and Tibetan Plateau summer drought and wetness in a high-resolution climate model. *International Journal of Climatology*, 31(6):832–846.

References

Cannon, F., Carvalho, L. M. V., Jones, C., and Bookhagen, B. (2014). Multi-annual variations in winter westerly disturbance activity affecting the Himalaya. *Climate Dynamics*, 44(1-2):441–455.

Chen, B., Xu, X.-D., Yang, S., and Zhang, W. (2012). On the origin and destination of atmospheric moisture and air mass over the Tibetan Plateau. *Theoretical and Applied Climatology*, 110(3):423–435.

Curio, J., Maussion, F., and Scherer, D. (2015). A 12-year high-resolution climatology of atmospheric water transport over the Tibetan Plateau. *Earth System Dynamics*, 6(1):109–124.

Curio, J. and Scherer, D. (2016). Seasonality and spatial variability of dynamic precipitation controls on the Tibetan Plateau. *Earth System Dynamics*, 7(3):767–782.

Dansgaard, W. (1964). Stable isotopes in precipitation. *Tellus*, 16(4):436–468.

Dimri, A. P., Niyogi, D., Barros, A. P., Ridley, J., Mohanty, U. C., Yasunari, T., and Sikka, D. R. (2015). Western Disturbances: A review. *Reviews of Geophysics*, 53(2):225–246.

Feng, L. and Zhou, T. (2012). Water vapor transport for summer precipitation over the Tibetan Plateau: Multidata set analysis. *Journal of Geophysical Research: Atmospheres*, 117(D20):1–16.

Feng, X., Liu, C., Rasmussen, R., and Fan, G. (2014). A 10-yr climatology of tibetan plateau vortices with NCEP climate forecast system reanalysis. *Journal of Applied Meteorology and Climatology*, 53(1):34–46.

Findell, K. L. and Eltahir, E. A. B. (2003). Atmospheric controls on soil moisture-boundary layer interactions: Three-dimensional wind effects. *Journal of Geophysical Research*, 108(838510):1–21.

Flohn, H. (1968). Contributions to a meteorology of the Tibetan Highlands. *Atmospheric Science Paper No. 130, Department of Atmospheric Science, Colorado State University, Colorado*.

Forsythe, N., Blenkinsop, S., and Fowler, H. J. . (2015). Exploring objective climate classification for the Himalayan arc and adjacent regions using gridded data sources. *Earth System Dynamics*, 6(1):311–326.

Galarneau, T. J., Hamill, T. M., Dole, R. M., and Perlwitz, J. (2012). A Multiscale Analysis of the Extreme Weather Events over Western Russia and Northern Pakistan during July 2010. *Monthly Weather Review*, 140(5):1639–1664.

Gao, Y., Cuo, L., and Zhang, Y. (2014). Changes in Moisture Flux over the Tibetan Plateau during 1979-2011 and Possible Mechanisms. *Journal of Climate*, 27(5):1876–1893.

Garreaud, R. D. (2007). Precipitation and circulation covariability in the extratropics. *Journal of Climate*, 20(18):4789–4797.

Gentine, P., Holtslag, A. a. M., D'Andrea, F., and Ek, M. (2013). Surface and Atmospheric Controls on the Onset of Moist Convection over Land. *Journal of Hydrometeorology*, 14(5):1443–1462.

Giovannettone, J. P. and Barros, A. P. (2009). Probing Regional Orographic Controls of Precipitation and Cloudiness in the Central Andes Using Satellite Data. *Journal of Hydrometeorology*, 10(1):167–182.

Guenther, F., Aichner, B., Siegwolf, R., Xu, B., Yao, T., and Gleixner, G. (2013). A synthesis of hydrogen isotope variability and its hydrological significance at the Qinghai–Tibetan Plateau. *Quaternary International*, 313-314:3–16.

Günther, F., Mügler, I., Mäusbacher, R., Daut, G., Leopold, K., Gerstmann, U. C., Xu, B., Yao, T., and Gleixner, G. (2011). Response of dD values of sedimentary n-alkanes to variations in source water isotope signals and climate proxies at lake Nam Co , Tibetan Plateau. *Quaternary International*, 236:82–90.

Hahn, D. and Manabe, S. (1975). The role of mountains in the south Asian monsoon circulation. *Journal of the Atmospheric Sciences*, 32:1515–1541.

Han, Y., Fang, X., Zhao, T., Bai, H., Kang, S., and Song, L. (2009). Suppression of precipitation by dust particles originated in the Tibetan Plateau. *Atmospheric Environment*, 43(3):568–574.

Hewitt, K. (2005). The Karakoram anomaly? Glacier expansion and the'elevation effect,'Karakoram Himalaya. *Mountain Research and Development*, 25(4):332–340.

Hoskins, B. J. and Ambrizzi, T. (1993). Rossby Wave Propagation on a Realistic Longitudinally Varying Flow. *Journal of the Atmospheric Sciences*, 50(12):1661–1671.

Houze, R. A. (2012). Orographic effects on precipitating clouds. *Reviews of Geophysics*, 50:RG1001.

Hren, M. T., Bookhagen, B., Blisniuk, P. M., Booth, A. L., and Chamberlain, C. P. (2009). δ18O and δD of streamwaters across the Himalaya and Tibetan Plateau: Implications for moisture sources and paleoelevation reconstructions. *Earth and Planetary Science Letters*, 288(1-2):20–32.

Immerzeel, W. W., Pellicciotti, F., and Bierkens, M. F. P. (2013). Rising river flows throughout the twenty-first century in two Himalayan glacierized watersheds. *Nature Geoscience*, 6(9):742–745.

Immerzeel, W. W., van Beek, L. P. H., and Bierkens, M. F. P. (2010). Climate Change Will Affect the Asian Water Towers. *Science*, 328(5984):1382–1385.

Janjic, Z. I. (2002). Nonsingular Implementation of the Mellor-Yamada Level 2.5 Scheme in the NCEP Meso model. *National Centers for Environmental Prediction Office Note*, #437:61.

Johansson, B. and Chen, D. (2003). The influence of wind and topography on precipitation distribution in Sweden: Statistical analysis and modelling. *International Journal of Climatology*, 23(12):1523–1535.

Joswiak, D. R., Yao, T., Wu, G., Tian, L., and Xu, B. (2013). Ice-core evidence of westerly and monsoon moisture contributions in the central Tibetan Plateau. *Journal of Glaciology*, 59(213):56–66.

Kang, S., Qin, D., Ren, J., Zhang, Y., Kaspari, S., Mayewski, P. a., and Hou, S. (2007). Annual Accumulation in the Mt. Nyainqentanglha Ice Core, Southern Tibetan Plateau, China: Relationships To Atmospheric Circulation over Asia. *Arctic, Antarctic, and Alpine Research*, 39(4):663–670.

Kuang, X. and Zhang, Y. (2005). Seasonal variation of the East Asian Subtropical Westerly Jet and its association with the heating field over East Asia. *Advances in Atmospheric Sciences*, 22(6):831–840.

Kurita, N. and Yamada, H. (2008). The Role of Local Moisture Recycling Evaluated Using Stable Isotope Data from over the Middle of the Tibetan Plateau during the Monsoon Season. *Journal of Hydrometeorology*, 9(4):760–775.

Lin, C., Chen, D., Yang, K., and Ou, T. (2018). Impact of model resolution on simulating the water vapor transport through the central Himalayas: implication for models' wet bias over the Tibetan Plateau. *Climate Dynamics*, 0(0):0.

Liu, J., Kang, S., Gong, T., and Lu, a. (2010). Growth of a high-elevation large inland lake, associated with climate change and permafrost degradation in Tibet. *Hydrology and Earth System Sciences*, 14(3):481–489.

Liu, W., Wang, L., Chen, D., Tu, K., Ruan, C., and Hu, Z. (2016). Large-scale circulation classification and its links to observed precipitation in the eastern and central Tibetan Plateau. *Climate Dynamics*, 46(11-12):3481–3497.

Liu, X. and Chen, B. (2000). Climatic warming in the Tibetan Plateau during recent decades. *International journal of climatology*, 1742:1729–1742.

Liu, X. and Yin, Z.-Y. (2001). Spatial and Temporal Variation of Summer Precipitation over the Eastern Tibetan Plateau and the North Atlantic Oscillation. *Journal of Climate*, 14(13):2896–2909.

Lu, N., Qin, J., Gao, Y., Yang, K., Trenberth, K. E., Gehne, M., and Zhu, Y. (2015). Trends and variability in atmospheric precipitable water over the Tibetan Plateau for 2000-2010. *International Journal of Climatology*, 35:1394–1404.

Luo, H. and Yanai, M. (1983). The Large-Scale Circulation and Heat Sources over the Tibetan Plateau and Surrounding Areas during the Early Summer of 1979. Part I: Precipitation and Kinematic Analyses. *Monthly Weather Review*, 111(5):922–944.

Ma, Y., Wang, Y., Wu, R., Hu, Z., Yang, K., Li, M., Ma, W., Zhong, L., Sun, F., Chen, X., Zhu, Z., Wang, S., and Ishikawa, H. (2009). Recent advances on the study of atmosphere-land interaction observations on the Tibetan Plateau. *Hydrology and Earth System Sciences*, 13(7):1103–1111.

Maussion, F., Scherer, D., Finkelnburg, R., Richters, J., Yang, W., and Yao, T. (2011). WRF simulation of a precipitation event over the Tibetan Plateau, China – an assessment using remote sensing and ground observations. *Hydrology and Earth System Sciences*, 15(6):1795–1817.

Maussion, F., Scherer, D., Mölg, T., Collier, E., Curio, J., and Finkelnburg, R. (2014). Precipitation Seasonality and Variability over the Tibetan Plateau as Resolved by the High Asia Reanalysis*. *Journal of Climate*, 27(5):1910–1927.

Medeiros, B., Hall, A., and Stevens, B. (2005). What controls the mean depth of the PBL? *Journal of Climate*, 18(16):3157–3172.

Mölg, T., Chiang, J. C. H., Gohm, A., and Cullen, N. J. (2009). Temporal precipitation variability versus altitude on a tropical high mountain: Observations and mesoscale atmospheric modelling. *Quarterly Journal of the Royal Meteorological Society*, 135(643):1439–1455.

Mölg, T., Maussion, F., and Scherer, D. (2014). Mid-latitude westerlies as a driver of glacier variability in monsoonal High Asia. *Nature Climate Change*, 4(1):68–73.

Norris, J., Carvalho, L. M. V., Jones, C., and Cannon, F. (2015). WRF simulations of two extreme snowfall events associated with contrasting extratropical cyclones over the western and central Himalaya. *Journal of Geophysical Research D: Atmospheres*, 120(8):3114–3138.

Patil, M. N., Patil, S. D., Waghmare, R. T., and Dharmaraj, T. (2013). Planetary Boundary Layer height over the Indian subcontinent during extreme monsoon years. *Journal of Atmospheric and Solar-Terrestrial Physics*, 92:94–99.

Roe, G. H. (2005). Orographic Precipitation. *Annual Review of Earth and Planetary Sciences*, 33(1):645–671.

Rose, B. E. J. and Lin, C. A. (2003). Precipitation from vertical motion: A statistical diagnostic scheme. *International Journal of Climatology*, 23(8):903–919.

Rüthrich, F. (2015). Lake-Related Cloud Dynamics on the Tibetan Plateau: Spatial Patterns and Interannual Variability. *October*, (617):5–7.

Saeed, S., Müller, W. a., Hagemann, S., and Jacob, D. (2010). Circumglobal wave train and the summer monsoon over northwestern India and Pakistan: the explicit role of the surface heat low. *Climate Dynamics*, 37(5-6):1045–1060.

Schiemann, R., Lüthi, D., and Schär, C. (2009). Seasonality and Interannual Variability of the Westerly Jet in the Tibetan Plateau Region*. *Journal of Climate*, 22(11):2940–2957.

Schiemann, R., Lüthi, D., Vidale, P. L., and Schär, C. (2008). The precipitation climate of Central Asia—intercomparison of observational and numerical data sources in a remote semiarid region. *International Journal of Climatology*, 28(3):295–314.

Shi, X., Wang, Y., and Xu, X. (2008). Effect of mesoscale topography over the Tibetan Plateau on summer precipitation in China: A regional model study. *Geophysical Research Letters*, 35(19):L19707.

Simmonds, I., Bi, D., and Hope, P. (1999). Atmospheric Water Vapor Flux and Its Association with Rainfall over China in Summer. *Journal of Climate*, 12:1353–1367.

References

Spiess, M., Schneider, C., and Maussion, F. (2015). MODIS-derived interannual variability of the equilibrium-line altitude across the Tibetan Plateau. *Annals of Glaciology*, 57(71):140–154.

Sugimoto, S., Ueno, K., and Sha, W. (2008). Transportation of Water Vapor into the Tibetan Plateau in the Case of a Passing Synoptic-Scale Trough. *Journal of the Meteorological Society of Japan*, 86(6):935–949.

Tao, S.-y. S. and Ding, Y.-h. (1981). Observational evidence of the influence of the Qinghai-Xizang (Tibet) Plateau on the occurrence of heavy rain and severe convective storms in China. *Bulletin of the American Meteorological . . .* , 62(1):23–30.

Thompson, L. G., Mosley-Thompson, E., Davis, M. E., Mashiotta, T. A., Henderson, K. A., Lin, P. N., and Tandong, Y. (2006). Ice core evidence for asynchronous glaciation on the Tibetan Plateau. *Quaternary International*, 154-155:3–10.

Tian, L., Masson-Delmotte, V., Stievenard, M., Yao, T., and Jouzel, J. (2001). Tibetan Plateau summer monsoon northward extent revealed by measurements of water stable isotopes. *Journal of Geophysical Research Atmospheres*, 106(D22):28081–28088.

Tian, L., Yao, T., MacClune, K., White, J. W. C., Schilla, A., Vaughn, B., Vachon, R., and Ichiyanagi, K. (2007). Stable isotopic variations in west China: A consideration of moisture sources. *Journal of Geophysical Research*, 112(D10).

Tian, W., Tian, H., Dhomse, S., and Feng, W. (2011). A study of upper troposphere and lower stratosphere water vapor above the Tibetan Plateau using AIRS and MLS data. *Atmospheric Science Letters*, 12(2):233–239.

Trenberth, K. E. (1999). Atmospheric Moisture Recycling: Role of Advection and Local Evaporation. *Journal of Climate*, 12(5):1368–1381.

Wang, B. (1987). The development mechanism for Tibetan Plateau warm vortices.

Webster, P. J., Magaña, V. O., Palmer, T. N., Shukla, J., Tomas, R. A., Yanai, M., and Yasunari, T. (1998). Monsoons: Processes, predictability, and the prospects for prediction. *Journal of Geophysical Research: Oceans*, 103(C7):14451–14510.

Webster, P. J., Toma, V. E., and Kim, H.-M. (2011). Were the 2010 Pakistan floods predictable? *Geophysical Research Letters*, 38(4):n/a–n/a.

Wu, Z., Li, J., Jiang, Z., and Ma, T. (2012). Modulation of the Tibetan Plateau snow cover on the ENSO teleconnections: From the East Asian summer monsoon perspective. *Journal of Climate*, 25(7):2481–2489.

Xu, G., Cui, C., Li, W., Zhang, W., and Feng, G. (2011). Variation of GPS precipitable water over the Qinghai-Tibet Plateau: Possible teleconnection triggering rainfall over the Yangtze river valley. *Terr. Atmos. Ocean. Sci.*, 22(2):195–202.

Xu, X., Lu, C., Shi, X., and Gao, S. (2008). World water tower: An atmospheric perspective. *Geophysical Research Letters*, 35(20):1–5.

Yanai, M., Li, C., and Song, Z. (1992). Seasonal Heating of the Tibetan Plateau and Its Effects on the Evolution of the Asian Summer Monsoon. *Journal of the Meteorological Society of Japan. Ser. II*, 70(1B):319–351.

Yang, K., Koike, T., Fujii, H., Tamura, T., Xu, X., Bian, L., and Zhou, M. (2004). The Daytime Evolution of the Atmospheric Boundary Layer and Convection over the Tibetan Plateau: Observations and Simulations. *Journal of the Meteorological Society of Japan*, 82(6):1777–1792.

Yang, K., Wu, H., Qin, J., Lin, C., Tang, W., and Chen, Y. (2014). Recent climate changes over the Tibetan Plateau and their impacts on energy and water cycle: A review. *Global and Planetary Change*, 112:79–91.

Yang, K., Ye, B., Zhou, D., Wu, B., Foken, T., Qin, J., and Zhou, Z. (2011). Response of hydrological cycle to recent climate changes in the Tibetan Plateau. *Climatic Change*, 109(3-4):517–534.

Yang, M., Yao, T., Gou, X., and Tang, H. (2007). Water recycling between the land surface and atmosphere on the Northern Tibetan Plateau—A case study at flat observation sites. *Arctic, Antarctic, and Alpine Research*, 39(4):694–698.

Yang, M., Yao, T., Wang, H., Tian, L., and Gou, X. (2006). Estimating the criterion for determining water vapour sources of summer precipitation on the northern Tibetan Plateau. *Hydrological Processes*, 20(3):505–513.

Yao, T., Masson-Delmotte, V., Gao, J., Yu, W., Yang, X., Risi, C., Sturm, C., Werner, M., Zhao, H., He, Y., Ren, W., Tian, L., Shi, C., and Hou, S. (2013). A review of climatic controls on δ 18 O in precipitation over the Tibetan Plateau: Observations and simulations. *Reviews of Geophysics*, 51(4):525–548.

Yao, T., Thompson, L., Mosbrugger, V., Zhang, F., Ma, Y., Luo, T., Xu, B., Yang, X., Joswiak, D. R., Wang, W., Joswiak, M., Devkota, L. P., Tayal, S., Jilani, R., and Fayziev, R. (2012a). Third Pole Environment (TPE). *Environmental Development*, 3:52–64.

Yao, T., Thompson, L., Yang, W., Yu, W., Gao, Y., Guo, X., Yang, X., Duan, K., Zhao, H., Xu, B., Pu, J., Lu, A., Xiang, Y., Kattel, D. B., and Joswiak, D. (2012b). Different glacier status with atmospheric circulations in Tibetan Plateau and surroundings. *Nature Climate Change*, 2(7):1–5.

Yasunari, T., Saito, K., and Takata, K. (2006). Relative Roles of Large-Scale Orography and Land Surface Processes in the Global Hydroclimate. Part I: Impacts on Monsoon Systems and the Tropics. *Journal of Hydrometeorology*, 7(4):626–641.

You, Q., Fraedrich, K., Ren, G., Ye, B., Meng, X., and Kang, S. (2012). Inconsistencies of precipitation in the eastern and central Tibetan Plateau between surface adjusted data and reanalysis. *Theoretical and Applied Climatology*, 109(3-4):485–496.

Zhang, B., Wu, Y., Zhu, L., Wang, J., Li, J., and Chen, D. (2011). Estimation and trend detection of water storage at Nam Co Lake, central Tibetan Plateau. *Journal of Hydrology*, 405(1-2):161–170.

Zhang, J. W. and Atkinson, B. W. (1995). Stability and wind shear effects on meso-scale cellular convection. *Boundary-Layer Meteorology*, 75(3):263–285.

Zhang, Y., Wang, D., Zhai, P., Gu, G., and He, J. (2013). Spatial Distributions and Seasonal Variations of Tropospheric Water Vapor Content over the Tibetan Plateau. *Journal of Climate*, 26(15):5637–5654.

A. Precipitation Seasonality and Variability over the Tibetan Plateau as Resolved by the High Asia Reanalysis

Maussion, F., D. Scherer, T. Mölg, E. Collier, **J. Curio**, and R. Finkelnburg, 2014: Precipitation Seasonality and Variability over the Tibetan Plateau as Resolved by the High Asia Reanalysis. *J. Climate*, 27, 1910–1927, doi: 10.1175/JCLI-D-13-00282.1.

Status: Published.

Own contribution:

- model simulation
- data post-processing
- scientific discussion

Precipitation Seasonality and Variability over the Tibetan Plateau as Resolved by the High Asia Reanalysis*

FABIEN MAUSSION, DIETER SCHERER, THOMAS MÖLG, EMILY COLLIER,+ JULIA CURIO, AND ROMAN FINKELNBURG

Chair of Climatology, Technische Universität Berlin, Berlin, Germany

(Manuscript received 14 May 2013, in final form 4 October 2013)

ABSTRACT

Because of the scarcity of meteorological observations, the precipitation climate on the Tibetan Plateau and surrounding regions (TP) has been insufficiently documented so far. In this study, the characteristics and basic features of precipitation on the TP during an 11-yr period (2001–11) are described on monthly-to-annual time scales. For this purpose, a new high-resolution atmospheric dataset is analyzed, the High Asia Reanalysis (HAR), generated by dynamical downscaling of global analysis data using the Weather Research and Forecasting (WRF) model. The HAR precipitation data at 30- and 10-km resolutions are compared with both rain gauge observations and satellite-based precipitation estimates from the Tropical Rainfall Measurement Mission (TRMM). It is found that the HAR reproduces previously reported spatial patterns and seasonality of precipitation and that the high-resolution data add value regarding snowfall retrieval, precipitation frequency, and orographic precipitation. It is demonstrated that this process-based approach, despite some unavoidable shortcomings, can improve the understanding of the processes that lead to precipitation on the TP. Analysis focuses on precipitation amounts, type, seasonality, and interannual variability. Special attention is given to the links between the observed patterns and regional atmospheric circulation. As an example of an application of the HAR, a new classification of glaciers on the TP according to their accumulation regimes is proposed, which illustrates the strong spatial variability of precipitation seasonality. Finally, directions for future research are identified based on the HAR, which has the potential to be a useful dataset for climate, glaciological, and hydrological impact studies.

1. Introduction

The Tibetan Plateau and adjacent mountain ranges (TP)—Himalayas, Karakoram, Pamir, Kunlun, and Qilian Shan (cf. Fig. 1)—play a crucial role for downstream hydrology and water availability in Asia (Immerzeel et al. 2010). Rainfall, snowmelt, and, to a lesser extent, glaciers dominate the hydrological budget of the TP (Bookhagen and Burbank 2010), but the relative importance of these factors varies largely between regions and watersheds (Kaser et al. 2010). Most glaciers in the Himalayas (Bolch et al. 2012) or on the Tibetan Plateau (Yao et al. 2012) are retreating, but they show contrasting patterns of shrinkage (Kääb et al. 2012). Local factors (e.g., exposition, topography, and debris coverage) partly account for these differences, but spatial and temporal heterogeneity of climate and climate change (Palazzi et al. 2013) play a role that has yet to be quantified, especially in the regions where in situ measurements are nonexistent.

The TP climate is under the combined and competitive influences of the East Asian and South Asian monsoons (Webster et al. 1998) and of the westerlies (Schiemann et al. 2009). The role of the TP as a controlling factor for the Asian monsoon system and for atmospheric circulation at hemispheric scale has been studied for a long time (Hahn and Manabe 1975) and continues to be a key research topic (e.g., Molnar et al. 2010; Wu et al. 2012). While the mechanical and thermal effects of the highly elevated TP on global circulation patterns has received much attention, the strength and nature of the couplings between the various monsoon

Denotes Open Access content.

* Supplemental information related to this paper is available at the Journals Online website: http://dx.doi.org/10.1175/JCLI-D-13-00282.s1.

+ Additional affiliation: Department of Earth and Atmospheric Sciences, University of Alberta, Edmonton, Alberta, Canada.

Corresponding author address: Fabien Maussion, Technische Universität Berlin, Chair of Climatology, Rothenburgstr. 12, 12165 Berlin, Germany.
E-mail: fabien.maussion@tu-berlin.de

DOI: 10.1175/JCLI-D-13-00282.1

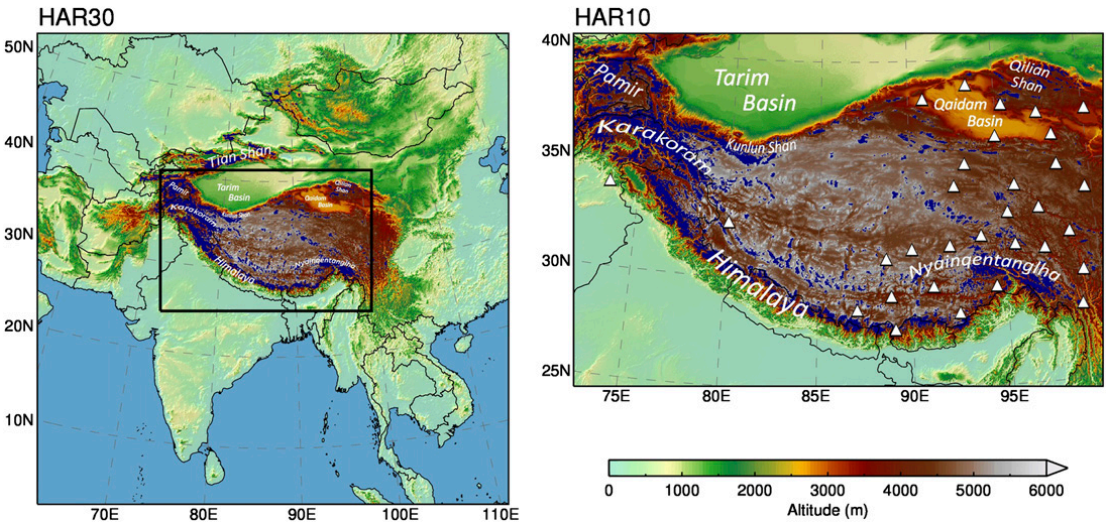

FIG. 1. Maps of the WRF model domains HAR30 (south-central Asia domain, 30-km resolution; 200 × 200 grid points) and HAR10 (High Asia domain, 10-km resolution; 270 × 180 grid points). Glacier outlines from the Randolph glacier inventory are drawn in blue, and the positions of the NCDC stations used for the validation are indicated by white triangles. Geographical locations mentioned in the text are indicated.

systems and the westerlies and especially their effects on TP precipitation variability remain less studied so far.

A substantial part of precipitation on the TP falls as snow. Spring TP snow cover has been proven to be a significant predictor for southwest Asian monsoon variability (Immerzeel and Bierkens 2010). The variability of snowfall frequency and intensity during spring/summer and related surface albedo conditions on glaciers also have a considerable impact on glacier mass balance. The timing and amount of snowfall in the early ablation (mass loss) season is a key process for the surface energy balance of glaciers and anomalous events (either dry or wet) initiate effects that can persist during the entire ablation season (e.g., Mölg et al. 2012; Yang et al. 2011, 2013). Glaciers on the TP are diverse in type regarding accumulation and ablation patterns, which are largely tied to precipitation amount and seasonality (Fujita 2008; Shi and Liu 2000).

The major reason for our lack of knowledge about the TP climate is the paucity of meteorological data. Permanent weather stations are scarce and confined to lower altitudes (Qin et al. 2009) and therefore are not representative of the high mountain climates. Global reanalysis datasets have coarse resolution that limits their representation of the mountainous topography. Of all climatological elements affected by topography, precipitation is probably the most complex and the most poorly represented by coarse-resolution grids (e.g., You et al. 2012; Bohner 2006).

Regional numerical weather prediction (NWP) models can be used to simulate precipitation fields and other meteorological variables at a high-spatiotemporal resolution. Longer time spans of years to decades can be simulated by NWP models by successive reinitialized model runs of shorter periods forced by large-scale observational datasets (e.g., Lo et al. 2008). In this study, we present a dataset generated using this method, that provides a tool to study atmosphere-related processes on the TP [the High Asia Reanalysis (HAR), described in section 2]. The HAR spans a period of more than 11 yr (October 2000–December 2011) and comprises two datasets with different spatial coverage and objectives: a domain of 30-km resolution including most parts of south and central Asia and a nested domain of 10-km resolution covering the TP and most parts of High Asia (Fig. 1). For simplicity, we use the acronym TP when referring to the Tibetan Plateau and surrounding mountain ranges as comprised in the 10-km-resolution High Asia domain.

The purpose of this study is twofold:

(i) describe the characteristics of precipitation (amount, type, seasonality, and variability) on the TP at monthly to annual time scales and obtain a more spatially detailed pattern than is possible from the few available observations (Fig. 1), as far as allowed by the accuracy and the resolution of the HAR and
(ii) provide some insights into the factors that lead to precipitation on the TP and propose perspectives for future research based on the HAR.

Producing accurate precipitation data using an atmospheric model is not trivial. Maussion et al. (2011, hereafter MA11) conducted a sensitivity analysis for a 1-month period during which strong rainfall and snowfall occurred on the TP and evaluated the model precipitation output

with (i) eight different physical parameterization schemes and (ii) several nesting and reinitialization configurations. No physical parameterization scheme outperformed the others for all the tests, but much effort went into choosing the model setup that performs best to produce the dataset presented in this study. In the first part of this paper, we assess the HAR precipitation output for the 11-yr period and evaluate its accuracy and potential errors. This evaluation is carried out by all available means; that is, by comparing the simulated precipitation with available surface and satellite observations but also by analyzing precipitation patterns and seasonality in the broader context of our current knowledge about precipitation in complex terrain and on the TP. The temporal resolution and extent of the HAR allows the analysis of processes from hourly to interannual time scales. In this study, we will not analyze diurnal cycles of precipitation or single stochastic weather events, although such aspects could also be addressed with the HAR dataset (see MA11).

In the following section, we describe the methods used to produce the HAR. The datasets used for the validation of the precipitation data are described in section 3. In section 4, we present and discuss the results. Section 5 shows an application example and provides a new map of glacier accumulation regimes based on precipitation seasonality. In section 6, we draw the conclusions of our study.

2. The High Asia Reanalysis dataset

To obtain gridded meteorological data at high-spatial and high-temporal resolutions, one general approach is to dynamically downscale a gridded global dataset that has been produced by data assimilation of a multitude of quality-controlled observations. Through data assimilation on the global scale, the resulting analysis or reanalysis dataset represents a physically consistent ''best guess'' of the state of the atmosphere at each time (usually at 6-h intervals). One of the basic requirements of our approach is that the downscaled data should represent as closely as possible the information that suitable observations would have delivered. This implies that the conditions at Earth's surface influencing atmospheric processes, particularly in the boundary layer, need to be described in sufficient spatial detail.

Lo et al. (2008) analyzed different dynamical downscaling methods and showed that consecutive reinitialized runs outperformed continuous long-term integrations with a single initialization, in particular when the reinitialization frequency was weekly instead of monthly. Other studies (e.g., von Storch et al. 2000) have successfully applied spectral nudging to continuous long-term integrations for dynamical downscaling, a technique that prevents the model from drifting away from the driving large-scale states while concurrently allowing the development of mesoscale processes. The major drawback of the latter method for our purposes is that no reinitialization takes place during which assimilated observations could possibly correct drifts in the land surface model or near-surface atmospheric variables.

MA11 tested different options for dynamical downscaling using reinitialization. Using almost the same domain as in this study, they showed for a test case that reinitialization sequences of daily runs outperformed weekly simulations. Based on these findings, we decided to follow a daily reinitialization strategy, which additionally prevents the land surface model from drifting away from the states provided by the analysis data. Several studies made use of this technique for regions of comparable environment (complex terrain and scarce observations): for example, Iceland (Bromwich et al. 2005), Greenland (Box et al. 2006), and the Arctic (Wilson et al. 2011).

The NWP model used to generate the HAR is the Advanced Research Weather Research and Forecasting model (WRF-ARW; Skamarock and Klemp 2008). The dataset consists of consecutive reinitialized model runs of 36-h time integration. Each run starts at 1200 UTC. The first 12 h from each run are discarded as spinup while the remaining 24 h of model output provide 1 day of the 11-yr-long time series. The model configuration used for the HAR is summarized in Table 1. The model is forced with the GFS operational model global tropospheric analyses [final analysis (FNL); dataset ds083.2], which are available every 6 h and have a spatial resolution of 1°. FNL data rely on numerous data sources, such as remote sensing data from Earth observing satellites assimilated together with surface and upper air reports from global observation networks. The data include pressure, geopotential height, temperature, dewpoint temperature, and wind direction and speed (National Centers for Environmental Prediction 2014). In the development phase of the HAR, the Interim European Centre for Medium-Range Weather Forecasts (ECMWF) Re-Analysis (ERA-Interim) dataset (Dee et al. 2011) was evaluated as a possible forcing dataset. We found that the accuracy of the HAR precipitation was improved when driven by FNL (Figs. S1–S3; see supplementary material). Moreover, initialization issues with ERA-Interim related to the treatment of snow cover in heavily glaciated grid cells[1] (Collier et al. 2013; Figs. S4–S6) and a summer cold bias on the TP further supported the choice of FNL.

[1] In ERA-Interim, snow depth is arbitrarily initialized at 10 m for grid cells with greater than 50% glacier coverage.

TABLE 1. HAR model strategy.

Map and grids	
Map projection	Lambert conformal
Center point of domain	30.0°N, 87.0°E
Number of vertical layers	28
Horizontal grid spacing	30 km and 10 km
Unstaggered grid points	200 × 200 and 270 × 180
Static geographical fields	U.S. Geological Survey (USGS) dataset at 10′ and 5′ resolution, glacier outlines from the RGI V1
Timing	
Simulation period	October 2000–September 2011
Time step	120 s and 40 s
Nesting strategy	
Nesting	Two-way nesting in cascade simulations
Forcing strategy	
Boundary conditions	National Centers for Environmental Prediction (NCEP) FNL from Global Forecast System (GFS) operational model global tropospheric analyses (1°, 6 hourly)
Sea surface temperature	NCEP Marine Modeling and Analysis Branch (MMAB) real-time global SST (RTG_SST) analysis (0.5°, daily)
Lake surface temperature	WRF model inland water module (avg_tsfc)
Initialization	Daily
Runs starting time	Daily, 1200 UTC
Runs duration	36 h
Spinup	12 h
Physical parameterization schemes	
Shortwave radiation	Dudhia scheme
Longwave radiation	Rapid Radiative Transfer Model (RRTM)
Cumulus parameterization	New Grell–Devenyi 3 sheme
Microphysics	Modified Thompson scheme
Land surface model	Noah land surface model (LSM)
PBL	Mellor–Yamada–Janjić turbulent kinetic energy (TKE)

In this study, a few minor setup changes with respect to MA11 were made, including upgrading the WRF model to version 3.3.1 and using the recently introduced inland water surface temperature initialization module. Since we expect the HAR dataset to be used as input data for hydrological and glaciological modeling, an adequate representation of ice-covered ground is important. Thus, we updated the original ice mask in the geographical land cover data with the Randolph glacier inventory, version 1.0 (RGI V1; Arendt et al. 2012). Since these modifications have a limited impact on the model output at regional scale (Collier et al. 2013), they will not be discussed here. The two-way nested cascading approach defined in MA11 has been followed here too. First the 10-km-resolution domain is run within the 30-km domain using the two-way nesting option, and then the 30-km-resolution domain is run alone to avoid inconsistencies due to the presence of the child domain. This allows us to consider the WRF model at 30 km (HAR30) and WRF model at 10 km (HAR10) as two different, complementary datasets.

Our approach using dynamical downscaling with short-term integration and daily reinitialization can be called ''regional reanalysis,'' following the ideas of, for example, Kanamitsu and Kanamaru (2007) or von Storch et al. (2000), who concluded that dynamical downscaling using spectral nudging may be seen as an indirect data assimilation technique. For the HAR we have not, however, performed data assimilation on the regional level, as is the case with ''true'' regional reanalyses like the North American Regional Reanalysis (NARR). Because of the scarcity of both surface observations and radio soundings as well as their inaccessibility, variational data assimilation is not possible for the TP. To our knowledge, such a comprehensive and process-based dataset is currently unique for the TP, and therefore the HAR is intended to fill a gap where other regional reanalyses are not available.

For the potential users of the dataset (atmospheric scientists, hydrologists, glaciologists, etc.), the WRF model output has been postprocessed for easy use. We provide separate data files per variable, per year, and per time aggregation (hourly, daily, monthly, and yearly), as well as vertically interpolated fields at standard pressure levels in addition to the model sigma levels. A webpage has been created for HAR users where the data can be downloaded (available at http://www.klima.tu-berlin.de/HAR). The range of applications of this dataset is rich and unexplored. So far, the HAR has been used by Mölg et al. (2012, 2014), who employed the HAR as input for a glacier energy and mass balance model; by Kropáček et al. (2013), who quantified the relation of air temperature and wind speed to the icing periods of large lakes on the plateau; and by Dietze et al. (2014), who analyzed sediment transport processes at four sites on the plateau.

We used the daily, monthly and yearly products from HAR30 and HAR10 (version 1) for this study. We consider the time span of October 2000–September 2011 but for simplicity we use the term ''decade'' for these 11 hydrological years. For the seasonality analyses we use the classical quarters: December–February (DJF), March–May (MAM), June–August (JJA), and September–November (SON). To avoid singularities we removed 10 and 5 grid points from the HAR30 and HAR10 domain boundaries, respectively. Unless specified otherwise, all figures and analysis are made using the original model grids.

3. Validation data and assessment methods

a. Weather stations

The HAR precipitation data are compared with rain gauge precipitation records from the ''Global Summary of the Day'' provided by the National Climatic Data Center (NCDC). We conduct our evaluation for the TP region. Thus, the weather stations selected for this study must satisfy two criteria: they are located within the HAR10 domain and are located above 2000 m MSL. We built monthly aggregated time series of precipitation rates (mm day^{-1}; day is abbreviated by d in figures) based on daily values and discarded months where less than 90% of the records were available. To ensure a correct reconstruction of the seasonal cycle at each station, we discarded the stations that did not include at least three valid months of each calendar month during the decade. After this filtering, 31 stations are left, of which 26 provide a gap-free time series, four contain a 1-month gap, and one has 51 valid months. The weather stations are not homogeneously distributed over the study region (Fig. 1), since they lie in more densely populated regions in the southern and eastern parts of the TP. In fact, some climatic precipitation regimes are not represented by this station population. To compare gridded precipitation data with the rain gauges, the nearest grid point is taken without interpolation (other interpolation methods—bilinear and cubic—did not change the results significantly). We use standard skill scores statistics for the assessment: mean deviation (MD; or mean bias), mean absolute deviation (MAD), and Pearson correlation coefficient r. For the daily precipitation occurrence statistics we use the Heidke skill score (HSS; Wilks 1995), computed from a contingency table (MA11, their Table 2). The HSS can only evaluate the detection or nondetection of discrete events; therefore, the tested events are defined as follows: precipitation exceeds a threshold T. The HSS indicates the capability of a simulation to be better or worse than a random simulation and ranges from -1 to 1 (1 for a perfect simulation and 0 for a random guess).

b. TRMM precipitation

Because of the uneven spatial distribution of the stations, we also compare the HAR precipitation output to precipitation estimates from the Tropical Rainfall Measuring Mission (TRMM). The TRMM precipitation estimates are derived from a combination of remote sensing observations calibrated against a large number of rain gauges on a monthly basis. In this study, the 3B42 (daily) and 3B43 (monthly) version 7 products are used (Huffman et al. 2007). The TRMM dataset covers the regions between 50°N and 50°S with a spatial resolution of 0.25°. It has been previously used to study convective activity on the TP (Yaodong et al. 2008) and in northern India (Medina et al. 2010), to study the diurnal cycle of precipitation over the TP (Zhou et al. 2008), and to validate atmospheric modeling studies (Chow and Chan 2009; MA11). The resolution of the TRMM 3B43 product (~28 km) allows a quantitative evaluation of HAR30 precipitation only.

As indicated by its name, TRMM was primarily designed for measuring tropical (i.e.: convective) rainfall. It has been shown that its accuracy on the TP is affected by sampling problems because of low grid resolution (Bookhagen and Strecker 2008; Yin et al. 2008). The authors of the latter study emphasize that TRMM performs poorly during winter, because of the presence of snow and ice over the TP (snow and ice on the ground scatter microwave energy in a similar fashion as ice crystals and raindrops in the atmosphere). Therefore, TRMM estimates in winter and more generally over the TP region should be analyzed with care.

Additionally, we used the 1998–2009 rainfall climatologies from Bookhagen and Burbank (2010). This dataset is processed from the TRMM 2B31 product and is a rainfall estimate at higher resolution than the TRMM 3B43 product (~5 km). Only the mean decadal climatologies are freely available, and they are computed for a slightly different period than the decade we consider. Therefore, we use the TRMM 2B31 dataset to qualitatively compare orographic precipitation with the HAR10 precipitation product.

4. Results and discussion

a. Seasonal climatologies at the synoptic scale

An overview of DJF and JJA climatologies derived from HAR30 is provided in Fig. 2. In DJF (left panel), a geopotential height (GPH) gradient produces strong westerly winds (Figs. 2c,e) over much of the domain (the GPH maximum, hidden by the color scale, is located at ~13°N). The winter monsoonal land to sea breeze (e.g., Qian and Lee 2000) characterizes the surface wind regime in the tropics (Arabian Sea, Bay of Bengal, and South China Sea; Fig. 2a). On the TP the westerlies dominate while in the north, surface winds are heterogeneous. The DJF season is mostly dry (Fig. 2a): precipitation occurs over land 1) in central Asia and western TP as a result of the orographic uplift of the westerly flow, 2) at coastal areas under moist sea-breeze flow (e.g., Vietnam, Malaysia, Sri Lanka), and 3) in southern China.

In JJA, the core Asian summer monsoons (ASM) season, the circulation patterns change dramatically.

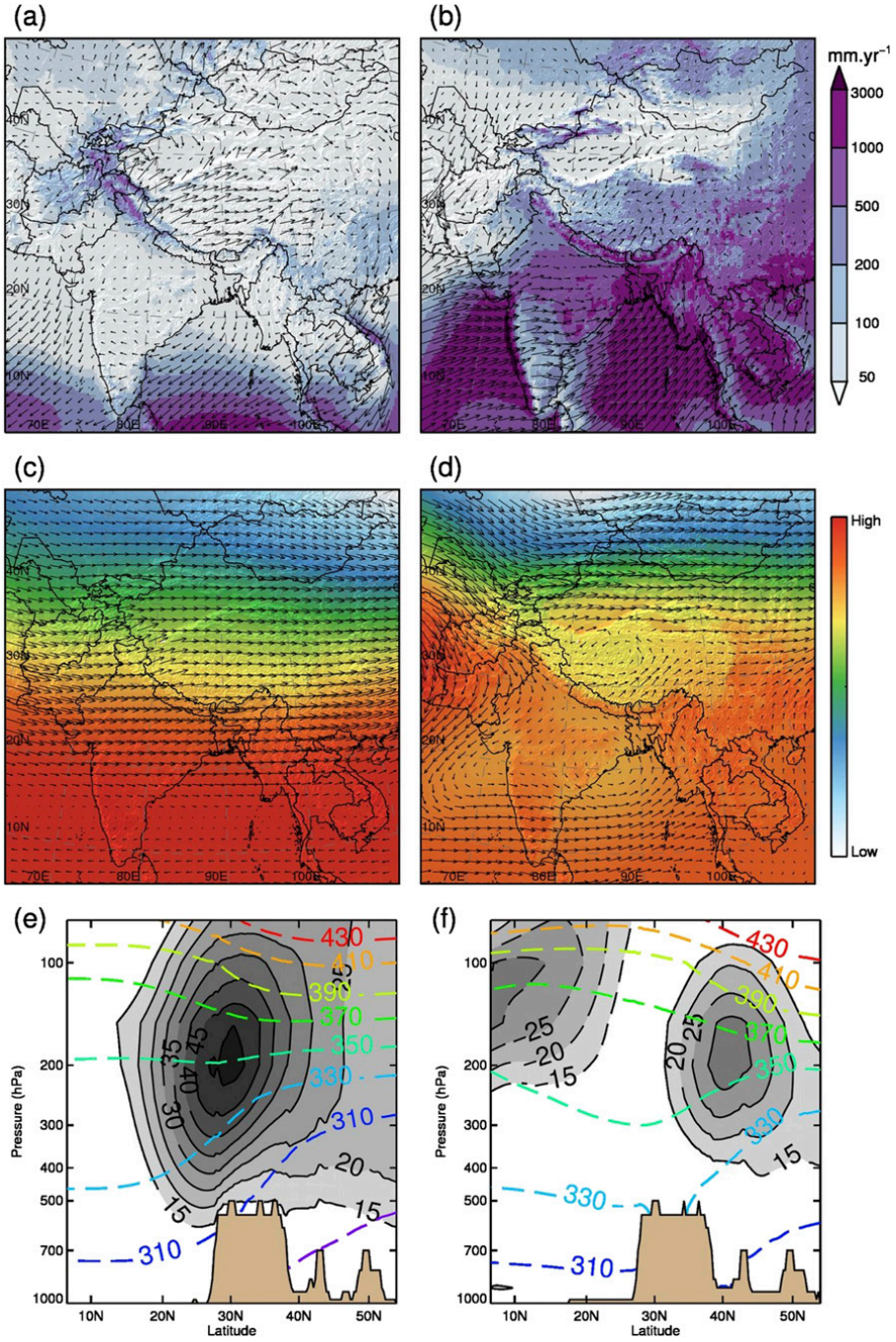

FIG. 2. Decadal (2001–11) seasonal means in the HAR30 dataset for (left) DJF and (right) JJA. (a),(b) Total precipitation and 10-m wind vectors (every fifth grid point). (c),(d) Geopotential height and horizontal wind vectors at the 500-hPa level. Note that the color scale represents a different range for winter (low: 5.24 km; high: 5.89 km) and summer (low: 5.67 km; high: 5.90 km). (e),(f) Horizontal wind speed ($m\,s^{-1}$; gray shades) and potential temperature (K; dashed color contours) along a latitude–pressure transect at 90°E. Dashed gray contours represent negative zonal wind.

The reversal of surface winds over oceans and coasts is characteristic of the monsoonal climate (Fig. 2b). The westerly flow is weaker and the main jet axis is shifted to the north (40°N; Fig. 2f) as a result of the summer hemisphere heating. Simultaneously, the tropical easterly jet forms in the upper troposphere. The warmest air in the free atmosphere is now located south of the TP as evident from the potential temperature field, as a result of both surface and convective heating. Two midtroposphere low pressure systems characterize the mean

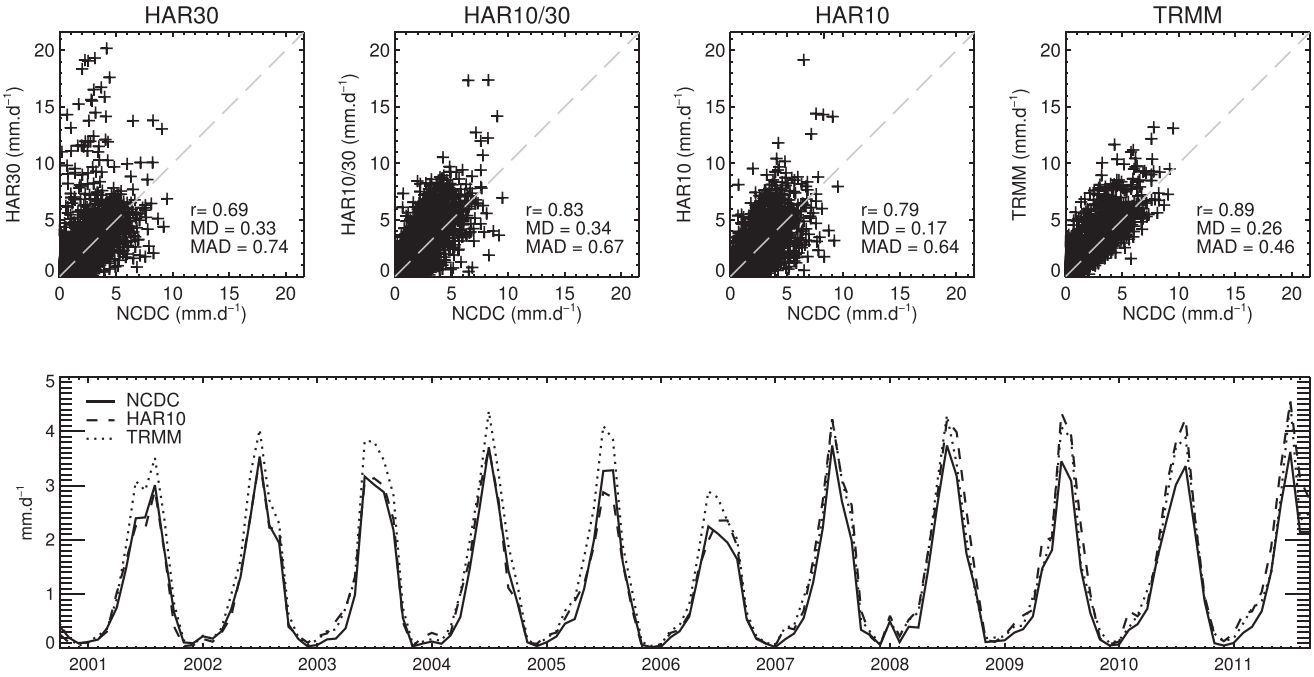

FIG. 3. Comparison of monthly precipitation rates (mm day^{-1}; 2001–11) with NCDC stations observations (31 stations; 4007 valid months). (top) Scatterplots of HAR30, HAR10/30, HAR10, and TRMM 3B43 and statistical scores *r*, MD (mm day^{-1}), and MAD (mm day^{-1}). HAR10/30 is constructed by spatially averaging HAR10 on the HAR30 grid. (bottom) Monthly precipitation time series (mm day^{-1}) averaged for all stations.

atmospheric circulation patterns at 500 hPa (Fig. 2d; Wang 2006): the monsoonal depression over India (which extends from the surface up to ~400 hPa) and the thermal low over the TP (confined to the TP boundary layer). Surface winds over the TP and partly over India follow the 500-hPa flow, with the exception of the Arabian Sea where surface winds are flowing in the opposite direction (they follow the Somali jet at ~850 hPa; not shown). The combined blocking effects of topography and of the Tibetan low seem to divide the 500-hPa westerly flow reaching the TP in a south and north stream. As a result of the ASM circulation, precipitation is observed at the Indian southwest coast, in Bangladesh, in the Indochinese peninsula, and in southeast China (Fig. 2b). The blocking effect of the Himalayas on the low-level atmospheric flow is clearly visible, as well as the orographically induced precipitation spells at the mountain ridges. The Pamir and Karakoram mountain ranges are mostly dry, but the Tien Shan is wetter than in DJF.

b. Comparison with observations

1) MONTHLY PRECIPITATION

We compare HAR and TRMM monthly precipitation with station observations in Fig. 3. The top panel shows the scatterplots and skill statistics for all stations and months. The results indicate an improvement between HAR30 and HAR10, as the former tends to overestimate precipitation and shows larger scatter. This confirms the findings of MA11 and other studies (e.g., Heikkila et al. 2011) that demonstrated the positive effect of higher resolution in complex terrain on simulated precipitation. The added value of higher resolution is also evident when spatially averaging the HAR10 dataset on the HAR30 grid (HAR10/30). The HAR10/30 still shows an improvement to HAR30 and has even slightly better correlation values than HAR10, while the other HAR10 scores remain better. The TRMM 3B43 product better explains the variance at the stations (higher correlation and lower MAD) but has a larger positive bias (MD).

Precipitation seasonality and interannual variability is well reproduced by the HAR (Fig. 3, bottom panel). Anomalous events on the TP, such as the driest year 2006 or the wet winter of 2008, are well represented. For the averaged time series, HAR10 is closer to observations than the TRMM 3B43 product (MD of 0.089 and 0.26 mm day^{-1} and MAD of 0.23 and 0.26 mm day^{-1}, respectively). However, the HAR diverges from the station data after 2007 in the summer months. The reasons for the disagreement are unclear, but the shift could be related to changes in the FNL assimilation system that occurred in 2007 (K. Manning 2013, personal communication). We compared HAR30 with the TRMM 3B43 product over the HAR30 domain and

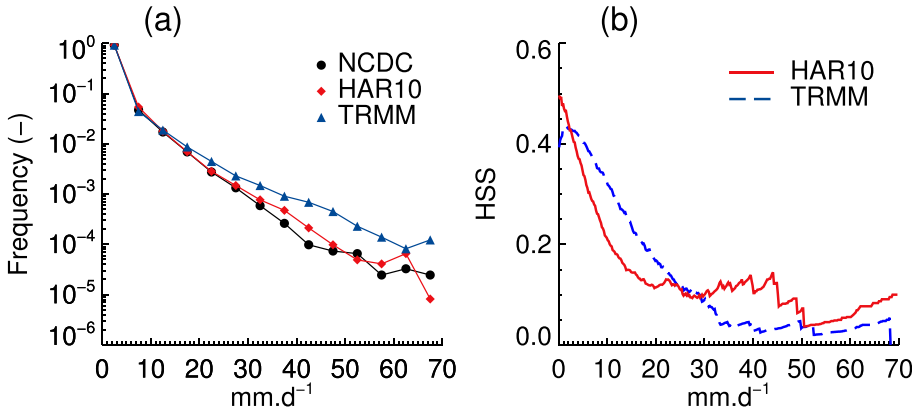

FIG. 4. (a) Histograms of daily precipitation amounts in the NCDC stations, HAR10, and TRMM data (note the logarithmic scale of the *y* axis) and (b) HSS for daily precipitation.

found that the statistical metrics are regular and constant throughout the decade, and no singularities could be detected (see Fig. S7 in the supplemental material). Similarly, we reproduced the analysis presented in Fig. 3 for all stations available in HAR10 (not only on the TP, thus doubling the number of stations) and found that (i) the updated scores confirms the results of Fig. 3 and (ii) the period 2007–11 does not appear to be singular (Fig. S8). Therefore, we argue that this shift either is only occurring on the TP or is an artefact resulting from the small number of stations used for the validation.

In Fig. S9 of the supplemental material, we present further validation analysis, this time by considering the mean seasonal cycle at each station location. Most stations have a characteristic summer precipitation regime but there are variations in both shape and magnitude that are captured by the HAR. It is worth noting that both TRMM and HAR show inconsistent deviations (positive or negative) at stations located close to each other. Since both datasets are produced with a spatially consistent methodology, these discrepancies are probably related to spatial sampling problems.

2) DAILY PRECIPITATION

One of the key objectives of the regional reanalysis is to represent past weather and therefore to be able to trace precipitation events (see MA11 for a day-by-day analysis of a severe precipitation event on the TP). Figure 4a shows the histograms of daily mean precipitation at the station locations for HAR10 and TRMM 3B42. The three histograms are close to each other for lower precipitation amounts (about 92% of all days are found in the 0–5 mm day^{-1} bin), but TRMM 3B42 overestimates the frequency of higher precipitation amounts (Zhou et al. 2008 also report that TRMM overestimates the frequency of precipitation in the diurnal variation). The HAR10 histogram is close to the stations, even for the extreme events. The HSSs of TRMM 3B42 and HAR10 are displayed in Fig. 4b. The HAR is closer to the stations for small thresholds, a feature that could be a result of the known problems of TRMM in detecting small raindrops and other issues related to irregular satellite overpasses (Kidd and Levizzani 2011). The HSSs decay rapidly for larger thresholds and faster for HAR10 than for TRMM 3B42. For higher amounts HAR10 performs better again, in accordance with the histograms presented in Fig. 4a.

c. *Precipitation over the TP and orography*

Figure 5a shows the decadal mean of HAR10 annual precipitation over the TP. There are large regional contrasts, from less than 50 mm yr^{-1} in the Tarim basin to more than 6000 mm yr^{-1} (35 grid points) in the southeast Himalayan foothills. As shown in Fig. 2b, the moist flow originating in Bay of Bengal is blocked by the Himalayas and redirected northwest following the range, generating an east–west precipitation gradient. The uplift caused by the Himalayan range generates an orographically induced "precipitation barrier," leaving the regions north of the range with drier air masses and less precipitation. On the TP, there is a clear southeast–northwest gradient, which is often attributed to the fact that most of the moisture is transported from the southeast by the monsoonal flow (e.g., Feng and Zhou 2012).

For completeness, we plotted TRMM 3B43 mean precipitation for the same period (Fig. 5b) and the 1998–2008 rainfall decadal mean from TRMM 2B31 (Fig. 5c). Similar features are observable in all three datasets: for example, the location of precipitation maxima, the gradients, the precipitation belt along the Himalayas, and the dry Tarim and Qaidam basins. However, HAR10 and TRMM 2B31 are more in agreement for detailed patterns such as the dry spell in the lee side of the

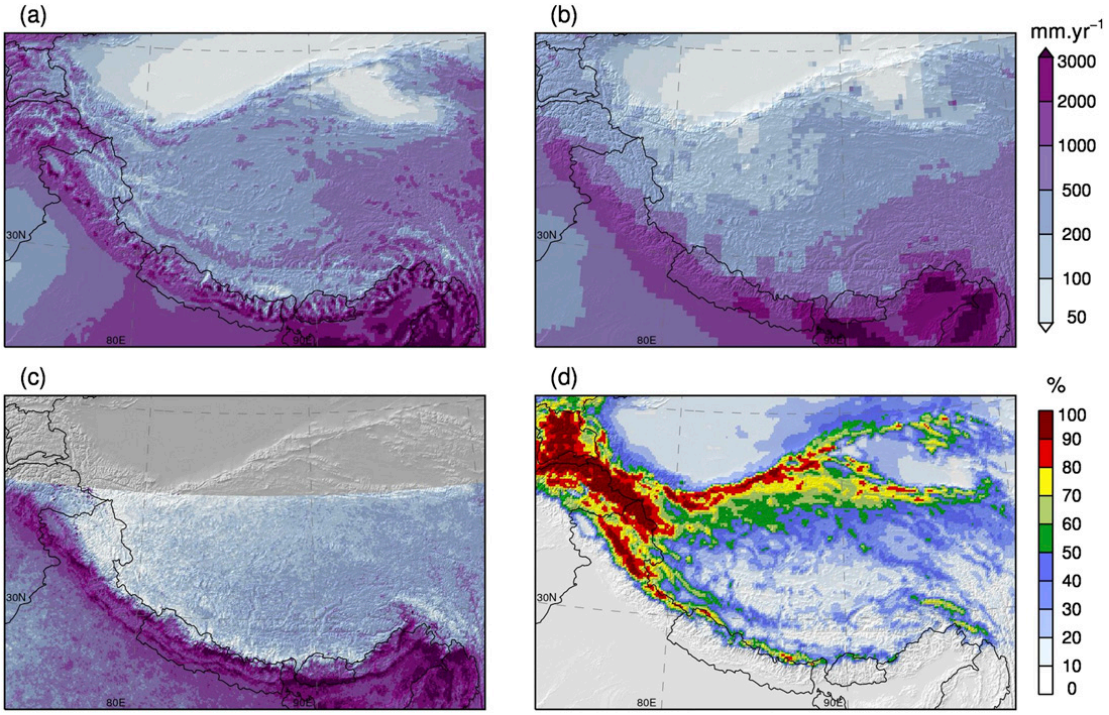

FIG. 5. Decadal means of annual precipitation for (a) HAR10 and (b) TRMM 3B43, (c) annual rainfall for TRMM 2B31, and (d) percentage of HAR10 precipitation falling as snow. Note that the decadal mean for TRMM 2B31 (1998–2008) covers a different period than HAR10 and TRMM 3B43 (2001–11).

Himalayas. The influence of orography is less pronounced in TRMM 3B43 on the TP, while it plays an obvious role in triggering precipitation in TRMM 2B31 and HAR10. The largest differences at regional scale between HAR10 and TRMM 3B43 are found in the Pamir and Karakoram regions and in northwestern Tibet. These regions experience mostly winter precipitation (Fig. 2a), with the majority falling as snow (Fig. 5d). The regions with large snowfall contribution to the total precipitation are the high mountains and the northwestern part of the TP, where temperatures are lower.

Interestingly, regions with larger discrepancies between TRMM and HAR10 correspond to areas with higher snowfall percentages. This is corroborated in Fig. 6, which shows the relative difference between TRMM 3B43 and HAR10 plotted against snowfall contribution at each grid point. There is a clear relationship between precipitation difference and snowfall, which is consistent with results of previous studies of possible TRMM detection errors of frozen precipitation (e.g., Yin et al. 2008). Although it is generally difficult to quantify the accuracy of the HAR snowfall data, there is support from studies in high mountains that the WRF model is able to reproduce observations (e.g., Mölg and Kaser 2011; Mölg and Scherer 2012). We repeat the analysis of Mölg and Scherer (2012) at one station location where snowfall information was available (Fig. S10 in the supplemental material) and found that the HAR captures well the phase of the precipitation compared with observations.

Bookhagen and Burbank (2010) suggested that two topographic classes can be defined along the Himalayas: either (i) the mean topography rises more or less steadily to an average elevation of 5 km (one-step topography) or (ii) it follows a two-step morphology in which the

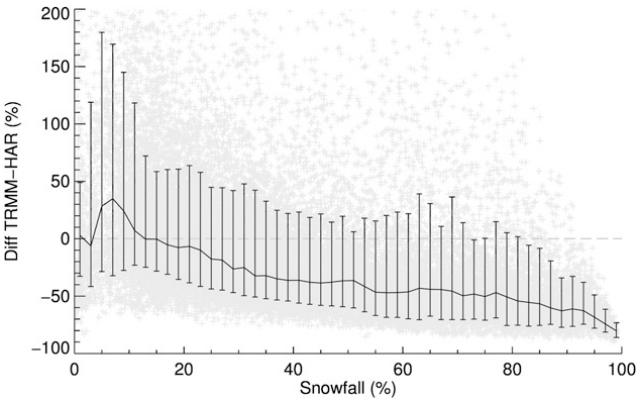

FIG. 6. Relative difference in annual precipitation between TRMM 3B43 and HAR10 with HAR10 as reference, as a function of annual snowfall fraction (%) in the HAR data. Each gray point represents one data point, and the curve represents 2%-wide binned median with 10% and 90% percentiles as error bars.

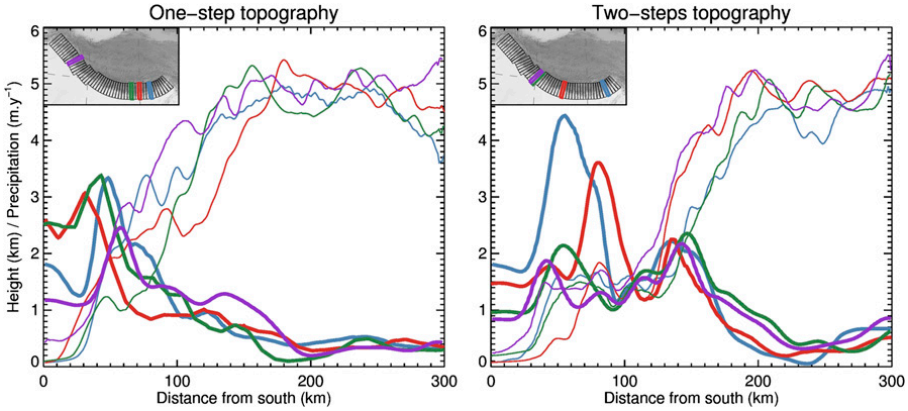

FIG. 7. Mean annual precipitation from HAR10 ($m\,yr^{-1}$; thick lines) and 30-km Shuttle Radar Topography Mission (SRTM30) topography (km; thin lines) along four 50-km-wide and 300-km-long south–north swaths. The swaths locations are indicated in the inset maps [swaths from Bookhagen and Burbank (2010)].

outer step corresponds to the Lesser Himalayas and the inner step to the Higher (Greater) Himalayas. The authors showed that precipitation in TRMM 2B31 mimics these two classes of topographic profiles. Such patterns are expected and known from the underlying processes of mountain–airflow interactions (e.g., Colle 2008). To evaluate HAR10 precipitation in this context, we computed the mean transect precipitation along several profiles and show examples of the two classes in Fig. 7. The HAR precipitation profiles follow similar features as the profiles in Bookhagen and Burbank (2010, their Fig. 7) but seem to slightly underestimate precipitation maxima, perhaps because of the coarser resolution of the HAR. This analysis underlines the importance of topography and snowfall for precipitation patterns on the TP and the added value of high-resolution modeling in this region.

Altogether, these results give confidence in the accuracy of the HAR with respect to the requirements of this study and indicate that it is free of a systematic precipitation error. Previous studies reported that the WRF model overestimates precipitation in mountainous terrain (e.g., Caldwell et al. 2009), but we find no evidence for this. Area averaged over the whole HAR10 domain, the model produces 15% more precipitation than TRMM 3B43 (734 versus 636 $mm\,yr^{-1}$, respectively), which we assume to be partly related to problems of TRMM snowfall retrievals.

d. Precipitation timing and seasonality on the TP

Figure 8 shows the contribution of each season to annual precipitation during the last decade. The Karakoram and Pamir regions form one coherent unit, with most precipitation falling in DJF and MAM and almost no precipitation in JJA. Precipitation in MAM shows two bands (north and south of the TP), indicating that these two spells have different origins. Most precipitation in the domain falls in JJA, especially in India and central TP but also in the northeasterly Qilian Mountains. In SON the patterns are fairly uniform, representing 10%–20% of the annual precipitation.

We analyze the seasonal cycle of precipitation in Fig. 9, this time by showing the contribution of each month to the annual precipitation, together with mean horizontal wind vectors at the 500-hPa level. With a height of approximately 5700 m, this level is a good indicator for the TP boundary layer flow. We start the description of the annual cycle in October, beginning of the hydrological year and end of the monsoon period. Low precipitation occurs in the southeast of the domain, and the winter precipitation season in the northwestern TP is starting. The seasonal cycle of precipitation in the northwest is tied to the location of the jet stream (Schiemann et al. 2008). Moisture is brought by southwesterly cyclones from the east of the Mediterranean and the Arabic Sea but under the stable winter conditions precipitation is mostly triggered by orography (e.g., Jiang 2003). From November to March, the 500-hPa zonal flow is constant and hardly perturbed by the mountains. The maximal winter precipitation intensity is reached in February. In March, the westerly jet starts to shift to the north, marking the beginning of the precipitation season in northern TP, which culminates in May–June. The first disturbances of the winter zonal flow occur in April, and the first indications for the formation of the Tibetan low appear in May. The center of this cyclonic system is not located in the south of the TP as one might expect because of stronger solar heating. Its location could be related to a combination of thermal and dynamical effects (Sugimoto and Ueno 2010).

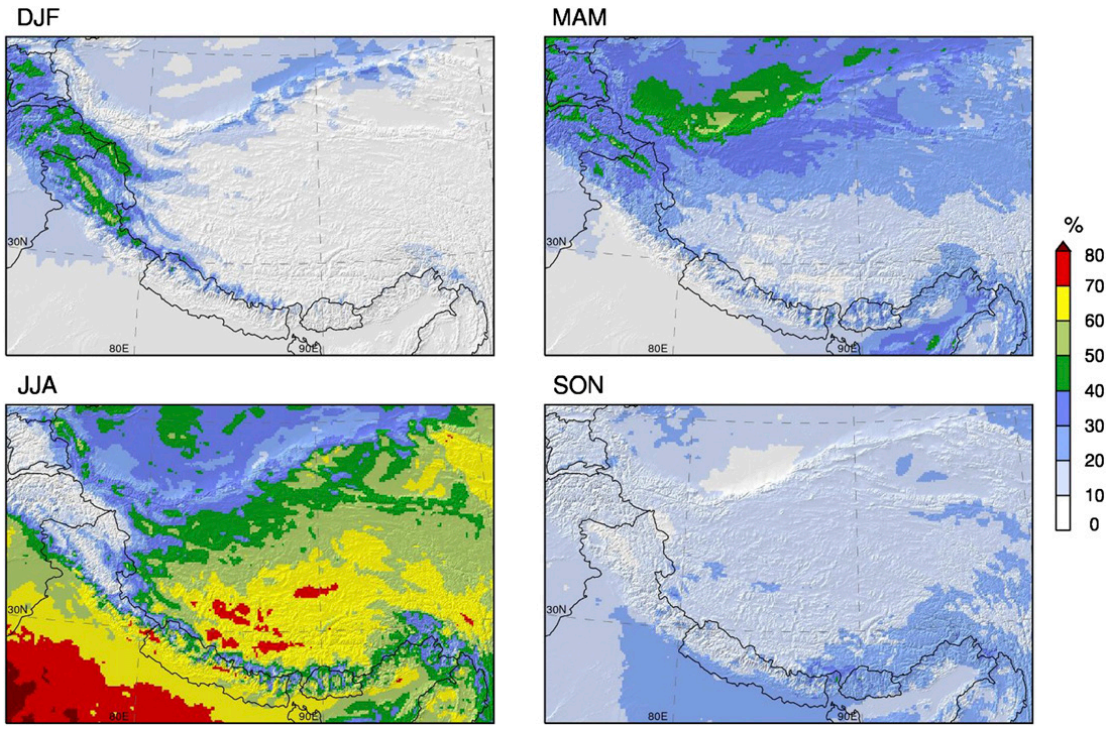

FIG. 8. Contribution (%) of DJF, MAM, JJA, and SON to the HAR10 mean annual precipitation.

The cyclonic circulation on the plateau is established months before the monsoonal circulation, characterized by a reversal of the flow south of the Himalayas. The circulation patterns on the TP during the transition phase (May–June) suggest a combined influence of southerly and westerly flows on precipitation on the TP. The circulation conditions remain stable in July and August, and the wet spell on the TP originates from its southern and eastern parts. There is an abrupt transition between the dry Pamir–Karakoram region and the wetter Pakistan lowlands. Finally, in September the Tibetan low decays and the remainder of the summer precipitation is evenly distributed over the TP.

e. *Precipitation frequency and role of convective precipitation*

Figure 10a shows the average number of precipitation days (>1 mm day^{-1}) per hydrological year. The number of precipitation days is related to precipitation amounts (cf. Fig. 5a), but this relationship is neither constant nor linear, as shown in Fig. 10c. As indicator for the occurrence of strong precipitation events, we count the smallest number of precipitation days needed to reach 50% of the yearly precipitation amounts (on average) and we divide it by the number of precipitation days shown in Fig. 10a to obtain Fig. 10b. A location with constant and regular precipitation days will then have a value of 50%, and a location with mostly light precipitation days but with a few strong precipitation events will have a lower value. We see in Fig. 10c that the number of days needed to reach 50% of the yearly precipitation is less dependent on the precipitation amount than precipitation frequency: it quickly reaches a value of approximately 25 days.

Most locations subject to strong precipitation events are located south of the TP. The most critical regions (where less than 15% of the precipitation days suffice to reach 50% of the annual precipitation amount) are not located in northeastern India, where most precipitation occurs, but in Pakistan and northwestern India, regions known to have experienced severe floods in the last decade (Webster et al. 2011) or cloud bursts (Kumar et al. 2012). On the plateau, Figs. 10a and 10b indicate less strong but more frequent precipitation events, in accordance with observational studies that documented the regularity of summer precipitation in central TP (Ueno et al. 2001) and a pronounced diurnal cycle related to frequent local convective activity (Liu et al. 2009).

The contribution of convective precipitation as diagnosed by the model physics to the annual precipitation is shown in Fig. 11. Precipitation is mostly convective in India, in the south ridge of the Himalayas and in large valleys, but barely any convection is triggered in higher mountains and in areas with frequent snowfall. Another large area of convective precipitation is found in central TP, in accordance with the results of several studies (e.g., Fu et al. 2006). Interestingly, the location of the center of the summer low pressure system on the TP (Fig. 9) does not match with the maximum occurrence

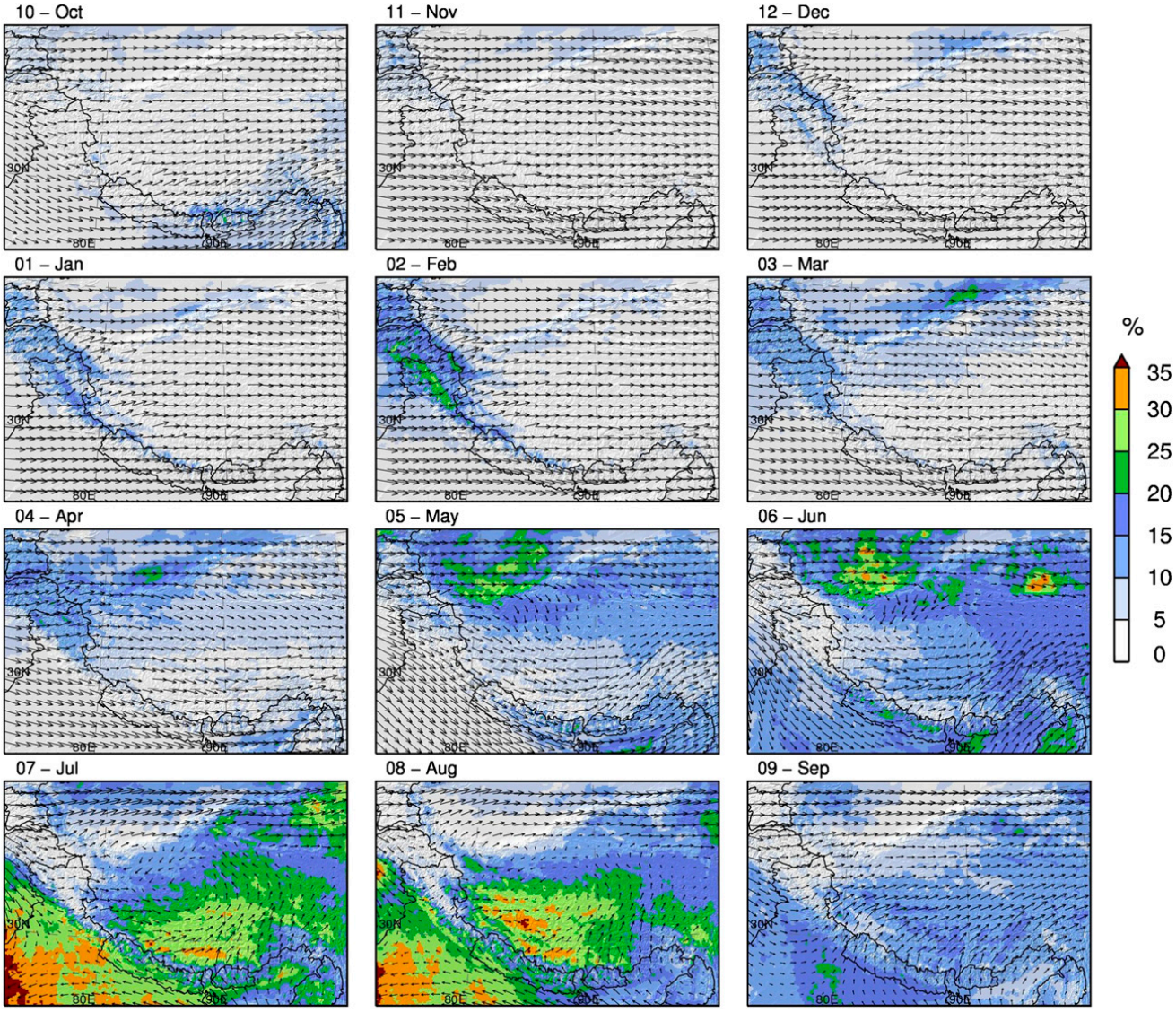

FIG. 9. Contribution (%) of each month to the HAR10 mean annual precipitation and mean monthly 500-hPa wind vectors (plotted every eighth grid point).

of convective precipitation, which is located more to the south. The location of the two areas of convective precipitation in Fig. 11 (central and eastern TP) matches well observations by Sugimoto and Ueno (2010, their Fig. 1).

f. Precipitation interannual variability

In addition to precipitation amount and regime, the variability of precipitation is important in characterizing a region's hydrological features. In Fig. 12, we describe interannual variability during the last decade considering hydrological years. We use the coefficient of variation c_v of annual precipitation, which is defined as the ratio between the standard deviation and the mean of precipitation. This metric provides more useful information than the standard deviation alone, since the latter is strongly related to precipitation amounts. The c_v is high in western and central TP and in northwestern India and is rather low in elevated areas and in the east (Fig. 12a). The relationship between the c_v and annual precipitation is shown in Fig. 12b. The c_v is, on average, only slightly related to precipitation for high amounts but much more for small amounts (e.g., Tarim and Qaidam basins). As proposed by Jurković and Pasarić (2013) based on the earlier work of Conrad (1941), we define the theoretical expected c_v as a decreasing hyperbolic function,

$$ec_v = \frac{B}{\overline{P} + C} + A, \tag{1}$$

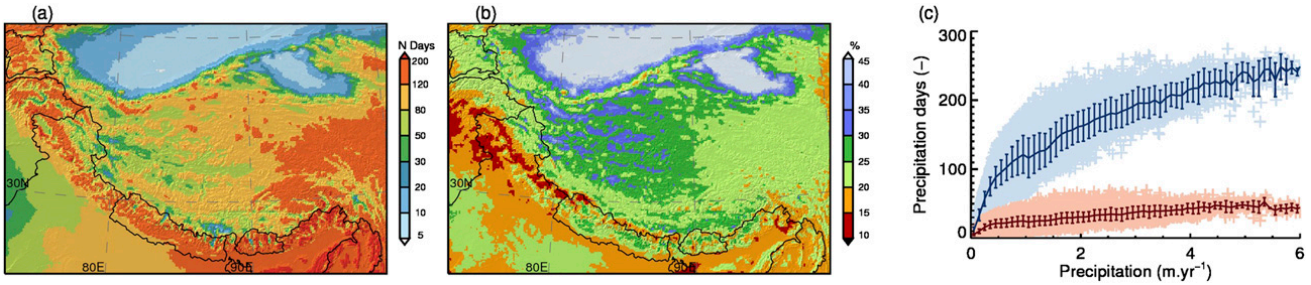

FIG. 10. Precipitation frequency and occurrence of large precipitation events. (a) Average number of precipitation days (>1 mm day^{-1}) per hydrological year (October–September). (b) Ratio (%) between the average number of days needed to reach 50% of the annual precipitation amount and the number of precipitation days per year. (c) Number of precipitation days (blue) and number of precipitation days needed to reach 50% of the annual precipitation amount (red) vs mean annual precipitation. The curves represent 0.1-m-wide binned means with $\pm 1\sigma$ error bars.

where $\overline{P}$ is the mean annual precipitation and A, B, and C are parameters to be obtained by least squares fitting. We obtain 17.17% for A, 5.99 m yr^{-1} for B, and 0.10 m yr^{-1} for C. Our constant A (representative of ec_v for high precipitation amounts) is similar to the one from Jurković and Pasarić (2013) of 15.37%. Unlike Jurković and Pasarić (2013), who computed ec_v for the whole globe, our ec_v is representative for the HAR10 region only. We use this theoretical curve to compute the c_v anomaly $c_v a$, which is defined as the difference between the c_v and the ec_v at each grid point. The resulting purple (brown) areas in Fig. 12c correspond to areas with higher (lesser) variability than "expected" in the domain. For instance, it appears that the relatively dry Qaidam basin has a high c_v but a negative $c_v a$, which means that it has a smaller interannual variability than expected from the annual precipitation amounts. Northwestern India and Pakistan show the strongest positive $c_v a$ (these regions correspond to the positive difference between the binned mean curve and the ec_v around 1 m yr^{-1} in Fig. 12b). The central and western TP also show more interannual variability than their neighboring TP areas.

In Fig. 13, we reproduce the analysis for the three precipitation seasons, DJF, MAM, and JJA. Precipitation in DJF has a spatially regular interannual variability, of about 20%–25%. The areas with higher variability are located at the southern edges of the Karakoram, where the influences of western disturbances that drive winter precipitation may be less continuous in this season. In MAM, the highest interannual variability is observable in the northwestern Tarim basin and, importantly, in the southeastern Himalayas (here the variability of the Indian summer monsoon onset probably accounts for a larger than average interannual variability of precipitation). The patterns of c_v and $c_v a$ in JJA resemble those of annual precipitation (Fig. 12c), which means that most of precipitation interannual variability is explained by summer precipitation variability.

5. An application example: Classification of glacier accumulation regimes

As discussed in the introduction, the TP hydrological cycle is strongly dependent on precipitation amounts and on seasonality. The works by Fujita (2008) and Mölg et al. (2012) emphasized the high sensitivity of glaciers on the TP to precipitation seasonality. Shi and Liu (2000) proposed a classification of the glaciers on the TP according to their continentality (maritime, subcontinental, and continental). Rupper and Roe (2008) proposed another grouping into three classes (western, eastern, and northern) according to the differences in spatial and temporal variability of the glaciers during the last glacial cycle.

In Fig. 14, we further propose a new classification based on precipitation seasonality, computed using an objective clustering approach. We used k-means clustering (e.g., Wilks 1995) to define five distinct classes that we named after the characteristics of their cluster centers. We recognize two dominant classes with winter (DJF) and summer (JJA) accumulation types and a third class with less elements having the maximum precipitation in MAM. Finally, we named two intermediate classes

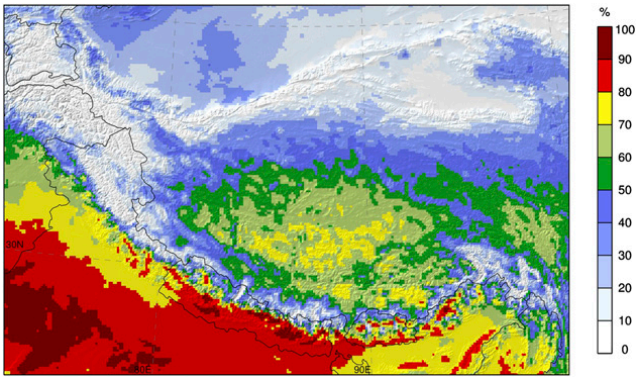

FIG. 11. Contribution (%) of convective precipitation to the total annual precipitation.

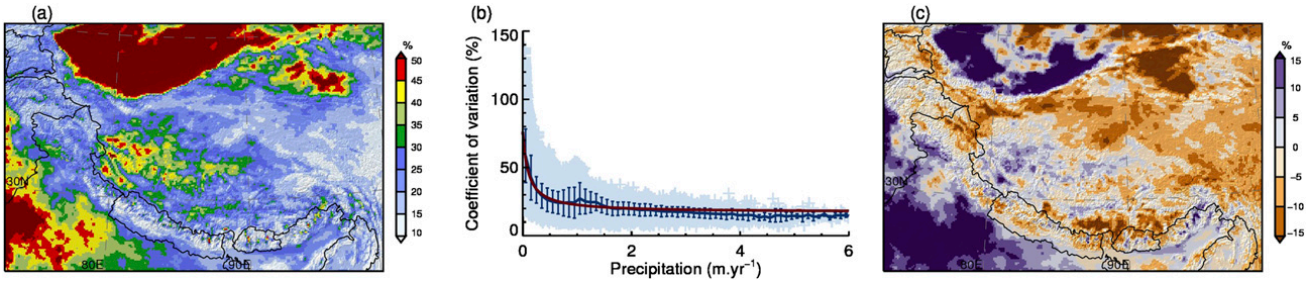

FIG. 12. Precipitation interannual variability for the 11 hydrological years (October 2000–September 2011). (a) Coefficient of variation (%) of annual precipitation. (b) Coefficient of variation vs annual precipitation. The blue curve represents 0.1-m-wide binned means with $\pm 1\sigma$ error bars. The red curve is the expected coefficient of variation obtained by fitting a hyperbolic curve to the data points [Eq. (1)]. (c) Anomaly of the coefficient of variation, defined as the difference between the coefficient of variation and the expected coefficient [red curve in (b)].

that tend to experience either winter (MAM/DJF) or summer (MAM/JJA) precipitation but with less pronounced centers. The mean seasonal cycles of each class are presented in Fig. 15. We recognize the three peaks of the DJF, MAM, and JJA classes and see that the two remaining classes have a less pronounced seasonality but different tendencies (MAM/DJF displays a February precipitation peak and precipitation almost all year-round; MAM/JJA experiences precipitation in MAM and JJA but less in winter). All classes but DJF have their minimum in November–December, while the DJF class has a minimum in June–July.

One striking feature is the clear difference between DJF (west) and JJA (central TP) regimes. The MAM cluster is mostly located in northern TP but a few glaciers can be found in southeast TP, together with a large region of mixed type glaciers, which correspond to the "maritime zone" defined by Shi and Liu (2000) or the "spring-accumulation type" zone proposed by Yang et al. (2013). Along the Himalayan range, we find glaciers of varying types over very short distances, which can be explained by the variability of precipitation regimes in the Himalayas. For example, Kansakar et al. (2004) identified as many as four different precipitation regimes for Nepal alone. The orientation of the glaciers and their location on the windward or lee side of the range also play a significant role, illustrating the importance of high spatial resolution in determining climatic influences on glaciers.

6. Conclusions

The TP precipitation regime is influenced by both the westerlies and the monsoons, as well as their interplay.

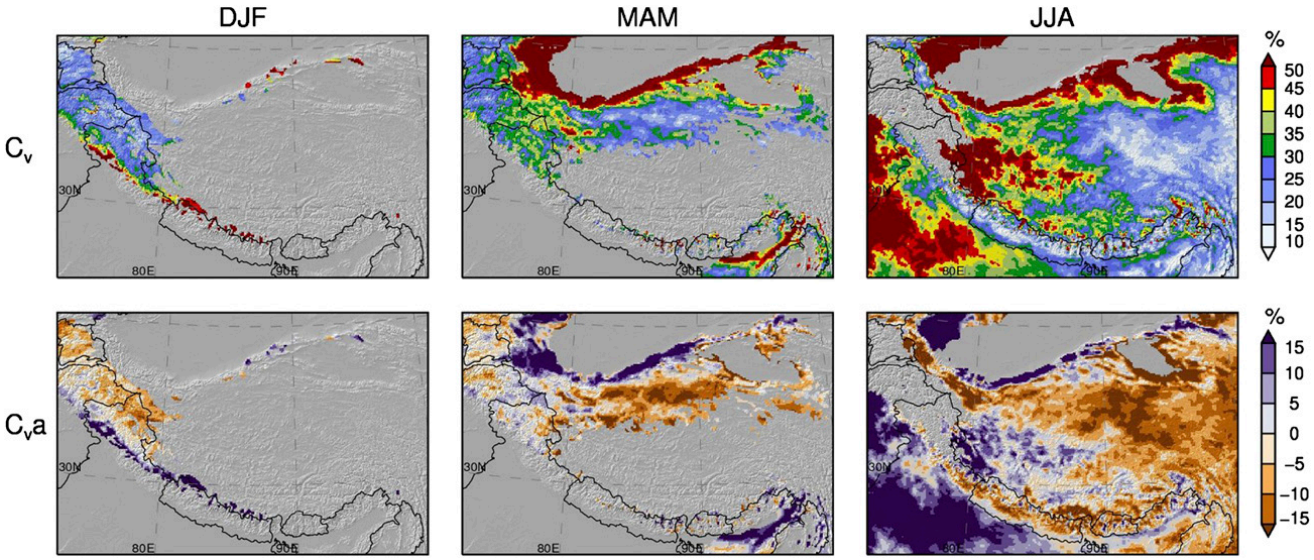

FIG. 13. Seasonal precipitation interannual variability for the 11 hydrological years (October 2000–September 2011). Coefficient of variation c_v and anomaly of the coefficient of variation c_va are shown, areas (i) where less than 25% of the annual precipitation occurs in the considered season and (ii) with less than 25-mm average seasonal precipitation are masked in gray. Precipitation in SON is too low and not presented here.

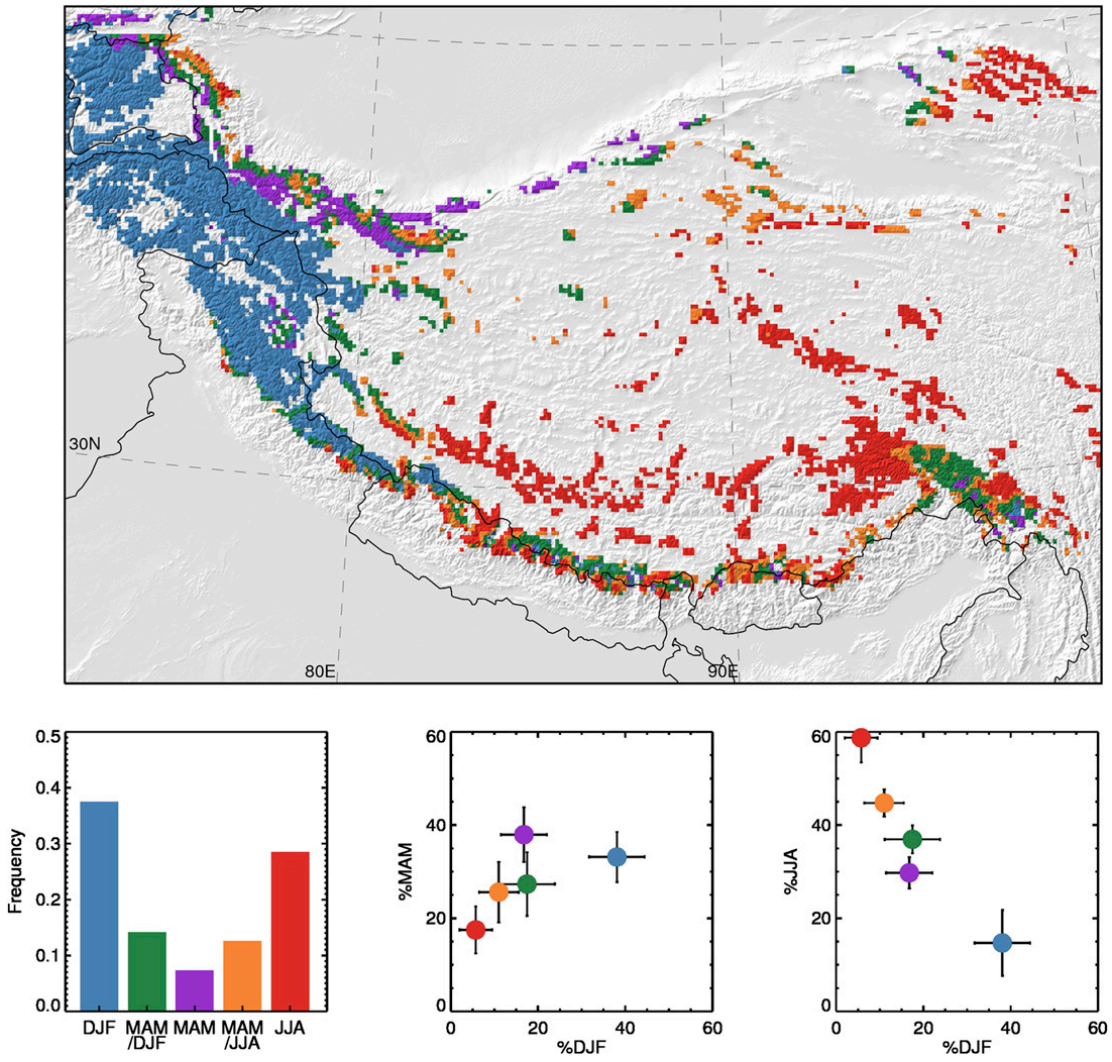

FIG. 14. Classification of glacier accumulation regimes according to precipitation seasonality. A *k*-means clustering algorithm is run on three input variables (percentage of precipitation falling in DJF, MAM, and JJA) and with five output clusters. We focus on glacierized grid points only. (bottom left) Histogram plot showing the relative occurrence of each class in the map with the color legend is described below. (bottom center),(bottom right) The clusters are named after their cluster centers characteristics. Since SON is a linear combination of the three other variables, it was not included in the clustering procedure.

The circulation dynamics create a complex puzzle for geophysicists or palaeoclimatologists attempting to reconstruct and understand the signals in various climate proxies. Furthermore, this task is made more difficult by our incomplete understanding of the present-day climate dynamics (e.g., Molnar et al. 2010). In this study, we did not attempt to explain and unravel all processes that drive precipitation on the TP, but we described the observed patterns and gave a framework for a better understanding of spatial and temporal variability. We showed that dynamical downscaling approaches like the HAR provide a way to resolve the full process chain of synoptic to regional dynamics for features such as precipitation and can provide details that are not represented in coarser datasets.

A crucial step was the evaluation of HAR precipitation in section 4. We demonstrated an improvement when increasing horizontal resolution from 30 to 10 km, quantitatively (by comparing to observations) as well as qualitatively (in the reproduction of documented orographic precipitation features). Further qualitative indices consolidated our confidence in the reliability of the HAR: for example, its realistic reproduction of both (i) the known relationship between the coefficient of variation and precipitation and (ii) the documented characteristics of precipitation on the TP (weak, frequent, and convective precipitation events). However, these considerations are qualitative and do not allow us to provide a quantitative uncertainty value of the HAR precipitation outputs. In this regard, integrated

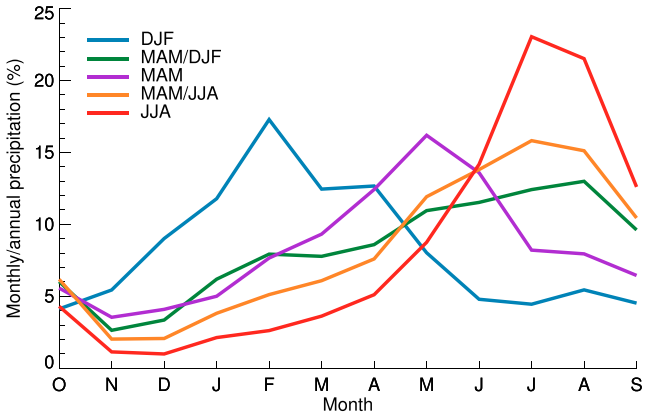

FIG. 15. Mean contribution of each month to annual precipitation for the five glacier clusters defined in Fig. 13.

approaches such as hydrological or glaciological modeling will aid evaluation at the basin scale. Furthermore, since validation and benchmarking are made difficult by scarce and imperfect observations, the new global precipitation measurement (GPM) system (Hou et al. 2014) or innovative cloud detection algorithms (Rüthrich et al. 2013) may help to improve the validation in the future.

In general, the annual cycle of precipitation on the TP is characterized by a winter precipitation regime in the west, a spring precipitation regime in northern and southern TP, and a summer precipitation regime elsewhere. This led some authors such as Shi (2002) to define the drivers of precipitation according to precipitation seasonality. In Fig. 1 of Shi (2002), the author draws a line along a southwest–northeast diagonal on the TP, symbolizing the limit between ''monsoonal precipitation'' and ''westerly precipitation.'' The use of these designations is interpreting ''synchronicity'' as ''causality.'' Our results do not contradict this view, as shown by the large domination of summertime precipitation on the TP. However, with a closer look at the seasonal cycle of precipitation on a monthly basis, we obtain more complex patterns than commonly assumed, especially on the central and northern TP, where spring precipitation represents a substantial part of the annual amounts. Recycling (moisture that originates and stays on the TP) could play a nonnegligible role in the TP hydrological cycle and should be quantified more precisely in the future. Recent studies that quantify moisture transport and provenance on the TP (e.g., Feng and Zhou 2012; Chen et al. 2012) focused on summer months and used atmospheric data from coarse-resolution global reanalysis. These studies could be complemented by similar approaches based on higher-resolution atmospheric datasets such as the HAR.

We identified regions with higher precipitation variability, either by analyzing the occurrence of strong precipitation events or by showing regional anomalies of the annual coefficient of variation. We see that both indicators are high for some regions: for example, in Pakistan and northwestern India. Located at the confluence zone of the westerly and monsoonal flows, this region may be more sensitive to variability of the synoptic atmospheric circulation. On the TP, precipitation days are of rather constant intensity during summer but the interannual variability in central and western TP is larger than in the neighboring TP regions. The drivers of interannual precipitation variability on the TP will be the subject of a future study.

Glaciers in different precipitation regimes will respond differently to changes in climate and shifts in precipitation seasonality. In this study, we proposed a new map of glacier accumulation regimes as one possible application for the HAR. Our analysis illustrates the high spatial variability of precipitation seasonality and provides a first approach for glacier energy and mass balance considerations. The map resulting from this cluster analysis emphasizes that glaciers on the TP cannot be considered as one entity with uniform mass balance sensitivity.

Acknowledgments. This work is supported by the German Federal Ministry of Education and Research (BMBF) Central Asia–Monsoon Dynamics and Geo-Ecosystems (CAME) program through the WET project (Variability and Trends in Water Balance Components of Benchmark Drainage Basins on the Tibetan Plateau) under the code 03G0804A and by the German Research Foundation (DFG) Priority Programme 1372, Tibetan Plateau: Formation–Climate–Ecosystems through the Dynamic Response of Glaciers on the Tibetan Plateau to Climate Change (DynRG-TiP) project under the codes SCHE 750/4-1, SCHE 750/4-2, and SCHE 750/4-3. Further support for TM came from the Alexander von Humboldt Foundation. We sincerely thank the developers of the WRF community model for providing such a comprehensive tool and B. Bookhagen for providing us the swaths locations and the TRMM 3B31 rainfall climatologies (available at http://www.geog.ucsb.edu/~bodo/TRMM/). All data analysis and graphics were realized with our own tools programmed in the IDL language and with the help of the Coyote IDL library. We made use of TRMM data provided by the GSFC DAAC and weather station data provided by the NCDC (available at http://www.ncdc.noaa.gov/oa/ncdc.html). We are grateful to three anonymous reviewers who made thoughtful comments and critics on an earlier version of this paper.

REFERENCES

Arendt, A., and Coauthors, 2012: Randolph glacier inventory [v1.0]: A dataset of global glacier outlines. Global Land Ice Measurements from Space Rep., 28 pp.

Bohner, J., 2006: General climatic controls and topoclimatic variations in Central and High Asia. *Boreas,* **35,** 279–295, doi:10.1111/j.1502-3885.2006.tb01158.x.

Bolch, T., and Coauthors, 2012: The state and fate of Himalayan glaciers. *Science,* **336,** 310–314, doi:10.1126/science.1215828.

Bookhagen, B., and M. R. Strecker, 2008: Orographic barriers, high-resolution TRMM rainfall, and relief variations along the eastern Andes. *Geophys. Res. Lett.,* **35,** L06403, doi:10.1029/2007GL032011.

——, and D. W. Burbank, 2010: Toward a complete Himalayan hydrological budget: Spatiotemporal distribution of snowmelt and rainfall and their impact on river discharge. *J. Geophys. Res.,* **115,** F03019, doi:10.1029/2009JF001426.

Box, J. E., and Coauthors, 2006: Greenland ice sheet surface mass balance variability (1988–2004) from calibrated Polar MM5 output. *J. Climate,* **19,** 2783–2800.

Bromwich, D. H., L. H. Bai, and G. G. Bjarnason, 2005: High-resolution regional climate simulations over Iceland using Polar MM5. *Mon. Wea. Rev.,* **133,** 3527–3547.

Caldwell, P., H.-N. S. Chin, D. C. Bader, and G. Bala, 2009: Evaluation of a WRF dynamical downscaling simulation over California. *Climatic Change,* **95** (3–4), 499–521, doi:10.1007/s10584-009-9583-5.

Chen, B., X.-D. Xu, S. Yang, and W. Zhang, 2012: On the origin and destination of atmospheric moisture and air mass over the Tibetan Plateau. *Theor. Appl. Climatol.,* **54,** doi:10.1007/s00704-012-0641-y.

Chow, K. C., and J. C. L. Chan, 2009: Diurnal variations of circulation and precipitation in the vicinity of the Tibetan Plateau in early summer. *Climate Dyn.,* **32,** 55–73, doi:10.1007/s00382-008-0374-x.

Colle, B. A., 2008: Two-dimensional idealized simulations of the impact of multiple windward ridges on orographic precipitation. *J. Atmos. Sci.,* **65,** 509–523.

Collier, E., T. Mölg, F. Maussion, D. Scherer, C. Mayer, and A. B. G. Bush, 2013: High-resolution interactive modelling of the mountain glacier–atmosphere interface: An application over the Karakoram. *Cryosphere,* **7,** 779–795, cp-10-91-2014/tc-7-779-2013.

Conrad, V., 1941: The variability of precipitation. *Mon. Wea. Rev.,* **69,** 5–11.

Dee, D. P., and Coauthors, 2011: The ERA-Interim reanalysis: Configuration and performance of the data assimilation system. *Quart. J. Roy. Meteor. Soc.,* **137,** 553–597, doi:10.1002/qj.828.

Dietze, E., and Coauthors, 2014: Sediment transport processes across the Tibetan Plateau inferred from robust grain-size end-members in lake sediments. *Climate* Past, **10,** 91–106, doi:10.5194/cp-10-91-2014.

Feng, L., and T. J. Zhou, 2012: Water vapor transport for summer precipitation over the Tibetan Plateau: Multidata set analysis. *J. Geophys. Res.,* **117,** D20114, doi:10.1029/2011JD017012.

Fu, Y., G. Liu, G. Wu, R. Yu, Y. Xu, Y. Wang, R. Li, and Q. Liu, 2006: Tower mast of precipitation over the central Tibetan Plateau summer. *Geophys. Res. Lett.,* **33,** L05802, doi:10.1029/2005GL024713.

Fujita, K., 2008: Effect of precipitation seasonality on climatic sensitivity of glacier mass balance. *Earth Planet. Sci. Lett.,* **276** (1–2), 14–19, doi:10.1016/j.epsl.2008.08.028.

Hahn, D., and S. Manabe, 1975: Role of mountains in South Asian monsoon circulation. *J. Atmos. Sci.,* **32,** 1515–1541.

Heikkila, U., A. Sandvik, and A. Sorteberg, 2011: Dynamical downscaling of ERA-40 in complex terrain using the WRF regional climate model. *Climate Dyn.,* **37** (7–8), 1551–1564, doi:10.1007/s00382-010-0928-6.

Hou, A. Y., and Coauthors, 2014: The Global Precipitation Measurement (GPM) mission. *Bull. Amer. Meteor. Soc.,* in press.

Huffman, G. J., and Coauthors, 2007: The TRMM Multisatellite Precipitation Analysis: Quasi-global, multiyear, combined sensor precipitation estimates at fine scale. *J. Hydrometeor.,* **8,** 38–55.

Immerzeel, W. W., and M. F. P. Bierkens, 2010: Seasonal prediction of monsoon rainfall in three Asian river basins: The importance of snow cover on the Tibetan Plateau. *Int. J. Climatol.,* **30,** 1835–1842, doi:10.1002/joc.2033.

——, L. P. H. van Beek, and M. F. P. Bierkens, 2010: Climate change will affect the Asian water towers. *Science,* **328,** 1382–1385.

Jiang, Q., 2003: Moist dynamics and orographic precipitation. *Tellus,* **55A,** 301–316, doi:10.1034/j.1600-0870.2003.00025.x.

Jurković, R. S., and Z. Pasarić, 2013: Spatial variability of annual precipitation using globally gridded data sets from 1951 to 2000. *Int. J. Climatol.,* **33,** 690–698, doi:10.1002/joc.3462.

Kääb, A., E. Berthier, C. Nuth, J. Gardelle, and Y. Arnaud, 2012: Contrasting patterns of early twenty-first-century glacier mass change in the Himalayas. *Nature,* **488,** 495–498, doi:10.1038/nature11324.

Kanamitsu, M., and H. Kanamaru, 2007: Fifty-seven-year California Reanalysis Downscaling at 10 km (CaRD10). Part I: System detail and validation with observations. *J. Climate,* **20,** 5553–5571.

Kansakar, S., D. M. Hannah, J. Gerrard, and G. Rees, 2004: Spatial pattern in the precipitation regime of Nepal. *Int. J. Climatol.,* **24,** 1645–1659, doi:10.1002/joc.1098.

Kaser, G., M. Grosshauser, and B. Marzeion, 2010: Contribution potential of glaciers to water availability in different climate regimes. *Proc. Natl. Acad. Sci. USA,* **107,** 20 223–20 227, doi:10.1073/pnas.1008162107.

Kidd, C., and V. Levizzani, 2011: Status of satellite precipitation retrievals. *Hydrol. Earth Syst. Sci.,* **15,** 1109–1116, doi:10.5194/hess-15-1109-2011.

Kropáček, J., F. Maussion, F. Chen, S. Hoerz, and V. Hochschild, 2013: Analysis of ice phenology of lakes on the Tibetan Plateau from MODIS data. *Cryosphere,* **7,** 287–301, doi:10.5194/tc-7-287-2013.

Kumar, M. S., M. S. Shekhar, S. S. V. S. R. Krishna, M. R. Bhutiyani, and A. Ganju, 2012: Numerical simulation of cloud burst event on August 05, 2010, over Leh using WRF mesoscale model. *Nat. Hazards,* **62,** 1261–1271, doi:10.1007/s11069-012-0145-1.

Liu, X., A. Bai, and C. Liu, 2009: Diurnal variations of summertime precipitation over the Tibetan Plateau in relation to orographically-induced regional circulations. *Environ. Res. Lett.,* **4,** 045203, doi:10.1088/1748-9326/4/4/045203.

Lo, J. C.-F., Z.-L. Yang, and R. A. Pielke Sr., 2008: Assessment of three dynamical climate downscaling methods using the Weather Research and Forecasting (WRF) model. *J. Geophys. Res.,* **113,** D09112, doi:10.1029/2007JD009216.

Maussion, F., D. Scherer, R. Finkelnburg, J. Richters, W. Yang, and T. Yao, 2011: WRF simulation of a precipitation event over the

Tibetan Plateau, China—An assessment using remote sensing and ground observations. *Hydrol. Earth Syst. Sci.,* **15,** 1795–1817, doi:10.5194/hess-15-1795-2011.

Medina, S., R. A. Houze Jr., A. Kumar, and D. Niyogi, 2010: Summer monsoon convection in the Himalayan region: Terrain and land cover effects. *Quart. J. Roy. Meteor. Soc.,* **136,** 593–616, doi:10.1002/qj.601.

Mölg, T., and G. Kaser, 2011: A new approach to resolving climate-cryosphere relations: Downscaling climate dynamics to glacier-scale mass and energy balance without statistical scale linking. *J. Geophys. Res.,* **116,** D16101, doi:10.1029/2011JD015669.

——, and D. Scherer, 2012: Retrieving important mass-balance model parameters from AWS measurements and high-resolution mesoscale atmospheric modeling. *J. Glaciol.,* **58,** 625–628, doi:10.3189/2012JoG11J258.

——, F. Maussion, W. Yang, and D. Scherer, 2012: The footprint of Asian monsoon dynamics in the mass and energy balance of a Tibetan glacier. *Cryosphere,* **6,** 1445–1461, doi:10.5194/tc-6-1445-2012.

——, ——, and D. Scherer, 2014: Mid-latitude westerlies as a driver of glacier variability in monsoonal High Asia. *Nat. Climate Change,* **4,** 68–73, doi:10.1038/nclimate2055.

Molnar, P., W. R. Boos, and D. S. Battisti, 2010: Orographic controls on climate and paleoclimate of Asia: Thermal and mechanical roles for the Tibetan Plateau. *Annu. Rev. Earth Planet. Sci.,* **38,** 77–102, doi:10.1146/annurev-earth-040809-152456.

National Centers for Environmental Prediction, cited 2014: NCEP ADP global upper air and surface weather observations (PREPBUFR format), May 1997—Continuing. National Center for Atmospheric Research Computational and Information Systems Laboratory Research Data Archive. [Available online at http://rda.ucar.edu/datasets/ds337.0.]

Palazzi, E., J. von Hardenberg, and A. Provenzale, 2013: Precipitation in the Hindu-Kush Karakoram Himalaya: Observations and future scenarios. *J. Geophys. Res. Atmos.,* **118,** 85–100, doi:10.1029/2012JD018697.

Qian, W., and D.-K. Lee, 2000: Seasonal march of Asian summer monsoon. *Int. J. Climatol.,* **20,** 1371–1386, doi:10.1002/1097-0088(200009)20:11<1371::AID-JOC538>3.0.CO;2-V.

Qin, J., K. Yang, S. Liang, and X. Guo, 2009: The altitudinal dependence of recent rapid warming over the Tibetan Plateau. *Climatic Change,* **97** (1–2), 321–327, doi:10.1007/s10584-009-9733-9.

Rupper, S., and G. Roe, 2008: Glacier changes and regional climate: A mass and energy balance approach. *J. Climate,* **21,** 5384–5401.

Rüthrich, F., B. Thies, C. Reudenbach, and J. Bendix, 2013: Cloud detection and analysis on the Tibetan Plateau using Meteosat and CloudSat. *J. Geophys. Res. Atmos.,* **118,** 10 082–10 099, doi:10.1002/jgrd.50790.

Schiemann, R., D. Luethi, P. L. Vidale, and C. Schaer, 2008: The precipitation climate of central Asia—Intercomparison of observational and numerical data sources in a remote semiarid region. *Int. J. Climatol.,* **28,** 295–314, doi:10.1002/joc.1532.

——, ——, and C. Schaer, 2009: Seasonality and interannual variability of the westerly jet in the Tibetan Plateau region. *J. Climate,* **22,** 2940–2957.

Shi, Y., 2002: Characteristics of late quaternary monsoonal glaciation on the Tibetan Plateau and in East Asia. *Quat. Int.,* **97–98,** 79–91, doi:10.1016/S1040-6182(02)00053-8.

——, and S. Liu, 2000: Estimation on the response of glaciers in china to the global warming in the 21st century. *Chin. Sci. Bull.,* **45,** 668–672.

Skamarock, W. C., and J. B. Klemp, 2008: A time-split nonhydrostatic atmospheric model for weather research and forecasting applications. *J. Comput. Phys.,* **227,** 3465–3485, doi:10.1016/j.jcp.2007.01.037.

Sugimoto, S., and K. Ueno, 2010: Formation of mesoscale convective systems over the eastern Tibetan Plateau affected by plateau-scale heating contrasts. *J. Geophys. Res.,* **115,** D16105, doi:10.1029/2009JD013609.

Ueno, K., H. Fujii, H. Yamada, and L. P. Liu, 2001: Weak and frequent monsoon precipitation over the Tibetan Plateau. *J. Meteor. Soc. Japan,* **79,** 419–434, doi:10.2151/jmsj.79.419.

von Storch, H., H. Langenberg, and F. Feser, 2000: A spectral nudging technique for dynamical downscaling purposes. *Mon. Wea. Rev.,* **128,** 3664–3673.

Wang, B., 2006: *The Asian Monsoon.* Springer-Praxis, 787 pp.

Webster, P. J., V. O. Magana, T. N. Palmer, J. Shukla, R. A. Tomas, M. Yanai, and T. Yasunari, 1998: Monsoons: Processes, predictability, and the prospects for prediction. *J. Geophys. Res.,* **103** (C7), 14 451–14 510.

——, V. E. Toma, and H. M. Kim, 2011: Were the 2010 Pakistan floods predictable? *Geophys. Res. Lett.,* **38,** L04806, doi:10.1029/2010GL046346.

Wilks, D. S., 1995: *Statistical Methods in the Atmospheric Sciences: An Introduction.* Academic Press, 467 pp.

Wilson, A. B., D. H. Bromwich, and K. M. Hines, 2011: Evaluation of polar WRF forecasts on the arctic system reanalysis domain: Surface and upper air analysis. *J. Geophys. Res.,* **116,** D11112, doi:10.1029/2010JD015013.

Wu, G., Y. Liu, B. He, Q. Bao, A. Duan, and F.-F. Jin, 2012: Thermal controls on the Asian summer monsoon. *Sci. Rep.,* **2,** 404, doi:10.1038/srep00404.

Yang, W., X. Guo, T. Yao, K. Yang, L. Zhao, S. Li, and M. Zhu, 2011: Summertime surface energy budget and ablation modeling in the ablation zone of a maritime Tibetan glacier. *J. Geophys. Res.,* **116,** D14116, doi:10.1029/2010JD015183.

——, T. Yao, X. Guo, M. Zhu, S. Li, and D. B. Kattel, 2013: Mass balance of a maritime glacier on the southeast Tibetan Plateau and its climatic sensitivity. *J. Geophys. Res. Atmos.,* **118,** 9579–9594, doi:10.1002/jgrd.50760.

Yao, T., and Coauthors, 2012: Different glacier status with atmospheric circulations in Tibetan Plateau and surroundings. *Nat. Climate Change,* **2,** 663–667, doi:10.1038/nclimate1580.

Yaodong, L., W. Yun, S. Yang, H. Liang, G. Shouting, and R. Fu, 2008: Characteristics of summer convective systems initiated over the Tibetan Plateau. Part I: Origin, track, development, and precipitation. *J. Appl. Meteor. Climatol.,* **47,** 2679–2695.

Yin, Z.-Y., X. Zhang, X. Liu, M. Colella, and X. Chen, 2008: An assessment of the biases of satellite rainfall estimates over the Tibetan Plateau and correction methods based on topographic analysis. *J. Hydrometeor.,* **9,** 301–326.

You, Q., K. Fraedrich, G. Ren, B. Ye, X. Meng, and S. Kang, 2012: Inconsistencies of precipitation in the eastern and central Tibetan Plateau between surface adjusted data and reanalysis. *Theor. Appl. Climatol.,* **109** (3–4), 485–496, doi:10.1007/s00704-012-0594-1.

Zhou, T., R. Yu, H. Chen, A. Dai, and Y. Pan, 2008: Summer precipitation frequency, intensity, and diurnal cycle over China: A comparison of satellite data with rain gauge observations. *J. Climate,* **21,** 3997–4010.

B. A 12-year high-resolution climatology of atmospheric water transport over the Tibetan Plateau

Curio, J., Maussion, F., and Scherer, D.: A 12-year high-resolution climatology of atmospheric water transport over the Tibetan Plateau, *Earth Syst. Dynam.*, 6, 109-124, doi:10.5194/esd-6-109-2015, 2015.

Status: Published.

Own contribution:

- design of the study
- HAR product generation
- data preparation
- data analysis
- scientific discussion
- graphics and tables
- writing

Earth Syst. Dynam., 6, 109–124, 2015
www.earth-syst-dynam.net/6/109/2015/
doi:10.5194/esd-6-109-2015

Earth System Dynamics
Open Access

A 12-year high-resolution climatology of atmospheric water transport over the Tibetan Plateau

J. Curio[1], **F. Maussion**[1,2], **and D. Scherer**[1]

[1]Chair of Climatology, Technische Universität Berlin, Berlin, Germany
[2]Institute of Meteorology and Geophysics, University of Innsbruck, Innsbruck, Austria

Correspondence to: J. Curio (julia.curio@tu-berlin.de)

Received: 7 September 2014 – Published in Earth Syst. Dynam. Discuss.: 2 October 2014
Revised: 6 February 2015 – Accepted: 22 February 2015 – Published: 13 March 2015

Abstract. The Tibetan Plateau (TP) plays a key role in the water cycle of high Asia and its downstream regions. The respective influence of the Indian and East Asian summer monsoon on TP precipitation and regional water resources, together with the detection of moisture transport pathways and source regions are the subject of recent research. In this study, we present a 12-year high-resolution climatology of the atmospheric water transport (AWT) over and towards the TP using a new data set, the High Asia Refined analysis (HAR), which better represents the complex topography of the TP and surrounding high mountain ranges than coarse-resolution data sets. We focus on spatiotemporal patterns, vertical distribution and transport through the TP boundaries. The results show that the mid-latitude westerlies have a higher share in summertime AWT over the TP than assumed so far. Water vapour (WV) transport constitutes the main part, whereby transport of water as cloud particles (CP) also plays a role in winter in the Karakoram and western Himalayan regions. High mountain valleys in the Himalayas facilitate AWT from the south, whereas the high mountain regions inhibit AWT to a large extent and limit the influence of the Indian summer monsoon. No transport from the East Asian monsoon to the TP could be detected. Our results show that 36.8 ± 6.3 % of the atmospheric moisture needed for precipitation comes from outside the TP, while the remaining 63.2 % is provided by local moisture recycling.

1 Introduction

The Tibetan Plateau (TP) is often referred to as the "world water tower" (Xu et al., 2008), as it is the source of many large Asian rivers such as the Indus, Ganges, Brahmaputra, Yellow River, Yangtze and Mekong. The TP is one of the most active centres in the word water cycle and constitutes an essential source of moisture for the downstream regions in East Asia (Immerzeel et al., 2010). The transport of moisture to the TP is crucial for a sustainable water supply in the downstream regions like the Yellow and Yangtze river valleys (Zhang et al., 2013). Moisture transport in and to the TP is influenced by mesoscale features (Sugimoto et al., 2008), but it is also driven by large-scale atmospheric circulation, most notably the monsoon systems (Webster et al., 1998) and the mid-latitude westerlies (Schiemann et al., 2009). The unique topography of the TP, with its large extent and an average altitude of more than 4000 m makes it of particular interest because of its interaction with large-scale circulation. The surrounding high mountain ranges, Himalaya, Karakoram, Pamir, Tien Shan and Kunlun Shan, act as a barrier for the atmospheric moisture transport.

During the last few decades the TP experienced climate changes of warmer and wetter conditions (Yang et al., 2011, 2014), which have a direct impact on the hydrological cycle. Precipitable water (PW) shows increasing trends in the eastern and western TP and decreasing trends in the central TP for the relatively short period of 2000–2010 (Lu et al., 2014). The poleward shift of the East Asian westerly jet in the period 1979–2011 and the assumed intensification of the monsoon system under climate change conditions (while Yao et al., 2012, described a recent weakening of the Indian summer monsoon) are supposed to cause large areas of the TP to become wetter (Gao et al., 2014). Lake expansion in the central TP has intensified during the last few decades, due

to global warming and its effects on the hydrological cycle of the TP (e.g. glacier retreat, permafrost degradation; Liu et al., 2010). The additional water vapour (WV), necessary for lake expansion, is assumed to come from outside the TP and therefore it is important for better understanding the WV sources and transport processes (Yang et al., 2014).

Many studies on atmospheric water transport (AWT) in and to the TP focus on the question of how the Indian and East Asian summer monsoon systems affect precipitation on the Tibetan Plateau, and how changes of the monsoonal circulation impact local and regional water resources (Gao et al., 2014; Immerzeel et al., 2013; Simmonds et al., 1999). Yao et al. (2012) and Bolch et al. (2012) list the Indian monsoon, the mid-latitude westerlies and the East Asian monsoon as drivers of climate variability in the TP. In previous studies, the influence of the westerlies and the monsoon system was examined on the basis of the precipitation timing and so is supposed to be limited to winter (westerlies) or summer (Indian and East Asian summer monsoon) (e.g. Hren et al., 2009; Tian et al., 2007; Yang et al., 2014). The origin of the atmospheric moisture over the TP plays a key role in recent research (e.g. Chen et al., 2012; Feng and Zhou, 2012). Their are three sources of moisture entering the TP: the Asian monsoon systems, the mid-latitude westerlies, and local moisture recycling. The general assumption is that the main WV source for summer precipitation in the TP is the Indian summer monsoon. Pathways for the moisture originating in the Arabian Sea, the Bay of Bengal and the westerlies are high mountain valleys in the southern and western border of the TP, e.g. the Brahmaputra Channel in the easternmost part of the Himalayas and the meridionally orientated valley in the central and western parts.

One method to identify the sources of moisture is to analyse the isotopic composition of precipitation, e.g. observed and modelled stable oxygen isotope ratios (δ^{18}O) and hydrogen isotope values (δD) (Araguás-Araguás et al., 1998; Tian et al., 2007; Yao et al., 2013) and the isotopic composition of the water in rivers and smaller water streams (Hren et al., 2009) and of climate proxies such as ice and sediment cores (Kang et al., 2007; Günther et al., 2011; An et al., 2012; Guenther et al., 2013; Joswiak et al., 2013). The latter ones can be used to analyse the moisture transport/conditions on the plateau and its source regions in the past. An et al. (2012) analysed a sediment core from Lake Qinghai in the north-east of the TP that reaches back 32 ka. They focused on the interplay of the westerlies and the Asian monsoon and showed that there is an anti-phase relationship with periods of dominant westerlies and periods with dominant Asian monsoon. Higher monsoon activity during the current warming period is found by studying variations in the monsoon intensity in the TP during the last 1000 years using data from sediment and ice cores (Günther et al., 2011). A shift in the isotope signals implies that the contribution of westerly moisture to the ice-core accumulation was relatively greater before the 1940s (Joswiak et al., 2013).

For the present-day conditions, various studies produce different results. Both the southern Indian Ocean (Indian summer monsoon) (Yao et al., 2013) and the Pacific Ocean (East Asian Monsoon) (Araguás-Araguás et al., 1998) are identified as the dominant moisture sources for summer precipitation in the TP. The analysis of stable isotopes of precipitation samples in western China show that the southern TP receives monsoon moisture in summer and westerly moisture in winter, while the moisture in western TP is delivered by the south-west monsoon (Tian et al., 2007). Hren et al. (2009), who sampled 191 stream waters across the TP and the Himalaya, found that the moisture entering the south-eastern TP through the Brahmaputra Channel originates in the Bay of Bengal. This monsoonal moisture is mixed with central Asian air masses the farther west and north in the TP the sampling site is located. The role of local moisture recycling as an additionally moisture source is also emphasized in many studies (e.g. Joswiak et al., 2013; Kurita and Yamada, 2008; Trenberth, 1999). Araguás-Araguás et al. (1998) found that it is dominant in winter and spring.

Another method to investigate the moisture transport in the TP is gridded atmospheric data sets, for example global reanalysis data, regional atmospheric models and remote sensing data. Chen et al. (2012) used backward and forward trajectories to identify the sources and sinks of moisture for the TP in summer. Their results show that for periods longer than 4 days backwards, the main moisture source is the Arabian Sea, while for shorter periods, the Bay of Bengal, the Arabian Sea and the north-western part of the TP contribute moisture in the same order of magnitude. The results from the forward tracking underline the relevance of the TP moisture for the precipitation in East Asia. Feng and Zhou (2012) found that the main WV transport for summer precipitation takes place through the southern border of the TP and originates in the Bay of Bengal and the Indian Ocean. They also point out that the southern branch of the mid-latitude westerlies transports moisture to the TP too, but its share is distinctly lower. Lu et al. (2014) analysed the atmospheric conditions and pathways of moisture to the TP for a wet and dry monsoon season and showed that differences in the atmospheric circulation have a direct impact on the moisture transport and on the PW over the TP. Meridionally orientated high mountain valleys in the Himalayas can channel water vapour and precipitation to the TP (Bookhagen and Burbank, 2010).

Previous studies relied on global reanalysis data sets to quantify the transport to the TP. Recently, a new high-resolution data set, the High Asia Refined analysis (HAR; Maussion et al., 2014), was made available. With a high spatial (30 and 10 km) and temporal (3 and 1 h) resolution, the data set allows us to analyse the AWT above the Tibetan Plateau differentiated in space and time. By using this new data set with a distinctly higher horizontal resolution than the global data sets, the question arises of whether or not the more realistic representation of the topography of the TP and

the surrounding high mountain ranges leads to an improvement in atmospheric moisture representation.

The objectives of the current study are threefold:

i. describe the characteristics of AWT over and to the TP as resolved by the HAR data set during the last decade, with focus on spatial patterns, seasonal evolution and vertical distribution,

ii. examine the barrier effect of the topography on AWT and detect the major transport channels to the plateau,

iii. and quantify the importance of increasing model spatial resolution on these transport channels.

Here we present a 12-year climatology of atmospheric water transport (AWT) over the TP and adjacent mountain ranges based on the HAR. We focus on the period 2001–2012 (referred to the "last decade" for convenience). First, we will look at the mean annual cycle of AWT (water vapour and cloud particles) to detect the mean patterns and transport channels. The vertical distribution of the transport is then analysed using selected model levels. We also compute vertical cross sections along the border of the TP to quantify the atmospheric water input and verify the importance of the detected transport channels. In the final step, we provide an estimation of the budget of AWT and its share of the precipitation falling on the TP.

2 Data and methods

2.1 The HAR data set

We use meteorological fields provided by the High Asia Refined analysis (HAR). The HAR is the result of the dynamical downscaling of the global gridded data set, the Operational Model Global Tropospheric Analyses (final analyses, FNL; data set ds083.2). These final analyses are available every 6 h and have a spatial resolution of 1 °. The model used for this purpose is the advanced research version of the Weather and Research Forecasting model (WRF-ARW, Skamarock and Klemp, 2008) version 3.3.1. The HAR provides products at a spatial resolution of 30 km and temporal resolution of 3 h for the first domain, covering most parts of central Asia (HAR30). A second nested domain (HAR10) covers high Asia and the TP with a spatial resolution of 10 km and temporal resolution of 1 h (Fig. 1). The data set is available online at http://www.klima.tu-berlin.de/HAR and described in detail by Maussion et al. (2011, 2014). The HAR provides meteorological fields at the surface and on 28 terrain-following vertical sigma levels. The data set covers a period of more than 12 years from October 2000 to December 2012 and is updated continuously. HAR products are available for different time aggregation levels: hourly (original temporal model resolution), daily, monthly and yearly.

The HAR precipitation data were compared to rain gauge observation and precipitation estimates from the Tropical Rainfall Measuring Mission (TRMM) by Maussion et al. (2011, 2014). The accuracy of the precipitation data is described more in detail in Sect. 4.2.

2.2 Moisture transport

Atmospheric water transport happens through WV transport and as cloud particle (CP) transport. In this study, we are interested in cloud particle transport but do not further distinguish between liquid (water droplets) and solid (ice) cloud particles which are both resolved by the model microphysics. WV and CP fluxes are calculated for each of the 28 original sigma levels, which are terrain following, based on the original temporal model resolution of 1 h (HAR10) and 3 h (HAR30) using the formula

$$Q = v_\mathrm{h} \rho q \Delta z, \tag{1}$$

where Q is the water vapour flux (kg m^{-1} s^{-1}) or cloud particle flux, v_h denotes the horizontal wind vector (m s^{-1}), ρ is the dry air density (kg m^{-3}) and q is the specific humidity (kg kg^{-1}). Δz is the thickness of each sigma level (m), this value is not constant but increases with increasing height above ground. Since the WRF model just provides mixing ratios (r) for the three atmospheric water components (water vapour, liquid water and ice), we first calculated the specific humidity for each component using the relationship

$$q = \frac{r}{(1+r)}. \tag{2}$$

Additionally, we integrated the fluxes over the whole atmospheric column to obtain the vertically integrated atmospheric water transport fluxes. The vertical integration is performed along the metric z coordinate along the model sigma levels from surface to top using the rectangle method.

$$Q = \int_{z=z_\mathrm{sfc}}^{z=z_\mathrm{top}} v_\mathrm{h} \rho q \, \Delta z \tag{3}$$

We calculated these fluxes for the original model levels and did not interpolate them to pressure levels to avoid information loss due to the interpolation. For the analyses, 10 and 5 grid points from the HAR30 and HAR10 domain boundaries, respectively, are removed to avoid lateral boundary effects.

To analyse the AWT towards the TP, we compute vertical cross sections along transects following the border of the TP. To be able to calculate a moisture budget, we defined a region which we henceforth call "the inner TP", with 14 transects attempting to follow the highest elevations in the mountain ranges and to cut across the high mountain valleys which we assume to be pathways for atmospheric moisture. A map with the transects is shown in Fig. 1. The u and v components of AWT are then rotated to the transect coordinate system to compute the normal fluxes towards the cross section.

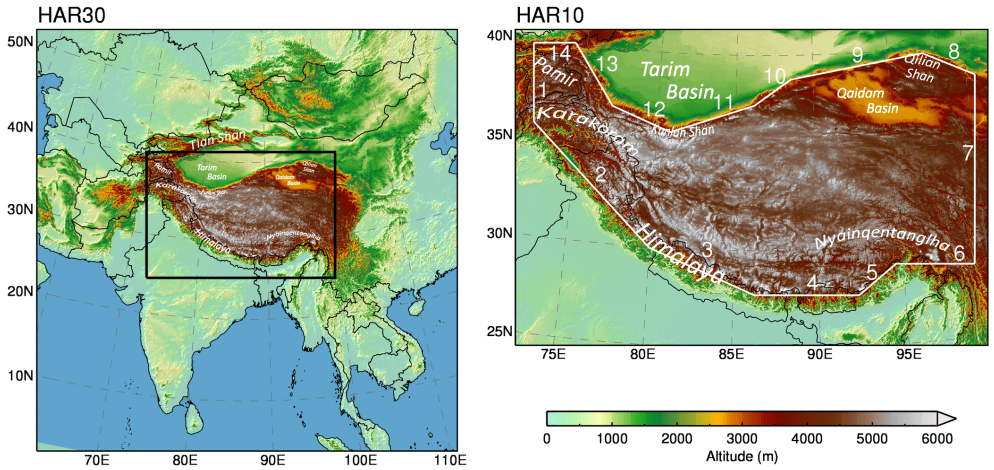

Figure 1. Maps of the Weather and Research Forecasting (WRF) model domains HAR30 (south-central Asia domain, 30 km resolution) and HAR10 (high Asia domain, 10 km resolution). The transects surrounding the Tibetan Plateau (numbered 1–14) are drawn in white. The region within the defined boundaries is called "inner TP" throughout the manuscript. Geographical locations are indicated (modified after Maussion et al., 2014).

2.3 ERA-Interim

To examine if our data set is able to reproduce the general characteristics of the WV flux, we compare the WV fluxes derived from HAR30 with ERA-Interim Reanalysis data (Dee et al., 2011). The ERA-Interim WV fluxes are available online as an integral over the atmospheric column for the eastward (u) and northward (v) components as monthly means. ERA-Interim has a horizontal resolution of 0.75°. To calculate the differences between the HAR30 and ERA-Interim WV fluxes, we transformed HAR30 data to the ERA-Interim grid by averaging the HAR30 grid points below each ERA-Interim grid point. The u and v components of the HAR fluxes were rotated to Earth coordinates first.

3 Results

3.1 Comparison of HAR30 and ERA-Interim water vapour fluxes

The general patterns and the magnitude of the WV transport amounts of HAR30 and ERA-Interim are in agreement (Fig. 2). Figure 2c shows the differences between HAR30 and ERA-Interim for July when the largest differences were found. The main differences between the two data sets are visible south of the eastern and central Tibetan Plateau along the southern slopes of the Himalayas. The WV transport through the Brahmaputra Channel towards the Tibetan Plateau is higher for ERA-Interim than for HAR30. This is probably due to differences in the representation of the orography, caused by different horizontal resolutions. HAR30 produces more transport westward along the Himalayas (upstream Ganges River), which is caused by more WV blockage. When the WV flux hits the Himalayas from the south it is mostly redirected to the west and follows the southern slopes of the Himalayas. Additionally there are differences in the Arabian Sea and the Bay of Bengal. Over the Arabian Sea, more water vapour is transported further to the south in the HAR30 data set. The transport direction in the ERA-Interim data set is more from the south-west to north-east. Therefore, the transport amount over the southern part of the Indian peninsula is also higher for HAR30. Because of that southward shift, the transport amount over the southern part of the Bay of Bengal is higher for HAR30 than for ERA-Interim and thus has a stronger northward component in the eastern part of the bay. So the South Asian Monsoon circulation has a modified shape in the HAR, possibly due to the influence of the southern branch of the mid-latitude westerlies which is more pronounced in HAR30. In winter, the differences are in general less pronounced (not shown).

3.2 Climatology of the atmospheric water transport (AWT)

Figure 3 displays the December–February (DJF) (left) and June–August (JJA) (right) decadal average of the vertically integrated atmospheric water transport (AWT) derived from HAR30. In winter (DJF), the AWT from west to east is dominant over the TP and most parts of high Asia. In the tropical ocean region, there is transport from east to west with the trade winds. The TP and the regions north of the plateau show small transport amounts, below 40 kg m^{-1} s^{-1}. For comparison, AWT reaches up to 450 kg m^{-1} s^{-1} over the South Chinese Sea off the coast of Vietnam. In summer (JJA), the pattern in the southern part of the domain is completely different from winter due to the circulation change related to the Indian summer monsoon (ISM). The largest amount of atmospheric water is now transported from west to east over the

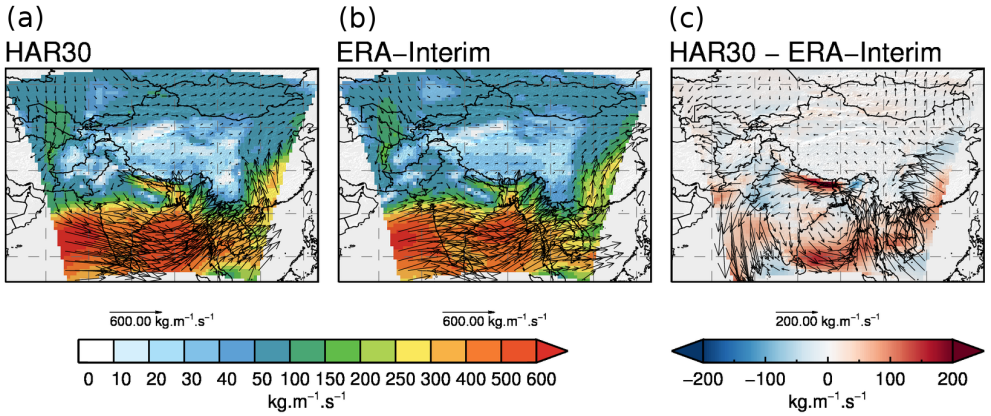

Figure 2. Decadal average of the vertically integrated water vapour flux (kg m^{-1} s^{-1}) in July for HAR30 **(a)**, ERA-Interim **(b)** and their difference **(c)**. The grid points without HAR30 data are masked out. Colour shading denotes strength of water vapour flux, arrows (plotted every second grid point) indicate transport direction (length of arrows is proportional to flux strength up to 600 kg m^{-1} s^{-1} for **(a)** and **(b)** and up to 200 kg m^{-1} s^{-1} for **(c)** and is constant afterwards for more readability).

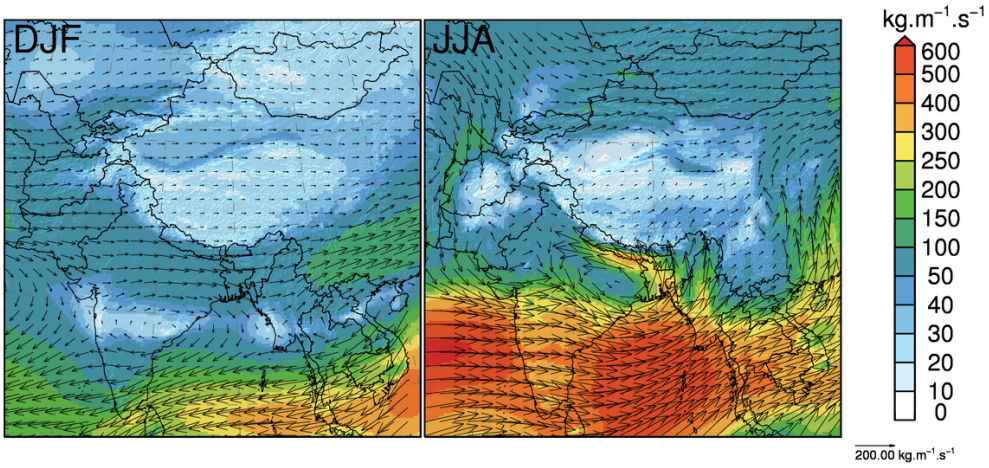

Figure 3. Decadal average of the vertically integrated water vapour flux (kg m^{-1} s^{-1}) in DJF (left) and JJA (right) for HAR30. Colour shading denotes strength of water vapour flux, arrows (plotted every sixth grid point) indicate transport direction (length of arrows is proportional to flux strength up to 200 kg m^{-1} s^{-1} and is constant afterwards for more readability).

Arabian Sea and the Bay of Bengal. Over the Bay of Bengal the flow gets a larger southerly component, and atmospheric water is directly transported to the southern slopes of the Himalayas. Over the TP the transport amount is still low in comparison.

3.2.1 Annual cycle of HAR10 water vapour (WV) transport

The annual cycle of vertically integrated WV transport (monthly decadal average) is provided in Fig. 4, and the WV transport spatially averaged for the inner TP is shown in Fig. 5. In winter, the westerlies are dominant in the whole domain, and therefore the available WV is transported eastward. The highest amounts of WV transport (50–200 kg m^{-1} s^{-1}) occur south of the Himalayas. Over the TP, the WV transport amount is distinctly lower (10–50 kg m^{-1} s^{-1}). The WV transport towards the TP can only take place through some high mountain valleys at the south-western border of the TP (western Himalayas, Karakoram, Pamir) and in the south-east of the TP where the Brahmaputra Channel is located. Additionally, the atmosphere over the TP is cold in winter and cannot hold large amounts of WV. The transport of WV over the TP further to the east is facilitated by lower elevated west–east orientated regions like the Yarlung Tsangpo (Brahmaputra) River course in the south. Therefore, the highest transport amounts are visible in the south-eastern and central southern TP.

From May to July the amount of transported WV in these regions increases and the region with higher transport extends to the central TP. This intensification of the transport is also visible in Fig. 5a and takes place before the actual mon-

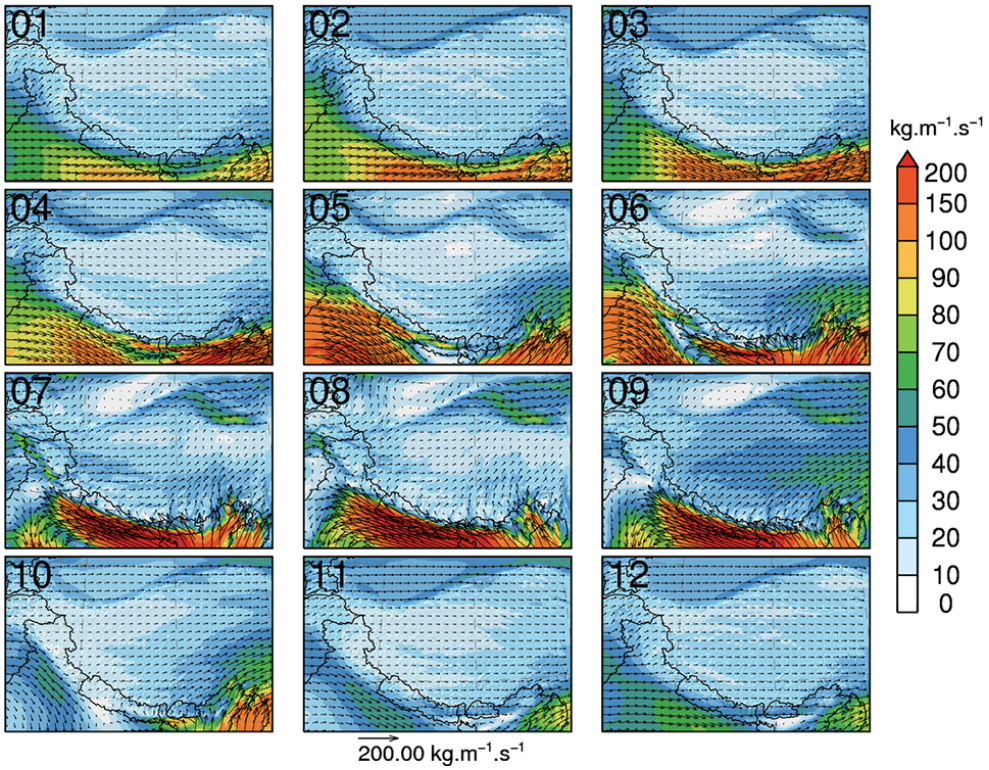

Figure 4. Decadal average of the vertically integrated water vapour flux ($kg\,m^{-1}\,s^{-1}$) in every month for HAR10. Colour shading denotes strength of water vapour flux, arrows (plotted every eighth grid point) indicate transport direction (length of arrows is proportional to flux strength up to $200\,kg\,m^{-1}\,s^{-1}$ and is constant afterwards for more readability).

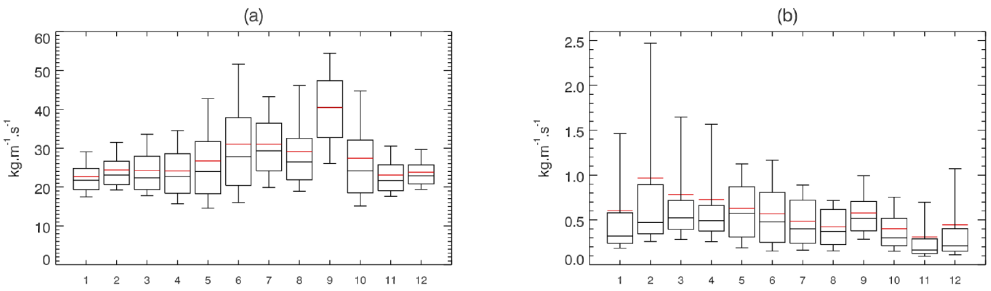

Figure 5. Box plots of the decadal average of the vertically integrated water vapour flux **(a)** and cloud particle flux **(b)** on the inner TP for HAR10 ($kg\,m^{-1}\,s^{-1}$). The boxes represent the range from the 25th to the 75th percentile. The boxes are divided by the median value (black) and the mean value (red). The whiskers represent the 10th and the 90th percentile, respectively. Note the different scales of the *y* axes.

soon season. Already by May, the WV flux south-east of the Himalayas obtains a more southerly component and the WV is no longer transported along the southern slopes, instead hitting the mountain ranges from the south. This results in an increase of the AWT amount north of the Himalayas. Due to the further evolution of the Indian summer monsoon, the transport intensifies over summer. However, large amounts of AWT from the Bay of Bengal northward to the Himalayas are blocked by the orographic barrier and redirected westward. This leads to high amounts of WV transport along the southern slopes of the Himalayas following the Ganges River course to the west. WV transport to the TP is possible where meridionally orientated valleys along this course exist.

The WV transport through the south-western border of the TP also increases over summer. This WV is not transported towards the TP by the monsoonal flow, but is rather provided by the southern branch of the mid-latitude westerlies. This is clearly visible in the transport patterns of the HAR30 domain (Fig. 3). Another hint for the contribution of the westerlies to the WV transport over the TP is the dominant transport direction in the southern TP from west to east. This eastward transport starts further west than the monsoonal flow reaches

along the southern slopes. So the WV from the Bay of Bengal cannot be the major source of the moisture transported in the westernmost regions of the TP.

In summer, the WV transport over the Qaidam Basin from north-west southward is nearly as high as in the monsoonal affected south-east of the TP. Figure 6, representing the decadal monthly average of HAR10 precipitation, shows a precipitation minimum in this region in summer, although large amounts of WV are transported to this region. Convection might be hindered by subsidence or high wind speeds (wind shear effect).

In September, we find the highest WV transport amounts over the TP. This intensification of the water vapour transport occurs because the precipitation in September (Fig. 6) is low compared to the summer months. The surface is wet due to the high precipitation rates in July and August and the temperatures are still relatively high, leading to high evaporation from the land surface. The evaporated moisture can be transported away from the source region and will not be rained out over the TP. Another reason for higher transport amounts is the wind speed recovery after the withdraw of the monsoon, which is visible in the 500 hPa wind field (Maussion et al., 2014), and facilitates higher evaporation rates and therefore higher transport amounts. In October there is only transport to the TP in the eastern and central parts of the Himalayas, because the monsoon circulation weakens and the fluxes do not reach as far westward into the Ganges valley as before. The flux from the westerlies reaches far more to the east along the southern slopes of the Himalayas (TP). In November, this pattern becomes more intense, there is no westward flux south of the Himalayas visible, the monsoon circulation collapses and wintertime conditions are established.

3.2.2 HAR10 cloud particle (CP) transport

The median value of HAR10 WV transport for the inner TP is between 20 and 40 $\mathrm{kg\,m^{-1}\,s^{-1}}$ over the whole year, while it is between 0.2 and 0.6 $\mathrm{kg\,m^{-1}\,s^{-1}}$ for the CP transport (Fig. 5). Differences in the annual cycle of the two components are clearly visible: the WV transport has its peak in summer and the CP transport in winter. To examine the relevance of CP transport for AWT, we looked at the transport patterns and amounts and calculated the contribution of the CP flux to AWT as a monthly decadal average in January and in July (Fig. 7). It shows that in winter in the Karakoram/Pamir/western Himalayas region, the CP flux can account for up to 25 % of the entire AWT. This pattern matches with the wintertime precipitation pattern in this region (Fig. 6). From April on (not shown), we find relatively high transport amounts (up to 2–3 $\mathrm{kg\,m^{-1}\,s^{-1}}$) in the south-east of the domain, but in summer the CP transport amount decreases in these two regions to very small values. Just over the central eastern parts of the plateau the amount increases to around 8 % of AWT. The percentage of CP in AWT is higher at higher elevations where the WV transport is lower because of lower temperatures. The relatively high percentage values over the Tarim Basin are related to the low AWT in general in this region

3.3 Vertical structure of the atmospheric water transport

We display the decadal average of AWT for selected vertical levels in Fig. 8. We selected the levels 1 (∼ 25 m above ground in Tibet), 5 (∼ 450 m above ground in Tibet), 8 (∼ 1200 m above ground in Tibet), 10 (∼ 2200 m above ground in Tibet), 12 (∼ 3200 m above ground in Tibet) and 15 (∼ 5500 m above ground in Tibet) because these levels show the most interesting features of the WV transport. The WV transport near the ground (level 1) is generally low in the TP and just a little bit higher south of the Himalayas, probably because of the lower surface wind speeds and of the stronger mixing in the boundary layer. The transport amount increases strongly up to level 12, where the largest transport occurs, due to higher wind speeds, higher moisture availability or both. Above this level, the WV transport starts to decrease and above level 17 (not shown) the transport amount is close to zero.

The general atmospheric circulation at different levels is visible in the transport patterns, but we have to consider that AWT is a complex mixture of wind and moisture availability. At the lower levels (1 and 5) we see the cyclonic circulation around the Tibetan heat low, with its centre in the central TP. At level 8, this structure shifts to the central northern TP. Level 12 and 15 (and levels in between) show an anticyclonic circulation around a centre in the southern TP, directly north of the Himalayas. This is the high-tropospheric Tibetan anticyclone that forms during May or early June (Flohn, 1968). In level 15 and 16, a second anticyclonic circulation is visible in the south-east of the domain, directly south of the Himalayas. Above these levels the anticyclonic circulation slowly weakens and a division into a northern part with transport from west to east, where the westerlies are dominant, and a southern part with transport from east to west is visible. Level 10, which lays between the cyclonic (level 1 and 5) and anticyclonic (level 12 and 15) circulation features, could be called the equilibrium level.

At level 5, monsoonal air and moisture is transported relatively far to the western (north-western) parts of the TP. Air from the south which originates in the tropical oceans (Indian summer monsoon) is included in the cyclonic circulation over the TP, but the WV does not seem to originate from the East Asian monsoon. In the higher levels (10–15), this cyclonic circulation is replaced by the westerlies and therefore extra-tropical air masses are transported to this region. Therefore, we find air masses and consequently moisture from different sources at one place. These results should be considered for the analysis of stable oxygen isotopes in precipitation samples, lake water, sediment and ice cores. Precipitation originating in the boundary layer will result in a monsoonal signal in the isotopes while precipitation originating

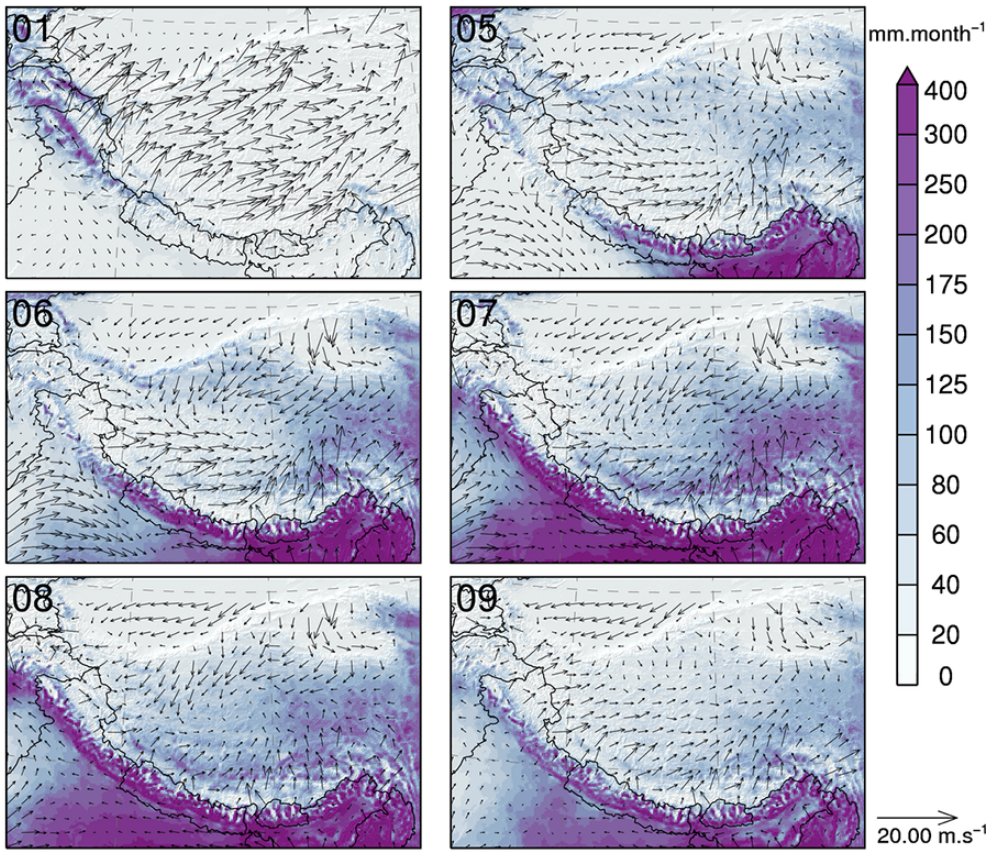

Figure 6. Decadal average of precipitation (mm month^{-1}) in January (01), May (05), June (06), July (07), August (08), and September (09) for HAR10. The arrows show the 10 m wind field (every ninth grid point plotted).

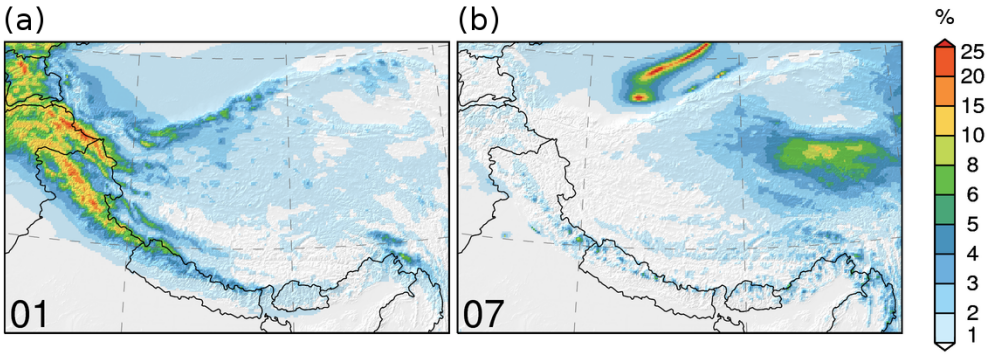

Figure 7. Decadal average of the contribution (%) of cloud particle flux to atmospheric water transport in January (01, **(a)**) and July (07, **(b)**) for HAR10.

from deep convection could have an isotope signature dedicated to the westerlies.

In the dry Tarim Basin north of the TP, we can see an anticyclonic circulation above the boundary layer at level 10 and transport of WV from north-east to south-west following the northern boundary of the TP. Therefore, the air at this level tends to descend. This means that just below this level clouds in the boundary layer are possible. These clouds can only provide small amounts of precipitation due to their low vertical extent. Above this level, the transport of WV is admittedly higher and in the opposing direction, but does not result in precipitation. Deep convection is inhibited by the subsidence tendency at the lower level.

In the south-western parts of the domain, in the border region between India and Pakistan, we can see the same feature, but there it leads to higher differences in the precip-

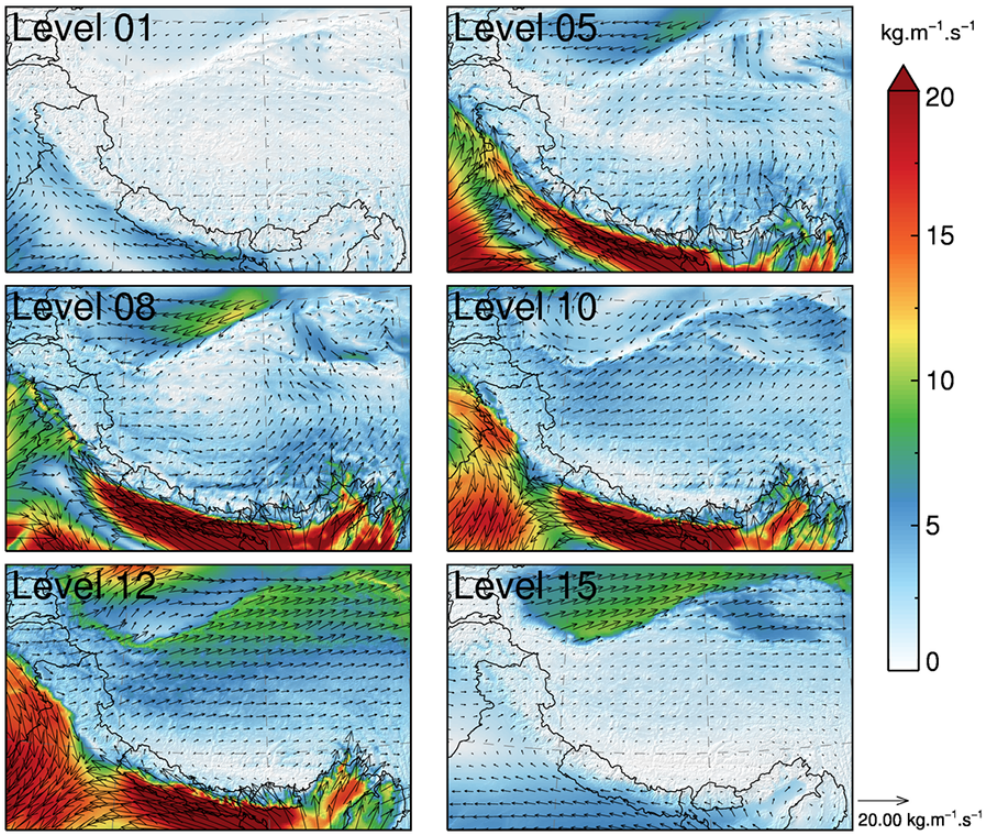

Figure 8. Decadal average of the water vapour flux ($kg\,m^{-1}\,s^{-1}$) for single selected model levels (1 ($\sim$ 25 m above ground in Tibet), 5 ($\sim$ 450 m above ground in Tibet), 8 ($\sim$ 1200 m above ground in Tibet), 10 ($\sim$ 2200 m above ground in Tibet), 12 ($\sim$ 3200 m above ground in Tibet) and 15 ($\sim$ 5500 m above ground in Tibet)) in July for HAR10. Colour shading denotes strength of water vapour flux, arrows (plotted every eighth grid point) indicate transport direction (length of arrows is proportional to flux strength up to 20 $kg\,m^{-1}\,s^{-1}$ and is constant afterwards for more readability).

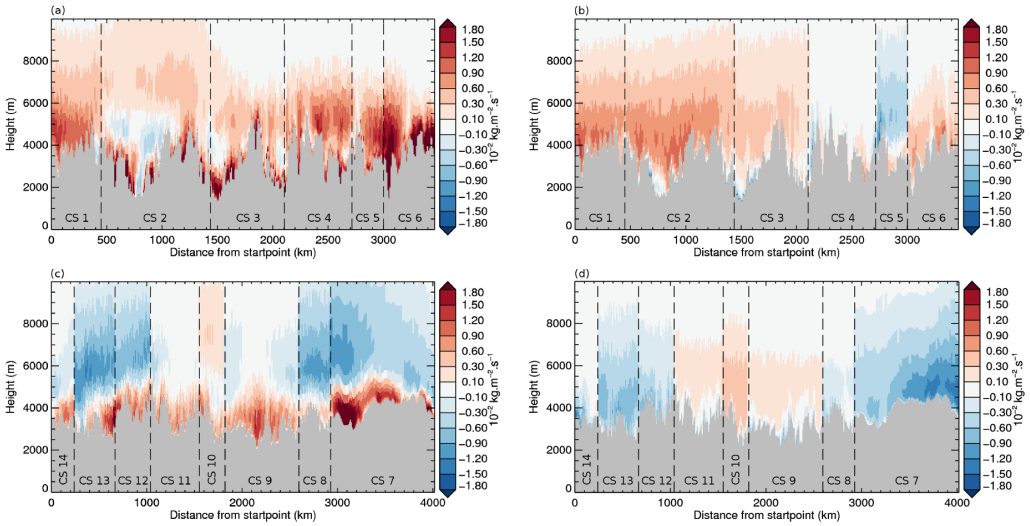

Figure 9. Decadal average of the atmospheric water transport ($10^{-2}\,kg\,m^{-2}\,s^{-1}$) for cross sections 1–6 (**a** and **b**) (from left to right, dashed lines indicate border between the cross sections) in July **(a)** and January **(b)**, and for cross sections 14–7 (**c** & **d**) in July **(c)** and January **(d)** for HAR10. Red colours denote transport towards the TP, while blue colours indicate transport away from the TP. The underlying topography is represented in grey.

itation patterns and affects a region with a higher population density. We see an anticyclonic circulation of the WV transport in the levels 10 and 12 (and in between). The transported amount is nearly as high as the WV transport associated with the ISM along the southern slopes of the Himalayas. However, if we look at the precipitation patterns, we see that there is a precipitation minimum in this region (Fig. 6). The development of deep convection is suppressed by subsidence. In the lower levels, the heat low over Pakistan (Bollasina and Nigam, 2010) is visible in the transport patterns (Fig. 8) and in the 10 m wind field (Fig. 6). Saeed et al. (2010) point out that the heat low over Pakistan connects the mid-latitude wave train with the Indian summer monsoon. In the surrounding region where we do not see this anticyclonic movement in the levels above the boundary layer, the large amounts of transported WV result in high amounts of precipitation. These results can provide an indication of the processes, which lead to the risk of droughts and floods (e.g. in July 2010) in Pakistan, as already analysed by Galarneau et al. (2012)

3.4 Transport towards the Tibetan Plateau through its borders

We calculated the WV input towards the TP through its borders (Fig. 9 and Table 1). For the southern boundary cross sections (CS 2–6) the highest transport amounts occur in summer (Fig. 9a) in the lower layers and decreases with increasing height. The largest fluxes occur in the regions where the elevation is lower compared to the direct surroundings, in the large meridionally orientated valleys (eastern Himalayas, in the region of the Brahmaputra channel). There, the areas of lower elevation are wider and the AWT from the Indian Ocean hits the mountain ranges directly from the south.

The AWT from the TP to the south is negligible in summer (Fig. 9a). It occurs mainly in CS 2 and a little in CS 3. This kind of recirculation may reflect northward transport. It takes place in the lower levels above a layer with high northward transport amounts. In winter (Fig. 9b), AWT is lower but the input of atmospheric moisture is still dominant.

The AWT through the western boundary (CS 1) (Fig. 9a and b, and Table 1) is higher in winter than in summer, as it is for CS 2 in the westernmost region of the Himalayas. These regions are dominated by atmospheric water input by extra-tropical air masses, transported to this region by the westerlies. In sum, the AWT in CS 2 is still almost as high as the AWT in CS 6. CS 6 contains the Brahmaputra Channel, which is often referred to as one of the main input channels for atmospheric moisture (Tian et al., 2001).

Table 1 shows the monthly decadal average of AWT input to the TP through the individual cross sections converted to a theoretical equivalent precipitation amount on the inner TP. We picked CS 1 and CS 6 for a closer comparison because CS 6 includes the Brahmaputra Channel and CS 1 is the western boundary, and they are of the same length. From November to April the transport through the western boundary (CS 1) is distinctly greater than that through CS 6. From May to October CS 6 shows higher transport amounts, but the differences are less than for the wintertime. In July the input of CS 1 is 90.47 % that of CS 6. This means that the input through the western boundary is around 90 % of the transport through the Brahmaputra Channel region. This is the month where the differences are smallest. We can see that for almost every month, CS 2–3 exhibits the largest input amounts. AWT through this cross section is controlled not only by the ISM but also by the southern branch of the mid-latitude westerlies.

The cross section for the eastern boundary (CS 7) shows that the TP is a source of atmospheric water for the downstream regions east of the TP for all months (Table 1 and Fig. 9c and d). In January, there is only eastward transport through the eastern boundary (Fig. 9d). In the other months (not shown except for July, Fig. 9c), we find additionally transport towards the TP in the lower layers near the surface. The transport towards the TP through eastern cross section has its peak in July (Fig. 9c) in the northern parts of the boundary where the elevation is distinctly lower than in the southern parts. Above this region, there is still eastward AWT away from the TP. However, if we look at the total of the AWT amount through the eastern boundary, we see that the transport from the plateau towards the east is also dominant in summer.

The transport through the northern boundary (CS 14–8) towards the TP (input) is lower than from the west and south in January and July (Fig. 9d and c, Table 1), although the circulation is directed to the boundary of the TP especially in summer. There, we find a strong gradient in altitude and fewer passages through which the atmospheric water could enter the TP than in the Himalayas. For the westernmost northern cross sections (14–12) the transport from the TP to the north is dominant. The reason for this is the north-eastward transport in the western TP, which also explains the lower transport amounts towards the TP. The AWT within the northern branch of the westerlies north of the TP is blocked by the high-altitude TP. AWT then follows the northern border of the TP to the east, where the elevation is lower in some regions (CS 9–11), e.g. at the border to the Qaidam Basin (CS 9). There, the input of atmospheric water to the TP is dominant for all months and the maximum input takes place in spring. AWT from the north to the Qaidam Basin is also visible in Fig. 4 for all months. This transport takes place in the lower layers of the atmosphere. The transport from the plateau northwards has its peak at the easternmost northern CS (CS 8) in July, August and September, when the TP can provide large amounts of atmospheric water, as shown in Sect. 3.2.1 in Fig. 4.

Table 1. Decadal average of the atmospheric water flux converted to a theoretical precipitation amount (mm month^{-1}) through vertical cross sections (1, 2–3, 4–5, 6, 7, 8, 9, 10–11, 12–14) and standard deviations (SD) for HAR10 (positive values denote transport towards the TP and negative values denote transport away from the TP). Decadal average of the precipitation (mm month^{-1}) and its standard deviation (SD) on the inner TP and of the contribution (%) of the atmospheric water flux to the precipitation for HAR10.

CS	1	2–3	4–5	6	7	8	9	10–11	12–14	1–14		
Month	West	SW 1–2	South 1–2	Brahmaputra	East	North-east	Qaidam	NW 5–4	NW 3–1	Sum	Inner TP precipitation	Ratio
01	12.8	41.2	-5.0	5.9	−34.0	−2.1	3.7	7.2	−17.7	12.1	22.9	52.6 %
02	15.8	47.4	−4.7	5.4	−31.5	−2.6	3.8	7.5	−21.1	20.0	33.5	59.7 %
03	19.8	35.4	−6.0	7.6	−37.8	−2.9	8.1	11.1	−23.9	11.5	33.9	33.9 %
04	17.8	33.4	−4.7	9.1	−36.2	−3.3	9.5	10.6	−22.8	13.4	42.7	31.4 %
05	17.1	21.5	9.1	21.3	−44.3	−5.6	8.5	10.4	−19.1	18.9	55.3	34.2 %
06	12.2	26.4	18.6	22.2	−42.4	−6.4	9.1	7.7	−14.5	32.9	72.3	45.5 %
07	14.9	34.4	24.3	16.5	−19.4	−12.2	4.2	5.3	−22.5	45.4	98.0	46.4 %
08	11.7	33.7	22.5	16.1	−22.9	−12.7	6.2	6.8	−22.6	38.8	91.8	42.2 %
09	12.3	44.0	20.3	19.0	−55.1	−11.3	2.4	5.1	−21.9	14.8	57.6	25.7 %
10	15.4	21.3	9.6	18.4	−56.3	−5.0	3.6	6.2	−17.3	−4.1	23.6	−17.5 %
11	16.9	24.4	−5.9	4.9	−35.5	−2.5	5.8	9.4	−20.5	−3.0	11.9	−25.2 %
12	15.0	36.5	−6.6	3.3	−34.2	−2.1	4.9	8.9	−20.5	5.3	15.8	33.7 %
Sum (mm yr^{-1})	181.6	399.6	71.7	149.8	−449.8	−68.8	70.1	96.2	−244.2	206.0	559.2	(36.8 ± 6.3) %
SD (mm yr^{-1})	59.4	47.6	15.5	22.1	44.1	8.4	12.7	12.8	24.5	42.6	77.1	
SD (%)	32.7 %	11.9 %	21.6 %	14.8 %	9.8 %	12.3 %	18.1 %	13.3 %	10.0 %	20.7 %	13.8 %	

Table 2. The same as Table 1 but for HAR30.

CS	1	2–3	4–5	6	7	8	9	10–11	12–14	1–14		
Month	West	SW 1–2	South 1–2	Brahmaputra	East	North-east	Qaidam	NW 5–4	NW 3–1	Sum	Inner TP precipitation	Ratio
01	13.6	43.1	−7.9	6.4	−35.9	−2.6	3.9	7.6	−19.9	8.3	24.3	34.0 %
02	16.7	49.8	−7.4	6.1	−33.7	−3.2	4.1	8.1	−23.8	16.8	35.7	47.0 %
03	21.5	36.9	−9.1	9.3	−41.1	−3.4	8.6	12.1	−27.5	7.3	36.7	19.9 %
04	19.6	35.2	−8.3	11.1	−39.5	−3.7	10.1	11.3	−26.6	9.2	46.0	20.0 %
05	19.0	21.4	7.5	23.3	−47.3	−5.9	9.2	10.9	−22.3	15.9	60.0	26.5 %
06	13.4	25.1	20.1	23.2	−47.1	−6.5	10.1	7.5	−16.1	29.8	76.2	39.1 %
07	16.2	32.2	27.6	14.1	−24.0	−12.6	4.9	3.9	−24.0	48.3	98.8	38.8 %
08	12.2	32.1	25.5	14.0	−27.3	−13.4	7.0	5.2	−23.7	31.6	91.8	34.5 %
09	13.4	43.2	22.8	19.3	−60.7	−12.1	2.9	4.5	−24.2	9.1	58.4	15.5 %
10	17.1	20.2	8.6	19.7	−59.2	−5.8	4.0	6.8	−20.3	−8.9	25.1	−35.6 %
11	18.4	24.5	−9.6	5.0	−37.1	−3.1	6.1	10.2	−23.6	−9.1	12.9	−71.1 %
12	16.0	38.2	−10.1	3.3	−35.9	−2.7	5.2	9.5	−23.0	0.4	16.7	32.7 %
Sum (mm yr^{-1})	197.2	401.9	59.7	154.9	−488.6	−75.0	76.1	97.4	−274.9	148.7	582.5	(25.5 ± 7.4) %
SD (mm yr^{-1})	25.4	53.2	18.3	23.5	212.7	9.4	13.8	13.5	27.8	47.4	81.0	
SD (%)	12.9 %	13.2 %	30.6 %	15.2 %	43.5 %	12.5 %	18.1 %	13.9 %	10.1 %	31.9 %	13.9 %	

3.5 Budget

Since we analysed AWT transport in and to the TP and quantified the input and output, the question arises of which amount of precipitation falling on the inner TP results from external moisture supply and which amount is provided by the TP itself from local sources and moisture recycling.

Table 1 displays the monthly decadal average of AWT through the individual cross sections and the sum for all cross sections, the precipitation falling on the inner TP and the ratios between them. To make the comparison with the precipitation easier, we converted the net atmospheric water input to a theoretical precipitation equivalent (mm month^{-1}). We obtain an annual mean AWT input of 206.0 mm yr^{-1} for HAR10. For the mean annual precipitation falling on the inner TP, a value of 559.2 mm yr^{-1} results. The ratio of net input of atmospheric water to the precipitation falling on the inner TP reveals that, on average, AWT through the borders accounts for 36.8 % of the precipitation during the year. Ac-

cording to this, the remaining 63.2 % of atmospheric water needed for precipitation must be provided by the TP itself. This moisture supply probably takes place via moisture recycling from local sources, e.g. evaporation from numerous large lakes, soil moisture, the active layer of permafrost, snow melt and glacier run-off. The ratio is highest in winter when the TP cannot provide moisture for precipitation by itself, followed by summer, where the largest net input occurs. In October and November the ratio is negative, which means that the TP provides more moisture than it receives from external sources. These are the 2 months where the output of moisture from the TP is larger than the input; this is possible because the moisture imported to the TP in summer is available for export in autumn. On a monthly basis, there is certainly a time lag between the moisture entrance and the precipitation, making the analysis of the monthly ratios difficult. The standard deviations for HAR10 (HAR30) in Table 1 (2) show that the atmospheric water input varies more between the years than the precipitation falling on the TP. This implies that the evaporation from local sources stabilises the precipitation falling on the inner TP.

4 Discussion

4.1 General discussion of results

The main WV input to the TP takes place through the southern and western boundaries, confirming the results of Feng and Zhou (2012), even if their western boundary is further east. The WV entering the TP through the eastern part of the southern boundary originates from the monsoonal air masses, while the WV entering the TP through the western boundary originates in the mid-latitude westerlies. The relatively high input through the western boundary shows that the westerlies are not fully blocked by the TP and not all moisture transported with them is redirected north or south. The magnitude of this WV input is similar to that of the input through the Brahmaputra channel. This agrees with the findings of Mölg et al. (2013), who found that the westerlies play a role for precipitation and glacier mass balance in summer also, and they challenged the assumption that the westerlies contribute moisture only in winter or just in the northernmost parts of the TP in summer (Hren et al., 2009; Tian et al., 2007). Our results show that there is direct atmospheric water transport through the western boundary by the mid-latitude westerlies in summer, which shoes that the westerlies are not fully blocked by the TP. The westerlies also contribute moisture to the TP through valleys in the western parts of the southern boundary by the southern branch of the westerlies. This implies that moisture entering the TP from the south-west can be transported there either by the westerlies or the monsoon, depending on the how far these systems extend eastward or westward along the southern slopes of the Himalayas, respectively. The examination of this structure will be the subject of a subsequent study. The main WV output from the TP takes place through the eastern border, as also found by Feng and Zhou (2012). The TP is a source of moisture for the downstream regions in the east throughout the year like the Yangtze River valley in China, agreeing the results from Chen et al. (2012) and Luo and Yanai (1983), that the TP contributes precipitation to its downstream areas in summer. Thus we can confirm the importance of the findings from Bin et al. (2013), Xu et al. (2011) and Chen et al. (2012), who called the TP a transfer or re-channel platform of moisture for the downstream regions in East Asia.

In our study, we could not find any contribution of the East Asian Summer Monsoon to the WV transport towards the TP, although it has thus far been assumed to have an influence on the TP (Yao et al., 2012; Bolch et al., 2012). The WV transported from east to the TP in the lower levels in summer (CS 7, Fig. 9c), also detected by Luo and Yanai (1983) and Feng and Zhou (2012), is not transported to this region by the East Asian Monsoon flow but by the eastern branch of the Indian summer monsoon flow. This is clear if we look at the transport patterns for HAR30 (Fig. 3). It is interesting that the HAR WV flux has a stronger westward component east of the TP than ERA-Interim (Fig. 2c) and still does not show any transport from east to west in the climate mean state. Since we focus on the mean climatology during our period of investigation, we cannot exclude the contribution of moisture from the East Asian summer monsoon (EASM) to the TP for single years or events, but at the same time we expect it to be visible in the mean if it is significant. Our hypothesis is that the transient weather systems could bring moisture from the east to the TP; however they are not visible in the means. It will be the goal of a future study to examine such weather systems in detail.

Prior studies focused on the WV transport and did not consider the CP flux. The assumption so far was that the CP transport is so small compared to the WV flux, that it does not have a significant influence on the atmospheric moisture transport. Our results show that the contribution of the CP flux to the entire AWT is not negligible in winter in the Pamir and Karakoram ranges (the western and south-western border of the TP), where it contributes up to 25 % of the entire AWT. The fact that the CP transport plays a role in the Karakoram and western Himalayas, the regions which are controlled mainly by the westerlies, lets us conclude that in this region moisture advection presumably plays a strong role. The horizontal motion is dominant in advective processes towards convection where the vertical motion is dominant. This leads to the fact that clouds developed in advective processes, for example frontal processes, can be transported further away from their origin than convective clouds.

The moisture supply from external sources provides around 36.8 % of the atmospheric water needed to produce the mean annual precipitation on the inner TP while the remaining part originates from the TP itself by local moisture recycling. These results highlights the importance of local moisture recycling as already emphasized by Kurita and Ya-

mada (2008), Joswiak et al. (2013) and Chen et al. (2012). For the northern Tibetan Plateau, Yang et al. (2006) detected that 32.06 % of the precipitation is formed by water vapour from ocean air mass and 46.86 % is formed by water vapour evaporated from local sources. They found that at least 21.8 % of the precipitation is formed by water vapour evaporated on the way and then transported by the monsoon circulation. Yang et al. (2007) also showed that for two flat observation sites in the central eastern part of the TP, the evaporation is 73 and 58 % of the precipitation amount. This is in a good agreement with our results that 63.3 % is provided by local moisture recycling. This moisture is provided by evaporation from numerous large lakes, soil moisture, the active layer of permafrost, snow melt and glacier run-off. The question arises over what will happen with the atmospheric water, which is transported to the TP. Does it remain in the TP or is it lost as run-off. Could this moisture input be an explanation for the observed lake level rises?

The comparison of the net atmospheric water input to the TP through the cross sections, the precipitation falling on the inner TP and the ratio between them for HAR10 (Table 1) and HAR30 (Table 2) show that the different horizontal resolutions result in differences between the two data sets. On an annual basis, the different horizontal resolutions result in an AWT input difference of 57.3 mm yr^{-1} and a precipitation difference on the inner TP of 23.3 mm yr^{-1}, where HAR30 has the lower AWT input but the higher precipitation amount. This leads to a difference of 11.3 percentage points in the ratio of AWT to precipitation between the HAR10 (36.8 %) and HAR30 (25.5 %) data sets. Nevertheless, HAR30 has, for almost every cross section and month, higher transport amounts for both input and output. Due to the fact that the output values are also higher, the annual net input for HAR30 is lower than for HAR10. On an annual basis HAR30 shows just three-fourths of the HAR10 AWT input. A possible explanation for lower transport amounts for individual cross sections in HAR10 could be that the higher horizontal resolution is overridden by higher orographic barriers due to better representation of the topography. Shi et al. (2008) showed that a higher horizontal resolution and more realistic representation of the topography is important for the development of disturbances leading to precipitation events in the downstream regions of the TP like the Yangtze River valley. Our study shows that for a quantification of AWT and the spatiotemporal detection of its major pathways and sources it is important to examine the complex topography of high Asia with high spatial resolution.

4.2 Sources of uncertainty

The uncertainty of the results depends on the accuracy of the data itself, the position of the cross sections used to calculate the budget and the vertical resolution of the data set.

Maussion et al. (2014) compared HAR precipitation with rain-gauge observations and the TRMM precipitation products 3B42 (daily), 3B43 (monthly) and 2B31 (higher resolution). They found an improvement when increasing the horizontal resolution from 30 to 10 km in comparison to the gauges. A slight positive bias could be detected against the same stations (0.17 mm day^{-1} for HAR10 and monthly precipitation values, their Fig. 3), comparable to that of TRMM 3B43 (0.26 mm day^{-1}). Converted to annual values (62 mm yr^{-1}) and compared to the value of HAR precipitation averaged over the inner TP (559 mm yr^{-1}), this bias remains significant. In a simple first-order approach, by assuming this bias to be constant over the region (and assuming no rain gauge undercatch), this would increase the part of moisture needed for precipitation coming from the outer TP from 36.8 to 41.4 %.

To determine if the position of the cross sections has an influence on our results, we replicated our budget analyses with the cross sections moved around 60 km towards the centre of the TP for the HAR10 data set. This results in new budget values for net atmospheric water input of 202.6 mm yr^{-1} (206.0 mm yr^{-1} with the old cross sections), and 506.3 mm yr^{-1} (559.2 mm yr^{-1}) precipitation falling on the inner TP. This result in a change of the percentage from 36.8 % (found for the original position of the cross sections) to 40 %. This is caused mainly by a change of the precipitation amount of −52.9 mm yr^{-1}, while the atmospheric water input is nearly the same (−3.4 mm yr^{-1}). This change is smaller than the standard deviation (6.3 %) of this ratio.

We analysed if the vertical resolution could have an influence on precipitation and moisture transport by creating a new series of simulations for the entire year of 2010, whereby we increased the number of vertical levels from 28 to 36 (all other settings kept unchanged). Precipitation patterns in the HAR10 domain remain very similar. Large absolute differences are found in the monsoonal affected regions south of the TP and the Himalayas. The largest relative differences occur in regions with very low precipitation rates, in the arid regions (e.g. Tarim Basin) north of the TP. The amounts and patterns of the vertically integrated atmospheric water transport match well with one another, relative differences are around ±5 % in the TP and only slightly higher in small regions south and north of the TP. The computation of the water budget for the year 2010 for 36 (28) vertical levels results in a net input of atmospheric water of 191.9 mm yr^{-1} (195.2 mm yr^{-1}), with 623.3 mm yr^{-1} (621.8 mm yr^{-1}) precipitation falling on the inner TP and an annual proportion of 30.8 % (31.4 %) for 2010. This shows that the results obtained with 28 vertical levels are reliable.

There is no other possible way to estimate the uncertainty of the computed fluxes than the rough comparison of ERA-Interim provided in Sect. 3.1. Certainly, the choice of the model set-up and the reinitialization strategy also influence our results. Put together, these uncertainties are not negligible but there is no indication that our core conclusions are significantly affected.

Due to the temporal averaging of the model results to monthly means, we ascertain the mean climatology, but lose the ability to analyse the data process based. The processes regarding the interplay of atmospheric water transport and precipitation will be the subject of a subsequent study at a higher temporal resolution (e.g. daily).

5 Conclusions

The TP experiences high precipitation variability leading to dry spells and droughts, as well as to severe snow- and rainfall events and subsequent floods. However, there are strong differences between regions and seasons which are not yet well understood on present-day climate conditions, making statements for past and future climates highly speculative. Therefore, in another study, we will analyse if there are significant differences in the AWT patterns in wet and dry years to find out whether the extremes are influenced by changes in atmospheric circulations or just in a change of the transported amount of atmospheric water. These results could then be compared with the results of Lu et al. (2014), who analysed the differences in the atmospheric circulation for wet and dry monsoon seasons of nearly the same period (2000–2010) using coarser-resolution data sets. Large-scale teleconnections, such as the influence of the North Atlantic Oscillation (NAO) mode during wet and dry periods, have been analysed for longer periods by, e.g. Liu and Yin (2001) and Bothe et al. (2009, 2011). An examination of the AWT patterns in the HAR during periods with positive or negative NAO index could be used to potentially reconfirm their findings using higher-resolution data. Interesting regional features, such as the large amount of atmospheric water over the dry Qaidam Basin, which does not result in precipitation, need to be studied in detail by analysing the reasons for precipitation suppression. Dust particles originating in the arid regions could play a role in precipitation suppression (Han et al., 2009).

Our first water budget estimate reveals that local moisture recycling is an important factor and provides more moisture than the input from external sources (on average 60 % versus 40 %). Moisture recycling has to be studied more in detail in the future to gain a better understanding of the water cycle in the TP. It would be interesting to analyse if and how the atmospheric water stored in snow in winter contributes to the atmospheric water transport and precipitation of the following warm season. Due to this storage term, the westerlies could play an even greater role in the hydrological cycle of some regions of the TP in summer. It is difficult to clearly differentiate between moisture provided by the large-scale circulations (mid-latitude westerlies and monsoon systems) or local moisture recycling because, for example, monsoonal moisture could reach the north-eastern parts of the TP via multiple moisture recycling as mentioned by Yang et al. (2006). Also, the mixing of water vapour sources as seen in the examination of the vertical structure of the transport shows that the general question of where the moisture comes from often cannot be answered by naming only one source. This can make the identification of moisture sources using isotope signals difficult. Therefore, the part of the atmospheric column where the precipitation actually forms has to be identified in addition to the development of a more in-depth analysis of the atmospheric water transport fluxes on individual levels. Additionally the other components of the water balance, e.g. evaporation and run-off, should be considered in further studies.

Acknowledgements. This work was supported by the German Federal Ministry of Education and Research (BMBF) Programme, Central Asia – Monsoon Dynamics and Geo-Ecosystems (CAME), within the WET project (Variability and Trends in Water Balance Components of Benchmark Drainage Basins on the Tibetan Plateau) under the code 03G0804A and by the German Research Foundation (DFG) Priority Programme 1372, Tibetan Plateau: Formation – Climate – Ecosystems, within the DynRG-TiP (Dynamic Response of Glaciers on the Tibetan Plateau to Climate Change) project under the codes SCHE 750/4-1, SCHE 750/4-2 and SCHE 750/4-3. The author F. Maussion acknowledges support by the Austrian Science Fund (FWF project P22443-N21). We would like to thank Oliver Bothe and a further anonymous referee for their thoughtful comments and critique.

Edited by: M. Werner

References

An, Z., Colman, S. M., Zhou, W., Li, X., Brown, E. T., Jull, A. J. T., Cai, Y., Huang, Y., Lu, X., Chang, H., Song, Y., Sun, Y., Xu, H., Liu, W., Jin, Z., Liu, X., Cheng, P., Liu, Y., Ai, L., Li, X., Liu, X., Yan, L., Shi, Z., Wang, X., Wu, F., Qiang, X., Dong, J., Lu, F., and Xu, X.: Interplay between the Westerlies and Asian monsoon recorded in Lake Qinghai sediments since 32 ka., Sci. Rep., 2, 619, doi:10.1038/srep00619, 2012.

Araguás-Araguás, L., Froehlich, K., and Rozanski, K.: Stable isotope composition of precipitation over southeast Asia, J. Geophys. Res., 103, 28721–28742, doi:10.1029/98JD02582, 1998.

Bin, C., Xiang-De, X., and Tianliang, Z.: Main moisture sources affecting lower Yangtze River Basin in boreal summers during 2004-2009, Int. J. Climatol., 33, 1035–1046, doi:10.1002/joc.3495, 2013.

Bolch, T., Kulkarni, A., Kääb, A., Huggel, C., Paul, F., Cogley, J. G., Frey, H., Kargel, J. S., Fujita, K., Scheel, M., Bajracharya, S., and Stoffel, M.: The state and fate of Himalayan glaciers, Science, 336, 310–314, doi:10.1126/science.1215828, 2012.

Bollasina, M. and Nigam, S.: The summertime "heat" low over Pakistan/northwestern India: evolution and origin, Clim. Dynam., 37, 957–970, doi:10.1007/s00382-010-0879-y, 2010.

Bookhagen, B. and Burbank, D. W.: Toward a complete Himalayan hydrological budget: Spatiotemporal distribution of snowmelt and rainfall and their impact on river discharge, J. Geophys. Res., 115, F03019, doi:10.1029/2009JF001426, 2010.

Bothe, O., Fraedrich, K., and Zhu, X.: The large-scale circulations and summer drought and wetness on the Tibetan Plateau, Int. J. Climatol., 30, 844–855, doi:10.1002/joc.1946, 2009.

Bothe, O., Fraedrich, K., and Zhu, X.: Large-scale circulations and Tibetan Plateau summer drought and wetness in a high-resolution climate model. Int. J. Climatol., 31, 832–846, doi:10.1002/joc.2124, 2011.

Chen, B., Xu, X.-D., Yang, S., and Zhang, W.: On the origin and destination of atmospheric moisture and air mass over the Tibetan Plateau, Theor. Appl. Climatol., 110, 423–435, doi:10.1007/s00704-012-0641-y, 2012.

Dee, D. P., Uppala, S. M., Simmons, a. J., Berrisford, P., Poli, P., Kobayashi, S., Andrae, U., Balmaseda, M. a., Balsamo, G., Bauer, P., Bechtold, P., Beljaars, a. C. M., van de Berg, L., Bidlot, J., Bormann, N., Delsol, C., Dragani, R., Fuentes, M., Geer, a. J., Haimberger, L., Healy, S. B., Hersbach, H., Hólm, E. V., Isaksen, L., Kållberg, P., Köhler, M., Matricardi, M., McNally, a. P., Monge-Sanz, B. M., Morcrette, J.-J., Park, B.-K., Peubey, C., de Rosnay, P., Tavolato, C., Thépaut, J.-N., and Vitart, F.: The ERA-Interim reanalysis: configuration and performance of the data assimilation system, Q. J. Roy. Meteorol. Soc., 137, 553–597, doi:10.1002/qj.828, 2011.

Feng, L. and Zhou, T.: Water vapor transport for summer precipitation over the Tibetan Plateau: Multidata set analysis, J. Geophys. Res.-Atmos., 117, D20114, doi:10.1029/2011JD017012, 2012.

Flohn, H.: Contributions to a meteorology of the Tibetan highlands. Atmospheric Science Paper No. 130, Department of Atmosphere Science, Colorado State University: Colorado, 1968.

Galarneau, T. J., Hamill, T. M., Dole, R. M., and Perlwitz, J.: A Multiscale Analysis of the Extreme Weather Events over Western Russia and Northern Pakistan during July 2010, Mon. Weather Rev., 140, 1639–1664, doi:10.1175/MWR-D-11-00191.1, 2012.

Gao, Y., Cuo, L., and Zhang, Y.: Changes in Moisture Flux over the Tibetan Plateau during 1979–2011 and Possible Mechanisms, J. Climate, 27, 1876–1893, doi:10.1175/JCLI-D-13-00321.1, 2014.

Günther, F., Mügler, I., Mäusbacher, R., Daut, G., Leopold, K., Gerstmann, U. C., Xu, B., Yao, T., and Gleixner, G.: Response of dD values of sedimentary n-alkanes to variations in source water isotope signals and climate proxies at lake Nam Co , Tibetan Plateau, Quaternary Int., 236, 82–90, doi:10.1016/j.quaint.2010.12.006, 2011.

Guenther, F., Aichner, B., Siegwolf, R., Xu, B., Yao, T., and Gleixner, G.: A synthesis of hydrogen isotope variability and its hydrological significance at the Qinghai–Tibetan Plateau, Quaternary Int., 313–314, 3–16, doi:10.1016/j.quaint.2013.07.013, 2013.

Han, Y., Fang, X., Zhao, T., Bai, H., Kang, S., and Song, L.: Suppression of precipitation by dust particles originated in the Tibetan Plateau, Atmos. Environ., 43, 568–574, doi:10.1016/j.atmosenv.2008.10.018, 2009.

Hren, M. T., Bookhagen, B., Blisniuk, P. M., Booth, A. L., and Chamberlain, C. P.: δ18O and δD of streamwaters across the Himalaya and Tibetan Plateau: Implications for moisture sources and paleoelevation reconstructions, Earth Planet. Sci. Lett., 288, 20–32, doi:10.1016/j.epsl.2009.08.041, 2009.

Immerzeel, W. W., van Beek, L. P. H., and Bierkens, M. F. P.: Climate change will affect the Asian water towers, Science, 328, 1382–1385, doi:10.1126/science.1183188, 2010.

Immerzeel, W. W., Pellicciotti, F., and Bierkens, M.: Rising river flows throughout the twenty-first century in two Himalayan glacierized watersheds, Nat. Geosci., 6, 742–745, doi:10.1038/ngeo1896, 2013.

Joswiak, D. R., Yao, T., Wu, G., Tian, L., and Xu, B.: Ice-core evidence of westerly and monsoon moisture contributions in the central Tibetan Plateau, J. Glaciol., 59, 56–66, doi:10.3189/2013JoG12J035, 2013.

Kang, S., Qin, D., Ren, J., Zhang, Y., Kaspari, S., Mayewski, P. A., and Hou, S.: Annual Accumulation in the Mt. Nyainqentanglha Ice Core, Southern Tibetan Plateau, China: Relationships To Atmospheric Circulation over Asia, Arctic, Antarct. Alp. Res., 39, 663–670, doi:10.1657/1523-0430(07503)[KANG]2.0.CO;2, 2007.

Kurita, N. and Yamada, H.: The Role of Local Moisture Recycling Evaluated Using Stable Isotope Data from over the Middle of the Tibetan Plateau during the Monsoon Season, J. Hydrometeorol., 9, 760–775, doi:10.1175/2007JHM945.1, 2008.

Liu, J., Kang, S., Gong, T., and Lu, A.: Growth of a high-elevation large inland lake, associated with climate change and permafrost degradation in Tibet, Hydrol. Earth Syst. Sci., 14, 481–489, doi:10.5194/hess-14-481-2010, 2010.

Liu, X. and Yin, Z.-Y.: Spatial and Temporal Variation of Summer Precipitation over the Eastern Tibetan Plateau and the North Atlantic Oscillation, J. Climate, 14, 2896–2909, doi:10.1175/1520-0442(2001)014, 2001.

Lu, N., Qin, J., Gao, Y., Yang, K., Trenberth, K. E., Gehne, M., and Zhu, Y.: Trends and variability in atmospheric precipitable water over the Tibetan Plateau for 2000–2010, Int. J. Climatol., doi:10.1002/joc.4064, in press, 2014.

Luo, H. and Yanai, M.: The large-scale circulation and heat sources over the Tibetan Plateau and surrounding areas during the early summer of 1979. Part I: Precipitation and kinematic, Mon. Weather Rev., 111, 922–944, doi:10.1175/1520-0493(1983)111<0922:TLSCAH>2.0.CO;2, 1983.

Maussion, F., Scherer, D., Finkelnburg, R., Richters, J., Yang, W., and Yao, T.: WRF simulation of a precipitation event over the Tibetan Plateau, China – an assessment using remote sensing and ground observations, Hydrol. Earth Syst. Sci., 15, 1795–1817, doi:10.5194/hess-15-1795-2011, 2011.

Maussion, F., Scherer, D., Mölg, T., Collier, E., Curio, J., and Finkelnburg, R.: Precipitation Seasonality and Variability over the Tibetan Plateau as Resolved by the High Asia Reanalysis*, J. Climate, 27, 1910–1927, doi:10.1175/JCLI-D-13-00282.1, 2014.

Mölg, T., Maussion, F., and Scherer, D.: Mid-latitude westerlies as a driver of glacier variability in monsoonal High Asia, Nat. Clim. Change, 4, 68–73, doi:10.1038/nclimate2055, 2013.

Saeed, S., Müller, W. A., Hagemann, S., and Jacob, D.: Circumglobal wave train and the summer monsoon over northwestern India and Pakistan: the explicit role of the surface heat low, Clim. Dynam., 37, 1045–1060, doi:10.1007/s00382-010-0888-x, 2010.

Schiemann, R., Lüthi, D., and Schär, C.: Seasonality and Interannual Variability of the Westerly Jet in the Tibetan Plateau Region*, J. Climate, 22, 2940–2957, doi:10.1175/2008JCLI2625.1, 2009.

Shi, X., Wang, Y., and Xu, X.: Effect of mesoscale topography over the Tibetan Plateau on summer precipitation in China: A regional model study, Geophys. Res. Lett., 35, L19707, doi:10.1029/2008GL034740, 2008.

Simmonds, I., Bi, D., and Hope, P.: Atmospheric Water Vapor Flux and Its Association with Rainfall over China in Summer, J. Climate, 12, 1353–1367, 1999.

Skamarock, W. C. and Klemp, J. B.: A time-split nonhydrostatic atmospheric model for weather research and forecasting applications, J. Comput. Phys., 227, 3465–3485, doi:10.1016/j.jcp.2007.01.037, 2008.

Sugimoto, S., Ueno, K., and Sha, W.: Transportation of Water Vapor into the Tibetan Plateau in the Case of a Passing Synoptic-Scale Trough, J. Meteorol. Soc. Japan, 86, 935–949, doi:10.2151/jmsj.86.935, 2008.

Tian, L., Masson-Delmotte, V., Stievenard, M., Yao, T., and Jouzel, J.: Tibetan Plateau summer monsoon northward extent revealed by measurements of water stable isotopes, J. Geophys. Res., 106, 28081–28088, doi:10.1029/2001JD900186, 2001.

Tian, L., Yao, T., MacClune, K., White, J. W. C., Schilla, A., Vaughn, B., Vachon, R., and Ichiyanagi, K.: Stable isotopic variations in west China: A consideration of moisture sources, J. Geophys. Res., 112, D10112, doi:10.1029/2006JD007718, 2007.

Trenberth, K. E.: Atmospheric Moisture Recycling: Role of Advection and Local Evaporation, J. Climate, 12, 1368–1381, doi:10.1175/1520-0442(1999)012<1368:AMRROA>2.0.CO;2, 1999.

Webster, P., Magana, V. O., Palmer, T. N., Shukla, J., Tomas, R. A., Yanai, M., and Yasunari, T.: Monsoons: Processes, predictability, and the prospects for prediction, J. Geophys. Res., 103, 14451–14510, doi:10.1029/97JC02719, 1998.

Xu, X., Lu, C., Shi, X., and Gao, S.: World water tower: An atmospheric perspective, Geophys. Res. Lett., 35, L20815, doi:10.1029/2008GL035867, 2008.

Xu, X., Shi, X., and Lu, C.: Theory and application for warning and prediction of disastrous weather downstream from the Tibetan Plateau (Vol. 1, 1–91), 2011.

Yang, K., Ye, B., Zhou, D., Wu, B., Foken, T., Qin, J., and Zhou, Z.: Response of hydrological cycle to recent climate changes in the Tibetan Plateau, Clim. Change, 109, 517–534, doi:10.1007/s10584-011-0099-4, 2011.

Yang, M., Yao, T., Wang, H., Tian, L., and Gou, X.: Estimating the criterion for determining water vapour sources of summer precipitation on the northern Tibetan Plateau, Hydrol. Process., 20, 505–513, doi:10.1002/hyp.5918, 2006.

Yang, M., Yao, T., Gou, X., and Tang, H.: Water recycling between the land surface and atmosphere on the Northern Tibetan Plateau—A case study at flat observation sites, Arc. Antarc. Alpine Res., 39, 694–698, 2007.

Yang, K., Wu, H., Qin, J., Lin, C., Tang, W., and Chen, Y.: Recent climate changes over the Tibetan Plateau and their impacts on energy and water cycle: A review, Global Planet. Change, 112, 79–91, doi:10.1016/j.gloplacha.2013.12.001, 2014.

Yao, T., Thompson, L., Yang, W., Yu, W., Gao, Y., Guo, X., Yang, X., Duan, K., Zhao, H., Xu, B., Pu, J., Lu, A., Xiang, Y., Kattel, D. B., and Joswiak, D.: Different glacier status with atmospheric circulations in Tibetan Plateau and surroundings, Nat. Clim. Change, 2, 663–667, doi:10.1038/nclimate1580, 2012.

Yao, T., Masson-Delmotte, V., Gao, J., Yu, W., Yang, X., Risi, C., Sturm, C., Werner, M., Zhao, H., He, Y., and Ren, W.: A review of climatic controls on δ 18 o in precipitation over the Tibetan Plateau: Observations and simulations, Rev. Geophys., 51, 525–548, doi:10.1002/rog.20023, 2013.

Zhang, Y., Wang, D., Zhai, P., Gu, G., and He, J.: Spatial Distributions and Seasonal Variations of Tropospheric Water Vapor Content over the Tibetan Plateau, J. Climate, 26, 5637–5654, doi:10.1175/JCLI-D-12-00574.1, 2013.

C. Seasonality and spatial variability of dynamic precipitation controls on the Tibetan Plateau

Curio, J. and Scherer, D.: Seasonality and spatial variability of dynamic precipitation controls on the Tibetan Plateau, *Earth Syst. Dynam.*, 7, 767-782, doi:10.5194/esd-7-767-2016, 2016.

Status: Published.

Own contribution:

- design of the study
- HAR product generation
- data preparation
- data analysis
- scientific discussion
- graphics and tables
- writing

Earth Syst. Dynam., 7, 767–782, 2016
www.earth-syst-dynam.net/7/767/2016/
doi:10.5194/esd-7-767-2016

Earth System Dynamics
Open Access
EGU

Seasonality and spatial variability of dynamic precipitation controls on the Tibetan Plateau

Julia Curio[1,a] **and Dieter Scherer**[1]

[1]Chair of Climatology, Technische Universität Berlin, Berlin, Germany
[a]now at: National Centre for Atmospheric Science, Department of Meteorology, University of Reading, Reading, UK

Correspondence to: Julia Curio (julia.curio@tu-berlin.de)

Received: 1 January 2016 – Published in Earth Syst. Dynam. Discuss.: 8 February 2016
Revised: 2 August 2016 – Accepted: 19 August 2016 – Published: 20 September 2016

Abstract. The Tibetan Plateau (TP) is the origin of many large Asian rivers, which provide water resources for large regions in south and east Asia. Therefore, the water cycle on the TP and adjacent high mountain ranges, in particular the precipitation distribution and variability play an important role for the water availability for billions of people in the downstream regions of the TP.

The High Asia Refined analysis (HAR) is used to analyse the dynamical factors that influence precipitation variability in the TP region, including the factors resulting in the enhancement and suppression of precipitation. Four dynamical fields that can influence precipitation are considered: the 300 hPa wind speed and wind speed 2 km above ground, the 300 hPa vertical wind speed, and the atmospheric water transport. The study focusses on the seasonality and the spatial variability of the precipitation controls and their dominant patterns. Results show that different factors have different effects on precipitation in different regions and seasons. This depends mainly on the dominant type of precipitation, i.e. convective or frontal/cyclonic precipitation. Additionally, the study reveals that the midlatitude westerlies have a high impact on the precipitation distribution on the TP and its surroundings year-round and not only in winter.

1 Introduction

The Tibetan Plateau (TP) has been called the "world water tower" (Xu et al., 2008) and is the origin of many rivers in high Asia, which provide water for billions of people downstream in south and east Asia. The TP is located in the transition zone between the midlatitude westerlies (Schiemann et al., 2009) and the Indian and east Asian summer monsoon systems (Webster et al., 1998). The TP shapes the hydroclimate of downstream regions by its influence on the large-scale circulation (Hahn and Manabe, 1975), caused by its large extent and height.

Since precipitation is a key feature of the water cycle of high Asia, it is important to analyse the factors controlling precipitation variability. Identifying which dynamic factors influence the precipitation may also help to estimate the impact of future climate change on precipitation variability.

Previous studies have stated that precipitation over the TP is controlled by the westerlies in winter and the Indian and east Asian summer monsoon in summer (e.g. Hren et al., 2009; Tian et al., 2007; Yang et al., 2014). This assumption is derived only from the precipitation timing, but Curio et al. (2015) and Mölg et al. (2014) have already shown that the midlatitude westerlies also have an impact on the summer precipitation.

There are many studies that have explored the influence of atmospheric circulation modes, e.g. the North Atlantic Oscillation, the Arctic Oscillation, and El Niño–Southern Oscillation, on the climate and precipitation in high Asia and on the monsoon systems (e.g. Bothe et al., 2010; Liu et al., 2016; Liu and Yin, 2001; Rüthrich et al., 2015). Less attention has been paid to the underlying processes controlling the precipitation variability over the TP and the surrounding high mountain ranges.

The High Asia Refined analysis (HAR) (Maussion et al., 2014), which is the result of the dynamical downscaling of an operational analysis and which covers more than 13 years at high spatial and temporal resolution, provides the opportunity for a process-based analysis of the precipitation and its variability.

The starting point of this study is the seasonality of the precipitation over the TP and the evaluation of the factors that control the precipitation over the TP and the surrounding high mountain ranges. This focusses on the timing, location, and strength of the factors that influence precipitation and its variability.

The main aim of this study is to describe the spatial and temporal correlation of selected dynamical variables and precipitation to reveal the underlying mechanisms through which the variables influence precipitation and therefore act as controls of precipitation variability.

We selected four variables as dynamic precipitation controls: horizontal wind speed at 300 hPa and at about 2 km above ground, the vertical wind speed at 300 hPa, and the vertically integrated atmospheric water transport. It is known that these factors have an influence on precipitation variability, but on the basis of coarse-resolution datasets it was not possible to analyse the relations in a spatially and temporally differentiated way like it is now with the HAR.

The different precipitation controls have effects on different spatial scales. While the horizontal and vertical wind speeds at 300 hPa (WS300 and W300) are large-scale controls, the horizontal wind speed in the boundary layer (WS10) is active on the mesoscale. The atmospheric water transport (AWT) connects the large scale with the mesoscale because it is effective on both scales and across large distances. We do not claim completeness for the list of precipitation controls but assume that these four factors belong to the most important dynamic precipitation controls. It is important to keep in mind that the precipitation controls are not independent of each other and can have combined effects on precipitation variability or cancel out each other; this will not be in focus of the current study.

In the following we will briefly introduce the selected precipitation controls and their possible impacts on precipitation variability.

The horizontal wind speed at the 300 hPa level has two main effects on precipitation variability. High WS300 can inhibit or cut off deep convection and thus suppress precipitation development (e.g. Findell et al., 2003; Zhang and Atkinson, 1995). In this case only shallow convection can form, which does not lead to considerable precipitation amounts. Mölg and Chiang (2009) showed that convective precipitation events on tropical mountain summits correspond to low horizontal wind speeds. On the other hand, higher wind speeds can have positive effects on moisture advection and orographic lifting and can, at lower levels, enhance evaporation from the surface and therefore convection (e.g. Johansson and Chen, 2003; Roe, 2005). This process is most interesting during the warm half of the year, when surface moisture from local sources like lakes, soil moisture, the active layer of permafrost, snow- and glacier melt is available. Moisture recycling plays an important role in precipitation on the TP (e.g. Araguás-Araguás et al., 1998; Trenberth, 1999); on average, more than 60 % of moisture needed for precipitation falling on the inner TP is provided by the TP itself (Curio et al., 2015).

The core of the subtropical westerly jet (SWJ) occurs at the 200 hPa level. Over the Tibetan Plateau the jet reaches down to 300 hPa and still has an effect there and also at lower levels. This was shown for the HAR by Maussion et al. (2014). The strength and location of the jet influences the hydro-climate of the Tibetan Plateau and central Asia (e.g. Schiemann et al., 2009). The precipitation seasonality in the north-western parts of the study region is especially related to the position of the jet (Schiemann et al., 2008). Garreaud (2007) pointed out that stronger than normal low-level westerlies lead to more precipitation on the windward side of meridionally orientated mountain ranges (orographic precipitation), while high wind speeds at mountain tops lead to rather dry conditions because of intensified downdrafts. This process is called the rain shadow effect. But he also shows this could lead to more precipitation on the lee side because more cloud particles are advected and disturbances can overcome the topographic barrier with the help of higher wind speeds, which would lead to more frontal or cyclonic precipitation. This case already shows that the influence each of the dynamic controls has on precipitation depends on many factors and that this influence varies highly regarding time and space.

The influence of the vertical wind speed on precipitation depends on the direction of the vertical wind, i.e. on whether it is an updraft or a downdraft (Rose et al., 2003). Updrafts have a positive impact on precipitation because they can boost or enhance convection and are a key element for orographic precipitation on the windward side of mountain ranges, while downdrafts (e.g. on the lee side of mountain ranges) and subsidence lead to the inhibition of convection and cloud dispersal. The expectation is that we have mainly positive correlations of vertical wind with precipitation: high upward winds cause higher precipitation and higher downward winds cause less precipitation.

Atmospheric water transport (AWT) is not only a dynamic precipitation control because it is a product of atmospheric moisture content and wind speed (and direction). The positive effect of AWT on precipitation variability due to moisture supply is described in, for example, Barros et al. (2006) and Giovannettone et al. (2009). Therefore, we assume that there is always a positive correlation between AWT and precipitation. But high AWT does not automatically lead to precipitation development, which was shown, for example, by Curio et al. (2015) for the Qaidam Basin where the prevailing atmospheric subsidence inhibits convection.

The main objectives of the study are three-fold:

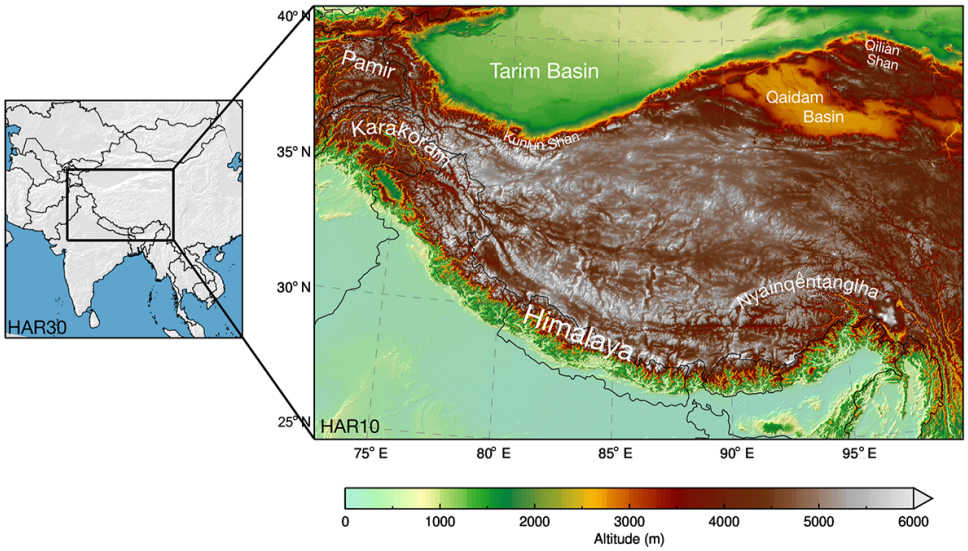

Figure 1. Map of the Weather and Research Forecasting (WRF) model domain HAR10 (high Asia domain) and its location nested in the larger domain HAR30 (south–central Asia domain). Geographical locations are indicated in white.

i. to analyse the impact of selected dynamic variables on the spatial and temporal variability of precipitation

ii. to examine whether the different factors that control precipitation variability act in the same way in different regions and at different times

iii. to gain a better understanding of the role of the midlatitude westerlies and the summer monsoon systems in the precipitation distribution on the TP.

In the following section, we describe the data and methods used in this study. Section 3 presents the precipitation seasonality on the TP and adjacent mountain ranges based on the HAR, using a cluster analysis. The focus of the study is the period 2001–2013. Afterwards we analyse the correlations between the four selected dynamic variables and precipitation regarding seasonality and spatial variability. A principal component analysis of this correlations is then used to detect the dominant patterns. The results and their uncertainties are discussed in Sect. 4. In Sect. 5, we draw conclusions from our study.

2 Data and methodology

2.1 The High Asia Refined analysis

This study is based on the HAR. The HAR has been produced using the advanced research version of the Weather and Research Forecasting model (WRF-ARW; Skamarock and Klemp, 2008) version 3.3.1 to dynamically downscale the Operational Model Global Tropospheric Analyses (final analyses, FNL; data set ds083.2), a global gridded data set. The HAR dataset, its modelling, forcing, and re-initialization strategies are described in detail by Maussion et al. (2011, 2014). The HAR data set currently covers the period from October 2000 to September 2014 and will be updated continuously. The first domain of the HAR encompasses most parts of south–central Asia with a spatial resolution of 30 km and temporal resolution of 3 h (HAR30). High Asia and the Tibetan Plateau are the focus of a second nested domain with a spatial resolution of 10 km and temporal resolution of 1 h (HAR10). A map of the HAR10 domain and its location in the parent domain HAR30 are shown in Fig. 1. In this study we analyse the processes on the TP and the surrounding high mountain ranges and therefore use the HAR10 data only. The calculation of the vertically integrated atmospheric water transport can be found in Curio et al. (2015). For this study the HAR data are used on a daily basis.

The HAR data set was validated by Maussion et al. (2014) by comparison with rain-gauge observations from the National Climatic Data Center (NCDC) and the satellite-derived gridded precipitation data from the Tropical Rainfall Measuring Mission (TRMM). The HAR shows a slightly positive bias in comparison with station data: 0.17 mm day^{-1} for HAR10 (0.26 mm day^{-1} for TRMM 3B43 product). The comparison with TRMM shows that HAR captures the general features of precipitation seasonality, variability, and spatial distribution. Maussion et al. (2014) found that the HAR10 precipitation averaged over the domain shows 15 % more precipitation than TRMM, but these differences are assumed to be related to the well-known underestimation of snowfall and light rain by TRMM. Convective precipitation is simulated in agreement with results from literature, but one has to keep in mind that the model uses a parameterization scheme for cumulus convection. A spatial resolution of 10 km is not high enough to resolve cumulus convection. The

HAR is able to reproduce orographic precipitation features as documented by Bookhagen and Burbank (2010). Maussion et al. (2014) state that these qualitative considerations cannot provide a quantitative uncertainty value. Curio et al. (2015) compared the HAR30 atmospheric water transport (AWT) with ERA-Interim (Dee et al., 2011). They found similar patterns; the differences being related to the different spatial resolutions and thus a better representation of the underlying topography by the HAR. In the HAR data, the blocking of AWT from the Bay of Bengal by the Himalayas is more pronounced, and the results show the importance of meridionally orientated high mountain valleys for moisture supply to the Tibetan Plateau. We have compared the 300 hPa wind of the HAR10 data set with ERA-Interim. Figure S1 (see the Supplement) shows that they are in a good agreement with each other. Due to the daily re-initialization strategy used to generate the HAR data set, the wind fields in higher levels cannot evolve as far away from the forcing data as this is possible for longer model runs. The question of how large the uncertainties of the HAR data and especially precipitation are and how we can estimate them is a topic which should be investigated more in detail. Since there are no other gridded data sets with a comparable high temporal and spatial resolution, the possibilities to validate the HAR are generally limited and will be the subject of future research.

2.2 Methodology

The selection of precipitation controls relies on well-studied relations of these factors with precipitation (e.g. Back and Bretherton, 2005; Garreaud, 2007; Shinker et al., 2006), but these controls were not investigated at high spatial and temporal resolution in high-mountain Asia until now.

The current study is based on the HAR10 data set for the study period 2001–2013 (all entire years available). Starting point of this study is an analysis of the precipitation seasonality on the TP using the k-means clustering method (e.g. Wilks, 1995). The percentages of monthly contribution to annual precipitation and not the precipitation amounts were used to define seven classes with different precipitation seasonality. This has the advantage that, in an area like high Asia where the differences in precipitation amounts vary strongly between regions and seasons, the regions were made comparable by this method. We conducted the cluster analysis with other numbers of classes (5–9), but the chosen number of seven classes led to the best ratio between coherent patterns and sufficient distinction between classes. This analysis follows the approach of Maussion et al. (2014), who used the clustering to detect glacier accumulation regimes on the TP. Their input data were restricted to glaciated areas only. Our current analysis expands the database to the entire TP and surrounding regions, using all grid points of the HAR10 domain.

For all further analysis daily averaged HAR data are used. Because we are only interested in precipitation days, the data set is stratified using a daily precipitation threshold. This is done month-wise. For example, all analyses for July depend on the data for each July day during the period 2001–2013; these are 31×13 days, i.e. 403 days in total. Precipitation days for a grid point are defined as days with a mean daily precipitation rate of at least 0.1 mm, which is a commonly used minimum value to define precipitation days (e.g. Polade et al., 2014; Liu et al., 2011; Bartholy and Pongracz, 2010; Frei et al., 1998). The threshold was basically used to filter out numerical artefacts and not to exclude events from the database.

The daily precipitation rate at each grid point is calculated as the mean precipitation rate for all grid points within an area of 15×15 grid points around the specific grid point. The time mask for precipitation days is then applied to the four variables used as precipitation controls. The number of precipitation days can vary distinctly between regions and seasons. Each of the dynamical variables is correlated with the precipitation using the Spearman rank correlation. This is done month-wise for all precipitation days in a specific month during the study period and for each grid point in the HAR10 data set. Using correlations avoids problems associated with the exact precipitation rates and amounts falling on the TP, which are hard to measure and to model exactly. The Spearman rank correlation uses the ranks of the values and not the values itself, which makes the correlations independent of the real data and more robust against outliers. This makes it easier to compare regions with very different precipitation amounts with each other and helps to reduce the effects of extreme events on the correlation results. We are aware of the fact that ranking the data leads to a slight information loss compared to the real values. We are sure that for our purpose the advantages are bigger than the disadvantages. Only correlations, which are significant at the 95 % level, are plotted. The statistical significance of the correlations was tested using a two-tailed test to determine the deviation from 0 (Numerical Recipes, The Art of Scientific Computing, 1992). The calculation oft the statistical significance is described more in detail in the Supplement. A principal component analysis (PCA) is performed for the results of the correlations with precipitation to detect the dominant relationships.

3 Results

3.1 Precipitation seasonality

Figure 2 shows the seven defined classes of precipitation regime and the mean annual cycle of monthly precipitation percentage in each class. It is clearly visible that the TP and the surrounding high mountain ranges show a spatial variability regarding precipitation seasonality. A class with a precipitation maximum in summer and a minimum in winter is dominant on the central TP and south of the Himalayas in India, Nepal, and Pakistan (blue, class 6). This class is the

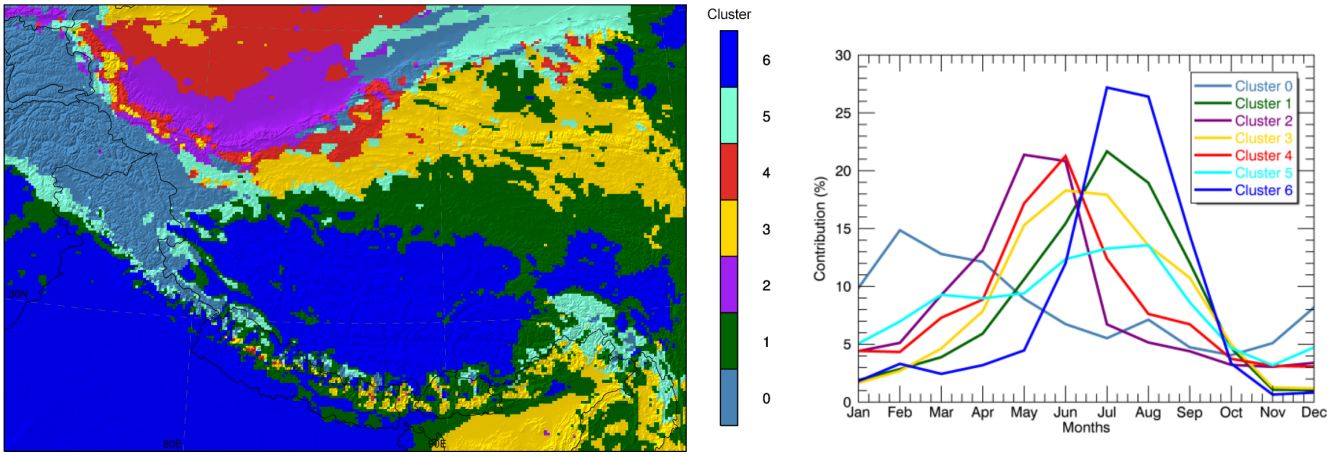

Figure 2. Precipitation clusters (left) and the mean annual cycle of percentage contribution of monthly precipitation to annual precipitation for each cluster (right).

monsoonal precipitation class because the precipitation percentage increases from June onwards, the onset period of the Indian summer monsoon. During July and August more than 50 % of the annual precipitation falls in this regions, while from October to May the monthly precipitation amount is below 5 % of the annual precipitation. The yellow class has a much broader and less pronounced summer precipitation maximum and the increase and decrease proceed with similar rates. The annual cycle of precipitation in this class is determined by the seasonal cycle of solar forcing and therefore convective activity. The green class represents a transition zone between the monsoonal and convective classes where the monsoon can have an influence but is not dominant. This means that both monsoonal precipitation and/or only solar-forced convective precipitation can occur.

The naming convention does not mean that the monsoonal class precipitation is not of convective nature, but it should emphasize that the precipitation (development/variability) is influenced by the monsoon, which is associated with the advection of tropical air masses. The monsoonal class is a subset of the convective class. The timing and strength of the precipitation maximum provides an indication of a different forcing. In the monsoonal class the precipitation maximum is higher, starts during the Indian summer monsoon onset, and persists for a shorter time period. The monsoonal class is divided into a northern and southern part by the Himalayas.

The grey-blue class experiences its precipitation maximum in winter and is dominated by the influence of the midlatitude westerlies. This class occurs mainly in the Pamir–Karakoram–western Himalayas (PKwH) region, as one coherent pattern, and additionally in the eastern part of the Tarim Basin. The precipitation maximum is much lower, but the minimum values are higher than in the classes dominated by summer precipitation, which shows that the intra-annual variability is lower and the values vary between 15 and 5 % but are never below 5 % in the mean. This could lead to the assumption that the influence of the midlatitude westerlies is more constant year-round, while the monsoon has a stronger but temporally more limited influence on precipitation on the TP.

The light blue class exhibits a more evenly distributed seasonality of precipitation during spring and summer with a minimum in November. This class surrounds the grey-blue cluster at the southern flank of the western Himalayas (western notch), in the south-eastern TP, and in the eastern Tarim Basin. It is interesting that the region in the south-east of the TP, where the Brahmaputra Channel enters the TP, belongs to a different class than the surroundings, which are divided between the three convectively dominated classes blue, yellow, and green. Maybe there is stronger influence from AWT, which would make this region more similar to the surroundings of the PKwH region regarding the factors controlling precipitation variability. Another possible reason could be the occurrence of extratropical cyclones which propagate eastward along the Himalayas and are then terrain-locked by the eastern notch of the Himalayas (Norris et al., 2015). This would lead to a higher moisture supply to the region and therefore higher amounts of orographic precipitation. This kind of terrain locking of the westerly flow in winter is described in detail for the western notch of the Himalayas by Norris et al. (2015). This mechanism would explain the higher shares of winter precipitation in the region around the Brahmaputra Channel and the affiliation to the same class occurring at the southern flank of the western Himalayas in the western notch.

The remaining two classes – red and purple – almost only appear in the Tarim Basin. They are both characterized by a spring and early summer precipitation regime but also show some differences. The amount of precipitation in the purple class increases sharply from March to May and June, where the maximum with a value of slightly above 20 % occurs. The decrease is even sharper so that in July already only 6 %

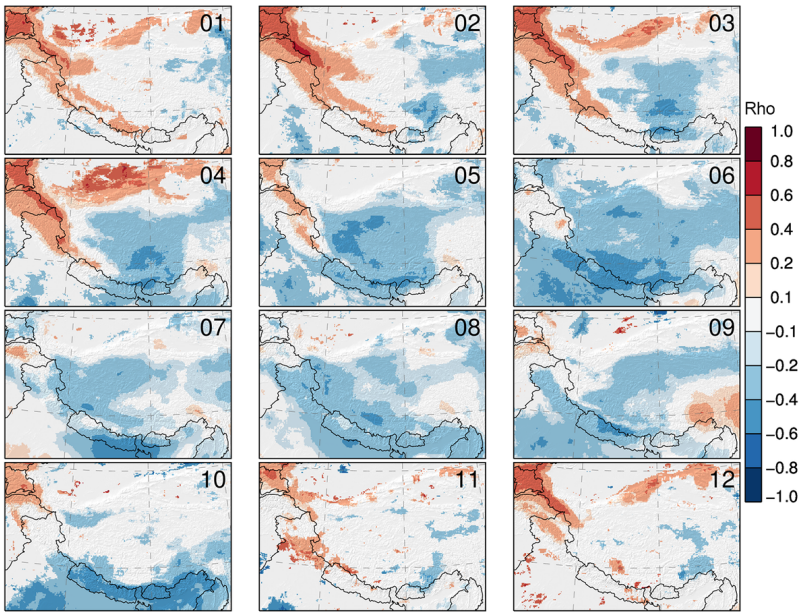

Figure 3. Coefficient of correlation (rho) between horizontal wind speed at 300 hPa (WS300) and precipitation for all months (01–12). Positive correlations are denoted in red, while negative correlations are denoted in blue.

of the annual precipitation occurs. The annual cycle of the red class seems to be delayed relative to the purple one, and the period of maximum precipitation is only 1 month long. In spring the values are lower but higher in late summer and autumn, while they are almost the same during winter.

The high mountain ranges of the Himalayas and Kunlun and Qilian Shan exhibit a complex structure of different classes over relatively short distances and therefore exhibit no coherent patterns. This holds true also for the border area between the Karakoram and the Tarim Basin. The mountainous region of the Pamir and Karakoram is represented by only one class, which implies that this region is mainly influenced by one atmospheric forcing (midlatitude westerlies) or that different controls have the same impact in this region. The other mountain ranges lie in regions where an interplay of different controls occur, and the temporal and spatial variability is larger on smaller scales.

3.2 Correlation of dynamic variables and precipitation

3.2.1 Horizontal wind speed

Horizontal wind speed at 300 hPa (WS300)

The correlations between WS300 and precipitation are shown in Fig. 3. There are high positive correlations in winter in the PMwH region; this is the time of the year when the majority of precipitation falls in this region (e.g. Curio et al., 2015; Maussion et al., 2014). The precipitation in the PMwH region is mainly cyclonic/frontal precipitation and is associated with western disturbances (Dimri et al., 2015). There are only negative correlations in the southern and eastern parts of the TP in winter, which enlarges over spring and covers mainly the whole central and north-eastern TP and large parts of the central Himalayas, with the highest negative correlations in the central TP. The reason for the negative correlations in these regions is that they are dominated by convective precipitation (e.g. Maussion et al., 2014), and higher wind speeds in winter inhibit the deep convection. This also explains why there are negative correlations almost everywhere in summer. The region of negative summer correlations covers almost the same area as the convective and monsoonal precipitation classes (Fig. 2) combined, so the impact of WS300 explains some of the precipitation classes. In spring there is a second region with positive correlations north of the TP in the Tarim Basin and the bordering Kunlun and Qilian Shan. This area is reached by the northern branch of the midlatitude westerlies, which delivers moisture for precipitation. The area around the Brahmaputra Channel exhibits slightly positive correlations, due to enhanced moisture transport by higher wind speeds. The region of high positive winter correlations exhibits no or slightly positive correlations in only a small area in summer, and in some parts of the region the positive correlations are replaced by negative ones. Since there is a non-negligible amount of precipitation falling in this region in summer ($\sim$ 20–40 %, see clusters 0 and 5 in Fig. 2), the lag/absence of positive correlations and the occurrence of negative correlations means that a different factor controls precipitation variability and/or the same control works in a different way due to higher shares of convective precipitation, especially in the eastern parts of the Pamir–Karakoram region.

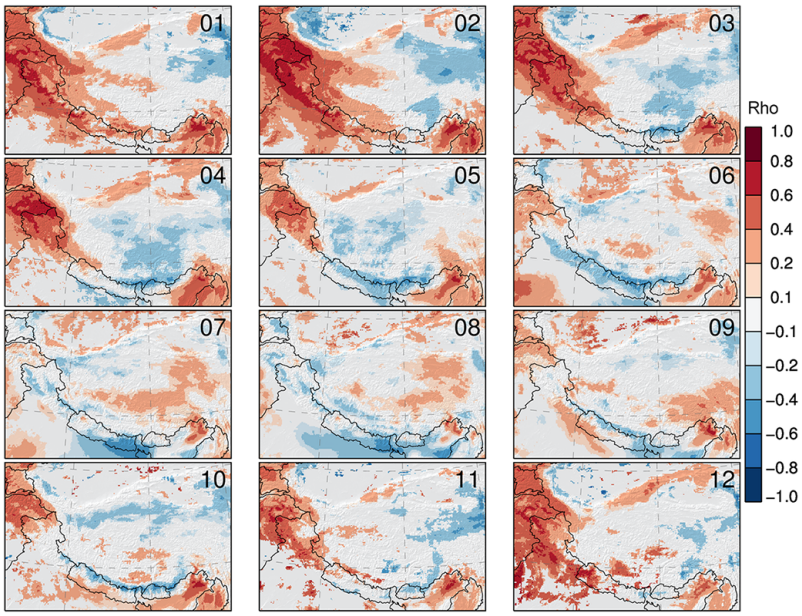

Figure 4. Coefficient of correlation (rho) between horizontal wind speed at model level 10 (WS10) and precipitation for all months (1–12). Positive correlations are denoted in red, while negative correlations are denoted in blue.

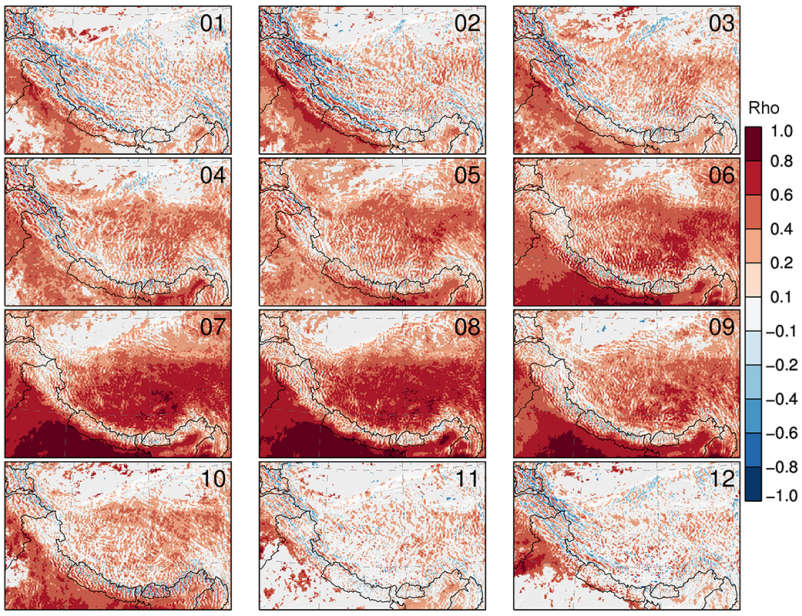

Figure 5. Coefficient of correlation (rho) between vertical wind speed at 300 hPa (WS300) and precipitation for all months (01–12). Positive correlations are denoted in red, while negative correlations are denoted in blue.

Horizontal wind speed at model level 10 (WS10)

Figure 4 shows that the correlations between WS10 and precipitation are positive in the PMwH region in winter as they are for WS300, but the region is larger, especially the region with correlations >0.6. The reason for the positive correlations is again the enhanced moisture supply due to higher wind speeds and therefore also more orographic precipitation. The positive correlations in the Brahmaputra Channel region (and south of it) are more pronounced, and the structure of the Brahmaputra Channel itself is clearly visible. The moisture supply is enhanced due to strengthened winds from the south, bringing moisture from the Indian Ocean to the Himalayas. There are high positive correlations between the WS10 and precipitation over the Tibetan Plateau in summer, while the correlations with WS300 are negative in sum-

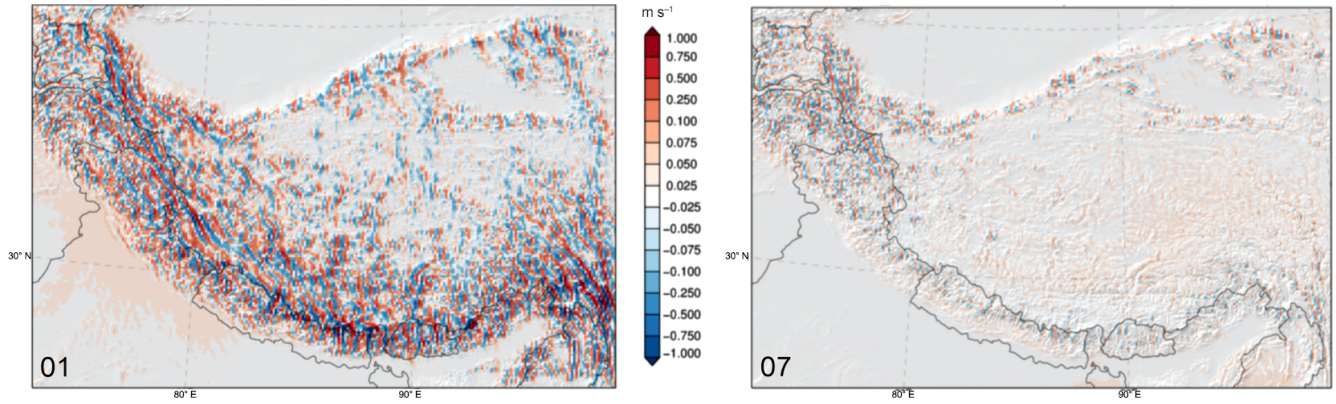

Figure 6. Mean vertical wind speed at 300 hPa for January (01) and July (07).

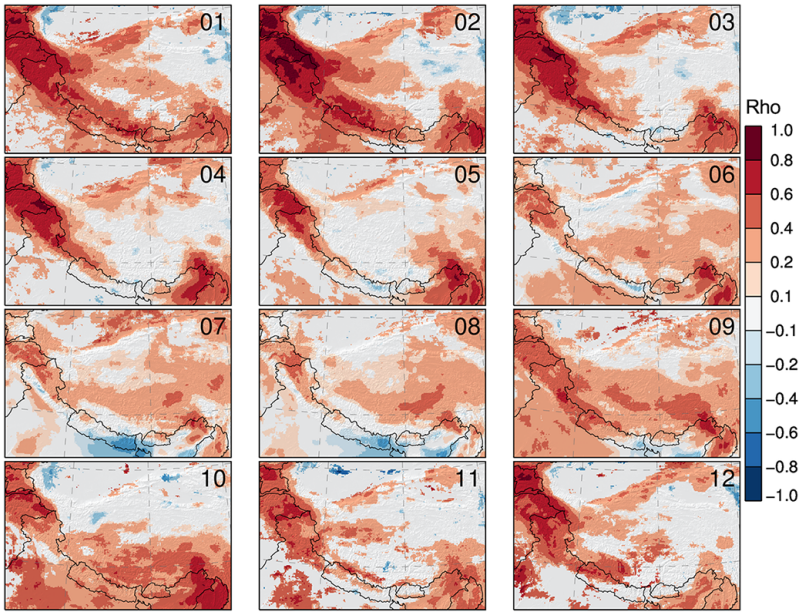

Figure 7. Coefficient of correlation (rho) between atmospheric water transport (AWT) and precipitation for all months (01–12). Positive correlations are denoted in red, while negative correlations are denoted in blue.

mer. This is because of the fact that the wind speed in the boundary layer can enhance evapotranspiration from the surface (e.g. lakes; snow-, glacier, and permafrost melt), which leads to more moisture in the lower atmosphere available for precipitation. This correlation again emphasizes the importance of moisture recycling on the TP. In winter the correlations on the TP are mainly negative because the effect of enhanced evapotranspiration is not active due to the fact that all potential moisture sources are frozen during this time of the year. Strong negative correlations occur south of the Himalayas and in northern parts of India in summer. When the air flow from the south hits the mountain barrier, parts of the flow are redirected to the south-east and north-west. The flow becomes divergent, which forces the air above to descend, which in turn leads to unfavourable conditions for growing convection and therefore precipitation.

3.2.2 Vertical wind speed

The correlations between vertical wind speed at 300 hPa (Fig. 5) and precipitation are mainly positive due to the positive effect of ascending air motion on precipitation development, as expected, especially in summer when most of the precipitation is convective. Therefore, the positive correlations are higher in summer than in winter when almost no precipitation falls on the TP, although the mean vertical wind speeds (up- and downdrafts) are higher in winter than in summer (Fig. 6). This shows that higher values of one precipitation control alone do not necessarily lead to higher correlations and therefore more precipitation but that usually other

conditions favourable for precipitation development have to occur. This supports the interpretation that precipitation variability is mostly caused by combined effects of different precipitation controls.

The high mountain ranges of the Pamir and Karakoram show a pattern of alternating positive and negative correlations between vertical wind speed and precipitation. It was expected that the correlations between the vertical wind speed would be positive on both sides of the mountain ranges. But the negative correlations can be explained physically. If an air flow hits a mountain range, the barrier causes orographically induced flow patterns, with updrafts on the windward side and downdraft on the lee side of the mountain range. This causes the precipitation to be smaller on average on the lee side because the downdrafts suppress precipitation development. In the case of a stronger horizontal flow to the mountains, there is stronger moisture advection and orographic precipitation, and therefore the downdrafts on the lee side are no longer able to suppress precipitation. This leads to the simultaneous occurrence of precipitation and downdrafts, which is the reason for the negative correlation patterns on the lee side of mountain ranges found in the western parts of the study region.

3.2.3 Atmospheric water transport (AWT)

Figure 7 shows the correlations between AWT and precipitation. The entire study region is dominated by positive correlations during the year (Fig. 7). The highest positive correlations occur in winter and early spring in the PKwH region, where the correlation coefficient exceeds 0.8 in most regions. This is the time of the year when the maximum precipitation occurs in this region (Fig. 2). The annual contribution of convective precipitation in this region is below 10 % (Maussion et al., 2014), but the region exhibits orographic precipitation triggered by the advection of moist air masses with the westerly flow and westerly disturbances (Cannon et al., 2014). Therefore, a higher moisture supply leads naturally to more precipitation. The positive correlations in the western parts of the study region persist during the course of the year, even if their extent and strength varies. The positive correlations extend to the TP, the whole Himalayan arc, and along the northern border of the TP (Kunlun and Qilian Shan). These seem to be the moisture supply routes along the branches of the midlatitude westerlies.

A second centre of positive correlation which is persistent is found in the extreme south-east of TP, the region where the Brahmaputra Channel enters the TP. This region exhibits less convective precipitation on annual timescales (Maussion et al., 2014), but it is surrounded by regions with high convective precipitation rates. This explains the fact that this region belongs to a different precipitation seasonality class than its surroundings (Fig. 2). In January and February, the Himalayan arc exhibits mostly positive correlations and connects the area in the western parts of the domain with the other positive centre in the south-eastern TP around the Brahmaputra Channel.

The spatial minimum of the positive correlations occurs in May, whereas the correlations are very high ($r > 0.6$) in the western and south-eastern centres. In May the central TP exhibits no significant correlations which may be caused by the fact that the AWT is very low on the TP in May (Curio et al., 2015). From then on the area with positive correlations enlarges but the strength of correlation decreases.

The minimum values of the positive correlations occur in July and August. But then there are positive correlations in the central TP, but they are not as high as in the western and south-eastern parts of the domain during winter and spring. This shows that the precipitation during this time of the year is mostly convective and that the moisture comes from local sources, so that the advection of moist air masses is less important. In large areas of the domain, the precipitation maximum occurs in July and August; ~ 30 % of the annual precipitation falls on the central and southern TP during this time (Maussion et al., 2014).

The regions where the highest positive correlations occur are the regions where the precipitation maximum occurs during winter, matching the grey-blue precipitation seasonality class (Fig. 2).

There are only a few regions and months where negative correlations occur, in the Tarim Basin during winter and in the central Himalayas and northern India during summer.

3.3 Principal components

So far the spatio-temporal variability of correlation between dynamical variables and precipitation for the TP and surrounding high mountain ranges has been discussed. To detect the dominant patterns in the relationship between the different variables and precipitation and to find the time of the year a control is most efficient, we conducted a principal component analysis (PCA) for each of the correlation sets. Because the dominant modes are the main interest, only the first two principal components (PCs) are analysed, which typically explain most of the variance of the data and can also explain important processes. For completeness, plots for all PCs can be found in the Supplement of this study (Figs. S2–S5). The explained variance of PC1 lies between 40 and 50 % and at around 20 % for PC2 for all sets of correlations. The higher PCs explain lower shares of variance, less than 10 % already for PC3 and only 1 % for PC12.

Figure 8 shows the scores of the first two principal components for the correlation between WS300 and precipitation and their monthly loadings. PC1 shows a pattern which looks like the winter pattern of the correlations in the western parts of the study region, the spring pattern of the northern region, and the summer pattern of the TP were combined. This is confirmed by the annual cycle of loadings for PC1. The highest positive loadings occur in winter and spring, which means that these months have the largest share of the domi-

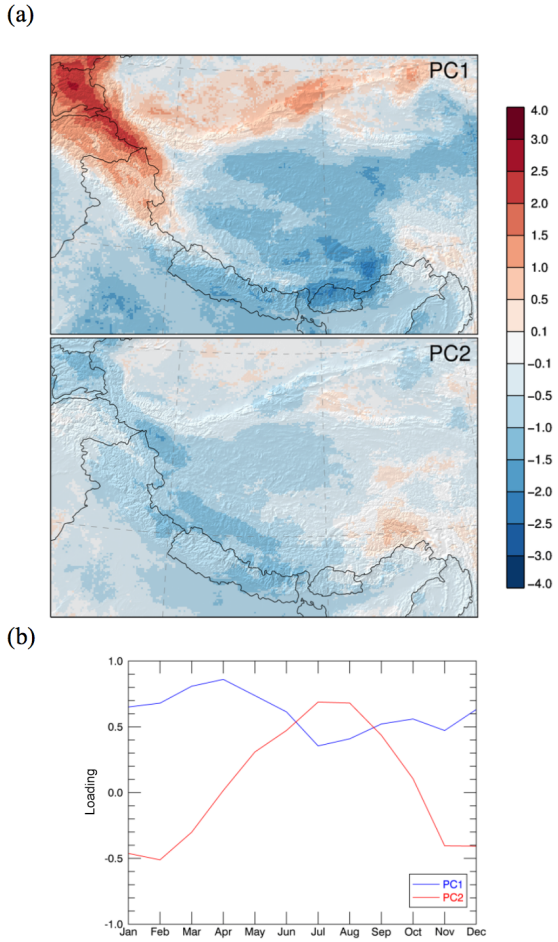

Figure 8. Scores of first two principal components PC1 and PC2 for the correlation between horizontal wind speed at 300 hPa (WS300) and precipitation **(a)** (positive values are denoted in red, while negative values are denoted in blue) and the monthly loadings **(b)** for both PCs.

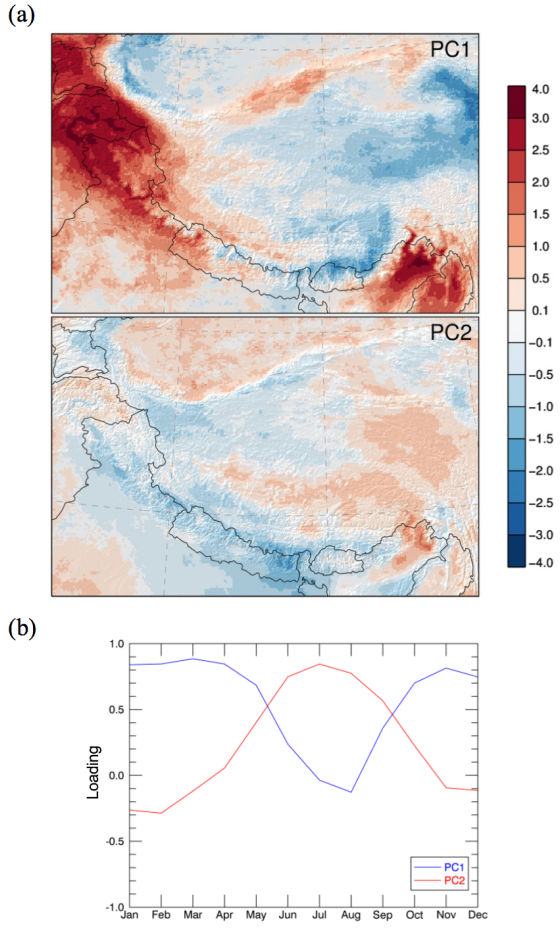

Figure 9. Scores of first two principal components PC1 and PC2 for the correlation between horizontal wind speed at model level 10 (WS10) and precipitation **(a)** (positive values are denoted in red, while negative values are denoted in blue) and the monthly loadings **(b)** for both PCs.

nant pattern. The loadings are high all year-round but highest in spring and lowest in July. This implies that this pattern is not particularly influenced by the monsoon system or, if it is, just in the onset period. We assume that the still relatively high loading is a result of the fact that there is high solar forcing and therefore convective activity on the TP which is negatively influenced by higher wind speeds at 300 hPa. The loadings of the second PC (PC2) show a completely different annual cycle. They are strongly negative in winter and strongly positive in summer; it is just in the transition seasons that the loadings are around zero. For this pattern winter and summer play a similar role, even with opposing arithmetic signs. This is an annual cycle pattern. The first two PCs together account for ∼ 60 % of the total variance of the data.

The first PC (PC1) for the correlation between WS10 and precipitation (Fig. 9a) shows a pattern dominated by the winter and early spring situation, high positive scores in the PKwH region and the region around the Brahmaputra Channel, and negative scores on the central and eastern TP. The loadings (Fig. 9b) are very high (∼ 0.8) from November to April. Only in July and August are the loadings slightly negative. The positive correlations during summer on the TP are not visible in PC1; they occur in PC2, which has loadings that have a directly opposing annual cycle, meaning high positive values in summer and slightly negative values in winter. The first two PCs together explain ∼ 65 % of the variance in the data.

All months exhibit high loadings for PC1 of the correlation between the vertical wind speed and precipitation. Fig. 10 shows the scores and the loadings of the first two PCs for the correlation of W300 with precipitation. Summer and early autumn conditions have the largest impact, while loadings are lowest in winter but still positive. Therefore, the high positive correlations in summer on the TP and in the lowlands south of the Himalayas are the dominant pattern, meaning that the vertical wind speed as a precipitation control is most

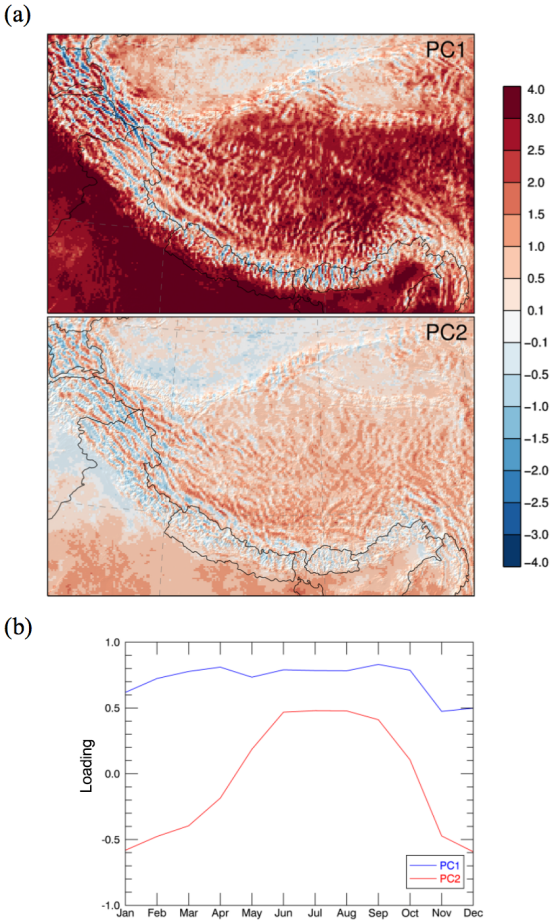

Figure 10. Scores of first two principal components PC1 and PC2 for the correlation between vertical wind speed at 300 hPa (W300) and precipitation **(a)** (positive values are denoted in red, while negative values are denoted in blue) and the monthly loadings **(b)** for both PCs.

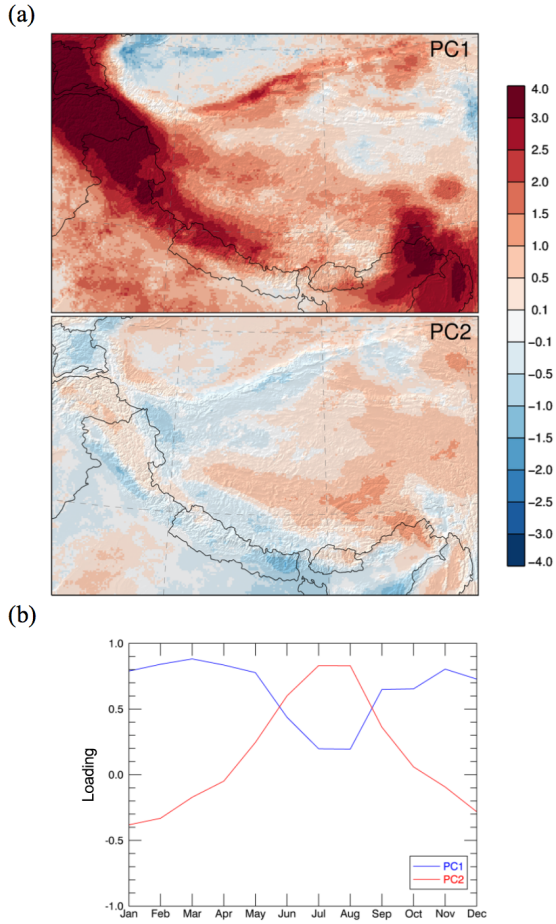

Figure 11. Scores of first two principal components PC1 and PC2 for the correlation between atmospheric water transport (AWT) and precipitation **(a)** (positive values are denoted in red, while negative values are denoted in blue) and the monthly loadings **(b)** for both PCs.

effective during that time of the year but has a mostly positive impact on precipitation year-round. PC2 exhibits much lower values. The annual cycle of the loadings shows that winter and summer both have high loadings (~ 0.5) but with different signs: positive in summer and negative in winter. Spring and autumn exhibit very low factor loadings and are more or less only transition periods between winter and summer. The first two PCs together explain $\sim 70\,\%$ of the variance in the data.

The loadings of the first two PCs of the correlation between AWT and precipitation (Fig. 11b) exhibit a similar annual cycle as the loadings of the correlation between WS300 and precipitation. For PC1 the loadings are high (between 0.6 and 0.9) in winter, spring, and autumn and low in summer (~ 0.2). This again emphasizes the finding that AWT is a precipitation control mainly in regions and seasons where moisture advection and frontal/cyclonic precipitation is dominant. The pattern of PC2 (Fig. 11a) is important mainly in summer months (loadings > 0.8 in July and August), while the winter months exhibit negative loadings.

In summary, the annual cycle of the loadings for each of the first two PCs, show a similar annual cycle. PC1 is mostly dominated by all seasons except summer and mainly by the winter and spring situations, whereas PC2 is determined by summer conditions. Winter conditions also have high loadings but with a negative sign, while spring and autumn only represent transition periods between these situations.

4 Discussion

4.1 General discussion of results

A main result of the current study is the high negative correlations between the 300 hPa horizontal wind speed and precipitation on the TP. This confirms the findings of Mölg et al. (2014), who showed that the flow strength at the 300 hPa level above the TP, during the onset period of the Indian

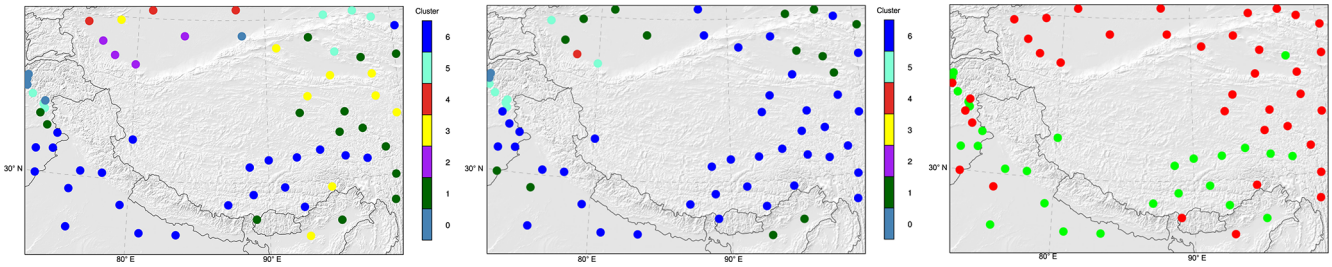

Figure 12. Map of precipitation clusters for HAR10 grid points (left) and the associated NCDC stations (middle). The map on the right shows whether the clusters match (green dots) or not (red dots).

summer monsoon, exhibits strong negative correlations with precipitation and explains 73 % of the interannual mass balance variability of the Zhadang glacier, located at the Nyainqênthangla range in the central TP. They argue that weak flow conditions favour convective cell growth. This together with the high positive correlations, in regions and seasons where frontal or cyclonic precipitation is dominant, shows the strong influence of the subtropical westerly jet (midlatitude westerlies) not only on the western parts of the study region but also on the TP itself, which previously has mostly been described as mainly influenced by the monsoon system (Hren et al., 2009; Tian et al., 2007; Yang et al., 2014).

Previous studies have stated that the precipitation on the TP is controlled by the midlatitude westerlies in winter and the Indian and east Asian summer monsoon in summer (e.g. Hren et al., 2009; Tian et al., 2007; Yang et al., 2014). This assumption is based only on precipitation timing, but Curio et al. (2015) and Mölg et al. (2014) have already shown that the midlatitude westerlies also have an impact on summer precipitation. The current study highlights their findings by the detection of the negative influence of the high horizontal wind speeds on precipitation (development, variability, amount) on the TP in summer.

Spiess et al. (2015) showed that in summer, increased horizontal wind speeds at 400 hPa have a positive effect on the height of the equilibrium line altitude at glaciers in different regions on the TP; they assumed that this could be caused by a reduction in convective precipitation due to high wind speeds. Exactly this process is shown by the strong negative correlations between horizontal wind speed at 300 hPa and precipitation in summer on the TP (Fig. 3).

The identified positive correlations of the wind speed in the boundary layer with precipitation in summer on the TP agree with the findings of Back and Bretherton (2005), who detected positive correlations between near-surface wind speed and precipitation only when convection can be triggered easily. Their study region was the Pacific ITCZ, but we assume that their findings are also valid for the TP in summer, where the convective activity is high and enough moisture is available at the surface.

The fact that the positive correlation of AWT with precipitation in summer on the central TP is not as high as in the western parts of the study region in winter means that here the convection is able to produce precipitation using the moisture from local sources, which emphasizes the importance of moisture recycling, as shown by Curio et al. (2015) using HAR data and by Chen et al. (2012), Joswiak et al. (2013), and Kurita and Yamada (2008), among others. Nevertheless, AWT still has a positive effect on precipitation, but it is not an essential control during this time of the year on the central TP.

Additionally, we calculated the vertically integrated atmospheric moisture content for the HAR and repeated the calculation of correlation for this variable. The results (Fig. S6 in the Supplement) show high positive correlations between the atmospheric moisture content and precipitation throughout the year, as expected. The correlation patterns can only explain parts of the precipitation variability on the TP. This highlights how highly effective the dynamic controls are on precipitation variability, differentiated in space and time.

4.2 Sources of uncertainties

As always the uncertainty of the results mainly depends on the accuracy of the data themselves, the aggregation of hourly data to daily means, and the statistical methods used to analyse the data. The HAR precipitation and other variables, e.g. wind speed and direction and temperature, have been validated against other gridded data sets – global reanalyses and remote sensing data – and observations from weather stations by Maussion et al. (2011, 2014), as described in Sect. 2.1.

NCDC station data were used to compare the results of the precipitation clustering approach with observations. Figure 12 shows the precipitation classes for the station data and for the associated HAR grid points and whether the obtained clusters regarding the mean annual cycle of monthly precipitation contribution to annual precipitation match (green dots) or not (red dots). Overall, 27 of the 65 stations (41.5 %) fall in the same cluster as the nearest HAR grid point. For 38 stations (58.5 %) this is not true, but most of them fall in clusters with a very similar annual cycle or in clusters which are spatially very close to the cluster to which the HAR grid point belongs. This is especially the case in the mountain regions in

Table 1. The percentage of NCDC stations falling in each of the seven possible HAR clusters. A value of 100 % would mean that all NCDC stations falls in the same cluster as the nearest HAR grid point.

		NCDC						
Cluster		0	1	2	3	4	5	6
HAR	0	40 %	0 %	0 %	0 %	0 %	40 %	20 %
	1	0 %	14.3 %	0 %	0 %	0 %	0 %	85.7 %
	2	0 %	50 %	0 %	0 %	25 %	25 %	0 %
	3	0 %	33.3 %	0 %	0 %	0 %	0 %	66.6 %
	4	0 %	33.3 %	0 %	0 %	0 %	33.3 %	33.3 %
	5	0 %	43 %	0 %	0 %	0 %	43 %	14 %
	6	0 %	13 %	0 %	0 %	0 %	0 %	87 %

the western, the south-eastern, and north-eastern parts of the domain, where at least four different clusters occur on very small spatial scales. Table 1 shows which percentage of the stations, which should all be in one specific class regarding their associated HAR grid points, falls in which of the seven possible classes. One has to take into account that there is always a distance up to a few kilometres between the NCDC stations and the respectively associated HAR grid point. This also can cause huge differences between the elevation and altitude of stations and grid points due to the complex topography of the study region, which in turn has an effect on the precipitation distribution. Additionally, the quality of the station data is not always satisfactory and the time series often show gaps, leading to a smaller database.

We decided to use the wind speed at the 300 hPa level because the wind shear at this height more strongly suppresses deep convection than at the 200 hPa level, where the core of the jet lays. Also we assumed that the results would not change overall using the wind speed at 200 hPa. To prove this, we repeated the correlation analysis between wind speed and precipitation for the wind speed at 200 hPa (Fig. S7 in the Supplement). The results are very similar. The correlations at the 300 hPa level (Fig. 3) are slightly higher because the negative effect of higher wind speeds on precipitation by cutting off deep convection is higher at this level than at 200 hPa.

We varied the k for clustering from 5 to 9 (Fig. S8 in the Supplement). We found 7 to be the optimal k for the recent study since it gave us good coherence within the classes and sufficient distinctions between them. We determined this qualitatively by looking at the plots for the different numbers of clusters. We first conducted the cluster analysis with five (Fig. S8a in the Supplement) clusters, like Maussion et al. (2014). But since we included a much higher number of grid points (we analysed the entire Tibetan Plateau), the results for the areas included in both analyses look slightly different, especially in the Karakoram and Tien Shan. By increasing the number of clusters to six (Fig. S8b in the Supplement), one cluster that covers most parts of the northern part of the study region – the northern Tibetan Plateau and Tarim Basin – breaks up into two clusters. Setting the number to seven (Fig. S8c in the Supplement), we get more variation in the Karakoram and Tien Shan which looks more similar to the cluster distribution achieved by Maussion et al. (2014). Using a higher number of clusters (Fig. S8d and e in the Supplement) led to the occurrence of more clusters of smaller size which are not as distinct from each other as the larger ones. In general, it would be interesting to have more clusters to get a higher spatial differentiation. But by increasing the cluster number the spatial coherence decreases and therefore the interpretability also decreases. We decided to use seven clusters as a compromise between higher spatial differentiation and less spatial coherence. Since the core areas of the clusters stay stable while changing the number of clusters, we assume that the clustering approach is suitable to analyse the seasonality of precipitation on the TP.

Of course using different parameterizations and higher spatial resolutions would change the precipitation values and the spatial and temporal distribution of the precipitation. But we assume that this would not change the main results of this study since we use rank correlations which are independent of the mean values and scaling of the input variables.

Using correlations we avoid problems regarding the exact precipitation rates falling on the TP. Additionally the use of the monthly percentage of annual precipitation as input for the cluster analyses, to detect the precipitation seasonality in different regions of the TP, makes it possible to compare regions, which exhibit distinctly different precipitation amounts. This is a general aspect to keep in mind; the decision to use mean daily data therefore has advantages and disadvantages. A major advantage is the possibility to analyse the processes from a climatological perspective, which cannot be done on the basis of monthly data. But it is clear that some information is lost by aggregation from hourly to daily data. To test, how sensitive the results are regarding the

use of different significance levels, we repeated the analysis with the significance level 0.01 for the correlation between wind speed in 300 hPa and precipitation (Fig. S9 in the Supplement) and compared the results with the results gained using 0.05 as significance level (Fig. 3). The resulting patterns do not change very much. The areas with negative and positive correlations are a little bit smaller, but the changes occur where the values are already lower (at the borders of the correlation patterns). The regions with the highest correlations stay stable and even small areas of positive or negative correlations do not disappear.

The number of precipitation days on which all analysis depends is variable regarding the analysed months and regions, but we assume that the condition of at least 13 precipitation days per grid point, applied for of all days of a specific month during the study period 2001–2013, ensures a reasonable data basis. Grid points which do not match this criterion are excluded from further analysis.

Since we only look at the first two PCs, it is possible that mechanisms controlling precipitation, which appear in higher PCs, are not considered in this study. The current study is limited to dominant patterns and thereby to the first two PCs because they together explain more than 60 % of the variance of the data. Patterns with lower explained variance and transient patterns will be the subject of a subsequent study.

5 Conclusion

Gaining a better understanding of the relationship between dynamical variables and precipitation and the underlying processes is important since precipitation is the key element of the hydrological cycle of the TP and the surrounding high mountain ranges. Precipitation variability has a large impact on the water availability in the densely populated downstream regions of India, Pakistan, and south-east Asia by directly governing river runoff by precipitation or with a time lag by snowmelt.

This study shows that different factors influence precipitation in different regions of the TP and adjacent high mountain ranges during different times of the year and in different ways. For example, the 300 hPa wind speed has a positive effect in the western parts of the study region in winter and spring, while it has a negative effect on precipitation on the TP during summer. This clearly shows that the impact of the midlatitude westerlies is strong, not only in winter by enhancing moisture advection for orographic and frontal precipitation in the western parts of the study region but also by cutting off deep convection during summer on the TP and in other regions and seasons where and when precipitation is mainly convective.

The negative effect of high horizontal wind speeds on precipitation plays an important role in regions and seasons which are dominated by convective precipitation, e.g. the Tibetan Plateau in summer (Maussion et al., 2014). The positive effect occurs in regions with mainly frontal/cyclonic or orographic precipitation. Precipitation benefits from enhanced moisture transport by strengthened atmospheric flow, especially when the moisture flow is lifted up by orographic forcing. This plays an important role in our study region because of the high mountain ranges surrounding the Tibetan Plateau.

Therefore, the TP and the entire study region can be partitioned by considering the dominant form of precipitation that occurs: cyclonic/frontal or convective precipitation. This enables us to more clearly determine the relevancy/importance of the monsoon system and the midlatitude westerlies for the precipitation distribution. The classification of precipitation has been determined by cluster analysis and shows a mostly monsoonally influenced class, a convective class, and a hybrid class in between. This highlights that it is not possible to draw an exact distinction regarding the extent of the monsoon and that there will always be a relatively broad area between monsoonally influenced precipitation and solely convection-dominated precipitation caused by the interannual variability of monsoon strength and other factors.

Perhaps it is possible to say that the precipitation on the central TP in summer is influenced by the monsoon system regarding moisture supply; however, moisture recycling is also important, and the midlatitude westerlies act as a control regarding the suppression or enhancement of precipitation due to the strong negative effect of high horizontal wind speeds on the development of deep convection.

A next step will analyse the combined effects of precipitation controls, since the current study has shown that the controls are not independent of each other. We intend to use a combination of PCA of the detected dominant patterns and cluster analysis to detect control regimes, as in Forsythe et al. (2015), to obtain a climate classification for the Himalayan arc and its surroundings. These regimes can perhaps help to explain regional features of glacier mass balance, like the so-called Karakoram anomaly (e.g. Hewitt, 2005) or observed lake level changes (e.g. Liu et al., 2010; Zhang et al., 2011), which show a different behaviour compared to the surrounding regions.

6 Data availability

The High Asia Refined analysis (HAR) is available at http://www.klima.tu-berlin.de/HAR. The ERA-Interim reanalysis, provided by the European Centre for Medium-Range Weather Forecasts (ECMWF), is available at http://www.ecmwf.int/en/research/climate-reanalysis/era-interim. The National Climatic Data Center (NCDC) provides weather station data from the "Global Summary of the Day", available at http://www.ncdc.noaa.gov/oa/ncdc.html.

The Supplement related to this article is available online at doi:10.5194/esd-7-767-2016-supplement.

Author contributions. Julia Curio and Dieter Scherer designed the study and discussed all results. Julia Curio carried out the analyses and prepared the paper with contributions from Dieter Scherer.

Acknowledgements. This work was supported by the German Federal Ministry of Education and Research (BMBF) Programme "Central Asia – Monsoon Dynamics and Geo-Ecosystems" (CAME) within the WET project ("Variability and Trends in Water Balance Components of Benchmark Drainage Basins on the Tibetan Plateau") under the code 03G0804A and by the German Research Foundation (DFG) Priority Programme 1372, "Tibetan Plateau: Formation – Climate – Ecosystems" within the DynRG-TiP ("Dynamic Response of Glaciers on the Tibetan Plateau to Climate Change") project under the codes SCHE 750/4-1, SCHE 750/4-2, SCHE 750/4-3. We would like to thank the four anonymous referees for their thoughtful comments, criticism, and suggestions on an earlier version of this paper.

Edited by: M. Werner
Reviewed by: four anonymous referees

References

Araguás-Araguás, L. and F. K.: Stable isotope composition of precipitation over southeast Asia, J. Geophys. Res., 103, 28721–28742, doi:10.1029/98JD02582, 1998.

Back, L. E. and Bretherton, C. S.: The relationship between wind speed and precipitation in the Pacific ITCZ, J. Climate, 18, 4317–4328, doi:10.1175/JCLI3519.1, 2005.

Barros, A. P., Chiao, S., Lang, T. J., Burbank, D., and Putkonen, J.: From weather to climate – Seasonal and interannual variability of storms and implications for erosion processes in the Himalaya, Geol. Soc. Am. Sp., 398, 17–38, doi:10.1130/2006.2398(02), 2006.

Bartholy, J. and Pongracz, R.: Analysis of precipitation conditions for the Carpathian Basin based on extreme indices in the 20th century and climate simulations for 2050 and 2100, Phys. Chem. Earth, 35, 43–51, doi:10.1016/j.pce.2010.03.011, 2010.

Bookhagen, B. and Burbank, D. W.: Toward a complete Himalayan hydrological budget: Spatiotemporal distribution of snowmelt and rainfall and their impact on river discharge, J. Geophys. Res., 115, F03019, doi:10.1029/2009JF001426, 2010.

Bothe, O., Fraedrich, K., and Zhu, X.: The large-scale circulations and summer drought and wetness on the Tibetan plateau, Int. J. Climatol., 30, 844–855, doi:10.1002/joc.1946, 2010.

Cannon, F., Carvalho, L. M. V., Jones, C., and Bookhagen, B.: Multi-annual variations in winter westerly disturbance activity affecting the Himalaya, Clim. Dynam., 44, 441–455, doi:10.1007/s00382-014-2248-8, 2014.

Chen, B., Xu, X.-D., Yang, S., and Zhang, W.: On the origin and destination of atmospheric moisture and air mass over the Tibetan Plateau, Theor. Appl. Climatol., 110, 423–435, doi:10.1007/s00704-012-0641-y, 2012.

Curio, J., Maussion, F., and Scherer, D.: A twelve-year high-resolution climatology of atmospheric water transport over the Tibetan Plateau, Earth Syst. Dynam., 6, 109–124, doi:10.5194/esd-6-109-2015, 2015.

Dee, D. P., Uppala, S. M., Simmons, a. J., Berrisford, P., Poli, P., Kobayashi, S., Andrae, U., Balmaseda, M. a., Balsamo, G., Bauer, P., Bechtold, P., Beljaars, a. C. M., van de Berg, L., Bidlot, J., Bormann, N., Delsol, C., Dragani, R., Fuentes, M., Geer, A. J., Haimberger, L., Healy, S. B., Hersbach, H., Hólm, E. V., Isaksen, L., Kållberg, P., Köhler, M., Matricardi, M., McNally, A. P., Monge-Sanz, B. M., Morcrette, J.-J., Park, B.-K., Peubey, C., de Rosnay, P., Tavolato, C., Thépaut, J.-N., and Vitart, F.: The ERA-Interim reanalysis: configuration and performance of the data assimilation system, Q. J. Roy. Meteorol. Soc., 137, 553–597, doi:10.1002/qj.828, 2011.

Dimri, A. P., Niyogi, D., Barros, A. P., Ridley, J., Mohanty, U. C., Yasunari, T., and Sikka, D. R.: Western Disturbances: A review, Rev. Geophys., 53, 225–246, doi:10.1002/2014RG000460, 2015.

Findell, K. L.: Atmospheric controls on soil moisture-boundary layer interactions: Three-dimensional wind effects, J. Geophys. Res., 108, 1–21, doi:10.1029/2001JD001515, 2003.

Forsythe, N., Blenkinsop, S., and Fowler, H. J.: Exploring objective climate classification for the Himalayan arc and adjacent regions using gridded data sources, Earth Syst. Dynam., 6, 311–326, doi:10.5194/esd-6-311-2015, 2015.

Frei, C., Schär, C., Lüthi, D., and Davies, H. C.: Heavy precipitation processes in a warmer climate, Geophy. Res. Lett., 25, 1431, doi:10.1029/98GL51099, 1998.

Garreaud, R. D.: Precipitation and circulation covariability in the extratropics, J. Climate, 20, 4789–4797, doi:10.1175/JCLI4257.1, 2007.

Giovannettone, J. P. and Barros, A. P.: Probing Regional Orographic Controls of Precipitation and Cloudiness in the Central Andes Using Satellite Data, J. Hydrometeorol., 10, 167–182, doi:10.1175/2008JHM973.1, 2009.

Hahn, D. and Manabe, S.: The role of mountains in the south Asian monsoon circulation, J. Atmos. Sci., 32, 1515–1541, 1975.

Hewitt, K.: The Karakoram anomaly? Glacier expansion and the'elevation effect, Karakoram Himalaya, Mt. Res. Dev., 25, 332–340, doi:10.1659/0276-4741(2005)025[0332:TKAGEA]2.0.CO;2, 2005.

Hren, M. T., Bookhagen, B., Blisniuk, P. M., Booth, A. L., and Chamberlain, C. P.: δ^{18}O and δD of streamwaters across the Himalaya and Tibetan Plateau: Implications for moisture sources and paleoelevation reconstructions, Earth Planet. Sci. Lett., 288, 20–32, doi:10.1016/j.epsl.2009.08.041, 2009.

Johansson, B. and Chen, D.: The influence of wind and topography on precipitation distribution in Sweden: Statistical analysis and modelling, Int. J. Climatol., 23, 1523–1535, doi:10.1002/joc.951, 2003.

Joswiak, D. R., Yao, T., Wu, G., Tian, L., and Xu, B.: Ice-core evidence of westerly and monsoon moisture contributions in the central Tibetan Plateau, J. Glaciol., 59, 56–66, doi:10.3189/2013JoG12J035, 2013.

Kurita, N. and Yamada, H.: The Role of Local Moisture Recycling Evaluated Using Stable Isotope Data from over the Middle of the

Tibetan Plateau during the Monsoon Season, J. Hydrometeorol., 9, 760–775, doi:10.1175/2007JHM945.1, 2008.

Liu, B., Xu, M., and Henderson, M.: Where have all the showers gone? Regional declines in light precipitation events in China, 1960–2000, Int. J. Climatol., 31, 1177–1191, doi:10.1002/joc.2144, 2011.

Liu, J., Kang, S., Gong, T., and Lu, A.: Growth of a high-elevation large inland lake, associated with climate change and permafrost degradation in Tibet, Hydrol. Earth Syst. Sci., 14, 481–489, doi:10.5194/hess-14-481-2010, 2010.

Liu, W., Wang, L., Chen, D., Tu, K., Ruan, C., and Hu, Z.: Large-scale circulation classification and its links to observed precipitation in the eastern and central Tibetan Plateau, Clim. Dynam., 46, 3481–3497, doi:10.1007/s00382-015-2782-z, 2016.

Liu, X. and Yin, Z.-Y.: Spatial and Temporal Variation of Summer Precipitation over the Eastern Tibetan Plateau and the North Atlantic Oscillation, J. Climate, 14, 2896–2909, doi:10.1175/1520-0442(2001)014<2896:SATVOS>2.0.CO;2, 2001.

Maussion, F., Scherer, D., Finkelnburg, R., Richters, J., Yang, W., and Yao, T.: WRF simulation of a precipitation event over the Tibetan Plateau, China – an assessment using remote sensing and ground observations, Hydrol. Earth Syst. Sci., 15, 1795–1817, doi:10.5194/hess-15-1795-2011, 2011.

Maussion, F., Scherer, D., Mölg, T., Collier, E., Curio, J., and Finkelnburg, R.: Precipitation Seasonality and Variability over the Tibetan Plateau as Resolved by the High Asia Reanalysis*, J. Climate, 27, 1910–1927, doi:10.1175/JCLI-D-13-00282.1, 2014.

Mölg, T. and Chiang, J.: Temporal precipitation variability versus altitude on a tropical high mountain: Observations and mesoscale atmospheric modelling, Q. J. Roy. Meteor. Soc., 135, 1439–1455, doi:10.1002/qj.461, 2009.

Mölg, T., Maussion, F., and Scherer, D.: Mid-latitude westerlies as a driver of glacier variability in monsoonal High Asia, Nature Clim. Change, 4, 68–73, doi:10.1038/nclimate2055, 2014.

NCDC: Global Summary of the Day, provided by the National Climatic Data Center (NCDC) available at: http://www.ncdc.noaa.gov/oa/ncdc.html, 2016.

Norris, J., Carvalho, L. M. V., Jones, C., and Cannon, F.: WRF simulations of two extreme snowfall events associated with contrasting extratropical cyclones over the western and central Himalaya, J. Geophys. Res., 120, 3114–3138, doi:10.1002/2014JD022592, 2015.

Numerical Recipes: The Art of Scientific Computing, second edition, Cambridge University Press, 1992.

Polade, S. D., Pierce, D. W., Cayan, D. R., Gershunov, A., and Dettinger, M. D.: The key role of dry days in changing regional climate and precipitation regimes, Sci. Rep., 4, 8 pp., doi:10.1038/srep04364, 2014.

Roe, G. H.: Orographic Precipitation, Ann. Rev. Earth Planet. Sci., 33, 645–671, doi:10.1146/annurev.earth.33.092203.122541, 2005.

Rose, B. E. J. and Lin, C. A.: Precipitation from vertical motion: A statistical diagnostic scheme, Int. J. Climatol., 23, 903–919, doi:10.1002/joc.919, 2003.

Rüthrich, F.: Lake-Related Cloud Dynamics on the Tibetan Plateau: Spatial Patterns and Interannual Variability, J. Climate, 28, 9080–9104, doi:10.1175/JCLI-D-14-00698.1, 2015.

Schiemann, R. and Lüthi, D.: The precipitation climate of Central Asia – intercomparison of observational and numerical data sources in a remote semiarid region, Int. J. Climatol., 28, 295–314, doi:10.1002/joc.1532, 2008.

Schiemann, R., Lüthi, D., and Schär, C.: Seasonality and Interannual Variability of the Westerly Jet in the Tibetan Plateau Region*, J. Climate, 22, 2940–2957, doi:10.1175/2008JCLI2625.1, 2009.

Shinker, J. J., Bartlein, P. J., and Shuman, B.: Synoptic and dynamic climate controls of North American mid-continental aridity, Quat. Sci. Rev., 25, 1401–1417, doi:10.1016/j.quascirev.2005.12.012, 2006.

Skamarock, W. and Klemp, J.: A time-split nonhydrostatic atmospheric model for weather research and forecasting applications, J. Comput. Phys., 227, 3465–3485, doi:10.1016/j.jcp.2007.01.037, 2008.

Spiess, M., Schneider, C., and Maussion, F.: MODIS-derived interannual variability of the equilibrium-line altitude across the Tibetan Plateau, Ann. Glaciol., 57, 140–154, doi:10.3189/2016AoG71A014, 2015.

Tian, L., Yao, T., MacClune, K., White, J. W. C., Schilla, A., Vaughn, B., and Ichiyanagi, K.: Stable isotopic variations in west China: A consideration of moisture sources, J. Geophys. Res., 112, D10112, doi:10.1029/2006JD007718, 2007.

Trenberth, K. E.: Atmospheric Moisture Recycling: Role of Advection and Local Evaporation, J. Climate, 12, 1368–1381, doi:10.1175/1520-0442(1999)012<1368:AMRROA>2.0.CO;2, 1999.

Webster, P., Magana, V., and Palmer, T.: Monsoons: Processes, predictability, and the prospects for prediction, J. Geophys. Res., 103, 14451–14510, 1998.

Xu, X., Lu, C., Shi, X., and Gao, S.: World water tower: An atmospheric perspective, Geophy. Res. Lett., 35, L20815, doi:10.1029/2008GL035867, 2008.

Yang, K., Wu, H., Qin, J., Lin, C., Tang, W., and Chen, Y.: Recent climate changes over the Tibetan Plateau and their impacts on energy and water cycle: A review, Global Planet. Change, 112, 79–91, doi:10.1016/j.gloplacha.2013.12.001, 2014.

Zhang, J. W. and Atkinson, B. W.: Stability and wind shear effects on meso-scale cellular convection, Bound.-Lay. Meteorol., 75, 263–285, doi:10.1007/BF00712697, 1995.

Zhang, G., Xie, H., Kang, S., Yi, D., and Ackley, S. F.: Monitoring lake level changes on the Tibetan Plateau using ICESat altimetry data (2003–2009), Remote Sens. Environ., 115, 1733–1742, doi:10.1016/j.rse.2011.03.005, 2011.